

AN EXPERIMENTAL AND ANALYTICAL STUDY ON THE
REFILLING AND REWETTING OF HOT
HORIZONTAL TUBES

by

AMAD ABDUL-RAZZAK, B.Sc., M.Sc.

A Thesis

Submitted to the School of Graduate Studies
in Partial Fulfillment of the Requirements
for the Degree
Doctor of Philosophy

McMaster University

(c) Copyright by Amad Abdul-Razzak, June 1990

REFILLING AND REWETTING
OF HOT HORIZONTAL TUBES

DOCTOR OF PHILOSOPHY (1990)
(Mechanical Engineering)

McMASTER UNIVERSITY
Hamilton, Ontario

TITLE: An Experimental and Analytical study on the Refilling
 and Rewetting of Hot Horizontal Tubes

AUTHOR: Amad Abdul-Razzak, B.Sc. (University Of Baghdad)
 M.Sc. (Strathclyde University)

SUPERVISOR: Professor M. Shoukri

NUMBER OF PAGES: xxiv, 269

ABSTRACT

This thesis contains the details of an experimental and analytical study on the refilling and rewetting of hot horizontal tubes. The experiments were conducted to refill and rewet two 25.4 mm I.D., 3 m long zircaloy tubes (1 mm and 2 mm wall thicknesses) under a wide range of initial and boundary conditions. In addition to obtaining the quenching rates and the various parametric effects, the data played an important role in understanding the nature of the quench front propagation and identifying the associated flow patterns. Moreover, the data were used to obtain quench curves at different axial and circumferential locations. These quench curves helped in investigating the parametric effects on the different modes of heat transfer associated with the rewetting process as well as giving valuable insight into the rewetting mechanisms involved in the process.

A rewetting criterion based on vapour film collapse in the film boiling region is proposed. This criterion suggests that surface rewetting is initiated when the vapour film thickness reduces down to a value equal to the sum of the amplitude of the liquid-vapour interface fluctuations and the solid surface roughness. Accordingly, a theoretical model for predicting the dynamic behaviour of the liquid-vapour interface in the film boiling region near the bottom of a horizontal tube was developed. This study showed that the hydraulic

disturbances represented by the system pressure fluctuations could induce interface fluctuations capable of rewetting the surface when the equilibrium vapour film thickness was close to the experimentally estimated critical value.

A two-fluid model incorporating the proposed rewetting criterion, as well as derived models for the partition factor and the film boiling heat transfer coefficient, was developed to predict the transients of the refilling and rewetting of hot horizontal tubes. This model is capable of predicting the experimentally observed thermal-hydraulic transients of the refilling and rewetting processes.

ACKNOWLEDGEMENTS

The author wishes to express his sincere gratitude to Professor M. Shoukri, his research supervisor, for his support, guidance and encouragement during the progress of research and for many valuable suggestions for improving the manuscript.

The author is also very grateful to Dr. A.M.C. Chan, for his advice, suggestions and critical examination of this work. Thanks are extended to Professor R.L. Judd, Dr. Wm.J. Garland, and Dr. M.A. El-Bestawi, members of the Ph.D. supervisory committee, for their continuous interest and encouragement.

Thanks are due to Mr. A.K. Ahluwalia, for his advice and help during the experimental program and to Mr. B. Tole, for his valuable help in transferring the data.

The author acknowledges with thanks the useful discussions he had with his colleagues, in particular, Mr. J. Ballyk.

The author thanks Ontario Hydro Research Division for the use of its laboratory and research facilities.

Thanks are also due to the Ministry of Higher Education and Scientific Research of Iraq for the financial support to the Author.

Finally, the author expresses his sincere appreciation to his wife Elham and children, Amane, Sura and Samy, for their understanding and patience during the work.

TABLE OF CONTENTS

	<u>PAGE</u>
ABSTRACT	iii
ACKNOWLEDGEMENT	v
TABLE OF CONTENTS	vi
LIST OF TABLES	xii
LIST OF FIGURES	xiii
NOMENCLATURE	xxi
 CHAPTER 1	
INTRODUCTION	1
 CHAPTER 2	
LITERATURE REVIEW	7
2-1	7
2-1-1	7
EXPERIMENTAL WORK ON REWETTING OF VERTICAL SURFACES	
2-1-2	10
CONCLUSIONS FROM THE EXPERIMENTAL WORK ON VERTICAL SURFACES	
2-1-3	12
THEORETICAL WORK ON REWETTING OF VERTICAL SURFACES	
2-1-3-1	12
CONDUCTION CONTROLLED MODELS	
2-1-3-2	18
THERMAL HYDRAULIC MODELS	
2-1-4	22
COMMENTS ON THE THEORETICAL WORK ON VERTICAL SYSTEMS	

		<u>PAGE</u>
2-2	REWETTING OF HORIZONTAL CHANNELS	23
2-2-1	COMMENTS ON THE THEORETICAL WORK ON HORIZONTAL CHANNELS	29
CHAPTER 3	EXPERIMENTAL FACILITY, INSTRUMENTATION AND MEASUREMENTS	35
3-1	TEST FACILITY	35
3-2	INSTRUMENTATION AND MEASUREMENTS	36
3-2-1	TEMPERATURE MEASUREMENTS	36
3-2-2	PRESSURE MEASUREMENTS	38
3-2-3	FLOW MEASUREMENTS	38
3-2-4	VOID FRACTION MEASUREMENTS	39
3-3	DATA ACQUISITION SYSTEM	42
3-4	EXPERIMENTAL PROCEDURE	43
3-5	TEST MATRIX	44
CHAPTER 4	EXPERIMENTAL RESULTS	54
4-1	THIN TUBE RESULTS	54
4-1-1	TRANSIENT PRESSURES AND INLET FLOW RATE	54
4-1-2	TRANSIENT WALL TEMPERATURES	55
4-1-3	TRANSIENT VOID FRACTION	57
4-2	THICK TUBE RESULTS	58
4-2-1	TRANSIENT PRESSURES AND INLET FLOW RATE	58
4-2-2	TRANSIENT WALL TEMPERATURES	58

		<u>PAGE</u>
4-2-3	TRANSIENT VOID FRACTION	60
4-3	REPRODUCIBILITY OF TEST RESULTS	61
CHAPTER 5	DATA ANALYSIS	75
5-1	REWETTING VELOCITY	75
5-2	FLOW REGIMES IDENTIFICATION	78
5-2-1	STRATIFIED REFILLING FRONT	79
5-2-2	INVERTED ANNULAR FLOW	81
5-2-3	ANNULAR FLOW	82
5-2-4	EFFECT OF TUBE WALL THICKNESS	84
5-3	QUENCHING CURVES	85
5-3-1	BACKGROUND	85
5-3-2	PRESENT ANALYSIS FOR QUENCH CURVES	87
CHAPTER 6	SURFACE REWETTING	126
6-1	BACKGROUND	126
6-1-1	LEIDENFROST TEMPERATURE	126
6-1-2	MINIMUM FILM BOILING LIMIT IN POOL BOILING	128
6-1-3	MINIMUM FILM BOILING TEMPERATURE IN CONVECTIVE FLOW SYSTEMS	134
6-2	COMPARISON WITH THE PRESENT DATA	141
6-3	THE CONCEPT OF MINIMUM VAPOUR FILM THICKNESS	142
6-4	EVALUATING THE AVAILABLE REWETTING CRITERIA IN REFILLING OF HOT HORIZONTAL TUBES	145

		<u>PAGE</u>
6-5	THE PROPOSED GENERAL REWETTING CRITERION	148
6-6	LIQUID-VAPOUR INTERFACE BEHAVIOUR IN FILM BOILING	150
6-6-1	REVIEW	150
6-6-2	EXPERIMENTAL RESULTS	151
6-7	DYNAMIC BEHAVIOUR OF THE LIQUID-VAPOUR INTERFACE OF FILM BOILING DURING REFILLING OF A HOT HORIZONTAL TUBE	153
6-7-1	THE MODEL	153
6-7-2	ANALYSIS AND DISCUSSION	158
6-7-2-1	EQUILIBRIUM VAPOUR FILM THICKNESS	158
6-7-2-2	DYNAMIC INTERFACE ANALYSIS	158
6-7-2-3	THE EFFECT OF SYSTEM PRESSURE FLUCTUATION ON THE CRITICAL VAPOUR FILM THICKNESS	161
6-8	A SIMPLE MODEL FOR EVALUATING THE PARTITION FACTOR β	162
CHAPTER 7	TWO-FLUID MODEL	185
7-1	INTRODUCTION	185
7-2	MODELLING OF MULTI-PHASE SYSTEMS	186
7-2-1	LOCAL INSTANTANEOUS CONSERVATION EQUATIONS	187
7-2-2	AVERAGING PROCEDURES	188
7-2-2-1	THE AVERAGED EQUATIONS	189
7-2-3	AUXILIARY RELATIONSHIPS	196

		<u>PAGE</u>
7-3	SIMPLIFIED TWO FLUID MODEL FOR THE REFILLING	197
	AND REWETTING OF HOT HORIZONTAL CHANNELS	202
7-4	NUMERICAL COMPUTATION	203
7-4-1	THE HYDRAULIC EQUATIONS	203
7-4-2	VAPOUR PHASE VELOCITY	205
7-4-3	THE ENERGY EQUATION OF THE LIQUID PHASE	206
7-4-4	WALL TEMPERATURE	207
7-5	INITIAL AND BOUNDARY CONDITIONS	211
7-5-1	INITIAL CONDITIONS	211
7-5-2	BOUNDARY CONDITIONS	212
7-6	AUXILIARY EQUATIONS FOR THE HYDRAULIC MODEL	213
7-6-1	WALL TO LIQUID FRICTION	213
7-6-2	WALL TO VAPOUR FRICTION	214
7-6-3	INTERFACIAL SHEAR	215
7-6-4	INTERFACIAL MASS TRANSFER	215
7-6-5	INTERFACIAL MOMENTUM TRANSFER	216
7-6-6	VAPOUR INERTIA	216
7-7	HEAT TRANSFER REGIMES	216
7-7-1	TRANSITION TO INVERTED ANNULAR FLOW REGIME	220
7-8	QUENCH MODEL	221
7-9	NUMERICAL PROCEDURE	223
7-10	NUMERICAL PREDICTIONS AND COMPARISON WITH	226
	EXPERIMENTAL RESULTS	
7-10-1	REFILLING AND REWETTING FRONTS	226

		<u>PAGE</u>
7-10-2	TRANSIENT WALL TEMPERATURE	227
7-11	CONVERGENCE STUDIES	229
7-12	PARAMETRIC STUDIES	230
CHAPTER 8	CONCLUSIONS	245
REFERENCES		249
APPENDIX A	TEST MATRIX	258
APPENDIX B	TWO-DIMENSIONAL HEAT CONDUCTION MODEL	265

LIST OF TABLES

<u>TABLE NO.</u>	<u>DESCRIPTION</u>	<u>PAGE</u>
2-1	ONE-DIMENSIONAL HEAT-CONDUCTION MODELS] [taken from Elias and Yadigaroglu (1978)]	31
2-2	TWO-DIMENSIONAL HEAT-CONDUCTION MODELS [taken from Elias and Yadigaroglu (1978)]	32
7-1	PARAMETRIC STUDIES	233
7-2	CONVERGENCE STUDIES .	234
7-3	SENSITIVITY TO CRITICAL VAPOUR FILM THICKNESS	234
A-1	TEST MATRIX OF THE THIN TUBE : FIRST GROUP	258
A-2	TEST MATRIX OF THE THIN TUBE : FIRST GROUP	259
A-3	TEST MATRIX OF THE THIN TUBE : FIRST GROUP	260
A-4	TEST MATRIX OF THE THIN TUBE SECOND GROUP : REPEATED RUNS	261
A-5	TEST MATRIX OF THE THICK TUBE	
A-6	TEST MATRIX OF THE THICK TUBE	
A-7	TEST MATRIX OF THE THICK TUBE	

LIST OF FIGURES

<u>FIG. NO.</u>		<u>PAGE</u>
1-1	METHODOLOGY OF LOCA ANALYSIS	4
1-2	SCHEMATIC OF PWR PRIMARY COOLANT SYSTEM	5
1-3	CANDU REACTOR SIMPLIFIED FLOW DIAGRAM	6
2-1	FLOW AND HEAT TRANSFER REGIMES OBSERVED DURING REFLOODING OF VERTICAL SYSTEMS [GROENEVELD AND YOUNG (1978)]	33
2-2	CHARACTERISTICS OF HORIZONTAL CHANNEL REWETTING [CHAN AND BANERJEE (1981)]	34
3-1	SCHEMATIC OF EXPERIMENT FACILITY	46
3-2	VIEW OF EXPERIMENTAL FACILITY	47
3-3	VIEW OF EXPERIMENTAL FACILITY	48
3-4	VIEW OF EXPERIMENTAL FACILITY	49
3-5	VIEW OF EXPERIMENTAL FACILITY	50
3-6A	THERMOCOUPLE AND GAMMA DENSITOMETER STATIONS ALONG THE TEST SECTION	51
3-6B	CIRCUMFERENTIAL THERMOCOUPLE LOCATIONS FOR THE THIN TUBE	51
3-7	THERMOCOUPLE LOCATIONS FOR THE THICK TUBE	52

<u>FIG. NO.</u>		<u>PAGE</u>
3-8	SCHEMATIC DIAGRAM OF THE GAMMA DENSITOMETER AND SIGNAL PROCESSING CIRCUIT	53
4-1	INLET AND OUTLET PRESSURE TRANSIENTS	62
4-2	TRANSIENT INLET FLOW RATE	62
4-3	TRANSIENT WALL TEMPERATURES AT DIFFERENT AXIAL LOCATIONS	63
4-4	TRANSIENT WALL TEMPERATURES AT DIFFERENT CIRCUMFERENTIAL LOCATIONS	64
4-5	TRANSIENT VOID FRACTION	65
4-6	INLET AND OUTLET PRESSURE TRANSIENTS	66
4-7	TRANSIENT INLET FLOW RATE	66
4-8	TRANSIENT WALL TEMPERATURES AT DIFFERENT AXIAL LOCATIONS	67
4-9	TRANSIENT WALL TEMPERATURES AT DIFFERENT CIRCUMFERENTIAL LOCATIONS	68
4-10	TRANSIENT WALL TEMPERATURES AT DIFFERENT RADIAL LOCATIONS	69
4-11	TRANSIENT VOID FRACTION	70
4-12	QUENCHING TIME VERSUS AXIAL LOCATION FOR REPEATED TEST RUNS	71
4-13	QUENCHING TIME VERSUS AXIAL LOCATION FOR REPEATED TEST RUNS	72

<u>FIG. NO.</u>		<u>PAGE</u>
4-14	QUENCHING TIME VERSUS AXIAL LOCATION FOR REPEATED TEST RUNS	73
4-15	QUENCHING TIME VERSUS AXIAL LOCATION FOR REPEATED TEST RUNS	74
5-1	REWETTING VELOCITY VERSUS MASS FLUX	95
5-2	REWETTING VELOCITY VERSUS MASS FLUX	96
5-3	REWETTING VELOCITY VERSUS MASS FLUX	97
5-4	REWETTING VELOCITY VERSUS MASS FLUX	98
5-5	REWETTING VELOCITY VERSUS MASS FLUX	99
5-6	REWETTING VELOCITY VERSUS MASS FLUX	100
5-7	REWETTING VELOCITY VERSUS MASS FLUX	101
5-8	REWETTING VELOCITY VERSUS MASS FLUX	102
5-9	REWETTING VELOCITY VERSUS MASS FLUX	103
5-10	REWETTING VELOCITY VERSUS MASS FLUX	104
5-11a	TRANSIENT CIRCUMFERENTIAL TEMPERATURE CURVES AT MODERATE FLOW RATES	105
5-11b	TRANSIENT VOID FRACTION AT MODERATE FLOW RATES	105
5-12	CHARACTERISTIC OF HORIZONTAL CHANNEL REWETTING AT MODERATE FLOW RATE	106
5-13	QUENCH LEVEL - VOID FRACTION VARIATION	107
5-14	QUENCH LEVEL - WATER LEVEL VARIATION	107
5-15a	HORIZONTAL ANNULAR FLOW	108

<u>FIG. NO.</u>		<u>PAGE</u>
5-15B	SPECULATED SECONDARY VAPOUR FLOW DURING REFILLING OF A HOT HORIZONTAL TUBE	109
5-16A	TRANSIENT CIRCUMFERENTIAL TEMPERATURE CURVES AT HIGH FLOW RATES AND HIGH TUBE HEAT CAPACITY	109
5-16B	TRANSIENT VOID FRACTION AT HIGH FLOW RATES AND HIGH TUBE HEAT CAPACITY	109
5-17A	TRANSIENT CIRCUMFERENTIAL TEMPERATURE CURVES AT LOW FLOW RATES AND LOW TUBE HEAT CAPACITY	110
5-17B	TRANSIENT VOID FRACTION AT LOW FLOW RATES AND LOW TUBE HEAT CAPACITY	108
5-18	DIMENSIONLESS QUENCH LEVEL VERSUS VOID FRACTION FOR STRATIFIED, ANNULAR AND INVERTED ANNULAR FLOW REGIMES	111
5-19A	TRANSIENT CIRCUMFERENTIAL TEMPERATURE CURVES FOR THE THICK TUBE	112
5-19B	TRANSIENT VOID FRACTION FOR THE THICK TUBE	112
5-20	A TYPICAL QUENCH CURVE AND THE CORRESPONDING TRANSIENT WALL TEMPERATURE	113
5-21	HEAT BALANCE ON AN ELEMENT OF THE TEST SECTION	114
5-22	COMPARISON BETWEEN THE HEAT FLUX OBTAINED FROM HEAT BALANCE AND RADIAL TEMPERATURE GRADIENTS AT THE QUENCHED SURFACE	115
5-23	QUENCH CURVES : EFFECT OF INITIAL TUBE TEMPERATURE	116

<u>FIG. NO.</u>		<u>PAGE</u>
5-24	QUENCH CURVES : EFFECT OF MASS FLUX	117
5-25	QUENCH CURVES : EFFECT OF SUBCOOLING	118
5-26	QUENCH CURVES : EFFECT OF AXIAL LOCATION	119
5-27	QUENCH CURVES : EFFECT OF CIRCUMFERENTIAL LOCATION	120
5-28	AXIAL HEAT CONDUCTION	121
5-29A	QUENCH CURVE FOR THE THICK TUBE : HEAT FLUX VERSUS TUBE TEMPERATURE	122
5-29B	QUENCH CURVE FOR THE THICK TUBE : HEAT FLUX VERSUS TIME	122
5-30A	AXIAL HEAT CONDUCTION FOR THE THICK TUBE : HEAT FLUX VERSUS TUBE TEMPERATURE	123
5-30B	AXIAL HEAT CONDUCTION FOR THE THICK TUBE : HEAT FLUX VERSUS TIME	123
5-31A	EFFECT OF TUBE WALL THICKNESS ON THE QUENCH CURVE : HEAT FLUX VERSUS TUBE TEMPERATURE	124
5-31B	EFFECT OF TUBE WALL THICKNESS ON THE QUENCH CURVE : HEAT FLUX VERSUS TIME	125
6-1	LEIDENFROST TEMPERATURE	167
6-2	FILM BOILING TERMINATION MECHANISMS	168
6-3	COMPARISON BETWEEN THE APPARENT QUENCH TEMPERATURE OF THE PRESENT EXPERIMENTS AND THAT PREDICTED BY CORRELATION [KIM & LEE (1979)]	169

<u>FIG. NO.</u>		<u>PAGE</u>
6-4	COMPARISON BETWEEN THE APPARENT QUENCH TEMPERATURE OF THE PRESENT EXPERIMENTS AND THAT PREDICTED BY CORRELATION [KIM AND LEE (1979)]	170
6-5	CRITICAL AND AVERAGE VAPOUR VELOCITIES VERSUS WATER LEVEL [CHAN AND BANERJEE (1981)]	171
6-6A	EFFECT OF INITIAL TUBE TEMPERATURE AND WATER SUBCOOLING ON THE CRITICAL WATER LEVEL	172
6-6B	EFFECT OF MASS FLUX ON THE CRITICAL WATER LEVEL	173
6-7	OVERALL GEOMETRY AND PROPOSED MODEL	174
6-8	EQUILIBRIUM VAPOUR FILM THICKNESS - MODEL PREDICTIONS AND EXPERIMENTS	175
6-9	DYNAMIC RESPONSE OF VAPOUR FILM TRIGGERED BY STEP CHANGE IN TUBE TEMPERATURE	176
6-10	EFFECT OF SUBCOOLING AND LIQUID VELOCITY ON THE DYNAMIC RESPONSE OF THE LIQUID-VAPOUR INTERFACE	177
6-11	DYNAMIC RESPONSE OF THE LIQUID-VAPOUR INTERFACE TRIGGERED BY PRESSURE PULSE	178
6-12	PRESSURE PULSE VERSUS CRITICAL VAPOUR FILM THICKNESS	179
6-13	PRESSURE PULSE VERSUS MAXIMUM AMPLITUDE OF INTERFACE FLUCTUATIONS	180

<u>FIG. NO.</u>		<u>PAGE</u>
6-14	INTEGRAL FORMULATION OF THE THERMAL BOUNDARY LAYER IN THE LIQUID PHASE	181
6-15	PARTITION FACTOR AT DIFFERENT TUBE WALL TEMPERATURES	182
6-16	PARTITION FACTOR AT DIFFERENT WATER VELOCITY	183
6-17	PARTITION FACTOR AT DIFFERENT SUBCOOLINGS	184
7-1	GENERAL TWO-PHASE CONTROL VOLUME	235
7-2	CONTROL VOLUME FOR THE AVERAGING PROCESS	235
7-3	STAGGERED NET USED FOR THE HYDRAULIC EQUATIONS	236
7-4	FINITE DIFFERENCE GRID USED FOR LIQUID TEMPERATURE CALCULATION	236
7-5	CONVECTIVE BOUNDARY CONDITION IN THE THREE-DIMENSIONAL FORMULATION	237
7-6	TWO-DIMENSIONAL FORMULATION WITH CONVECTIVE BOUNDARY CONDITIONS	237
7-7	REGIONS OF HEAT TRANSFER FOR MODERATE TUBE HEAT CAPACITY AND MODERATE MASS FLUX	238
7-8	REGIONS OF HEAT TRANSFER FOR HIGH TUBE CAPACITY AND HIGH MASS FLUX	239
7-9	REFILLING AND QUENCH FRONT PROPAGATION	240
7-10	EFFECT OF MASS FLUX ON STRATIFICATION	240
7-11	TRANSIENT TEMPERATURE CURVES AT DIFFERENT AXIAL LOCATIONS FOR LOW MASS FLUX	241

<u>FIG. NO.</u>		<u>PAGE</u>
7-12	TRANSIENT TEMPERATURE CURVES AT DIFFERENT CIRCUMFERENTIAL LOCATIONS FOR LOW MASS FLUX	242
7-13	TRANSIENT TEMPERATURE CURVES AT DIFFERENT AXIAL LOCATIONS FOR HIGH MASS FLUX	243
7-14	TRANSIENT TEMPERATURE CURVES AT DIFFERENT CIRCUMFERENTIAL LOCATIONS FOR HIGH MASS FLUX	244
B-1	NODAL NETWORK FOR THE TWO-DIMENSIONAL ANALYSIS	269
B-2	NODAL NETWORK FOR CALCULATION OF SURFACE HEAT FLUX	269

NOMENCLATURE

<u>SYMBOL</u>	<u>DESCRIPTION</u>	<u>UNITS</u>
a_g	vapour to wall contact area per unit volume	1/m
a_i	vapour-liquid interfacial area per unit volume	1/m
a_L	liquid to wall contact area per unit volume	1/m
A	cross sectional area of the tube	m^2
C_p	specific heat at constant pressure	J/kg K
D	tube diameter	m
e	specific internal energy	J/kg
f	friction factor	
g	gravitational acceleration	m/s^2
G	mass flux	$kg/m^2.s$
h	heat transfer coefficient or enthalpy	$W/m^2 K$ J/kg
h_{fg}	latent heat of evaporation	J/kg
h_q	quench level	m
H_c	critical water level	m
H_L, h_L	water level	m
\bar{J}	generalized flux term	
k	thermal conductivity	W/m K
\dot{m}	rate of interfacial mass transfer	$kg/m^3.s$
\hat{n}	normal unit vector	

<u>SYMBOL</u>	<u>DESCRIPTION</u>	<u>UNITS</u>
N	attenuated flux of gamma beam	counts/s
N_0	incident flux of gamma beam	counts/s
Nu	Nusselt number	
p	pressure	N/m^2
p_{cr}	critical fluid pressure	N/m^2
P_L	hydrostatic liquid pressure	N/m^2
P_G	vapour pressure in the film boiling region	N/m^2
Pr	Prandtl number	
q	heat flux	W/m^2
q_{min}	minimum heat flux	W/m^2
r	radial distance coordinate	m
R	tube radius	m
S	sensitivity of the gamma densitometer	
t	time	s
T	temperature	$^{\circ}C$
T_{cr}	critical fluid temperature	$^{\circ}C$
T_{min}	minimum film temperature	$^{\circ}C$
u	velocity	m/s
u_{crit}	critical vapour velocity	m/s
U	rewetting velocity	m/s
\bar{U}	velocity vector	m/s
V	averaged volume or velocity of vapourization	m^3 m/s
x	quality	

<u>SYMBOL</u>	<u>DESCRIPTION</u>	<u>UNITS</u>
y	distance from the bottom of the tube	m
y_h	hydraulic depth	m
z	distance along tube axis	m

<u>GREEK SYMBOLS</u>	<u>DESCRIPTION</u>	<u>UNITS</u>
α	void fraction	
β	partition factor	
δ	vapour film thickness	mm
$\dot{\delta}$	vapour-liquid interface velocity	m/s
$\ddot{\delta}$	vapour-liquid interface acceleration	m/s ²
Δt	time step	s
Δz	axial cell size	m
ϵ	emissivity or statistical error	
ϕ	generalized source term	
ψ	generalized intensive quantity	
λ	wave length	m
μ	dynamic viscosity	N.s/m ²
θ	angle from the bottom	degree
ρ	density	kg/m ³
σ	surface tension or Stefan Boltzman constant	N/m W/m ² .K ⁴
$\bar{\sigma}$	stress tensor	N/m ²
τ	shear stress	N/m ²
$\bar{\tau}$	shear tensor	N/m ²

<u>SUBSCRIPT</u>	<u>DESCRIPTION</u>
c	coolant
CHF	critical heat flux
G	vapour
i	interfacial
I	inside
K	phase
L	liquid
O	outside
SAT	saturation
SUB	subcooled

CHAPTER 1

INTRODUCTION

Surface wetting is the establishment of continuous liquid contact with a dry hot surface. This phenomenon is encountered in nuclear engineering, cryogenic engineering, metallurgy and other industrial applications. In nuclear engineering, surface rewetting is of fundamental importance for the re-establishment of normal and safe temperature levels following dry-out during a postulated loss of coolant accident (LOCA) in a water cooled nuclear reactor.

The interest in various safety aspects related to the design and operation of nuclear reactor installations resulted in considerable efforts in thermal-hydraulic research. The main concern in reactor thermal hydraulic safety analysis is the effectiveness of the emergency core cooling systems in arresting the temperature rise in the core following a hypothetical LOCA. This requires the development and verification of computational tools which can predict the sequence of events which occur in the reactor cooling circuit during a postulated LOCA. Accordingly, mathematical models are developed and experiments are conducted to test individual system components as well as the integrated system.

The approach used for developing sound tools for thermal-hydraulic analysis of LOCA is shown in figure 1-1. The final analysis tool is essentially in the form of a computer code. The code is based on numerical solution of a set of conservation laws governing the system behaviour which is complemented by a set of constitutive (closure) equations. In developing the mathematical model, and in choosing the closure relationships, experimentation is required. As shown in figure 1-1, experimental results play an important role in formulating the physical model, validating assumptions, developing and evaluating required constitutive relations and finally verifying code calculations.

Heat transport systems vary according to reactor design. In the Boiling Water Reactors (BWR) and the Pressurized Water Reactor (PWR), the reactor core is placed in a vessel. The fuel rods in the core are arranged in vertical arrays. A diagrammatic arrangement of a PWR is shown in figure 1-2. Top spray cooling for BWR and bottom reflooding for PWR are used. Following the blow-down phase, the emergency core cooling system injects cooling water into the primary system until the core is totally rewet and refilled with water.

In the CANDU pressurized heavy water reactor, a horizontally oriented calandria is used instead of a reactor vessel. The calandria tank is penetrated by horizontal channels containing fuel bundles. Low pressure heavy water moderator is held in the calandria tank surrounding the horizontal channels which are comprised of two concentric tubes, the calandria and pressure tubes with an insulating gap of inert gas between them. The pressure tubes containing the fuel

bundles are each connected by feeder pipes to inlet and outlet horizontal headers located above the core. The headers are connected to the steam generators and to the emergency core cooling system. A simplified flow diagram for the heat transport system of the CANDU reactor is shown in figure 1-3. Accordingly, the hydrodynamics of the rewetting process is different from that of vertical systems because of the gravity forces which may cause flow stratification and hence different quenching behaviour around the tube.

A review of the literature on the rewetting of hot surfaces indicated that while an enormous amount of published information on the rewetting of hot vertical surfaces is available, data on rewetting of horizontal channels is limited and relatively recent. The objective of this study is to understand the basic physical processes taking place during the refilling and rewetting of hot horizontal tubes. More specifically, the research program was designed to achieve the following:

- i- Obtain detailed experimental data on the refilling and rewetting of hot horizontal tubes of different thicknesses.
- ii- Identify the flow patterns which could exist near the quench front during the refilling and rewetting process.
- iii- Identify the basic governing physical mechanisms of surface rewetting in horizontal tubes.
- iv- Develop a criterion for surface rewetting relevant to hot horizontal tubes.
- v- Incorporate the rewetting model into a general two-fluid model for predicting the refilling and rewetting of hot horizontal tubes.

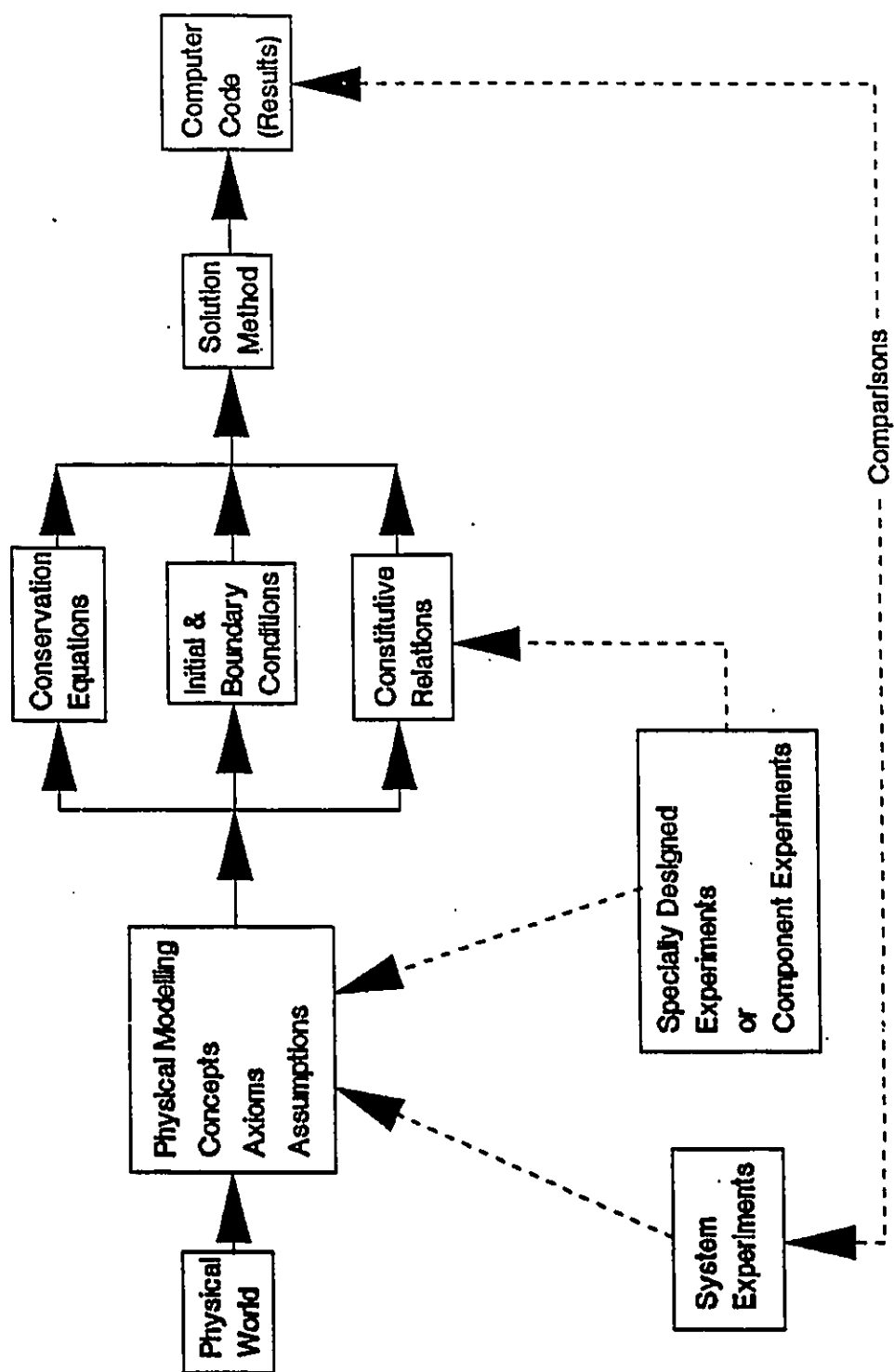


FIGURE 1-1 METHODOLOGY OF LOCA ANALYSIS

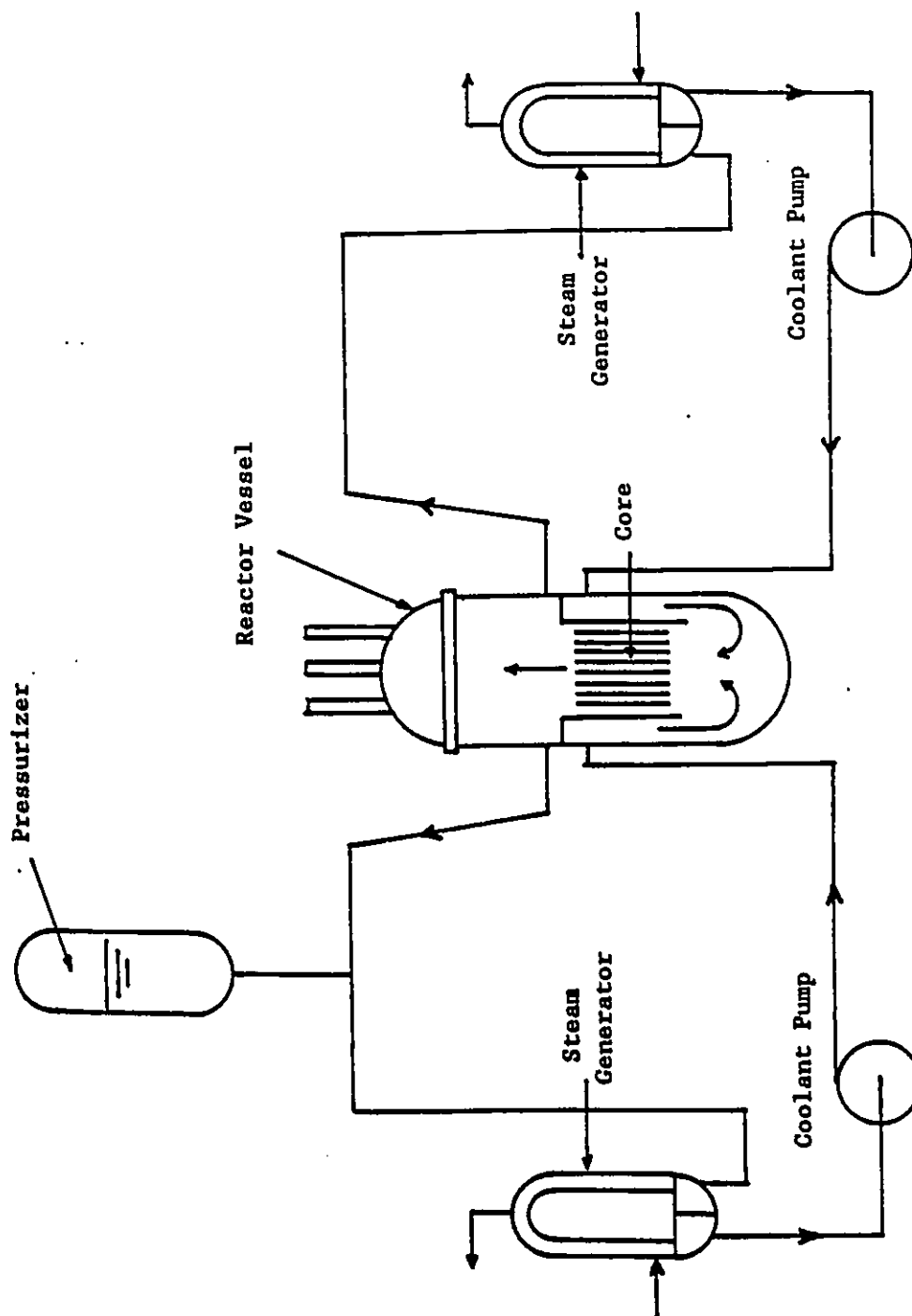


FIGURE 1-2 SCHEMATIC OF PWR PRIMARY COOLANT SYSTEM

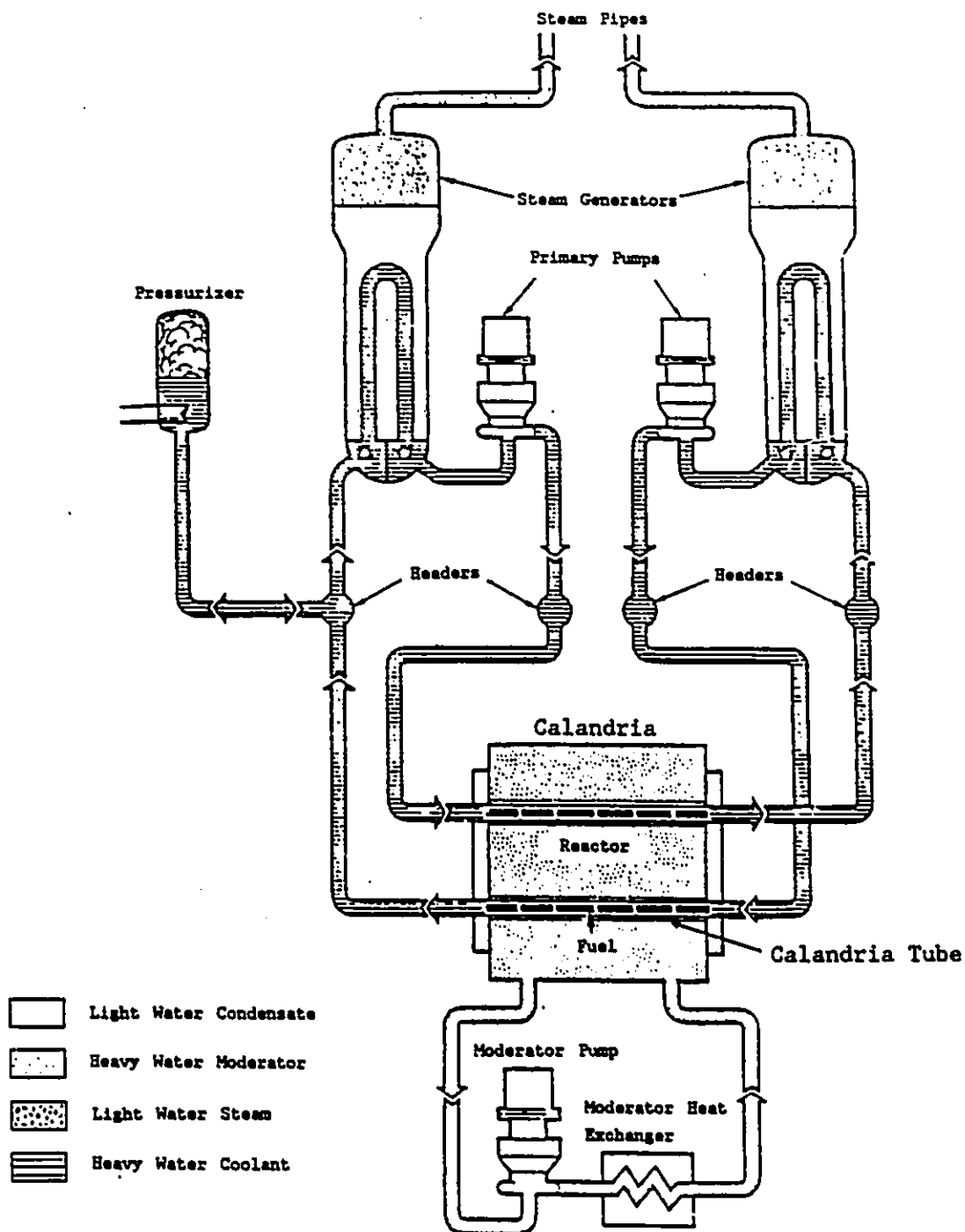


FIGURE 1-3 CANDU REACTOR SIMPLIFIED FLOW DIAGRAM

CHAPTER 2

LITERATURE REVIEW

Although considerable experimental and theoretical work has been done to investigate the rewetting of hot vertical surfaces, little has been done for horizontal systems. This chapter is a review of the literature on both vertical and horizontal systems.

2-1 REWETTING OF VERTICAL SURFACES;

The literature on rewetting vertical surfaces has been extensively reviewed by Yadigaroglu et al (1975), Sawan and Carbon (1975), Butterworth and Owen (1975), Elias and Yadigaroglu (1978), Chan (1980) and Raj (1984). However, a brief updated review is presented below.

2-1-1 EXPERIMENTAL WORK ON REWETTING OF VERTICAL SURFACES;

Experiments were performed both with single heated tubes or rods in annuli and with arrays of heated rods simulating fuel bundles. The purpose of the experiments conducted on single tubes or rods was to gain an understanding of the basic physical mechanisms involved in the rewetting phenomena. The bundle experiments were conducted mainly to check the effectiveness of the emergency core cooling systems in rewetting the core in case of a LOCA. To simulate the behaviour of the emergency core cooling systems in PWRs and BWRs, experiments on the

rewetting of vertical surfaces are carried out for either upward coolant flow (bottom flooding) or falling liquid film (top spray cooling). All of the transient quenching experiments were conducted in a similar manner. The rod or tube or cluster of rods were preheated to the desired initial temperature. Quenching was then initiated by injecting cooling water and the main parameter of interest was the rewetting velocity. The independent parameters investigated were normally the initial test section temperature, the coolant flow rate, the inlet subcooling, the system pressure and the wall thickness and physical properties of the test section.

In a few investigations the arrival of the rewetting front at any axial location was determined by visual observation and the rewetting velocity was estimated accordingly. However, the usual method of estimating the rewetting velocity was based on surface temperature measurements. The arrival of the rewetting front at any axial location is identified by a sharp drop in surface temperature marking the end of the low heat transfer mode of film boiling and the start of the efficient heat transfer modes of transition and nucleate boiling. The rewetting velocity was calculated based on the time required for the rewetting front to travel between two given axial locations.

Some of the previous experimental studies, conducted mainly with single vertical rods or tubes, are outlined below. The general conclusions that can be made from these studies are discussed in the following section.

One of the earliest works on rewetting of hot vertical rods by top spray cooling was reported by Shires et al (1964) where the

mechanism of falling film flow and heat transfer for vertical rods were investigated. Tests were run both with single heated rods (15.87 mm O.D.) and with a cluster of seven rods.

Experiments on rewetting of a vertical stainless steel tube (12.7 mm O.D., by 1.62 mm thick) in a steam environment at pressures ranging from 690 to 6900 kPa were reported by Bennett et al (1966).

Elliot and Rose (1970 and 1971) did a series of experiments to measure the quenching rate in a steam environment for a range of water flow rates and in pressure up to 5300 kPa. Zircaloy, stainless steel and inconel tubes were used.

Results of quenching experiments of a single rod and a tubular test section at atmospheric pressure were reported by Andreoni and Courtand (1972) and Andreoni et al (1974).

Martini and Premoli (1973) conducted bottom flooding experiments in tubular and annular test sections.

Piggott and Duffey (1975) presented the results of both top and bottom rewetting experiments. This included falling film rewetting experiments on two types of fuel pins and a range of tubes and heaters. Comparisons were made between falling film and bottom flooding experiments. The effects of surface finish, cladding material and filling material were also discussed.

Experimental work on single channel rewetting was reported by Groeneveld and Young (1978) and Lee et al (1978), where the parametric effects of mass flux, inlet subcooling, wall thickness and power input on rewetting heat transfer and quench velocity were investigated.

De Salve and Panella (1980) reported bottom flooding

experiments in tubes with different wall thicknesses and lengths.

An experimental investigation of the heat transfer characteristics during the rewetting of a vertical channel was reported by Zvonarev et al (1984). The cross section of the channel was designed to simulate the sub-channel formed between four tubes. The heat transfer modes accompanying the rewetting process were discussed.

Kawaji et al (1985) investigated the flow regimes and heat transfer characteristics in constant injection rate and forced oscillation reflooding of a vertical tube. The flow regimes identified above the quench front in constant injection, high reflooding rate tests were inverted annular, transition and dispersed flow. In constant injection, low reflooding rate tests, annular droplet flow and dispersed flow regimes existed below and above the quench front, respectively. In forced oscillation tests, the flow regime near the quench front alternated periodically between inverted annular and annular droplet flow during the upstroke and downstroke of an oscillation cycle respectively. Accordingly, the heat transfer rate was found to rise (or fall) whenever the local void fraction decreased (or increased).

2-1-2 CONCLUSIONS FROM THE EXPERIMENTAL WORK ON VERTICAL SURFACES:

- 1) During the reflooding of hot vertical systems, two different flow regimes can occur near the quench front as shown in figure 2-1. At very low reflooding rates, the liquid near the quench front is saturated and an annular flow regime exists. At higher reflooding rates, the liquid near the quench front is subcooled and a long

liquid or two-phase column is formed above the quench front, separated from the wall by a thin film of vapour. This flow regime is generally referred to as the inverted-annular flow pattern.

- ii) The rewetting velocity decreases as the initial wall temperature increases.
- iii) The rewetting velocity increases with flow rate.
- iv) Increasing the coolant subcooling increases the rewetting velocity.
- v) Surface roughness has been found to increase the rewetting velocity.
- vi) The rewetting velocity is decreased with increasing surface heat capacity. Similar effect has been found by increasing the wall thickness or introducing a filler material.
- vii) Internal heat generation (decay heat) within the hot surface decreases the rewetting velocity.
- viii) Higher rewetting rates are obtained with increasing system pressure for both top and bottom flooding.
- ix) Falling film experiments with low flow rate and subcooling resulted in almost constant rewetting velocity at different axial locations. However, bottom flooding with subcooled water showed that the local rewetting velocity decreases as the rewetting front propagates upward. This is attributed to the decrease in local subcooling.
- x) Precursory cooling downstream the quench front in bottom flooding was reported to be more significant than that in top spraying.

2-1-3 THEORETICAL WORK ON REWETTING OF VERTICAL SURFACES:

The theoretical models which have been developed for simulating the rewetting of vertical systems can be classified into the well known conduction controlled models and thermal-hydraulic models.

2-1-3-1 CONDUCTION CONTROLLED MODELS:

In conduction controlled models, it is assumed that the quench velocity is determined by the rate at which heat can be conducted from the dry hot side through the wall to the wetted side where it is removed by boiling. In these models all thermal and hydraulic processes associated with the quench process are frozen by assuming a constant quench velocity and using a moving coordinate system which moves with a speed equal to the quench velocity. The obtained quasi-steady heat conduction equation in one or two dimensional form is solved either analytically or numerically assuming that the wall temperature at the quench front equals the sputtering temperature.

The two-dimensional conduction equation in a wall is

$$\frac{\partial^2 T}{\partial y^2} + \frac{\partial^2 T}{\partial z^2} = \frac{1}{\alpha} \frac{\partial T}{\partial t} \quad (2.1)$$

where $\alpha = k/\rho c$ is the thermal diffusivity. Assuming constant quench front velocity U and that the temperature field in the wall is invariant in a coordinate system moving with the quench front, then

$$\frac{\partial T}{\partial t} = -U \frac{\partial T}{\partial z} \quad (2.2)$$

From equations (2.1) and (2.2) the quasi-steady heat conduction equation becomes

$$\frac{\partial^2 T}{\partial y^2} + \frac{\partial^2 T}{\partial z^2} + \frac{\rho c U}{k} \frac{\partial T}{\partial z} = 0 \quad (2.3)$$

A one-dimensional model is obtained by assuming uniform temperature in the transverse direction, i.e., $T = T(z)$ only. Physical modelling of the phenomena provides the necessary convective boundary conditions in the form of heat transfer coefficients along the wall being cooled by the advancing quench front.

The solution of the above problem is usually given in the form of a dimensionless temperature distribution, $\theta = (T - T_{SAT})/(T_q - T_{SAT})$, which is dependent on the Biot number, $Bi = h\delta/k$, the Peclet number, $Pe = U\delta\rho c/k$, and the dimensionless initial wall temperature, $\theta_w = (T_w - T_{SAT})/(T_q - T_{SAT})$. In the above equations δ is the wall thickness. T_{SAT} and T_q are the saturation temperature and quench temperature respectively.

One-Dimensional Models.

One dimensional solutions were first proposed by Semeria and Martinet (1965) and Yamanouchi (1968). The problem was divided into a wet region with a uniform heat transfer coefficient and a dry region with zero heat transfer coefficient. The wall temperature at the quench front is assumed to equal the sputtering temperature. Unreasonably high heat transfer coefficients had to be used to predict quench velocities comparable to the observed values.

Thompson (1972) solved the one dimensional heat conduction equation numerically using a temperature dependent heat transfer coefficient in the wet region. However unreasonable results, similar to

those obtained by Yamanouchi, were obtained.

Sun et al (1975) expanded the one dimensional model to include precursory cooling (the effect of cooling by the droplet-vapour mixture in the region immediately ahead of the quench front). This was accomplished by introducing an exponentially decaying heat transfer coefficient ahead of the quench front. The decay rate was related to the coolant mass flow rate. It was found that the falling film rewetting velocity can increase substantially with precursory cooling. As the precursory cooling decreases the solution approaches the two region model with zero heat transfer coefficient for the dry region presented by Yamanouchi.

Sun et al (1974) presented a three-region analytical model. The quench process was divided into a dry region ahead of the quench front, a sputtering region right behind the wet front, and a region of continuous liquid film further upstream. Constant heat transfer coefficients were used in the three different regions. The result reduces to the two region solution obtained by Yamanouchi in the limit when the sputtering region goes to zero. In this three region model, reasonable heat transfer coefficient for the sputtering region was obtained.

A multi-region, one-dimensional model was presented by Elias and Yadigaroglu (1976). Increasing the number of regions considered was to further improve the representation of the large variation of the heat transfer coefficients near the wet front. The wall was modelled as a thin plate with internal heat generation which receives a variable heat flux from one side while cooled from the other side. It was found

that the predicted temperature profiles in the vicinity of the quench front and the rewetting velocity vary according to the number of regions used in the model. However, asymptotic values were reached when the number of regions was greater than 5.

A list of one dimensional heat conduction models presented by Elias and Yadigaroglu (1978) are shown in table 2-1.

Two-Dimensional Models:

The one dimensional models were successful in correlating the experimental data for low flow rates and small Biot numbers. For high flow rates, extremely high values of the heat transfer coefficients in the wet region must be assumed in order to fit model predictions with experimental data. Accordingly, two-dimensional models were presented.

Duffey and Porthouse (1973) solved the two-dimensional slab case analytically for a two-region model. Constant wet side heat transfer coefficient was considered. A series solution was obtained by separation of variables. A first order solution was obtained by retaining only the first term in the series expansion. It was shown that for very small Biot numbers, the solution reduces to the one dimensional solution as expected.

Thompson (1972) solved the two dimensional problem numerically with a wet side heat transfer coefficient that was allowed to be temperature dependent. Thompson (1974) extended this two dimensional model to include the wall heat generation term. The effect of various parameters such as wall thickness, thermal conductivity, volumetric heat capacity and heat generation on the rewetting rate was studied.

The analysis revealed that the thermal perturbation due to the advancing interface requires a finite time to propagate through the wall and that there exists a critical wall thickness beyond which the rewetting rate is independent of wall thickness.

Other two-dimensional rewetting models with a step change in the heat transfer coefficient at the quench front (two-region models) were presented by Coney (1974) considering a slab geometry (i.e., for the cladding) and by Blair (1975) and Yeh (1975) considering a cylindrical geometry (i.e., for a solid rod). The common method of solution was the separation of variables obtaining a series expansion for each region. The coefficients of the two series were determined by matching the temperatures and their axial derivatives at the interface separating the two regions, i.e., at the quench front.

Yeh (1980) and Olek (1989) extended the above two-dimensional approach with two heat transfer regions to model a composite geometry of cylindrical fuel rod and cladding.

Another modification of the two-dimensional model considered three or more heat transfer regions. Sawan and Temraz (1981) proposed a two-dimensional, three-region model which included dry, wet and sputtering regions. The solution technique was similar to that in two-region models, i.e., by separation of variables and matching temperatures and their derivatives at the region boundaries. The results of this model were compared with the simpler analytical one and two dimensional models. It was concluded that the one dimensional solution is valid for high initial surface temperatures at all values of Biot number and for low initial surface temperatures at small values

of Biot number ($Bi \leq 1$). The two-dimensional, two region model was considered valid only for low initial surface temperatures with large Biot numbers.

Bonakdar and Mcassey (1981) proposed a multi region, two-dimensional model. However, results were presented for a three region example involving dry, wet and sputtering regions. The same solution method by separation of variables was followed. It was concluded that the sputtering region controls the rewetting process if its length exceeds one quarter of the cladding thickness, and that two dimensional effects exist upstream of the wet front for approximately two to three slab thicknesses. The results showed good agreement with experimental data only in the low to moderate coolant flow rate range.

Werner et al (1988) developed a finite element model for the rewetting problem. Instead of using a quasi-steady approach by assuming a constant rewetting velocity and adopting moving coordinates, this approach used the element activation technique for the transient heat conduction analysis of a moving convective boundary. Accordingly, this model was capable of incorporating a time varying rewetting velocity. However, a simple example of constant rewetting velocity and an advancing step function for the heat transfer coefficient (i.e., two-region model) was presented to provide initial validation of the model. The results compared well with the analytical model of Coney (1974).

Olek et al (1988) considered the rewetting of hot surfaces by falling liquid films as a conjugate heat transfer problem. The main motive of this approach was to remove the need of supplying the heat

transfer coefficient required by all of the conduction controlled models discussed above. The liquid film was assumed to move at a constant speed and to have a uniform thickness. Moreover, the temperature of the film-free surface was assumed constant and equal to the inlet liquid temperature. An iterative procedure was followed to calculate the rewetting velocity, with the requirement that the temperature be equal to an assumed rewetting temperature at the triple interface line within an acceptable error tolerance. The rewetting velocity predicted by this model showed good agreement with experimental results for low flow rates. However, this model underpredicts the quench front velocity for high flow rates. Moreover, it was found that, by increasing flow rate, the zone which characterizes the quench phenomenon becomes smaller and the heat transfer coefficient becomes higher.

A list of two-dimensional models as presented by Elias and Yadigaroglu (1978) is shown in table 2-2.

2-1-3-2 THERMAL-HYDRAULIC MODELS:

Many theoretical models have introduced the thermal-hydraulic aspects of the process so that the wall transient conduction may be coupled with the thermal hydraulic phenomena in the system. Such models were mostly developed to simulate bottom flooding tests. In these models the conservation equations of the two-phase flow are solved. Accordingly, heat transfer coefficients based on the local flow conditions are selected to provide the boundary conditions for the solution of the transient conduction equation. Some of these models are

discussed below.

A one-dimensional single channel thermal-hydraulic model of bottom reflooding was presented by Ghiaasiann et.al (1982). The model solved either radial or axial heat conduction formulation. The coolant side was assumed to consist of three regions, single phase liquid, churn-turbulent two-phase and single phase steam. In the single phase liquid region, the energy equation was solved by assuming constant flow velocity and density. This region was assumed to terminate above the elevation at which $T_w \geq (T_{SAT} + 100)^{\circ}C$. In the two-phase flow region, a quasi-steady treatment of the thermal hydraulic phenomena was used to predict the two phase region's thickness. This was done by assuming that the total pressure drop across this region is equal to the equivalent collapsed liquid water head above the quench front. Different heat transfer correlations for the different regions were used. The heat transfer coefficients in the film and transition boiling regions were calculated from existing correlations which were modified to account for the observed experimental trends. Surface rewetting was assumed when the film boiling heat transfer coefficient was higher than or equal to the transition boiling heat transfer coefficient. The solutions obtained assuming only either axial or radial conduction showed little difference in the overall behaviour. Moreover, reasonable agreement between model predictions of the transient quench front location and the experimental results was obtained.

Chun and Chung (1982) presented a thermal hydraulic model for LOCA in a PWR. The physical model consisted of a finite vertical fuel

rod whose initial surface temperature distribution was similar to a chopped cosine function. Flow characteristics were determined by solving the conservation equations of the two-phase flow, where six different flow regions were assumed and well-known heat transfer and flow transition correlations were used. The criterion for surface rewetting was defined in terms of Leidenfrost temperature, using a correlation developed by Henry (1974). The thermal behaviour of the cladding surface obtained from this model agreed well with experimental data at high flooding rates, while the deviations become relatively larger at lower flooding rates.

Kawaji and Banerjee (1987) and (1988) presented a two-fluid model of the inverted annular and dispersed droplet flows encountered in reflooding of a tubular flow channel. The model consists of mass, momentum and energy conservation equations derived from a generalized, one-dimensional, two-fluid model. The phasic pressure difference terms were included in the momentum equations of both phases. In the first paper (1987), linear stability analysis of the hydraulic equations was discussed. For inverted annular flow, the phasic pressure difference terms were shown to be important in achieving stability to short wavelength numerical instabilities, and allowed prediction of long wave length Kelvin-Helmholtz instabilities, which appear physically as interfacial waves. For dispersed flow, the system was predicted to be unstable if the Weber number, defined in terms of the mean droplet diameter and relative velocity, exceeded a critical value of 8. The second paper (1988), dealt with solving the two-fluid model equations using constitutive equations that were formulated separately for

individual transfer mechanisms. The tube wall temperature was obtained by solving a two-dimensional heat conduction equation with fine mesh nodalization in the quench front region where severe axial and radial temperature gradients exist. In regions far from the quench front, a lumped parameter technique was used and a one-dimensional heat conduction equation was solved. The wall temperatures were matched at the boundaries between the two regions. Instead of using a rewetting criterion or quench temperature correlation to mark the end of film boiling, the quench speeds extracted from the experimental data was used in the model. This was done to decouple the heat transfer and hydrodynamic aspects of reflooding from the rewetting problem and analyze them independently. For dispersed flow, a size distribution of droplets was considered and both single and multi-field equations of motion were solved to calculate the droplet transport. The numerical results showed that most of the important heat transfer and hydrodynamic aspects of the experimental results were predicted reasonably well, supporting the mechanisms considered. In particular, a wall-droplet interaction heat transfer mechanism was found to be effective in explaining the experimentally observed strong dependence of heat transfer rate on liquid volume fraction in the dispersed flow region.

De Salve and Panella (1987) presented a model which predicts the thermal-hydraulics during the reflooding of a tubular channel. Three main time-dependent control volumes were considered on the basis of the prevailing flow regimes: the single phase (liquid) region, and the two-phase regions (bubbly, churn, annular or inverted annular and

the dispersed flow regions). The continuity and energy equations for the coolant were coupled to a one-dimensional (axial) conduction equation for the wall. The model is capable of handling a transition from bubble-churn to annular flow for low mass flux and a transition from bubble to inverted annular flow for high mass flux. In calculating the void fraction, the usual correlations based on the drift flux model were used for the two-phase region between the point net vapour generation and the transition point to the stable film boiling, while correlations were derived for the inverted annular and the dispersed flow patterns. The quench temperature was calculated by a correlation based on a Leidenfrost temperature calculation proposed by Baumeister and Simon (1973). This correlation was modified to include the mass flux effect. The model predictions of the wall temperature histories at different elevations compared fairly well with experimental results except at the highest axial locations. Moreover, the experimental collapsed liquid level compared fairly well with that of the model prediction.

2-1-4 COMMENTS ON THE THEORETICAL WORK ON VERTICAL SYSTEMS;

The approach of the conduction controlled models has passed through different stages of development, starting with the simplest case of one-dimensional, two-region models and up to the two-dimensional multi-region models. All of these models are based on the assumptions of constant rewetting velocity and constant rewetting temperature. These assumptions could be justified in the case of rewetting by falling liquid film with low flow rate and low subcooling.

However, increasing the flow rate and subcooling could result in variations of the rewetting velocity and the rewetting temperature along the surface. These variations were more evident in bottom reflooding experiments. Accordingly, heat conduction models are not appropriate under these conditions of high flow rates and subcooling.

In the thermal hydraulic models, the transient conduction in the solid wall is coupled to the thermal hydraulic characteristics of the system. This incorporates various aspects of flow and heat transfer regimes involved in the process with the use of various flow and heat transfer transition criteria and correlations. The transition criterion which defines the conditions at which the surface rewets is the most important since it is accompanied by the most drastic change in heat transfer rates (film to transition and nucleate boiling) taking place during the process. This requires better understanding of the mechanics and conditions at which surface rewets. However, in almost all cases, very little attention has been paid to the analysis of the rewetting criterion. Instead, empirical correlations for the apparent quench temperature were typically used.

2-2 REWETTING OF HORIZONTAL CHANNELS.

The rewetting process in horizontal channels has been investigated to a lesser extent because except for CANDU reactors, all other designs involve a vertically oriented reactor core. The few reported investigations on refilling and rewetting of hot horizontal channels are discussed below.

Lee et al (1978), reported an experimental investigation on

rewetting circular tubes. The test facility allowed experiments to be carried out for different test section orientations between horizontal and vertical. The test sections were:

- 1- Stainless steel: 4 m long, 19.1 mm O.D. and 1.65 mm thick.
- 2- Stainless steel: 3.5 m long, 19.1 mm O.D. and 0.89 mm thick.
- 3- Inconel: 4 m long, 15.9 mm O.D. and 1.02 mm thick.

The parameters varied were:

- Coolant flow rates: 100 kg/m².s to 400 kg/m².s
- Initial wall temperature: 270 °C to 800 °C
- Inlet water temperature: 10 °C to 80 °C and
- Test section orientation: horizontal to vertical

The main observations were quite similar to those of vertical systems in that increasing initial wall temperature and wall thickness decreased the rewetting velocity, while increasing subcooling and mass flux increased the rewetting velocity. Moreover, for similar initial and inlet conditions rewetting times in horizontal tubes were found to be 20 to 30% greater than rewetting times in vertical tubes.

Salcudean and Bui (1980) and Salcudean et al (1981) modelled the process of rewetting in horizontal channels by adopting the same well-known conduction controlled models. In the first paper (1980), the three dimensional heat conduction equation was solved numerically. The model assumed an inclined rewetting front propagating at uniform velocity to account for the expected stratification during rewetting of

a horizontal tube. Two regions of heat transfer: a dry region, with precursory cooling taking place, and a rewetted region were considered. Accordingly, a step functional variation of the heat transfer coefficient was used. As expected, precursory cooling was found to have a significant effect on the rewetting velocity. Moreover, the circumferentially conducted heat was predicted to be one order of magnitude lower than that of the axially transmitted heat. In the second paper (1981), a two-dimensional (axial and circumferential) numerical solution for the wall heat conduction during the rewetting of hot horizontal channels was developed. The model assumed an inclined rewetting front propagating with uniform velocity. Three distinct heat transfer regions, dry region with no precursory cooling, dry region with precursory cooling and wet region were considered. As expected, it was found that increasing the heat transfer coefficient or the length of the precursory cooling region increased the rewetting velocity. A similar effect was obtained by increasing the assumed rewetting temperature.

Chan and Banerjee (1981) reported an experimental and theoretical work on the refilling and rewetting of hot horizontal tubes in a series of three papers. In the first paper, the experimental work was discussed. The experiments were carried out on a zircaloy tube 2 m long, 19.6 mm O.D., and 0.898 mm thick. Thirty thermocouples were spot-welded onto the outside surface at twelve locations equally spaced along the test section. The circumferential temperature variations were measured at five locations at which wall temperatures at the top, bottom, and mid-side were obtained. Other thermohydraulic parameters

measured during the transients included : inlet and exit fluid temperatures, pressure drop, inlet water volumetric flow rates, volume averaged void fractions at two locations using gamma densitometers, and total power input to the test section. The main parameters varied were the test section initial wall temperature (280-600 °C) and the inlet flow rate (35-110 ml/s). The experiments showed that the refilling and rewetting process in a horizontal channel could be visualized as sketched in figure 2-2. The results confirmed that the rewetting velocity decreases as the initial tube temperature increases or the inlet flow rate decreases. Moreover, it was found that the rewetting velocity and the rewetting temperature varied along the tube. In addition to that the rewetting temperature varied along the circumference with the highest values obtained at the top side of the tube. Accordingly, it was concluded that the conduction controlled models are not applicable ,in general, to the process of rewetting horizontal tubes.

The second paper of Chan and Banerjee (1981b) dealt with the development of a mathematical model to analyze the refilling and rewetting process in hot horizontal tubes. The model was derived from the generalized one-dimensional two-fluid model. Variation of the liquid pressure due to gravity was retained in the model. The resulting governing equations were the hydraulic equations for the liquid phase, which were coupled to the vapour phase through interfacial terms, and the thermal equations of the liquid phase and the channel wall. The hydraulic equations were solved by an explicit finite difference characteristics technique, while the thermal equations were solved by

explicit finite difference method. The model was used first to predict the refilling of a cold horizontal tube. Good agreement between the numerical results and experimental data was obtained.

The third paper of Chan and Banerjee (1981c) dealt with the application of the two-fluid model to the refilling and rewetting of hot horizontal tubes. A quench initiation model based on the occurrence of a Kelvin-Helmholtz instability at the vapour film-liquid interface was proposed. The initiation of instability was related to the collapsed height of the water level by a simple model. The water level necessary to initiate the interfacial instability and consequently initiate quenching, was called the critical water level. It was postulated that when the critical water level is reached surface quenching is initiated at the bottom of the tube. This is followed by an upward circumferential propagation of the quench front. A linear function relating the quench level and the water level imposing a simultaneous water and quench level arrival at the top side of the tube was assumed. The critical water level was adjusted numerically to predict the experimentally measured rewetting velocity. The predicted temperature transient curves at different axial locations along the tube agreed reasonably well with the experimental results. Moreover, numerical results were found to be relatively insensitive to the interfacial transfer models used.

Sollychin (1983) reported a flow visualization study on the refilling of an annular horizontal channel formed by two concentric tubes. The inner tube was heated and the outer tube was transparent. Based on flow visualization, it was concluded that hydrodynamics could

play an important role in the process of rewetting horizontal channels.

Raj (1984) reported experiments on rewetting horizontal rectangular and annular channels. The rectangular channel was 240 mm long with a cross section of 24 mm wide and height ranges between 5-20 mm. Only the bottom side was heated. In these experiments only the inlet flow rate and the temperature transients of the bottom side at five axial locations were measured. The annular channel was made of two concentric stainless-steel tubes. The outer tube was 26.6 mm I.D. and the inner tube had a 1.2 m long heated length. Inner tubes of 15 mm O.D. with 1.5 mm wall thickness, and 17.2 mm O.D. with 2.3 mm wall thickness were used. Measurements obtained during experiments were surface temperature transients at five different axial locations along the inner heated tube, inlet flow rate and pressure drop along the channel. The parameters investigated for the rectangular channel were water flow rate (0.1 to 0.5 kg/min) and initial surface temperature (200-500 °C) while for the annular channel, water flow rate up to 9.5 kg/min, initial surface temperature (200-600 °C) and heat generation rate up to 1160 W/m were examined. The experiments showed significant stratification and varying rewetting velocity along the channel. However, all the hydrodynamic aspects were neglected and the problem was represented by a two-region two-dimensional (r,z) conduction controlled model where even the circumferential variation due to stratification was neglected.

Ahluwalia et al (1985) reported experiments on the reflooding of a hot horizontal channel. The test section was a zircaloy tube, 3 m long, 25.4 mm I.D. with a 2.54 mm wall thickness. In addition to axial

and circumferential temperature measurements, radial temperature measurements were made during the transients. This was achieved by attaching sub-miniature thermocouples to the tube wall at different distances from the inner surface. Other parameters measured during the transients included i) inlet and outlet fluid temperature ii) inlet and outlet pressures iii) cross-sectional average void fraction at two axial locations iv) inlet volumetric flow rate, and v) momentum flux at the discharge. The parameters varied were initial tube temperature (290 to 590 °C), inlet flow rate (0.16 to 0.62 kg/s) and inlet water temperature (20 to 80 °C). It was noticed that the local rewetting velocity may vary along the tube. The results showed also that the rewetting velocity increases with mass flux and subcooling and decreases with increasing initial tube temperature. Moreover, the apparent quench temperature increased with increasing tube temperature and inlet water subcooling.

2-2-1 COMMENTS ON THE WORK ON HORIZONTAL CHANNELS.

- i) The general parametric effects of flow rate, subcooling, initial tube temperature and wall thickness on the rewetting velocity are similar to those found in rewetting of vertical surfaces.
- ii) The experimental investigations showed clearly that rewetting velocity as well as the rewetting temperature vary along the channel.
- iii) All the experimental investigations indicated that refilling and rewetting of hot horizontal channels is characterized by flow stratification due to gravity effects.

- iv) Significant circumferential variation in the temperature transients was observed. The rewetting temperature varied along the circumference with the highest values obtained at the top side of the channel.
- v) It is clear from the above findings that the hydrodynamic effects can not be ignored and a realistic thermal hydraulic model should be used to simulate the refilling and rewetting of hot horizontal channels. However, identification of the flow patterns accompanying the quench front at various initial and boundary conditions as well as a physically sound rewetting criterion are also needed.

TABLE 2-1
ONE-DIMENSIONAL HEAT-CONDUCTION MODELS
[taken from Elias and Yadigaroglu (1978)]

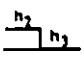


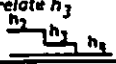

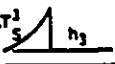



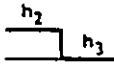
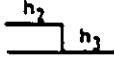
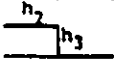

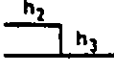
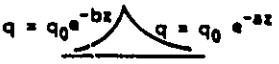

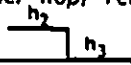

Reference	Experimental Data Correlated	Heat-Transfer Coefficient $W/(m^2)(^{\circ}C)$ $Btu/(hr)(ft^2)(^{\circ}F)$	Quench Temperature $^{\circ}C(^{\circ}F)$	Comments and Heat-Transfer Coefficient Profile
Yamanouchi Semeria and Martinet	Yamanouchi	$h_2 = 2 \times 10^3 - 10^6$ $4 \times 10^4 - 2 \times 10^3$ $h_3 = 0$	150(302)	
Sun et al	Yamanouchi Duffey and Porthouse	$h_2 = 1.7 \times 10^4$ (3000)	260(500)	Precursory Cooling Included 
Sun et al	Yamanouchi Duffey and Porthouse (only low-flow-rate data)	$h_1 = 570$ (100) ? $h_2 = 1.7 \times 10^4$ (3000) $h_3 = 0$	260(500)	Sputtering Region Between Location of Incipience of Boiling and Quench Front 
Chun and Chon	Cose et al	$h_2 = 2.56 \times 10^4$ (4500) $h_3 = 170$ (30) $h_4 = 0$	260(500)	Calculated Length of Dispersed Flow Region and Mass Carry-Over to Correlate h_3 
Ishii	Bennett et al	$h_1 = h_{CHF}$ $h_2 = 4 \times 10^3$ (7×10^4) $h_3 = 0$	260-390 (500-740)	1. Sputtering Region Between CHF and Quench Front 2. Correlated vs Pressure Range of 6.9-69 Bars abs (100-1000 psia) 3. Defined Thermal Penetration Length in Sputtering Region 
Thompson	Bennett et al	$h_1, h_2 \sim 7 \times 10^6$ (1.2×10^6) (Peak Values) $h_3 = 0$	$T_s + 100^{\circ}C$ ($T_s + 180^{\circ}F$)	High-Pressure Data 6.9-69 Bars abs (100-1000 psia) $h_2 = R\Delta T_s^{1/4}$ 
Elias and Yadigaroglu	Duffey and Porthouse (only low-flow-rate data)	$h_1 = 170$ (100) h_2, h_3, h_4, \dots = Boiling-Curve Approximation	260(500)	
Andreoni	Andreoni	h_1 , from Jens-Lottes Correlation h_2 , Extracted from rewetting Data h_3 , from Experimental Data	$T_s + 200^{\circ}C$ ($\sim T_s + 360^{\circ}F$)	
Yoo	No Experimental Data Correlated			Constant Internal Heat Generation Included: Assumes Parabolic Radial Temperatures Profile 

TABLE 2-2
TWO-DIMENSIONAL HEAT-CONDUCTION MODELS
[taken from Elias and Yadigaroglu (1978)]

Reference	Experimental Data Correlated	Heat-Transfer Coefficients, (W/(m ²)(°C) (Btu/(hr)(ft ²)(°F)	Quench Temperature °C(°F)	Comments and Heat-Transfer Coefficient Profile
Duffey and Porthouse	Yoshioka and Hasewaga Yamanouchi Duffey and Porthouse Andreoni Martini and Premoli Thompson Campanile and Pozzi	$h_2 = 10^4 - 2 \times 10^4$ (1700-3.5 × 10 ³) $h_3 = 0$	190-250 (375-480)	
Coney	Bennett et al	$h_2 = 0.94 - 1.3 \times 10^4$ (1.6-2.3 × 10 ³) $h_3 = 0$	$T_s + 68^\circ\text{C}$ ($T_s + 122^\circ\text{F}$)	Pressure Range 6.9-69 Bars abs (100-1000 psia) 
Blair	Thompson	$h_2 = 1.7 \times 10^4$ (3000) $h_3 = 0$	260(500)	Cylindrical Geometry 
Yen	No Experimental Data Correlated			Cylindrical Geometry 
Yoshioka and Hasewaga	Yoshioka and Hasewaga	$h_2 = \text{Function of Wall Temperature and Wet-Front Velocity}$ $h_3 = 0$		
Edwards and Mather		$h_{\max} = 2 - 4 \times 10^3$ (3.5-7 × 10 ³)		$q = q_0 e^{-bz}$ 
Thompson	Bennett et al	$h_1, h_2 = 4 - 8 \times 10^3$ (0.7-1.3 × 10 ³) (Peak Values) $h_3 = 0$	$T_s + 100^\circ\text{C}$ ($\sim T_s + 180^\circ\text{F}$)	Numerical Solution $h_2 = R \Delta T_s^3$ 
Tien and Yao	No Experimental Data Correlated			Wiener-Hopf Technique 
Dua and Tien	Duffey and Porthouse Yamanouchi	$h_2 = 1.7 \times 10^4$ (3000) $q_3 = q_0 / Ne^{-az}$	260 (500)	Wiener-Hopf Technique with Precursory-Cooling 

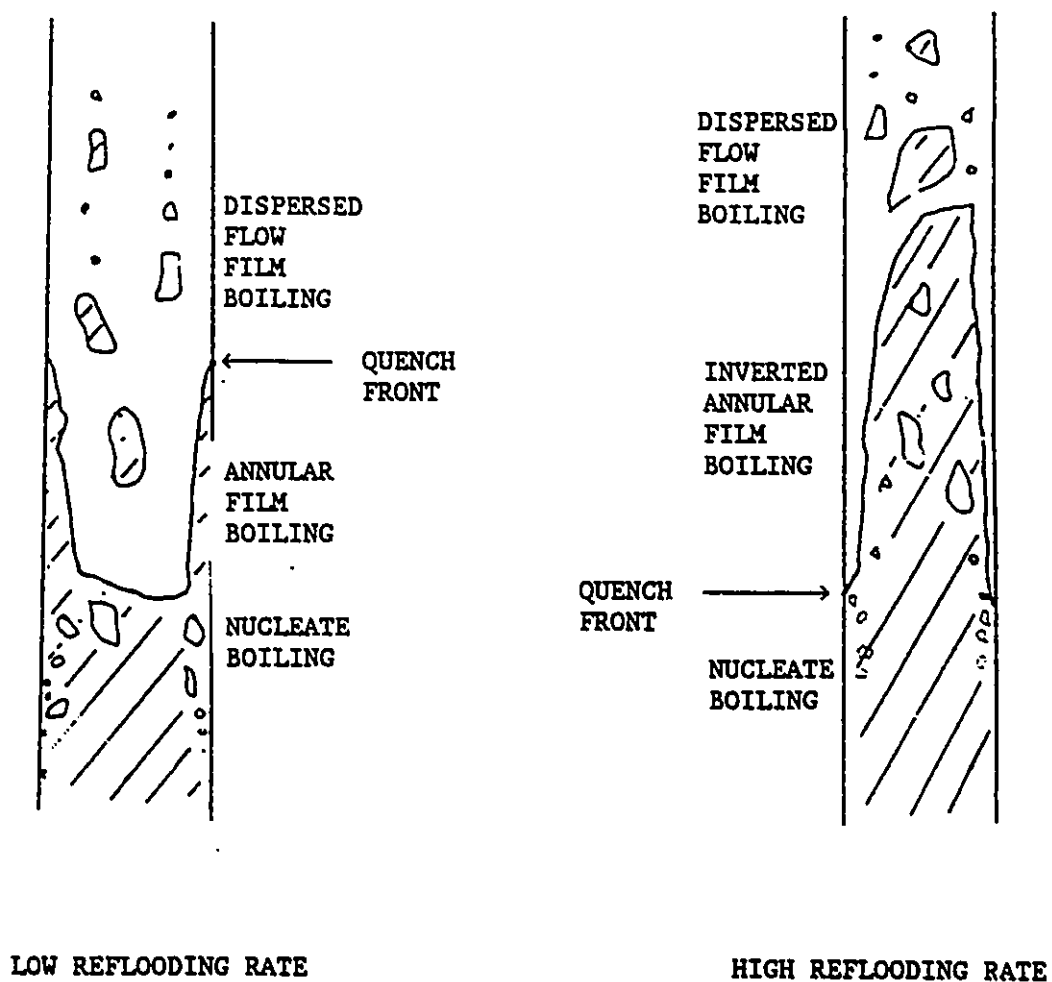


FIGURE 2-1 FLOW AND HEAT TRANSFER REGIMES OBSERVED DURING
REFLOODING OF VERTICAL SYSTEMS.

[Groeneveld and Young (1978)]

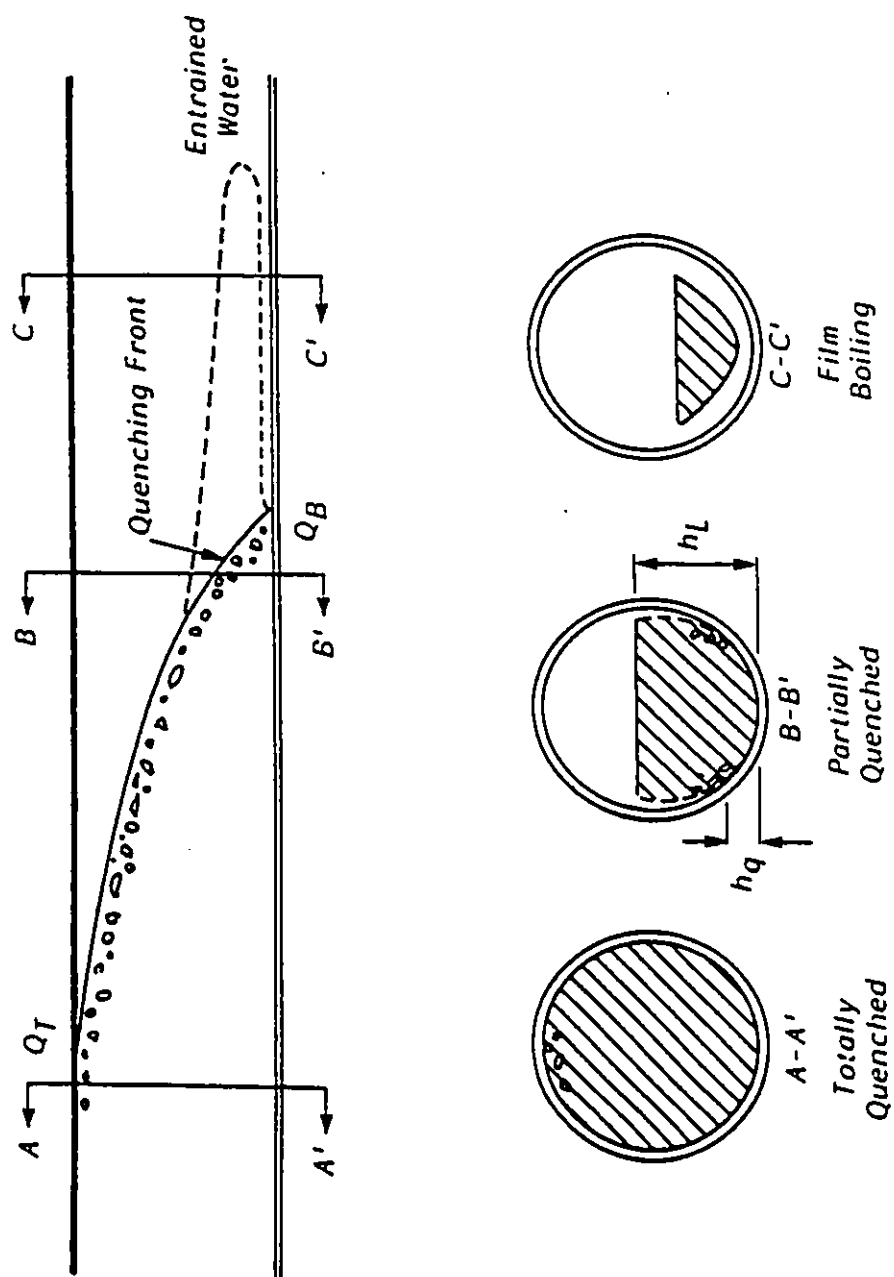


FIGURE 2-2 CHARACTERISTIC OF HORIZONTAL CHANNEL REWETTING

[Chan and Banerjee (1981)]

CHAPTER 3

EXPERIMENTAL FACILITY, INSTRUMENTATION AND MEASUREMENTS

3-1 TEST FACILITY.

The test facility used in conducting the experiments on the rewetting and refilling of hot horizontal tubes is shown schematically in figure 3-1 and photographically in figures 3-2 to 3-5. The facility was designed to heat the test tube to a prescribed temperature and then inject controlled inlet flow of coolant water having a prescribed inlet temperature and nominal flow rate to refill the tube. The test section was direct resistance heated. Two 3 m long zircaloy tubes of 25.4 mm I.D. with different thicknesses were tested. The wall thicknesses tested were 1 mm and 2 mm.

The head tank was a 3 m high, 1000 L galvanized water tank supplied from the mains. The head tank pressure was regulated up to 1.5 atmospheres by using a Bristol Instruments pneumatic controller. The outlet from the head tank was connected to two in-line 270 l electric water heaters to heat the coolant water to temperatures up to 80 °C.

The outlet from the hot water tanks was connected to a turbine flow meter, a pneumatically actuated quick closing ball valve and the test section. The test section was supported at three axial locations to avoid lateral deformation due to the difference in quenching time of the bottom and top sides of the tube. No restrictions to axial

expansion or contraction are made. Downstream of the test section is a 1 meter long lexan tube (for viewing purposes) which directs the flow into a galvanized discharge tank open to the atmosphere.

A by-pass line is branched off the main line downstream of the turbine flow meter into the discharge tank. This line also has a pneumatically actuated quick closing valve. The two pneumatic valves are connected such that when one is opened the other is simultaneously closed. This is to adjust the flow to the required condition in the by-pass line first, then inject it into the test section to achieve a developed flow at the initiation of the test runs. An 8 kVA variable transformer was interconnected with the primary side of a 220 V input step-down transformer. The secondary side of the step-down transformer was supplied with a 15 V terminal tap which was then connected to the zircaloy tube in order to heat it to the desired temperature.

3-2 INSTRUMENTATION AND MEASUREMENTS:

The parameters measured during the transients were

- i) Test Section Temperatures.
- ii) Inlet and Exit Fluid Temperatures.
- iii) Inlet and Exit Pressures.
- iv) Inlet Volumetric Flow Rates.
- v) Void Fractions at a given axial location.

3-2-1 TEMPERATURE MEASUREMENTS:

The wall temperatures along the thin tube (1 mm thickness) were measured by thermocouple wires spot welded on the outside surface of

the tube at five axial locations as shown in figure 3-6a. The first, second, fourth and fifth axial locations were instrumented at the bottom, mid-side and top of the tube. The third axial location was instrumented with thermocouples at seven circumferential positions. They covered half the circumference from the bottom to the top of the tube. They were separated by 30° angles. All thermocouple locations are shown in figures 3-6a and 3-6b. Subminiature thermocouples were used to obtain fast response to temperature changes. They were 0.5 mm stainless steel sheathed type K thermocouples (Chromel-Alumel) with 0.089 mm exposed wires. The response time given by the supplier (Omega Engineering Inc.) was less than 30 ms when the junctions were alternatively exposed to still water at 93°C and 37°C respectively.

For the thick tube (2 mm thickness), temperatures at different radial locations were measured as well by spot welding 0.075 mm type K bare thermocouple wires onto the bottom of 0.875 mm diameter holes drilled to different depths from the outside surface of the tube. The deepest holes were 0.127 mm away from the inner surface. Temperature measurements were made at the same axial locations used for the thin tube. All thermocouple locations for the thick tube are shown in figure 3-7. To avoid a secondary contact between the bare thermocouple wires inside the hole, they were separated by insulating adhesive cement. The terminals of the bare wires were spot welded to a 0.5 mm stainless steel sheathed thermocouple extension wires of the same type (K). An error analysis for a similar thermocouple assembly was conducted by Elphick et al (1985), where the normalized temperature measurement error was found to be less than 0.06. The temperature measurement

errors were normalized with respect to temperature difference between inner and outer surfaces. The response time for these thermocouples is expected to be faster than those used with the thin tube since they have a smaller diameter. For the outer surface temperature measurements, 0.5 mm stainless steel sheathed thermocouple wires (similar to those used for the thin tube) were used by direct spot welding. A picture showing some of these thermocouples is given in figure 3-5.

Other temperatures measured were the fluid temperature upstream and downstream of the tube. For this purpose 1.25 mm diameter, type K thermocouples were used.

3-2-2 PRESSURE MEASUREMENTS:

The transient pressure during the rewetting process was measured by two Shaevitz type P720 pressure transducers. They were located just upstream and downstream of the test section. The transducer signals were conditioned and amplified to give an analog voltage output in the range of ± 5 volts. The voltage output was calibrated against known pressure supplied by standard weights using a hydraulic bench.

3-2-3 FLOW MEASUREMENTS:

The inlet volumetric flow rate was measured using a Flow Technology standard line turbine type flow meter. Its operating range is 7 l/min to 115 l/min. The signal from a turbine flow meter is a voltage pulse with a frequency proportional to the flow rate. Since

analog voltage is required by the data acquisition system, a frequency to voltage converter was used to give an output voltage up to 5 Volts. The flow meter was calibrated by measuring the time required for collecting a given volume of water at the exit of the channel.

3-2-4 VOID FRACTION MEASUREMENTS.

A single-beam gamma densitometer operating in the count mode was used for transient void fraction measurements at the third axial measuring station along the test section as shown in figure 3.6a.

The basic principle of the gamma ray attenuation technique is that the intensity of a collimated gamma beam decreases exponentially as it passes through matter. The attenuated flux of a collimated beam is related to the incident flux by

$$N = N_0 e^{-\mu x} \quad (3.1)$$

where N is the emerging flux, N_0 is the incident flux, μ is the material absorption coefficient and x is the beam path length through the absorber.

Consider a test section of width L and wall thickness t with an absorption coefficient of μ_w . If the test section is completely filled with vapour ($\alpha = 1$) or liquid ($\alpha = 0$) equation 3.1 may be written

$$N_{(\alpha=1)} = N_0 e^{-2\mu_w t} e^{-\mu_g L} \quad (3.2)$$

or

$$N_{(\alpha=0)} = N_0 e^{-2\mu_w t} e^{-\mu_l L} \quad (3.3)$$

respectively, where μ_g and μ_l are the gas and liquid absorption coefficients. If the test section is filled with a mixture of the two

phases where the total volume occupied by gas divided by the test section volume is denoted as α (the void fraction) equation 3.1 becomes

$$N_{\alpha} = N_0 e^{-2\mu_w t} e^{-\alpha\mu_g L} e^{-(1-\alpha)\mu_1 L} \quad (3.4)$$

From equations 3.2 and 3.3

$$\frac{N_{(\alpha=0)}}{N_{(\alpha=1)}} = e^{(\mu_g - \mu_1)L} \quad (3.5)$$

and from equations 3.2 and 3.4

$$\frac{N_{\alpha}}{N_{(\alpha=1)}} = e^{(\mu_g - \mu_1)(1-\alpha)L} \quad (3.6)$$

Equations 3.5 and 3.6 can be used to obtain the void fraction as

$$\alpha = \frac{\ln(N_{\alpha}/N_{\alpha=0})}{\ln(N_{\alpha=1}/N_{\alpha=0})} \quad (3.7)$$

However, the exponents in equations 3.5 and 3.6 are small and these equations may be approximated by the first two terms of an exponential series expansion, i.e.,

$$\frac{N_{(\alpha=0)}}{N_{(\alpha=1)}} = 1 + (\mu_g - \mu_1)L \quad (3.8)$$

and

$$\frac{N_{\alpha}}{N_{(\alpha=1)}} = 1 + (\mu_g - \mu_1)(1-\alpha)L \quad (3.9)$$

Combining equations 3.8 and 3.9 yields the linear interpolation equation

$$\alpha = \frac{N_{\alpha} - N_{(\alpha=0)}}{N_{(\alpha=1)} - N_{(\alpha=0)}} \quad (3.10)$$

In designing the gamma densitometer, the procedure described by

Chan and Banerjee (1981) was followed. A 60 mCi cobalt 57 line source was used. The gamma beam was collimated to form a thin rectangular beam (50.8 mm x 12.7 mm) covering the entire cross section. A NaI(Tl) scintillator was used for gamma detection. The densitometer was mounted vertically for better void fraction measurement in the stratified flow regime. A schematic diagram of the gamma densitometer and the signal processing circuit are given in figure 3-8.

Measurement errors associated with a single-beam gamma densitometer can be estimated based on i) geometric and flow regime related errors, and ii) statistical error (Chan and Banerjee (1981)). The first type depends on the test tube geometry, flow conditions and densitometer design (e.g., beam profile). The statistical error is given approximately by Chan and Banerjee (1981) as

$$\epsilon_{\alpha} = 1 / (S \sqrt{N_{\alpha}}) \quad (3.11)$$

where S is the sensitivity of the gamma beam to the water content in the test section defined as

$$S = (N_{\alpha=1} - N_{\alpha=0}) / \bar{N} \quad (3.12)$$

where \bar{N} is the average value, $\bar{N} = (N_{\alpha=1} + N_{\alpha=0})/2$.

A fairly narrow window was used in the single-channel analyzer to count only those photons within a narrow energy band, i.e., almost monoenergetic photons were counted. Accordingly, the low energy level noise was eliminated. Also, in order to increase the densitometer sensitivity to the water content low energy gammas were used. Accordingly, a Co-57 source with principal photon energy of 122 KeV was used instead of the usual Cesium 137 which has a principal photon

energy of 662 KeV.

The gamma densitometer was calibrated both statically and dynamically prior to its use in the present work. Lucite pieces were machined to simulate the liquid phase for different flow regimes; namely stratified, annular and inverted annular flow. Lucite was used because its gamma ray absorption coefficient is very close to that of water. The static calibration was done using tubes similar to those used in the present experiments in which the machined lucite pieces were inserted. The dynamic calibration was carried out in a specially designed test section in which the void fraction was allowed to fluctuate. The error was within 10%. The calibration results were reported by Yuzda and Pham (1986).

For the present set up, the water sensitivity S ranged between 0.27 and 0.3. With an integration time of 0.1 second, the statistical error ϵ_a was estimated in the range of 0.4% to 2%.

The gamma densitometer was located at the third axial station of the tube (1.65 m from inlet) where the detailed circumferential temperature distribution is obtained.

The measured void fraction is actually a volume averaged void fraction. However, because of the narrow beam used in this work, the term "area averaged" will be used in this thesis.

3-3 DATA ACQUISITION SYSTEM:

A Digital Equipment Corporation MINC PDP11/23 computer was used for data acquisition. It consists of the PDP11/23 central processor (32K words of core memory and 128K words of virtual memory), two hard

disc drives, CRT, line printer and a plotter. The RT-11 operating system used allows for interactive programming on industry standard high-level and assembly languages. There were two analog to digital (A/D) converters: a DEC ADV-11 and a Data Translation DT 1764.

The MINC ADV-11 A/D converter module has twelve high-level (-5 V to +5 V) channels. Two MINC thermocouple preamplifier modules were connected to and multiplexed by the ADV-11. These provided sixteen low level input channels suitable for thermocouples.

The DT 1764 A/D converter is a wide range unit which was hardware configured for -25 mV to +25 mV input range. It can handle 32 double-ended inputs, suitable for thermocouples.

The outputs from the pressure transducers, turbine flow meter and gamma densitometer were connected to the data acquisition system through the high level channels. The low level channels were used for the temperature measurements.

The system was capable of scanning 48 channels at a rate of forty scans per second (25 ms per scan).

3-4 EXPERIMENTAL PROCEDURE:

A. consistent operating procedure was followed throughout the experiments. The experimental procedure is summarized in the steps;

- 1- Set the computer for data acquisition.
- 2- Check the water subcooling.
- 3- Check the pressure transducers, adjust the zero offset if necessary.
- 4- Check the output of the thermocouples to be sure they are working properly.

- 5- Check that the electronics of the gamma densitometer are properly set.
- 6- Turn on the water supply and adjust the flow rate to the desired value. Obtain the full tube ($\alpha=0$) calibration condition for the gamma densitometer.
- 7- Actuate the pneumatic valves so that the water now flows through the bypass line.
- 8- Blow remaining water droplets by compressed air.
- 9- Switch on the transformer and raise the power slowly with intermittent air blowing, if necessary, until the dry condition for all tube stations is ensured by monitoring all thermocouple readings.
- 10- Obtain the empty tube ($\alpha=1$) calibration condition for the gamma densitometer.
- 11- Continue raising the power slowly until a steady desired tube temperature is achieved with reasonably uniform axial and circumferential readings.
- 12- Set the scanning program, switch off transformer, actuate the pneumatic valve so that water flows through the zircaloy tube and start scanning simultaneously.

3-5 TEST MATRIX:

The conditions tested during the experiments were in the ranges:

- | | |
|----------------------------|-------------------------------------|
| - Inlet mass flux | 420 - 1300 $\text{kg/m}^2.\text{s}$ |
| - Inlet water temperature | 20 - 80 $^{\circ}\text{C}$ |
| - Initial tube temperature | 290 - 590 $^{\circ}\text{C}$ |

The thin zircaloy tube (1 mm thickness) was tested by conducting two groups of test runs. The first group consisted of 54 test runs conducted at six inlet flow rates, three initial tube temperatures and three inlet water temperatures. The complete test matrix including the dates when the experiments were conducted is shown in tables A-1 to A-3 of Appendix A.

The second group of tests were conducted for four selected initial and boundary conditions, to test the reproducibility of the results. A total of 20 test runs (five repeated runs for each case of initial and boundary conditions) were conducted. These are shown in table A-4 of Appendix A.

The thick zircaloy tube (2 mm) was tested by conducting 45 test runs. Five inlet flow rates, three initial tube temperatures and three inlet water temperatures were considered. The test matrix of the thick tube (2 mm) is given in tables A-5 to A-7 of Appendix A.

Moreover, data obtained from experiments conducted on a similar test section with a different tube wall thickness (2.54 mm) was available (Ahluwalia et al (1984)) and is analyzed together with the present data.

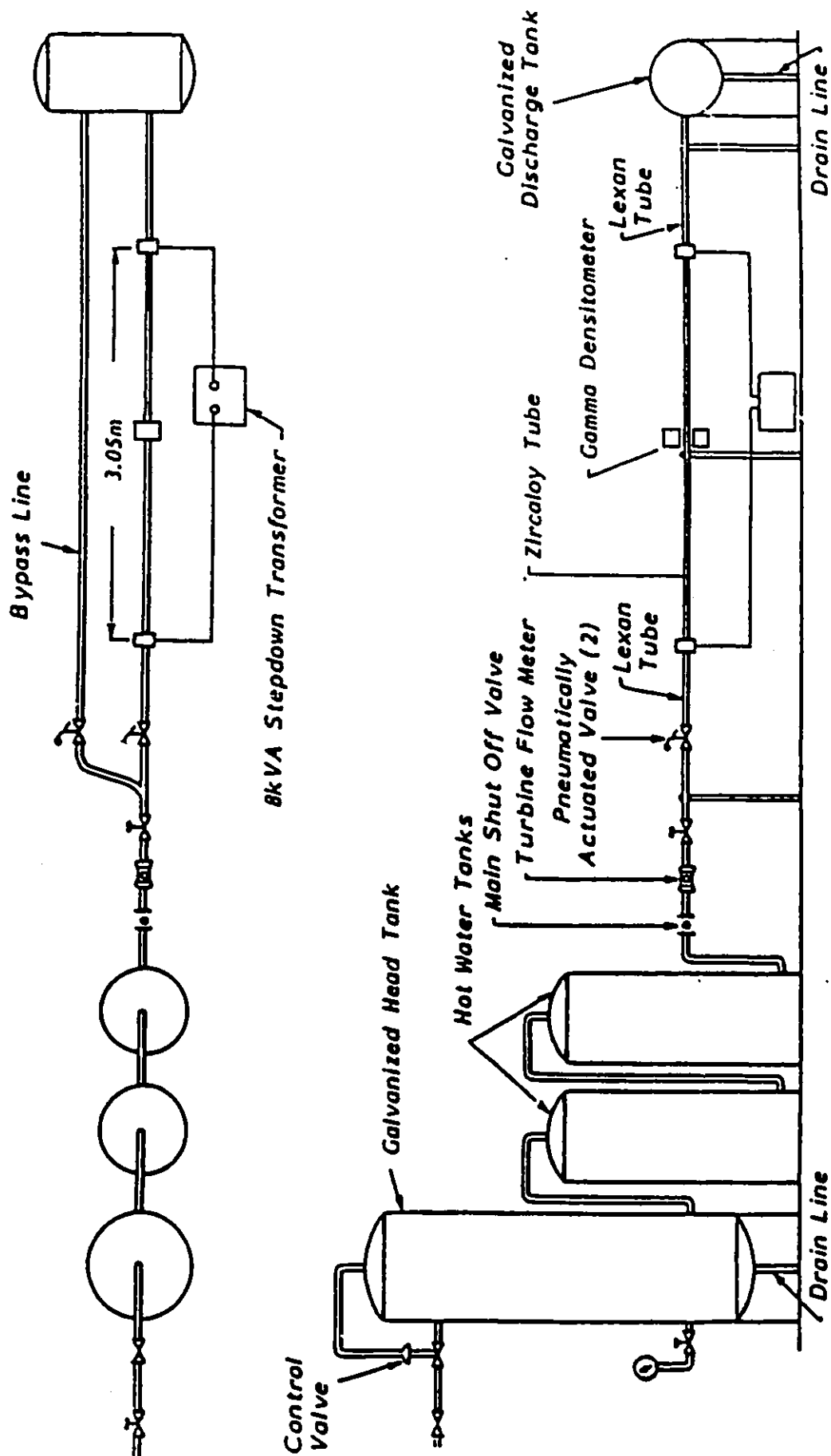
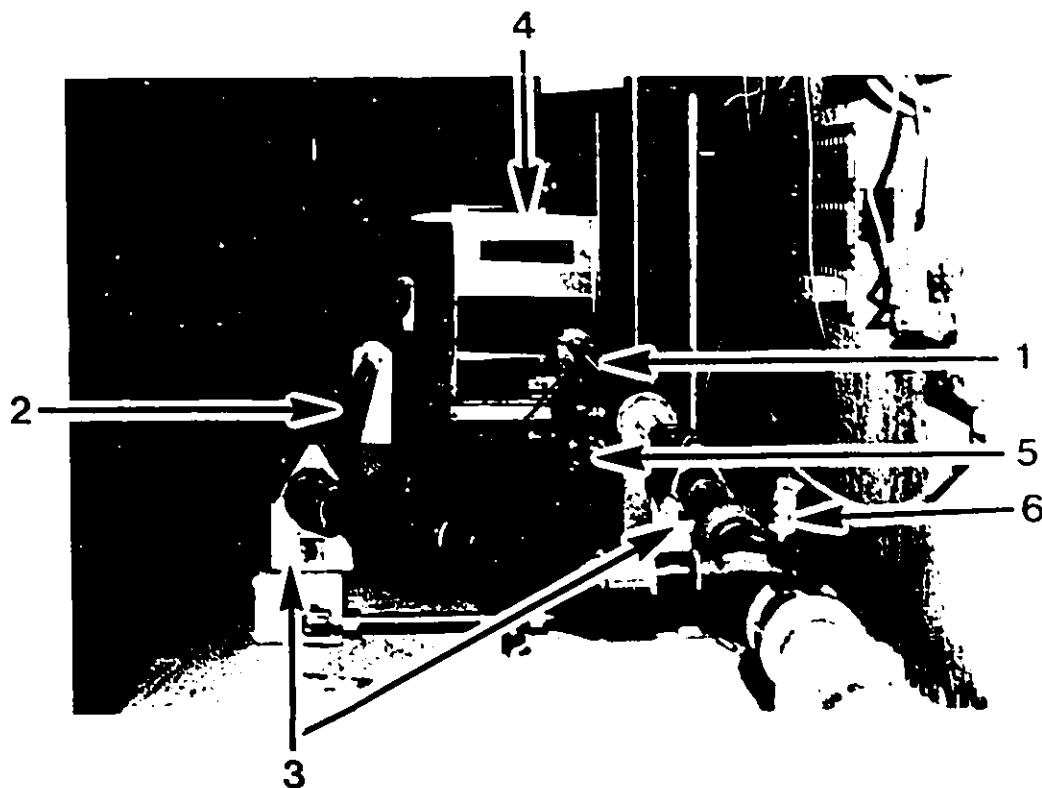


FIGURE 3-1 : SCHEMATIC OF EXPERIMENTAL FACILITY.



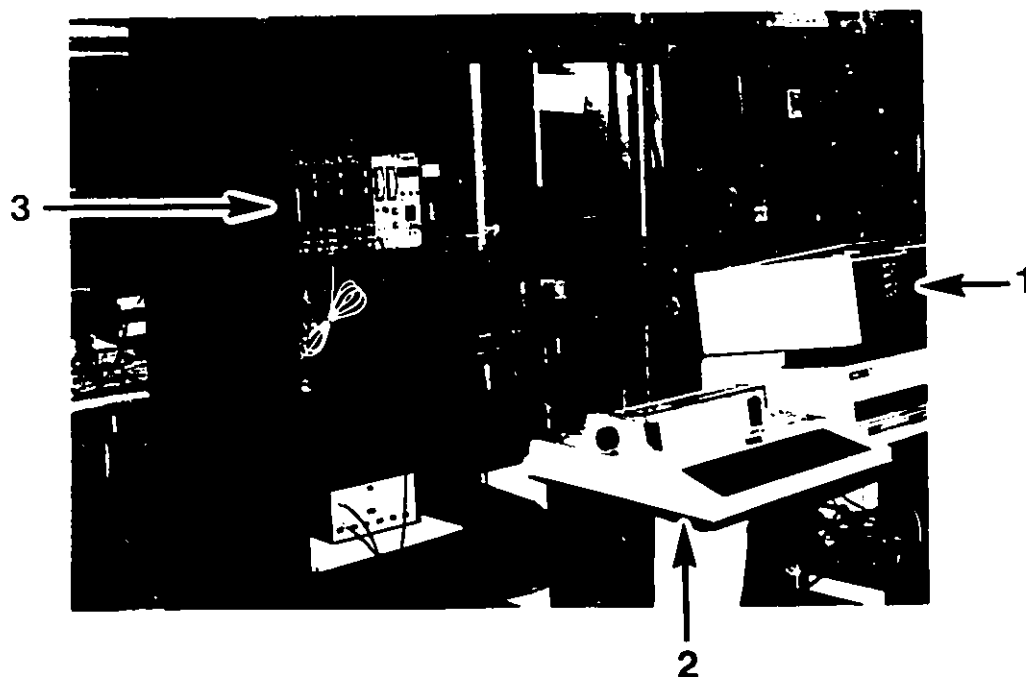
- 1- Test Section
- 2- Bypass Line
- 3- Gamma Densitometer

FIGURE 3-2 : VIEW OF EXPERIMENTAL FACILITY.



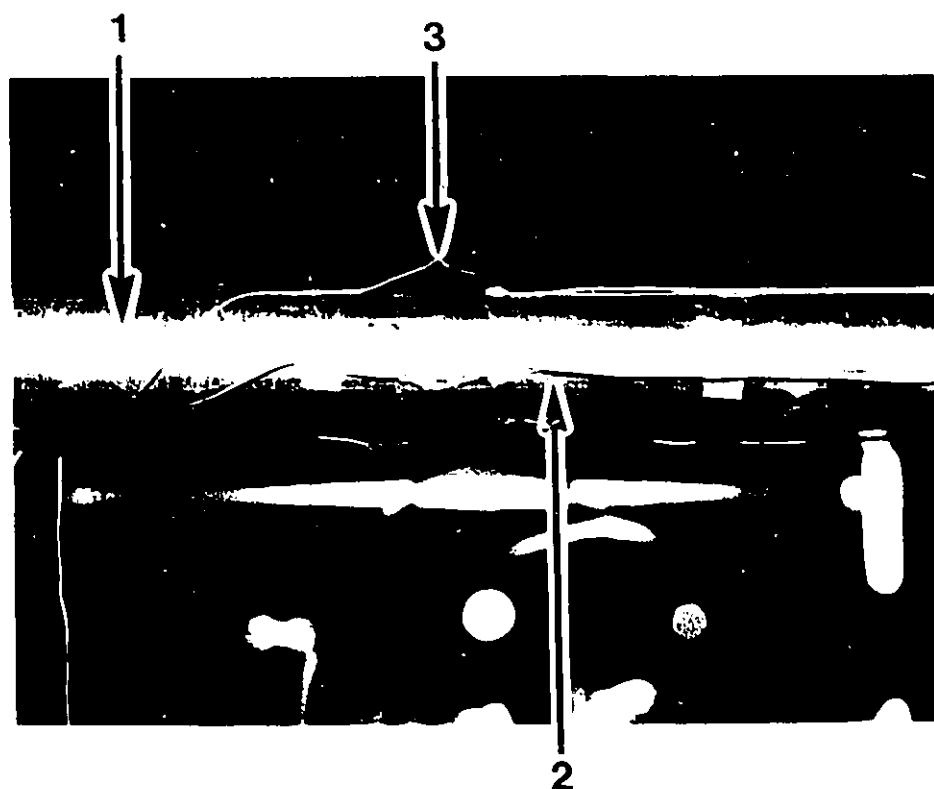
- 1- Test Section
- 2- Bypass Line
- 3- Pneumatic Valves
- 4- Gamma Densitometer
- 5- Pressure Transducer
- 6- Flow Meter

FIGURE 3-3 : VIEW OF EXPERIMENTAL FACILITY.



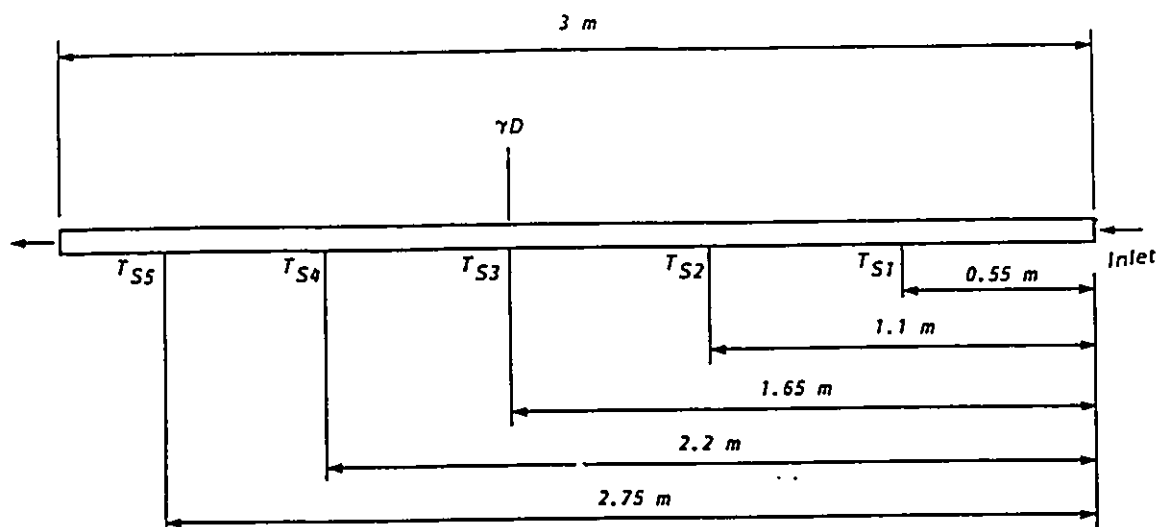
- 1- Computer
- 2- Printer
- 3- Gamma Densitometer Signal Processing Instruments

FIGURE 3-4 : VIEW OF EXPERIMENTAL FACILITY.



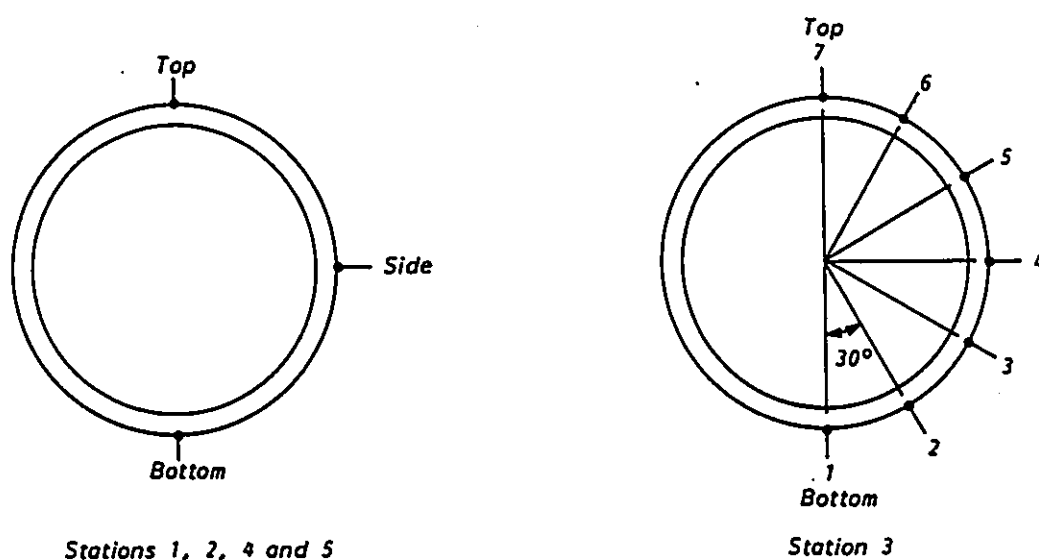
- 1- Test Section
- 2- Thermocouple Spot Welded on the Outside Surface
- 3- Thermocouple for an Inner Radial Location.

FIGURE 3-5 : VIEW OF EXPERIMENTAL FACILITY.



γD = Gamma Densitometer Station
 T_S = Thermocouple Station

**FIGURE 3-6a : THERMOCOUPLE AND GAMMA DENSITOMETER STATIONS
 ALONG THE TEST SECTION.**



**FIGURE 3-6b : CIRCUMFERENTIAL THERMOCOUPLE LOCATIONS FOR
 THE THIN TUBE.**

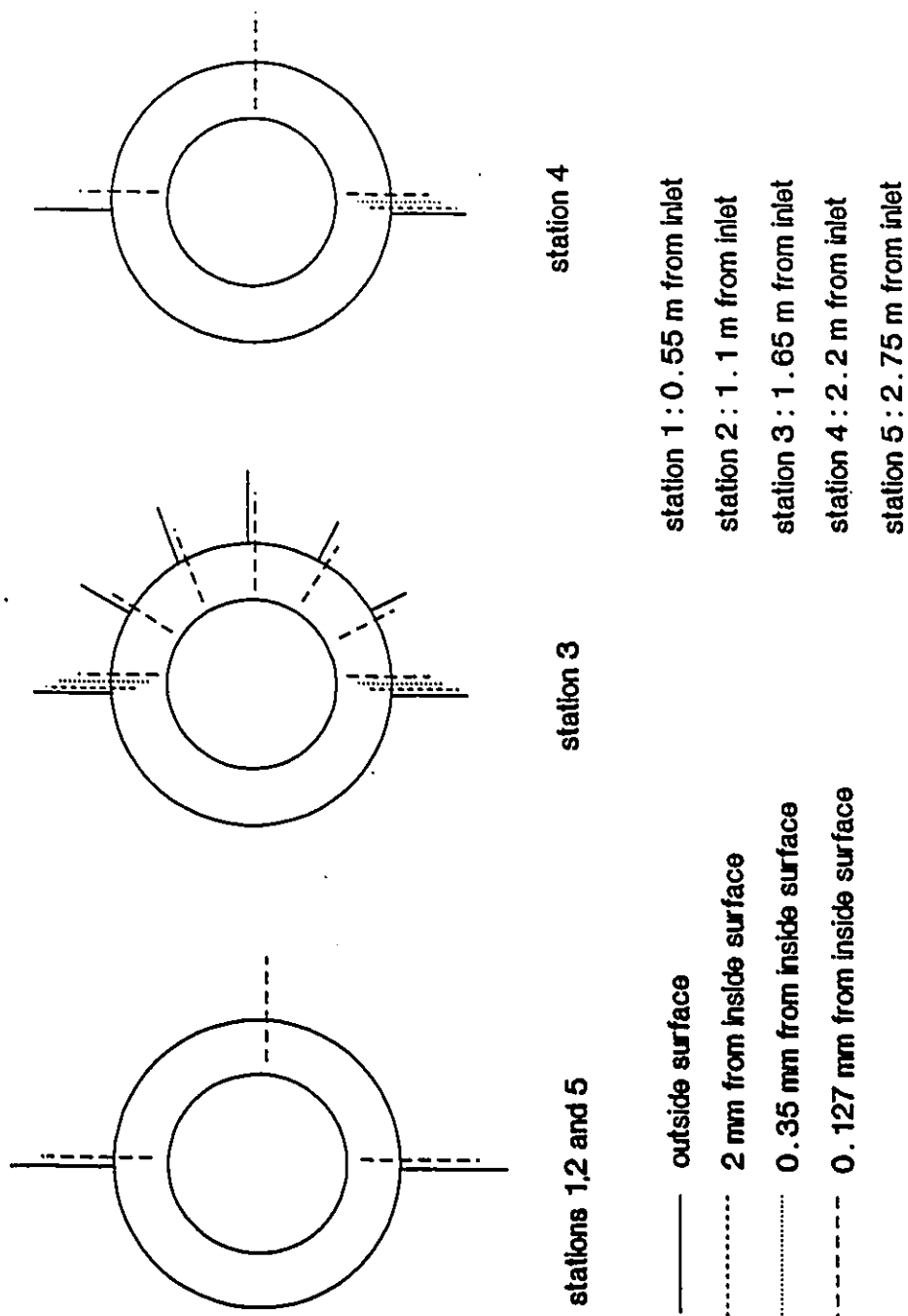
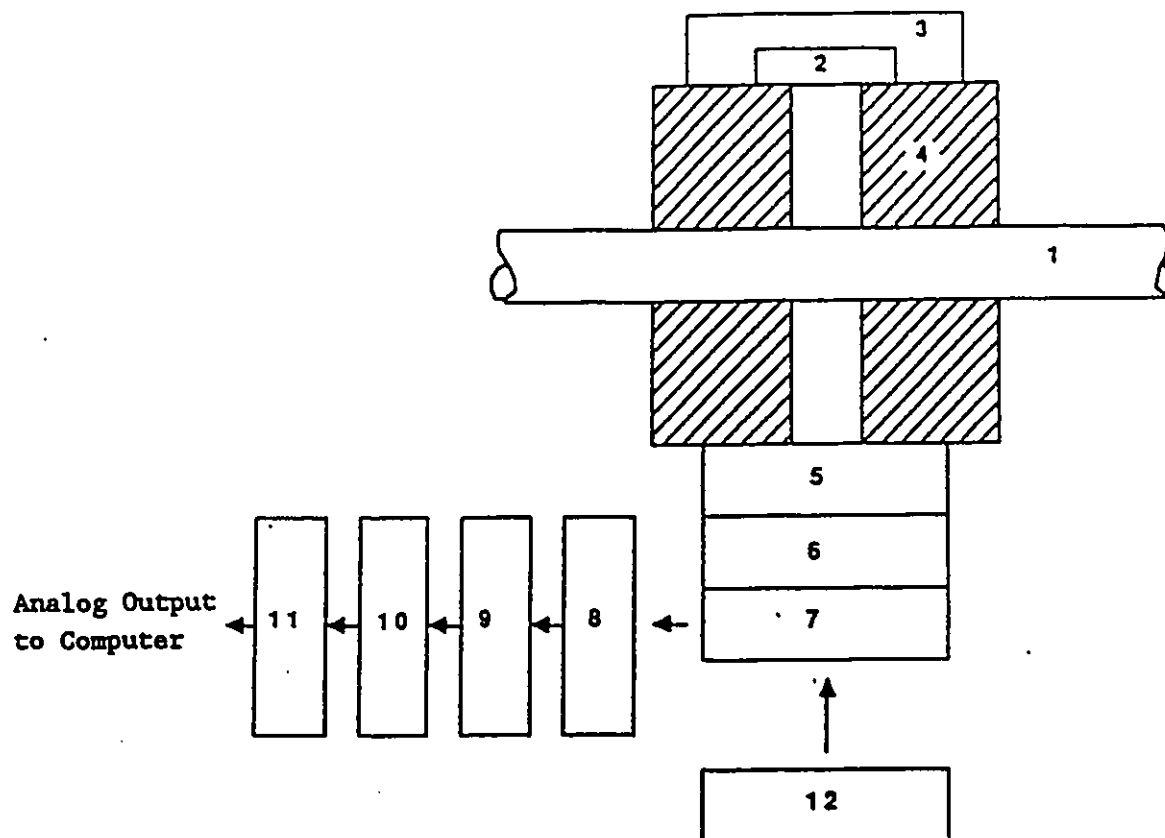


FIGURE 3-7 : THERMOCOUPLE LOCATIONS FOR THE THICK TUBE.



- | | |
|------------------------|------------------------------------|
| 1- Test Section | 7- Voltage Divider |
| 2- Sealed Source | 8- Pre-Amplifier |
| 3- Shielding Container | 9- Amplifier - Discriminator |
| 4- Collimator | 10- Pre-Scaler |
| 5- Scintillator | 11- Frequency to Voltage Converter |
| 6- Photo Multiplier | 12- High Voltage Source |

**FIGURE 3-8 : SCHEMATIC DIAGRAM OF THE GAMMA DENSITOMETER
AND SIGNAL PROCESSING CIRCUIT.**

CHAPTER 4

EXPERIMENTAL RESULTS

In this chapter, the results of typical runs are examined. Due to the large volume of data obtained in the present work, only two complete sets of data representing two experimental runs, one for each of the two tube thicknesses tested, are presented herein. Some data trends are also discussed. A more detailed data analysis is given in chapter 5.

4-1 THIN TUBE RESULTS:

The results of a typical run for the thin tube (1 mm wall thickness) are presented in this section. The test conditions of this run are 490 °C initial tube temperature, 50 °C inlet water temperature and 480 kg/m².s mass flux.

4-1-1 TRANSIENT PRESSURES AND INLET FLOW RATE:

Figure 4-1 shows the test section inlet and outlet pressure transients. This indicates an oscillatory nature of the process. Figure 4-2 shows the corresponding transient inlet flow rate. The dependency of the transient flow rate on the system pressure is clear such that the flow retards when the pressure in the tube increases and vice versa. The end of the fluctuations in both system pressure and inlet flow rate marks the end of the rewetting process.

In general, the amplitude of pressure and flow fluctuations was found to increase with increasing initial tube temperature, inlet water temperature, and inlet flow rate.

4-1-2 TRANSIENT WALL TEMPERATURES:

The transient wall temperatures presented in this section are the outside surface temperatures.

The transient wall temperature curves, at the five axial locations, are shown in figure 4-3 for the bottom and top sides of the tube. The bottom temperature curves start with a very slow temperature drop before the arrival of the refilling front as the heat transfer rate from the tube is very low. The arrival of the refilling front is indicated by an increase in the rate of temperature drop due to film boiling. The film boiling period is followed by a sharp drop in temperature down to near saturation as the heat transfer mode changes to transition and nucleate boiling. The curve then levels off as the heat is transferred by single phase forced convection. The instant at which the sharp drop in temperature occurs indicates the initiation of quenching. The wall temperature at which the sharp drop starts is called "the apparent quench temperature".

The main difference in the wall temperature curves of the bottom side at different axial locations is the length of the film boiling period. Longer film boiling periods are encountered as the water advances along the tube. Consequently, the apparent quench temperature decreases. This is mainly related to the decrease in local subcooling as the refilling front advances along the tube.

The top side temperature curves of figure 4-3 differ from the bottom side curves in that a clear film boiling period is not observed. This was true for all moderate flow rates and moderate tube heat capacity (i.e., tube wall thickness and temperature). However, increasing the flow rate and the tube heat capacity resulted in top side temperature curves similar to those of the bottom with a distinct film boiling period. This will be discussed later in conjunction with the flow regime identification in chapter 5. Figure 4-3 also shows that at any axial location, surface quenching is first initiated at the bottom of the tube.

It was found clearly that by increasing the initial tube temperature and inlet water temperature as well as decreasing inlet flow rate, the film boiling period became longer. Consequently, lower apparent quench temperature and slower axial quench propagation were encountered. Moreover, decreasing the inlet water temperature resulted in steeper drop in the transient wall temperatures.

Figure 4-4 shows the seven circumferential transient wall temperature curves at the third axial location (1.65 m from inlet). These curves indicate that quenching is first initiated at the bottom of the tube. The quench front then propagates circumferentially upward quenching the whole cross section. At higher circumferential locations, the corresponding film boiling period is seen to decrease such that the top side of the tube has no distinct film boiling period. The effect of increasing the inlet flow rate and the tube heat capacity on the circumferential tube temperatures was found to extend the film boiling region up to the top of the tube. As mentioned earlier, this will be

discussed later in chapter 5.

4-1-3 TRANSIENT VOID FRACTION:

Figure 4-5 shows the transient void fraction at 1.65 m from inlet. Although only the area averaged void fraction is measured, valuable information is obtained by cross-correlating it with the simultaneous circumferential temperature distribution measured at the same axial location. This was the basis for identifying the flow regimes associated with the quench front as will be discussed in detail later in chapter 5. For example, it is clear from figures 4.4 and 4.5 that at the instant the film boiling period starts at the bottom side of the tube, the void fraction starts to drop, indicating the arrival of the refilling front. The drop in void fraction is gradual suggesting a continuing slow increase in water inventory during the film boiling period. After quenching is initiated at the bottom of the tube, the void fraction decreased at a faster rate down to zero, at which time the top thermocouple shows the sharp drop in temperature indicating the complete quenching and filling of the tube cross section. The void fraction at which quench is initiated at the bottom of the tube is about 0.4 indicating that, for this run, the collapsed water level, during the film boiling period, increased to fill about 60% of the tube at quench initiation. This suggests that the quench front is associated with a stratified flow pattern.

The above was true for all moderate flow rates. Increasing the flow rate resulted in sharper drop in void fraction at the instant of the refilling front arrival (see figure 5-16). This is expected since

increasing flow rate results in reducing stratification.

4-2 THICK TUBE RESULTS:

The results of a typical test run for the thick tube (2 mm wall thickness) are presented in this section. This test run has the closest available test conditions to those of the thin tube run presented in the previous section. The test conditions are 480 °C initial tube temperature, 60 °C inlet water temperature and 480 kg/m².s mass flux.

4-2-1 TRANSIENT PRESSURES AND INLET FLOW RATE:

Figure 4-6 shows the test section inlet and outlet pressure transients while figure 4-7 shows the corresponding transient inlet flow rate. Similar to the corresponding transient thin tube results, the oscillatory nature and dependency of flow rate on the system pressure are indicated. However, the oscillations are more pronounced due to the higher heat capacity of the tube (thicker wall) which resulted in higher vapour generation rate.

Increasing initial tube temperature, inlet water temperature and inlet flow rate mostly resulted in increasing the amplitude of the pressure and flow rate fluctuations.

4-2-2 TRANSIENT WALL TEMPERATURES:

The temperature curves presented in figures 4.8 and 4.9 are those measured by the thermocouples placed close to the inner tube surface ,i.e., at 0.127 mm from the inner surface of the tube. Using fine thermocouples which are located very close to the inner surface of

the tube made it possible to capture the details of the inner surface transients.

Typical transient wall temperature curves for the thick tube (2 mm wall thickness) at the five axial locations are shown in figure 4-8 for the bottom and top sides of the tube. In general, these temperature curves show similar characteristics to those of the thin tube. However, the main difference is that the temperature drop in the film boiling period, at the bottom side of the tube, is slower due to the higher heat capacity of the thick tube which is associated with a higher vapour generation rate. Accordingly, the film boiling region is longer for the thick tube resulting in a slower axial quench front propagation. This is clear by comparing quench times (times at which the sharp drop in the temperature curves start) of the bottom and top temperature curves with the corresponding quench times of the thin tube shown in figure 4-3. For example, the top side of the fifth axial station (2.75 m from inlet) quenches at about 15 s after initiation of water injection, while the corresponding time for the thin tube, shown in figure 4-3, is about 10 s. It was found clearly that increasing the initial tube temperature, inlet water temperature and decreasing inlet flow rate increase the quenching time.

Figure 4-8 shows that temperature curves, in particular those for the top side of the tube, may indicate an oscillatory quench process. This oscillatory quench behaviour at the top side of the tube can be caused by temporary liquid-solid contact due to liquid surface waves at the top of the stratified refilling front (see chapter 5). This effect was more pronounced in the thick tube case due to the

expected higher vapour generation rate, i.e., higher vapour velocity, leading to higher amplitude of the liquid surface waves.

Figure 4-9 shows the seven circumferential transient temperature curves at the third axial station (1.65 m from inlet). Again in general, similar trends to those of the thin tube are observed. However, the oscillatory nature of the process can be noticed.

Figure 4-10 shows the transient wall temperature measurements at different radial locations from the inner surface of the tube. These temperature curves indicate that, prior to quench initiation, the tube wall temperature is almost uniform across the thickness. This is due to the low rate of cooling in this region. However, radial temperature variations are clear during quenching (transition and nucleate boiling regions) due to the high cooling rate. As expected, the closest thermocouple to the inner (quenched) surface, shows the sharpest drop in temperature, while the outer thermocouple shows the slowest drop in temperature. Moreover, it was noticed that increasing the flow rate and subcooling resulted in higher radial temperature variations.

4-2-3 TRANSIENT VOID FRACTION.

Figure 4-11 shows the transient void fraction at the third axial station (1.65 m from inlet). It indicates clearly that during the refilling process the void fraction is not decreasing as smoothly as in the corresponding thin tube curve shown in figure 4-5. This is due to the oscillatory quench process resulting in fluctuating void fraction.

Figure 4-11 shows that the time at which the bottom side is quenched (about 9 s as indicated by figure 4-9), the void fraction is about 0.22. This is compared with a corresponding void fraction of about 0.4 for the thin tube as discussed earlier. This is because the high heat capacity of the thick tube results in longer film boiling period. Accordingly, the liquid inventory is increased before quench initiation. Moreover, figure 4-11 shows that the void fraction drops to zero, indicating the complete filling of the tube cross section, at about 12 s after inlet water injection. This is compared with about 7 s for the corresponding thin tube curve shown in figure 4-5.

4-3 REPRODUCIBILITY OF TEST RESULTS.

The data showed high degree of reproducibility as indicated by all measured parameters. To avoid repetition only quenching times are shown here. Quenching time for an axial station is defined as the time elapsed between initiating water injection at the test section inlet and the time at which the quench front reaches that specific station. The reproducibility of the second group of tests conducted on the 1 mm thick tube (table A-4 of appendix A) is demonstrated in figures 4-12 to 4-15. Each one of these figures shows the quenching time versus axial location for five repeated runs conducted at the same initial and boundary conditions. These figures indicate that the experimental results were reproducible. Moreover, figure 4.12 clearly shows that quenching times for the top side of the tube are longer than those of the bottom side of the tube due to stratification. Further discussion of the quench times and rewetting velocities are given in chapter 5.

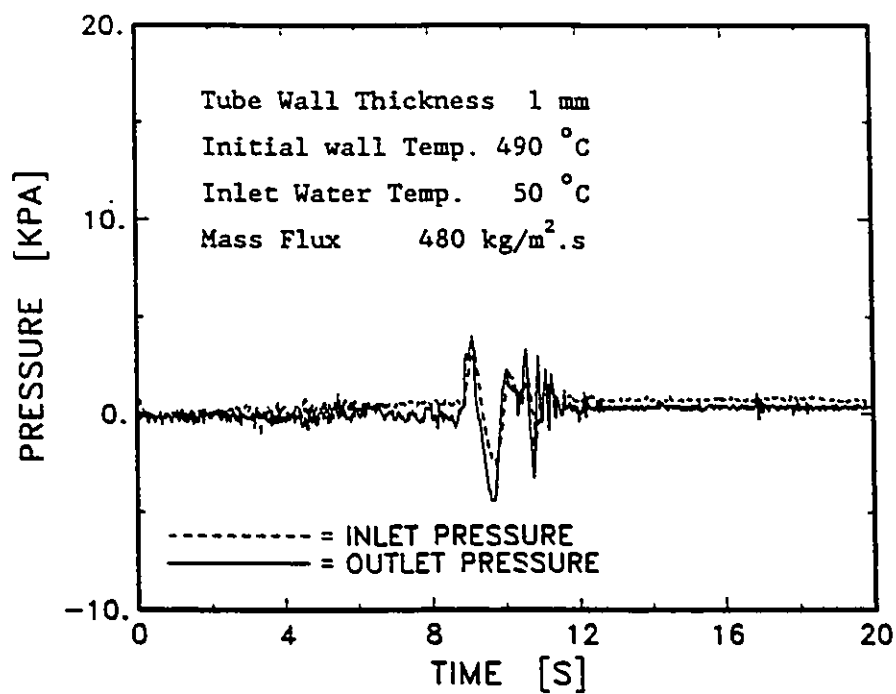


FIGURE 4-1: INLET AND OUTLET PRESSURE TRANSIENTS

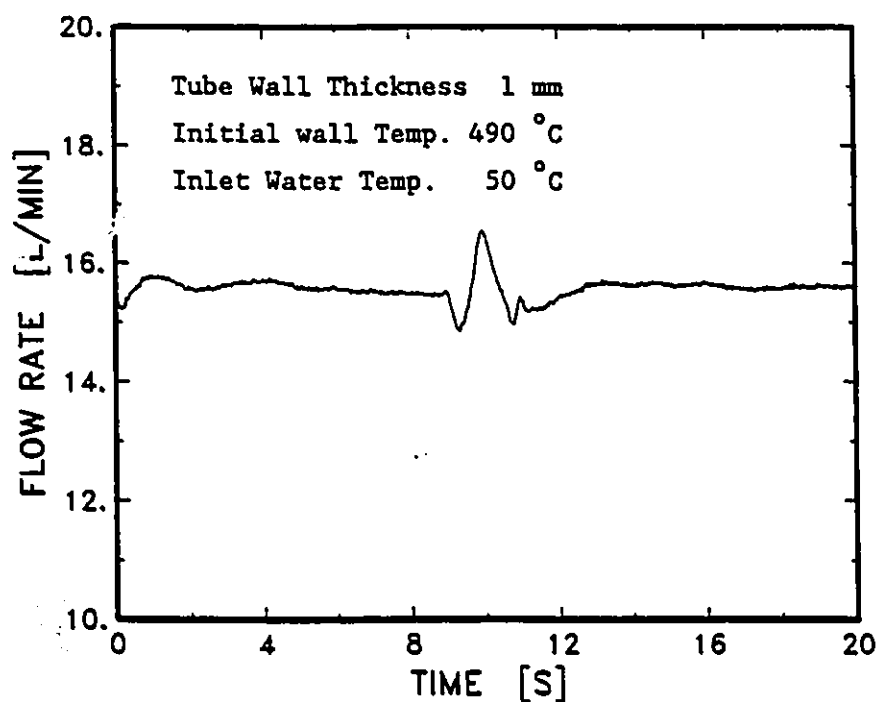


FIGURE 4-2: TRANSIENT INLET FLOW RATE

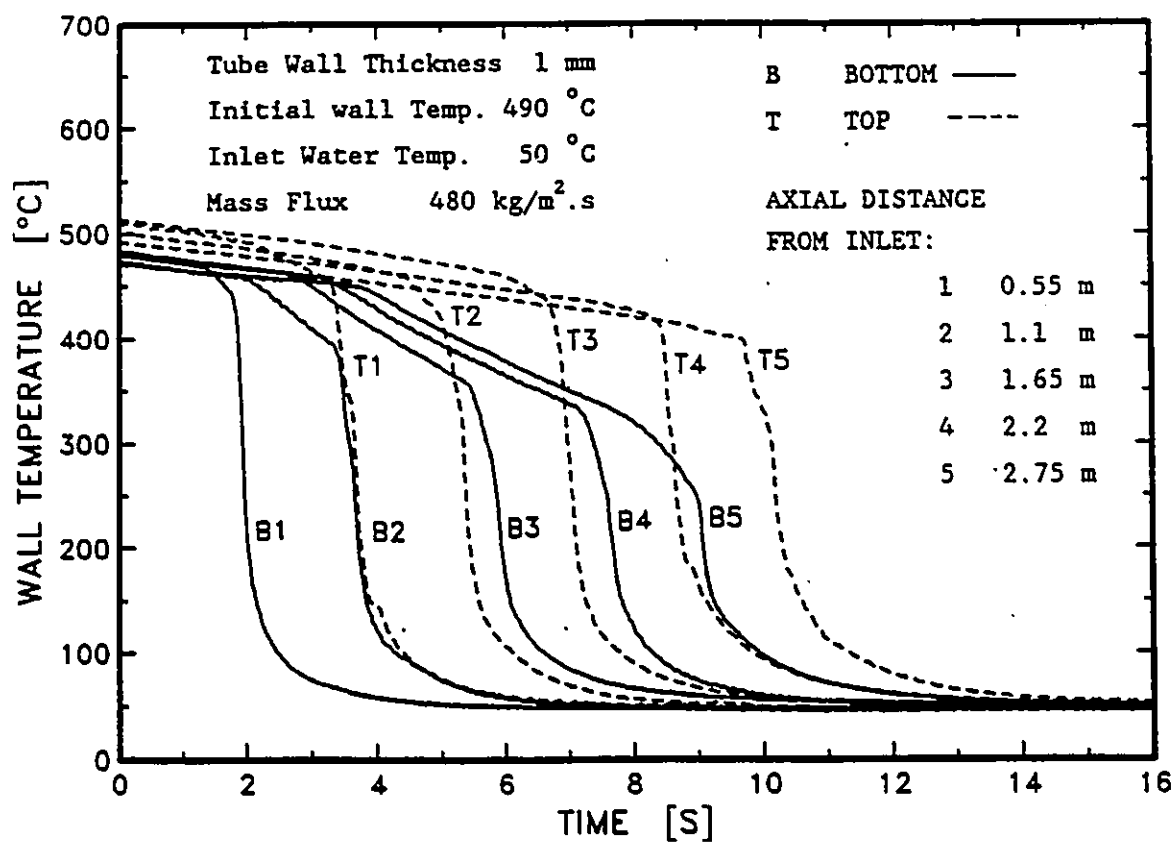


FIGURE 4-3 TRANSIENT WALL TEMPERATURES AT DIFFERENT AXIAL LOCATIONS

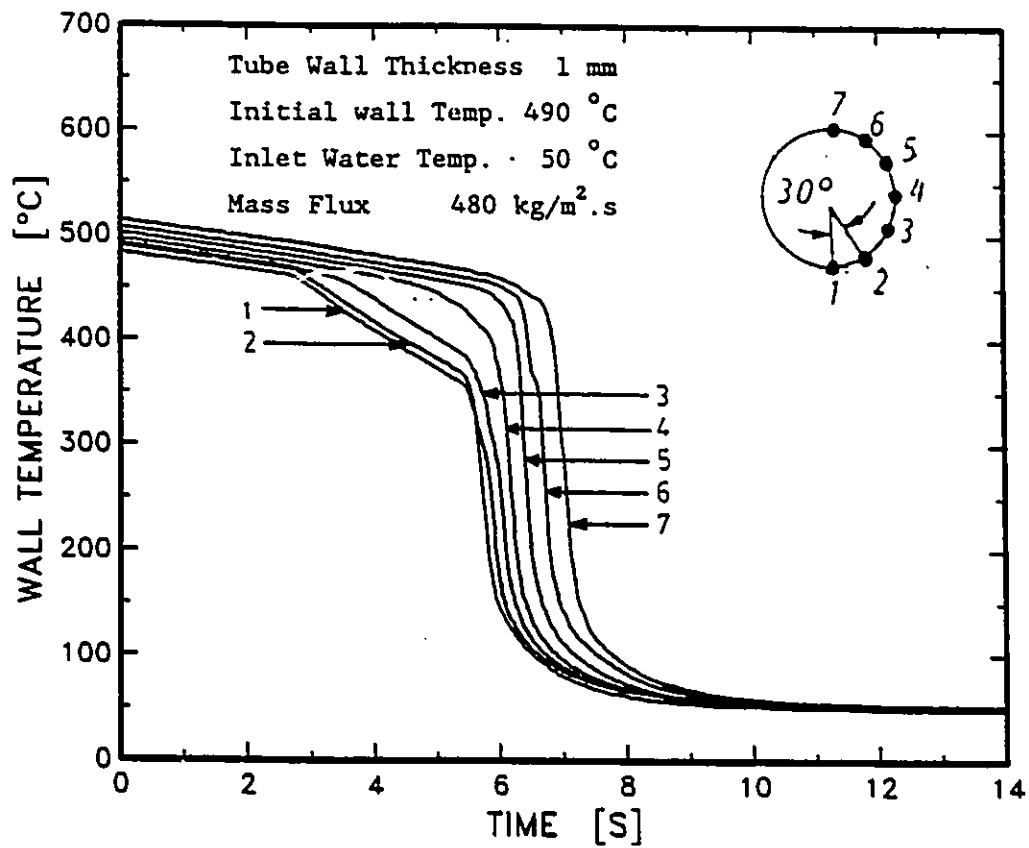


FIGURE 4-4 TRANSIENT WALL TEMPERATURES AT DIFFERENT CIRCUMFERENTIAL LOCATIONS

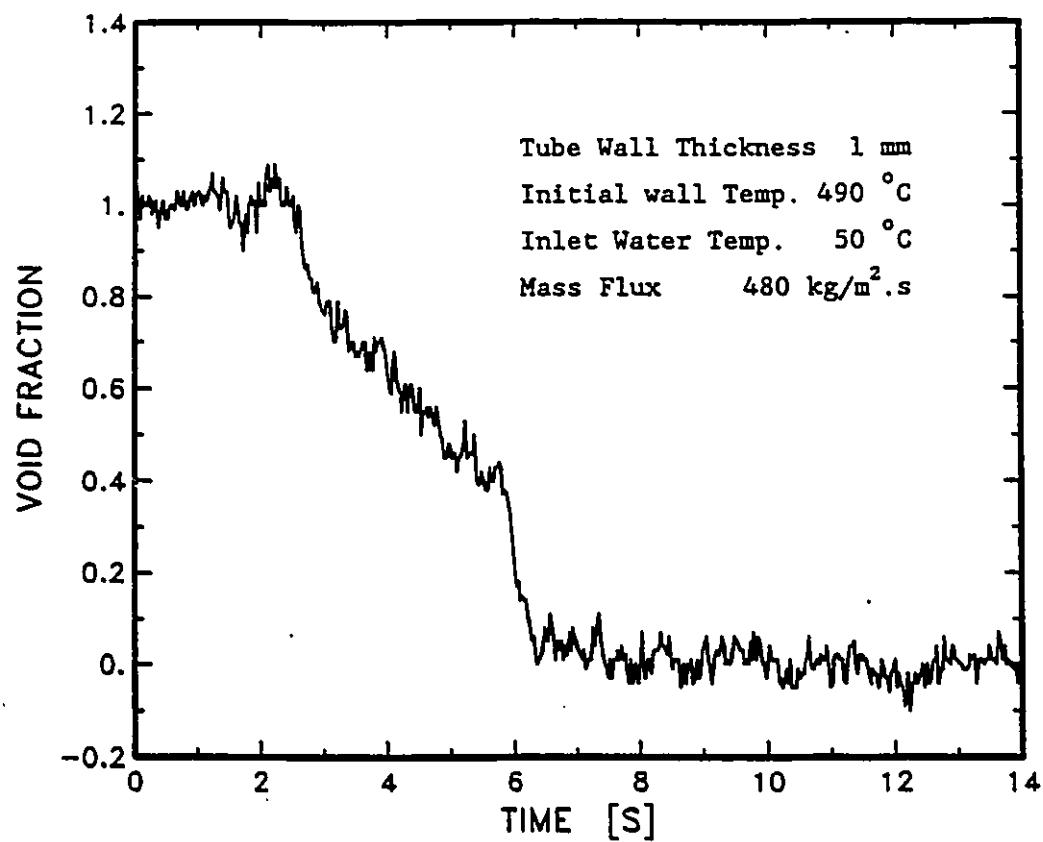


FIGURE 4-5 TRANSIENT VOID FRACTION

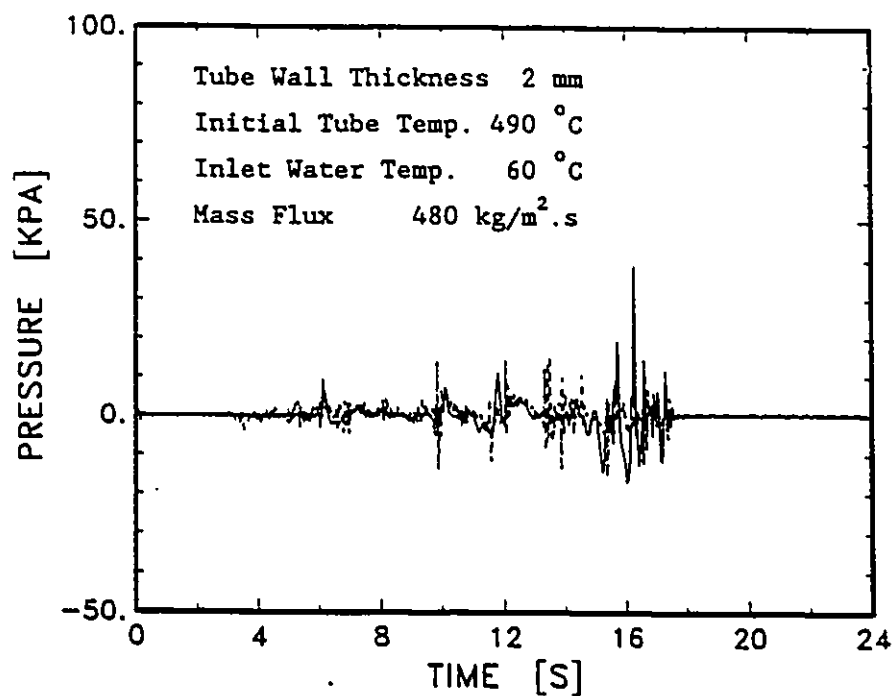


FIGURE 4-6 INLET AND OUTLET PRESSURE TRANSIENTS

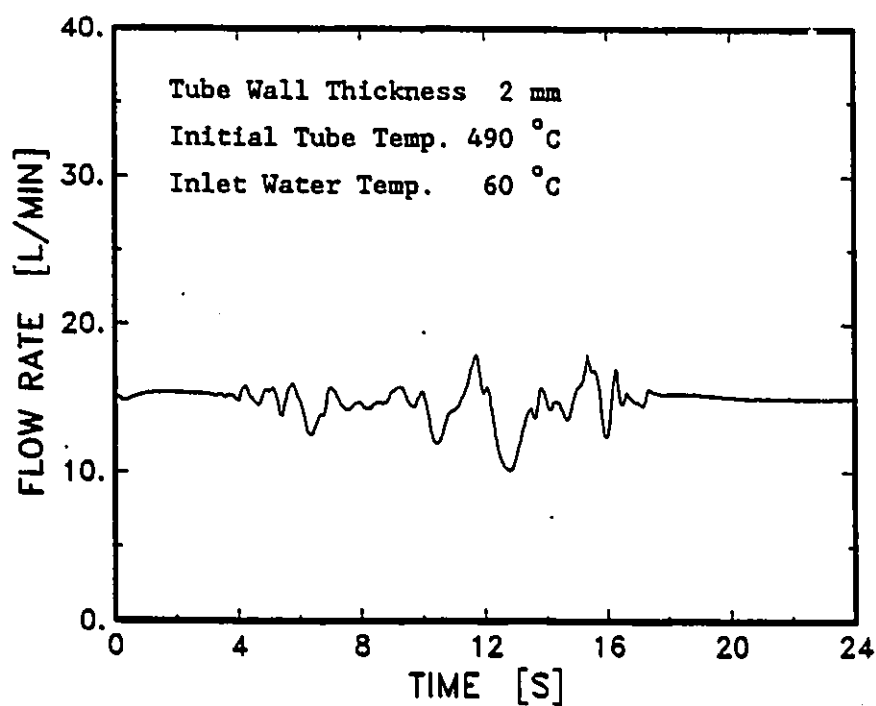


FIGURE 4-7 TRANSIENT INLET FLOW RATE

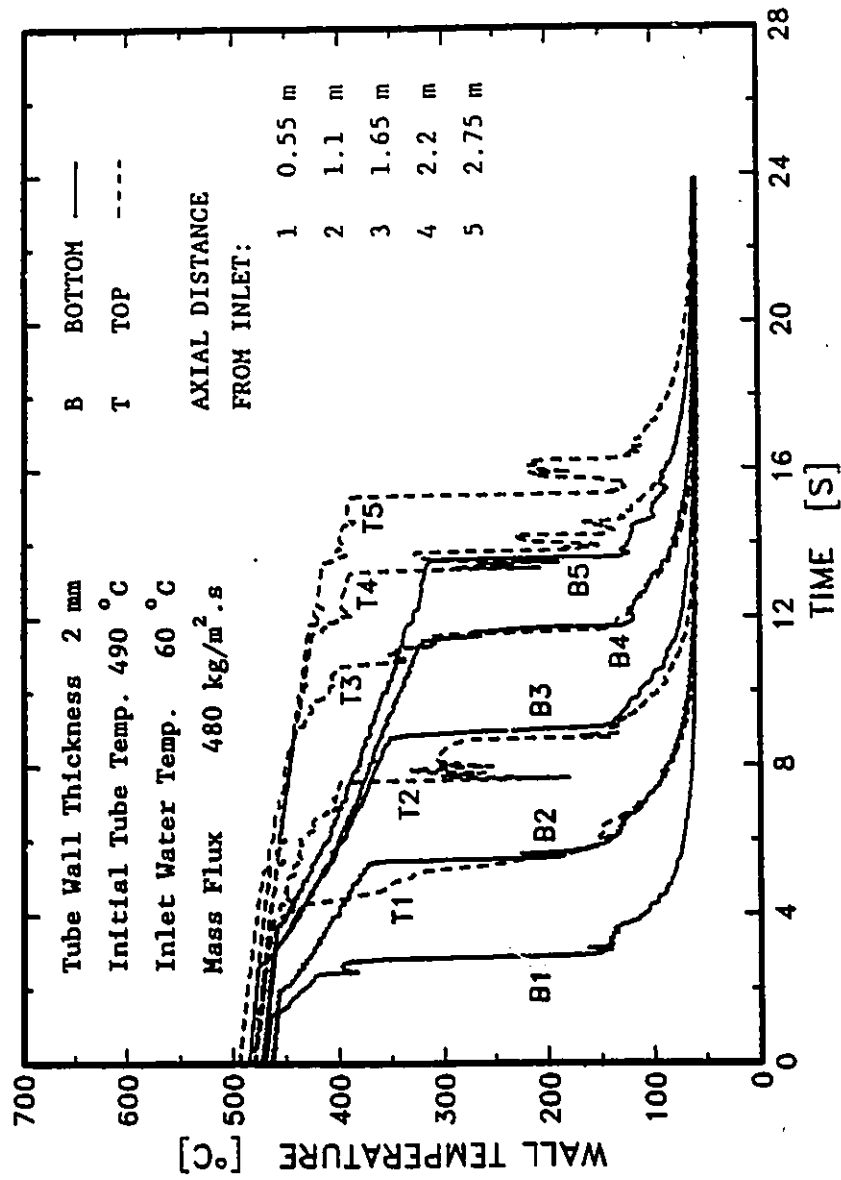


FIGURE 4-8 TRANSIENT WALL TEMPERATURES AT DIFFERENT AXIAL LOCATIONS

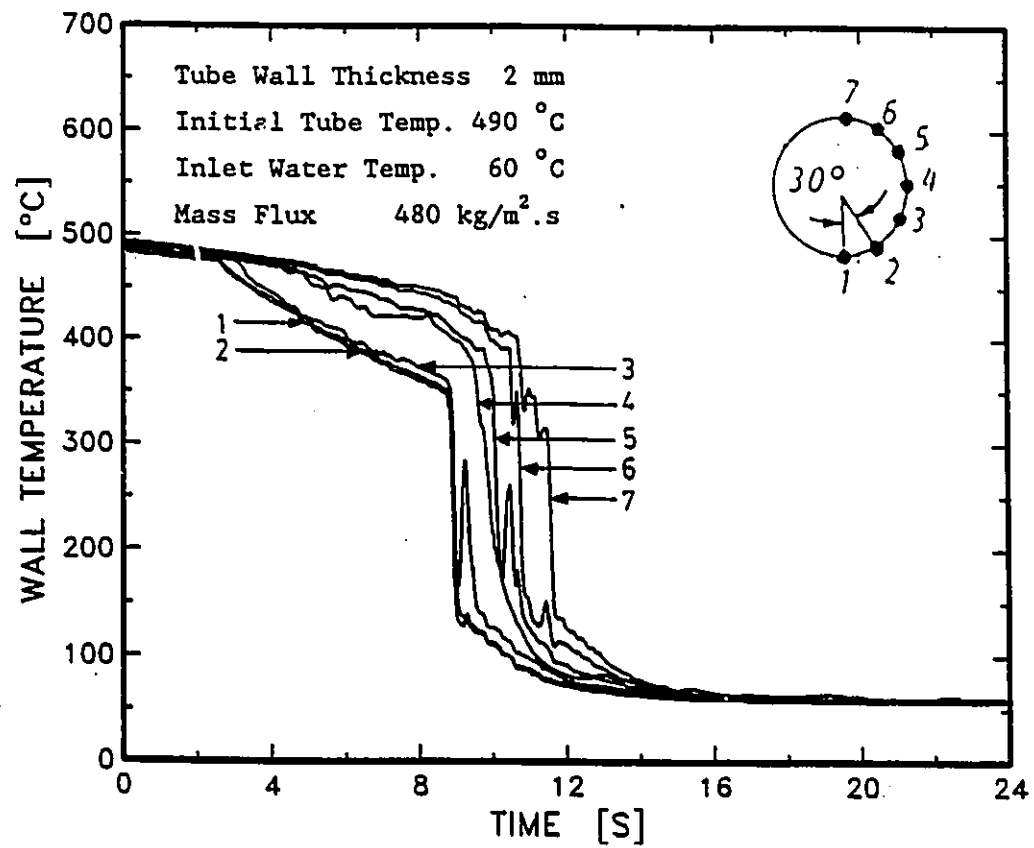


FIGURE 4-9 TRANSIENT WALL TEMPERATURES AT DIFFERENT CIRCUMFERENTIAL LOCATIONS

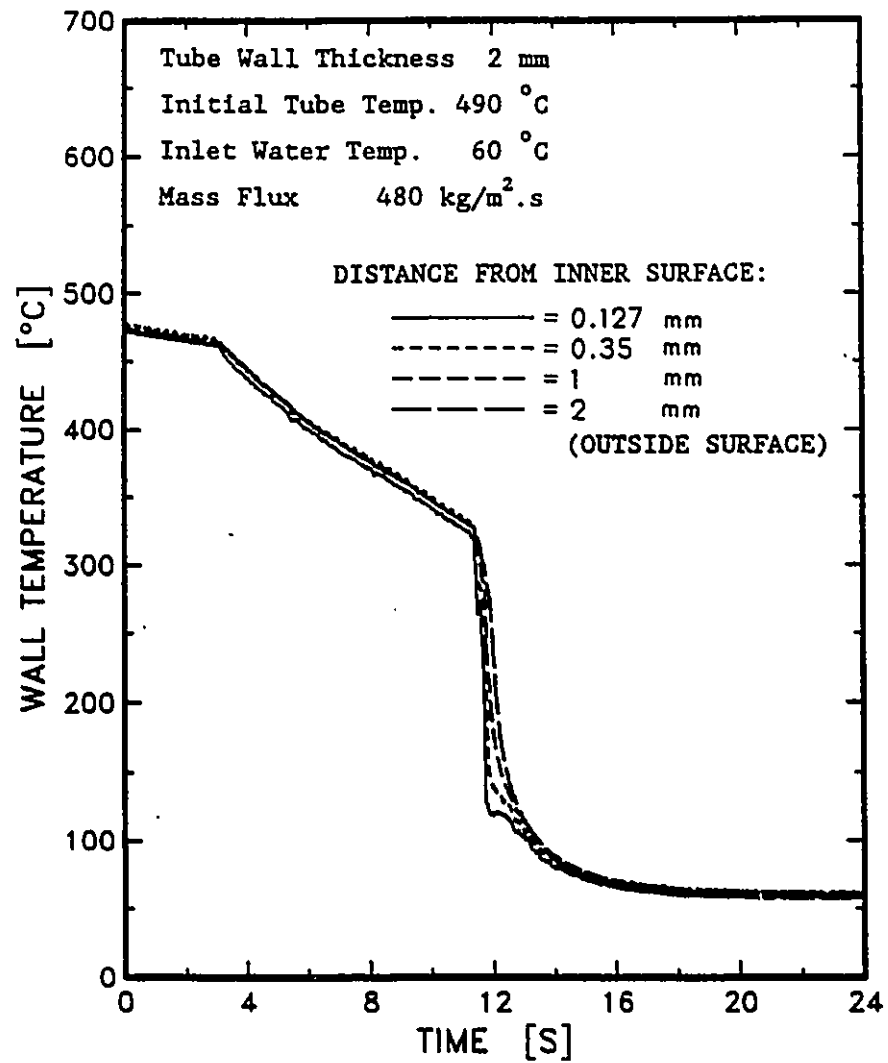


FIGURE 4-10 TRANSIENT WALL TEMPERATURES AT DIFFERENT RADIAL LOCATIONS

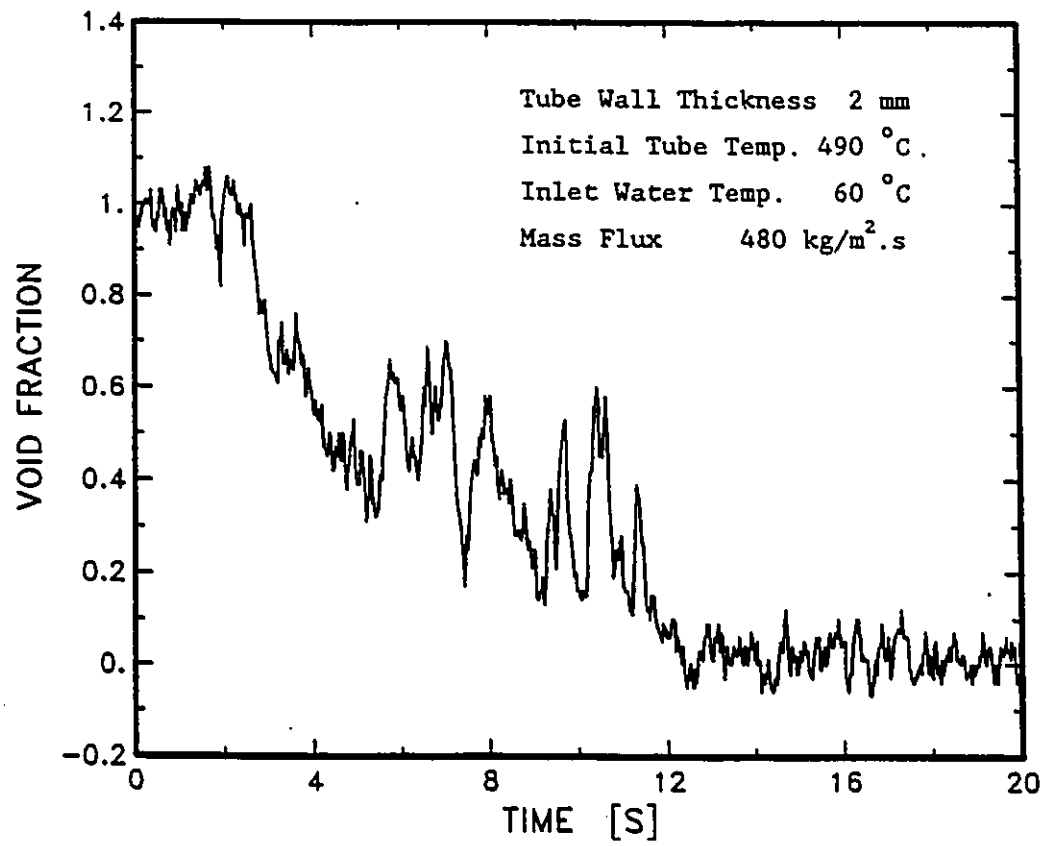


FIGURE 4-11 TRANSIENT VOID FRACTION

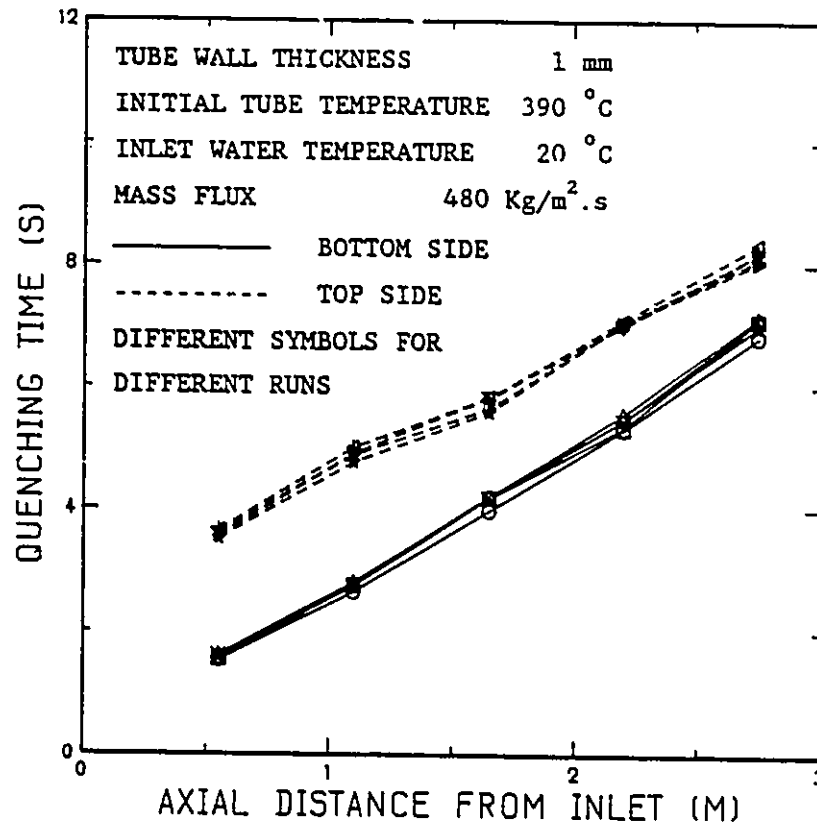


FIGURE 4-12 QUENCHING TIME VERSUS AXIAL LOCATION FOR REPEATED TEST RUNS

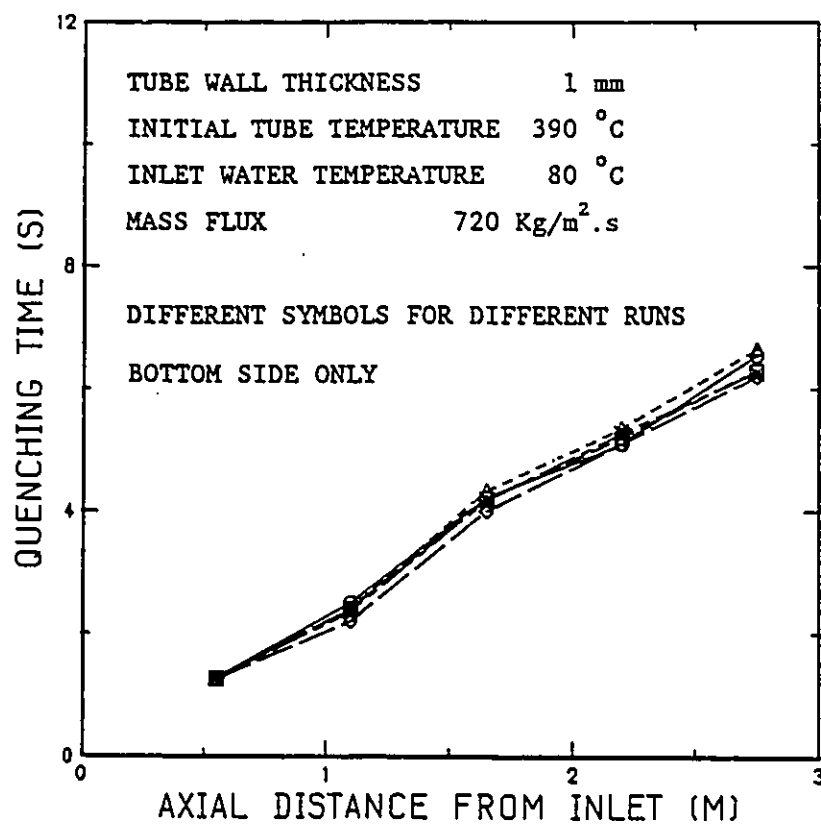


FIGURE 4-13 QUENCHING TIME VERSUS AXIAL LOCATION FOR REPEATED TEST RUNS

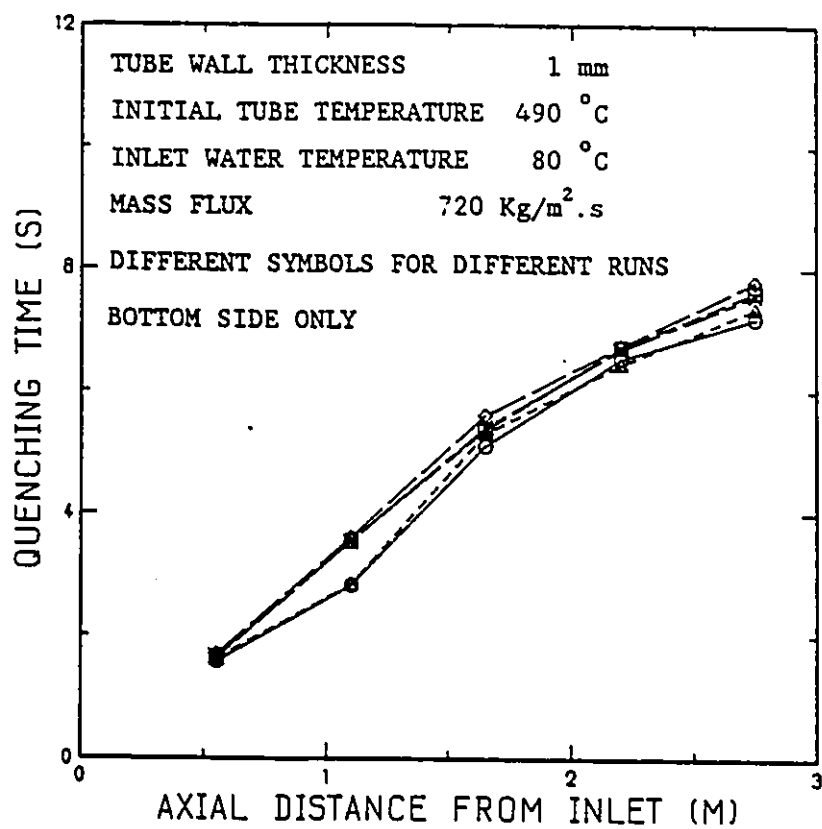


FIGURE 4-14 QUENCHING TIME VERSUS AXIAL LOCATION FOR REPEATED TEST RUNS

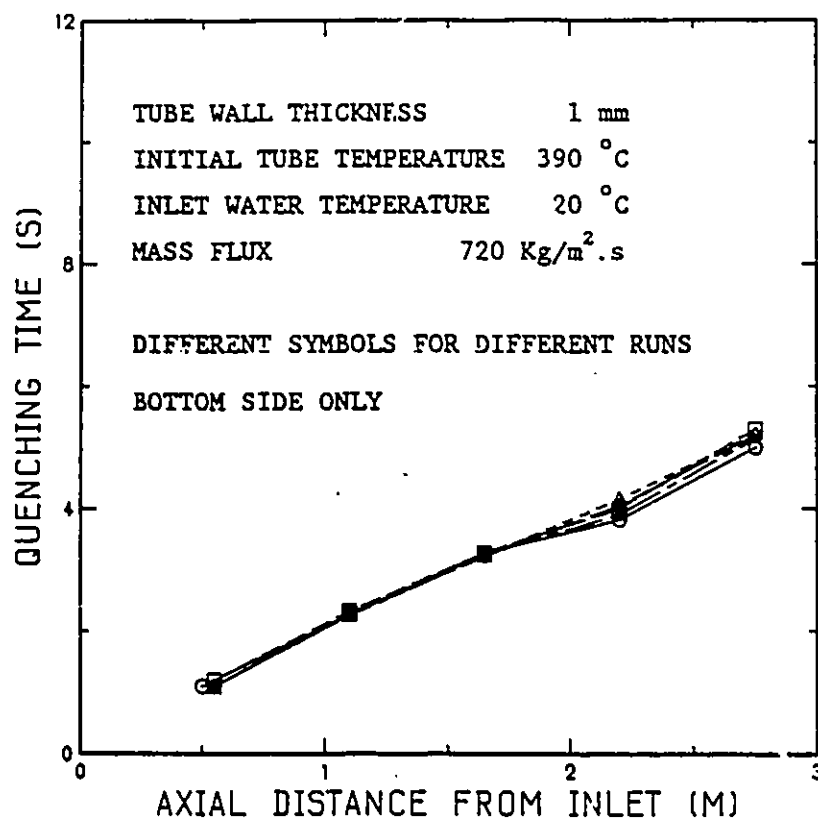


FIGURE 4-15 QUENCHING TIME VERSUS AXIAL LOCATION FOR REPEATED TEST RUNS

CHAPTER 5

DATA ANALYSIS

5-1 REWETTING VELOCITY:

Rewetting velocities are normally calculated from the transient wall temperature curves by calculating the time difference between the sharp drop in wall temperature at different axial locations.

Figures 5-1 to 5-6 show the rewetting velocities, calculated at the third axial measuring station (1.65 m from inlet) as a function of water mass flux for both tubes (1 mm and 2 mm thickness) at different initial tube and inlet water temperatures. The rewetting velocities were calculated at the third axial station (1.65 m from inlet) where the detailed circumferential temperature distribution and void fraction measurements were conducted. This was done by measuring the difference in time between the sharp drop in wall temperature at the bottom of the second axial station (1.1 m from inlet) and the fourth axial station (2.2 m from inlet). Superimposed on the figures is the nominal inlet water velocity corresponding to cold refilling.

As shown, the rewetting velocity is usually lower than the inlet water velocity, with the exception of the conditions shown in figure 5-1, which correspond to the thin tube case having the lowest initial tube temperature (290 °C) and a very low mass flux ($<480 \text{ kg/m}^2 \cdot \text{s}$). The same phenomenon was observed by Chan (1980), where it was stated that the bottom side rewetting velocities could be higher than

inlet water velocity, since the flow is stratified and the leading edge can acquire a velocity which is considerably higher than the average inlet flow velocity especially for low inlet flow rates. However, in the present work rewetting velocities higher than the inlet velocity were also observed at the top side of the tube under the same above conditions. Analysis of the flow regimes associated with the quench front propagation, given in the next section, indicates that under the above limited conditions of very low flow rate and tube heat capacity, the quench front may lead a skewed annular flow where the rewetting velocity could be higher than the inlet water velocity. Groneveld and Young (1978) showed that for bottom flooding of hot vertical tubes with low initial wall temperature and injection rate, the rewetting velocity was higher than the collapsed liquid velocity. Moreover, Chan and Yadigaroglu (1980) and Kawaji et al (1985) reported the existence of annular flow pattern during the reflooding of hot vertical tubes under similar conditions of low initial tube temperature and injection rate. It was argued by Groneveld and Young (1978) that rewetting velocities could be higher than the cold flooding velocity since quenching occurs almost instantaneously on arrival of the liquid film which propagates ahead of the collapsed liquid core.

Figures 5-1 to 5-6 show clearly that increasing mass flux and water subcooling increases the rewetting velocity. The deviation from the cold injection velocity increases with increasing initial tube wall temperature.

The effect of the initial tube temperature is shown in figures 5-7 and 5-8. These figures indicate that increasing the initial tube

temperature decreases the rewetting velocity.

The effect of the tube wall thickness is shown in figures 5-9 and 5-10 where the data from Ahluwalia et al (1985) are also included. These figures indicate that the rewetting velocity decreases as the tube wall thickness increases.

The above findings on the effect of different parameters (mass flux, subcooling, initial tube temperature and tube wall thickness) on the rewetting velocity agree well with the previous investigations for both vertical channel reflooding and horizontal channel rewetting as discussed in chapter 2.

For a given inlet flow rate, the decrease of the rewetting velocity with increasing initial tube temperature, inlet water temperature and tube wall thickness (heat capacity) may be attributed to increase in resistance to flow caused by increasing vapour generation rate in the tube. Having higher vapour generation rate increases the initial vapour film thickness around the advancing refilling front during the film boiling region which can delay the quenching process. It is interesting to note, accordingly, that decreasing the rewetting velocity was always associated with longer duration of the film boiling region.

For a given run, it was found that local rewetting velocity varied along the tube. This is clearly shown by the quenching time curves in figures 4-12 to 4-15 since the slope of these curves represents the reciprocal of the rewetting velocity.

5-2 FLOW REGIMES IDENTIFICATION:

The simultaneous transient void fraction and tube wall temperature measurements were used to obtain the shape of the advancing refilling and rewetting fronts. In general, the results were used to reconstruct the shape of the advancing refilling front as well as characterizing the flow regime and phase distribution near the quench front. The rewetting of the tube surface at any location and the axial circumferential propagation of the quench front were clearly identified from the transient temperature measurements since tube quenching is characterized by a sharp drop in temperature. Accordingly, at a given axial location, the quench level (h_q), defined in figure 5-12, can be evaluated by observing the circumferential temperature distributions. The transient void fraction measurements, however, were used to identify the arrival of the refilling front and to evaluate the average water level (h_L) as predicted from geometrical considerations, assuming a smooth stratified water surface (see figure 5-12 for the definition of h_L). The relationship between void fraction (α) and the collapsed water level (h_L) for stratified flow in a circular tube is

$$\alpha = 1 - \left(\frac{1}{\pi R^2} \right) \left\{ R^2 \cos^{-1}[(R-h_L)/R] - (R-h_L)(2Rh_L-h_L^2)^{0.5} \right\} \quad \text{for } h_L < R \quad (5.1)$$

and

$$\alpha = \left(\frac{1}{\pi R^2} \right) \left\{ R^2 \cos^{-1}[(h_L-R)/R] - (R-h_L)(2Rh_L-h_L^2)^{0.5} \right\} \quad \text{for } h_L \geq R \quad (5.2)$$

where h_L and R are the collapsed liquid level and radius of the tube respectively.

In general, three different flow regimes associated with the

refilling and rewetting of hot horizontal tubes were observed; stratified, inverted annular and annular flow regimes.

5-2-1 STRATIFIED REFILLING FRONT.

Figures 5-11a and 5-11b show typical of results obtained for moderate inlet flow rates (up to $800 \text{ kg/m}^2\text{s}$). Starting with the empty tube ($\alpha=1$), the tube temperature decreased slowly due to the low rate of heat transfer by forced convection to the steam flow ahead of the refilling front (figure 5-11a). The arrival of the refilling front was indicated by the sudden drop in void fraction (figure 5-11b, point a). The bottom thermocouple and the adjacent one showed a corresponding steeper drop in temperature, typical of film boiling, which ended when the vapour film collapsed causing surface quenching (point b) as indicated by a sharp drop in temperature. During the film boiling period, the void fraction measurement showed a gradual drop which indicated a continuing increase in water inventory. After quenching was initiated at the bottom of the tube, the void fraction decreased at a faster rate down to zero, at which time the top thermocouple showed the sharp drop in temperature indicating the complete quenching and filling of the tube cross section. The above finding supports what was proposed by Chan and Banerjee (1981), that a stratified "liquid tongue" stretching out from the quench front cools the bottom portion of the dry surface in front as shown in figure 5-12. The axial length of the water tongue can be obtained from the measured time duration of film boiling and the rewetting velocity. As the stratification of the advancing refilling front is confirmed from figures 5-11a and 5-11b,

the shape of the interface can be deduced from the data as shown below.

The relationship between the void fraction and the quench level as determined by the thermocouple measurement is shown in figure 5-13 for different inlet water subcooling. The data clearly show that the void fraction decreased significantly to a critical value before the initiation of quenching at the bottom of the tube ($h_q = 0$). The data also show that this critical void fraction was dependent on the inlet water temperature. Quench initiation was followed by fast circumferential propagation of the quench front (i.e., an increase in h_q) while the void fraction, i.e., the collapsed water level, remained almost constant. This was then followed by slower circumferential propagation of the quench front accompanied by a general decrease in void fraction, i.e., an increase of the collapsed water level until the entire cross section was quenched. Superimposed on figure 5-13 are the predictions of equations 5.1 and 5.2 which represent the refilling of a cold tube. Therefore, the experimental data falling on the left of the dotted curve in figure 5-13 indicate that the quench level is lower than the collapsed water level, while those on the right side suggest that the quench level is higher than the collapsed water level.

Figure 5-14 shows the same set of data plotted to relate the quench level and the corresponding collapsed water level as predicted by equations 5.1 and 5.2. This shows that since quenching was delayed, the quench level was lagging behind the collapsed water level, but it eventually overtook the water level as the latter increased, filling more than half the tube. Under this condition, the water surface became depressed in the middle, forming a semi-annular shape. This observation

can be explained by the effect of the interfacial shear stresses as discussed below.

It is known that secondary flows could be set-up in flows over surfaces of unequal roughness in a direction such that turbulence-rich fluid is transported into regions of lower turbulence intensity. This mechanism was adopted by Laurinat (1982) and Laurinat et al (1984) in modelling the steady annular flow in horizontal tubes. It was postulated that, because of asymmetrical water film distribution, the interfacial roughness at the bottom of the tube will be larger than that at the top. This rougher interface at the bottom presents more resistance to the vapour flow in the axial direction and results in a circumferential (secondary) vapour flow pattern as shown in figure 5-15a. In the present situation, two factors would enhance this phenomenon. Firstly the difference in the interfacial shear on the surface of the liquid and the dry upper portion of the tube would be larger than that associated with an annular flow. Secondly, the upward flow of vapour venting from the vapour film would enhance the secondary flow and impose further interfacial stresses in the vapour film region shearing the liquid circumferentially upward. Accordingly, the postulated flow pattern is shown in figure 5-15b.

5-2-2 INVERTED ANNULAR FLOW:

Increasing the inlet flow rate ($G > 800 \text{ kg/m}^2\text{s}$) reduced stratification such that the flow regime at the quench front approached an inverted annular pattern at the highest flow rates considered. The higher the tube heat capacity (tube temperature and tube wall

thickness) the longer the inverted annular flow regime tended to be. This is shown in figures 5-16a and 5-16b. The void fraction decreased below 0.2 well before the arrival of the quench front, and the upper thermocouple showed a period of gradual temperature decrease typical of film boiling, indicating the presence of a subcooled liquid core extending ahead of the quench front. It should be noted that the rewetting of the bottom surface was always ahead of the rewetting of the top. However, the delay between the quenching of the top and the bottom of the tube decreased with increasing inlet flow rate. This regime is similar to the well known inverted annular flow observed in flooding of vertical tubes with high flow rates as was reported by Kawaji and Banerjee (1987) and Ishii and Jarlais (1986) among others. This similarity between the refilling of hot horizontal tubes and the flooding of hot vertical tubes for high mass flux is expected since increasing the injected mass flux in a horizontal tube will decrease the significance of gravitational effects leading to less flow stratification.

5-2-3 ANNULAR FLOW.

For the thin tube (1 mm wall thickness), at the lowest initial wall temperature (about 300 °C), and an inlet mass flux less than 480 kg/m².s, a different behaviour was observed. Particularly for high subcooling, quenching started at the bottom of the tube at relatively high void fraction and ended at the top of the tube when it was still not full of liquid as shown in figures 5-17a and 5-17b. It is speculated that the quenching front may lead a collapsed liquid core,

forming a short region of a skewed annular flow with an inclined quench front. This can explain the rewet velocity being slightly higher than the inlet velocity under these conditions as was reported earlier. This phenomenon was only observed in three runs of low wall heat capacity, i.e., for thin-walled tube. Some other runs under similar conditions have clearly shown formation of annular flow like behaviour, i.e., existence of film boiling at the top side of the tube while the void fraction is still very high, followed by breaking down to stratified flow behaviour. This change in behaviour was found to take place with decreasing inlet subcooling. This skewed annular flow pattern is similar to the annular flow pattern observed in flooding hot vertical tubes with low flow rate and initial tube temperature as was reported by Groneveld and Young (1987), Chan and Yadigaroglu (1980) and Kawaji et al (1985). However, due to gravitational effects, such a flow pattern in horizontal tubes would be skewed such that the minimum thickness and length of the liquid film occurs at the top side of the tube and the maximum thickness and length of the liquid film occurs at the bottom of the tube. Kawaji et al (1985) reported that flow visualization experiments on flooding hot vertical tubes showed that periodic bursts of vapour occur in the boiling zone followed by upward ejection of liquid. This could be responsible for breaking up the liquid core leading to the short annular flow since quenching occurs almost instantaneously upon arrival of the liquid front. In the case of horizontal tubes, another mechanism could exist, i.e., the liquid film is driven circumferentially upward, to cover the whole cross section, by the speculated vapour secondary flow discussed in section 5-2-1.

The relationship between the void fraction and the dimensionless quench level (quench level/diameter) for the three discussed flow regimes is shown in figure 5-18. Runs T.R. 22, T.R. 54 and T.R. 1 (see Appendix A for test conditions) were selected to represent the stratified, inverted annular and annular flow respectively. As shown, quenching is initiated at the bottom of the tube at void fraction equal to 0.94 in the annular flow, 0.6 in the stratified flow and 0.19 in the inverted annular flow. Moreover, the annular flow curve shows that quenching the top side of the tube is reached when the tube is not completely full.

5-2-4 EFFECT OF TUBE WALL THICKNESS:

Experiments carried out on the thick tube (2 mm wall thickness) showed only the first two flow patterns, i.e., stratified and inverted annular. However, due to the higher wall heat capacity, the vapour generation rate was significantly higher and the duration of the film boiling region was longer. As a result, the length of the liquid tongue which preceded the quench front was longer than that observed for the thin tube for the same inlet flow rate, water subcooling and initial tube temperature. This trend is clearly demonstrated in figures 5-19a and 5-19b, where a long period of film boiling was encountered at the bottom of the tube associated with a nearly constant void fraction, or liquid level. However, when quenching was initiated at the bottom of the tube, it propagated quickly to cover the entire cross section with a sudden drop in void fraction to almost zero value.

5-3 QUENCHING CURVES:

Quenching curves are boiling curves constructed from transient rewetting data. The importance of investigating quenching curves is to identify and evaluate the various modes of heat transfer associated with the rewetting process. However, for the same set of data, different quench curves could be obtained depending on the method of reducing the data. A typical quench curve and the corresponding transient wall temperature are shown in figure 5-20. This figure shows the different heat transfer regimes associated with the rewetting process.

5-3-1 BACKGROUND:

Extensive experimental studies have been carried out on the development of quenching curves under pool boiling conditions. The effect of different parameters were included such as initial wall temperature, surface configuration, heat capacity (wall thickness and type of material), surface condition, type of coolant, and the method of heating and quenching. The results were consistent in that, for systems with sufficient thermal capacity, the quenching curves are similar to the corresponding steady-state boiling curves. The main difference was in the value of the critical heat flux where quenching curves showed lower values. For details refer to Peyayopanakul and Westwater (1978), Lin and Westwater (1982), Nishikawa et al (1984), Veres and Florschuetz (1971) and Owens and Florschuetz (1972).

Under forced convective conditions, high thermal capacity test sections were used by Cheng et al (1978) and Ueda et al (1983) who used

water and freon-113 respectively. The results indicated that boiling curves obtained via both transient cooling , i.e., quenching and steady state boiling methods are in good agreement. Moreover, the results of Cheng et al (1978) indicated that:

- i) Transition boiling heat flux increased with increasing inlet subcooling and mass flux.
- ii) Subcooling and mass flux had no effect on nucleate boiling.
- iii) Heat flux in the film boiling regime remained constant over a fairly wide range of wall superheats.

Chen et al (1979) conducted tests on reflooding of circular tubes using water. Quenching curves were obtained over a wide range of experimental parameters using outside tube surface temperature measurements. The main findings were

- i) No significant difference in quenching curves obtained for different wall thickness at the same initial and inlet conditions.
- ii) In the nucleate boiling region, the surface heat flux is independent of the initial wall temperature.
- iii) Critical heat flux and the surface heat flux in the transition boiling region decrease with increasing axial distance from the inlet along the test section. No significant effect of axial location on surface heat flux was observed in the nucleate boiling region.
- iv) Film boiling heat flux decreases with increasing distance from the inlet.

Ueda et al (1983) and Ueda and Inoue (1984) experimentally studied the rewetting of a hot surface by a falling film of R-113 liquid at atmospheric pressure and different subcooling. Using the

temperature transient measured at the wall surface, a two dimensional conduction equation in the wall was solved numerically to derive the quenching curve. It was found that the quenching curve is little affected by the wall thickness and is independent of the liquid film flow rate and the initial wall superheat. The surface heat flux increases with increasing subcooling.

Refilling and rewetting of a hot horizontal tube using water was studied experimentally by Ahluwalia et al (1985). The temperature distribution in the radial direction was used to obtain the inner surface temperature by extrapolation using a third order polynomial least squares fit. Quenching curves were obtained by calculating the radial temperature gradient at the inner (quenched) surface. The quench curves obtained were different from conventional boiling curves. Nucleate boiling was not observed and the surface heat flux was considerably higher than that in the conventional boiling curve. This method of deriving the quench curves is further discussed in the next section.

5-2-2 PRESENT ANALYSIS FOR QUENCH CURVES:

For the case of the thin tube (1 mm wall thickness), the temperature was assumed uniform across the thickness. Circumferential conduction is also neglected as the thickness to diameter ratio is very small. Accordingly, the quench curves were generated utilizing the measured temperature transients at the outside surface of the tube. The surface heat flux to the coolant was extracted from the data by using an energy balance for a control volume occupying a length Δz of the

tube as shown in figure 5-21.

$$\rho C_p A \Delta z \frac{\partial T}{\partial t} = (q_z - q_{z+\Delta z}) - q_{out} - q_{in} \quad (5.3)$$

where

A is the cross sectional area of the tube wall

$$= (\pi/4) (D_o^2 - D_i^2)$$

$q_z - q_{z+\Delta z}$ is the net axial conduction into the element

$$= k A (\partial^2 T / \partial z^2) \Delta z$$

q_{out} is the heat transfer rate from the element to the surroundings

$$= \bar{q}_{out} \pi D_o \Delta z$$

q_{in} is the heat transfer rate from the element to the coolant

$$= \bar{q}_{in} \pi D_i \Delta z$$

ρ and C_p are the tube wall density and specific heat capacity respectively.

In estimating the axial heat conduction term, the approach given by Chen et al (1979) is followed. Assuming a constant rewetting velocity (U), the axial temperature gradient ($\partial T / \partial z$) could be represented by $(1/U)(\partial T / \partial t)$. Accordingly, the axial conduction term $kA[\partial^2 T / \partial z^2]$ is approximated by $(kA/U^2)(\partial^2 T / \partial t^2)$ when the rewetting velocity (U) deduced from the experiment is used.

Substituting for the axial heat conduction and the heat loss terms, equation 5.3 is reduced to give the inner surface heat flux

$$\bar{q}_{in} = \frac{(D_o^2 - D_i^2)}{4 D_i} \left[\frac{k}{U^2} \frac{\partial^2 T}{\partial t^2} - \rho C_p \frac{\partial T}{\partial t} \right] - \bar{q}_{out} \frac{D_o}{D_i} \quad (5.4)$$

\bar{q}_{out} is calculated by

$$\bar{q}_{out} = h_{out} (T - T_{su}) \quad (5.5)$$

where h_{out} is the combined heat transfer coefficient due to radiation and natural convection ($h_{rad} + h_{nc}$) and T_{su} is the surrounding temperature.

h_{rad} is calculated by

$$h_{rad} = \sigma \epsilon \frac{(T_A^4 - T_{suA}^4)}{(T_A - T_{suA})} \quad (5.6)$$

T_A and T_{suA} are the absolute temperatures of the tube wall and surrounding respectively. The Stefan-Boltzmann constant is represented by σ and ϵ is the tube wall emissivity.

h_{nc} is calculated by a simplified relation given by Holman (1976)

$$h_{nc} = 1.32 \left[\frac{T - T_{su}}{D_o} \right]^{0.25} \quad (5.7)$$

For the thick tube (2 mm wall thickness), the radial temperature variation across the tube wall thickness could be significant. Accordingly, it is not appropriate to use the outside surface temperature in obtaining quench curves. However, circumferential heat conduction can be neglected as the tube thickness to diameter ratio is relatively low (less than 8%). This is supported by the three-dimensional conduction analysis by Salcudean and Bui (1980) and Salcudean and Rahman (1980) where it was shown that in calculating the local heat flux during the rewetting of horizontal tubes, the circumferential heat flow is an order of magnitude less than the axial heat flow even for considerable stratification.

Therefore, a semi-analytical method for obtaining the quench curves for the thick tube is proposed. The two-dimensional heat conduction equation in the tube wall is solved numerically with the experimentally measured transient inside and outside surface temperatures used as boundary conditions. The inner surface temperature is obtained by extrapolating the four measured radial temperatures using a third order polynomial least squares fit. Variable radial mesh size with the finest mesh near the quenched (inner) surface was used. Solving for temperatures of the inner mesh points, the surface heat flux is obtained from a heat balance for a boundary control volume. The finite difference approach and the method of calculating the surface heat flux are outlined in Appendix B.

Ahluwalia et al (1985) suggested generating quenching curves by calculating the surface heat flux utilizing the radial temperature gradient at the inner (quenched) surface. The radial temperature distribution was obtained by fitting a third order polynomial through four radial measurements and extrapolating the fitted curve to the inner surface. This approach resulted in unusually high values of the maximum heat flux as compared to other investigations. Figure 5-22 shows a comparison between two quench curves, one obtained by the present two-dimensional model and the second by the approach suggested by Ahluwalia et al (1985). The quench curve obtained by the present two-dimensional model was generated by imposing the inner and outer surface temperatures and solving for the inner mesh points. Then, surface heat fluxes were obtained by conducting a heat balance on the inner boundary cells. The quench curve predicted by the approach

suggested by Ahluwalia et al (1985) was obtained by calculating the surface heat fluxes from the radial temperature gradients at the inner surface. This was done by utilizing the inner mesh temperatures which were obtained by the present two-dimensional model. Four radial locations, identical to those at which temperatures were measured during the experiments conducted by Ahluwalia, were used to fit the third order polynomial. Figure 5-22 shows that the calculated heat flux by the present two-dimensional model is significantly lower than that predicted by the approach suggested by Ahluwalia et al (1985). The maximum heat flux predicted by the present two-dimensional model agrees with published data on maximum heat flux in flow boiling.

It is expected that the surface heat flux predicted from radial temperature measurements (by calculating temperature gradients at the inner surface) to be very sensitive to the method of fitting the data. The above analysis indicates that the method suggested by Ahluwalia et al (1985) overpredicts the heat flux in the transition and nucleate boiling regions significantly. Moreover, using radial temperature gradients would introduce significant uncertainties in calculating surface heat flux in the inefficient heat transfer regimes like film boiling since the temperature is almost uniform in the radial direction due to slow cooling.

A more practical method of obtaining quench curves for thick tubes could be achieved by using the lumped approach, i.e., equation 5.4, for which the average transient tube temperature is calculated by integrating the transient radial temperature distribution. This was done for the 2 mm wall thick tube tested in the present study by

obtaining a third order polynomial least square fit first, then integrating over the wall thickness to obtain the mean temperature.

The effect of initial tube temperature is shown in figure 5-23. The apparent quench temperature increases as the initial wall temperature increases. Also, the maximum heat flux and surface heat flux in the transition boiling region will be higher. No significant effect in the nucleate boiling region was observed.

The effect of the inlet flow rate and inlet water subcooling is shown in figures 5-24 and 5-25 respectively. Increasing either parameter clearly reduces the duration of the film boiling region. Hence the apparent quench temperature will be higher leading again to an increase in the maximum heat flux and surface heat flux in the transition boiling region, with no significant effect in the nucleate boiling region.

For a given experimental run, the heat transfer characteristics of the rewetting process can vary at different axial locations as the local flow conditions e.g. liquid subcooling, will change along the tube. Figure 5-26 shows the quench curves derived from the temperature transients at different axial locations. As shown, the maximum heat flux and surface heat flux in the transition region decreased with increasing axial distance from the inlet. This is also associated with an increase in the duration of the film boiling period as well as a decrease in the apparent quench temperature. The above changes along the tube are the result of local subcooling decrease.

The quenching characteristics at different circumferential locations are shown in figure 5-27. The film boiling period decreases

as the circumferential distance from the bottom increases. This leads to an increase in maximum heat flux and transition boiling heat flux. Although well established film boiling regions can be observed near the bottom side of the tube, the top part of the tube appears not to experience a significant film boiling duration. Quenching the upper part of the tube is delayed until it is reached by the rising water inventory.

Figure 5-28 shows the axial heat conduction term, i.e.,

$$\left[\frac{D_o^2 - D_i^2}{4 D_i} \left(\frac{k}{U^2} \frac{\partial^2 T}{\partial \tau^2} \right) \right]$$

for the top and bottom quench curves presented in figure 5-27. This indicates that following the initiation of surface quenching, the axial heat conduction is characterized by two distinguished negative and positive zones. The negative zone identifies the transition boiling regime when the net axial heat conduction into the tube element is negative since the tube temperature gradient increases in this period. In other words, the net axial heat conduction out the tube element is positive because as the surface rewets, the surface heat transfer increases drastically and heat is drawn by axial conduction from the hot downstream side. The positive zone identifies the nucleate boiling region when the net axial heat conduction into the tube element is positive since the tube temperature gradient decreases in this regime. The transition point between these two zones at which axial heat conduction is zero, identifies the tube wall temperature at which the maximum heat flux occurs. However, this analysis indicates that the

axial heat conduction is insignificant since it represents a very small fraction of the total heat flux, for example, it is less than 0.08% of the total heat flux for the case presented in figure 5-28. This agrees with the findings of Chen et al (1979).

Figure 5-29a shows the quench curve for a test run conducted on the 2 mm thick tube utilizing the extracted mean temperature as discussed earlier. Figure 5-29b shows the same case when the heat flux is plotted against time. Figures 5-30a and 5-30b shows the corresponding axial heat conduction curves. These curves, in general, are similar to those obtained for the thin tube (1 mm wall thickness).

The effect of tube wall thickness on the quench curve is shown in figure 5-31a . The same curves are reproduced in figure 5-31b to show heat flux against time. These figures show that for the same initial tube temperature, subcooling and flow rate, the heat flux as well as quenching time increases with tube wall thickness. Subsequently the rewetting velocity decreases as wall thickness increases as was discussed earlier in section 5-1.

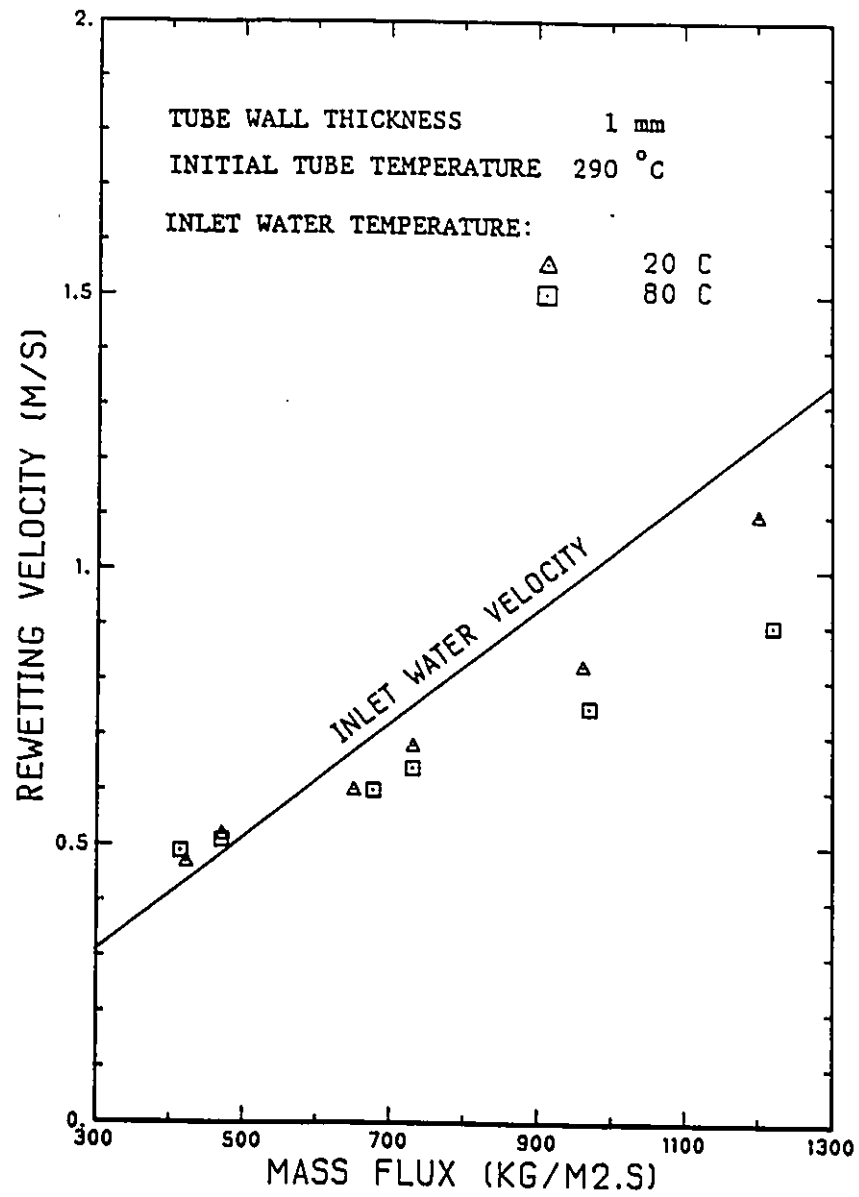


FIGURE 5-1 REWETTING VELOCITY VERSUS MASS FLUX

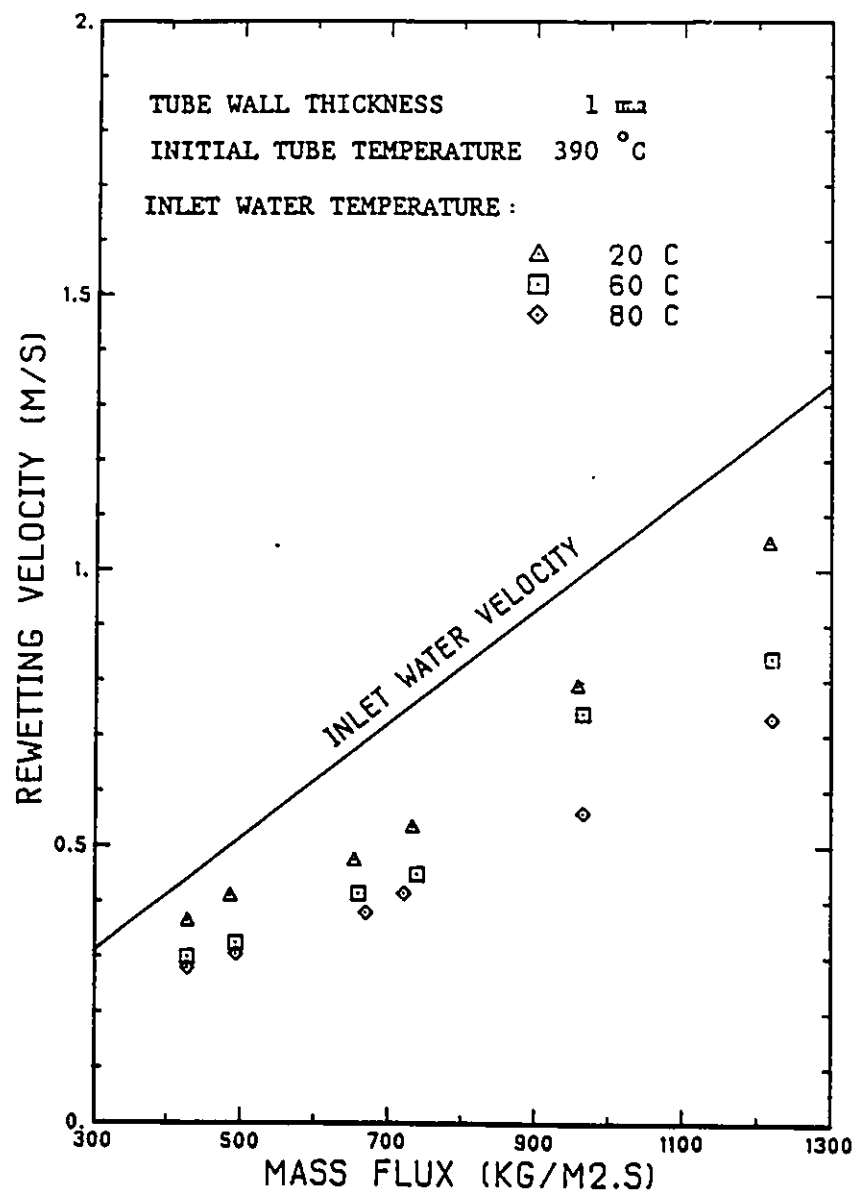


FIGURE 5-2 REWETTING VELOCITY VERSUS MASS FLUX

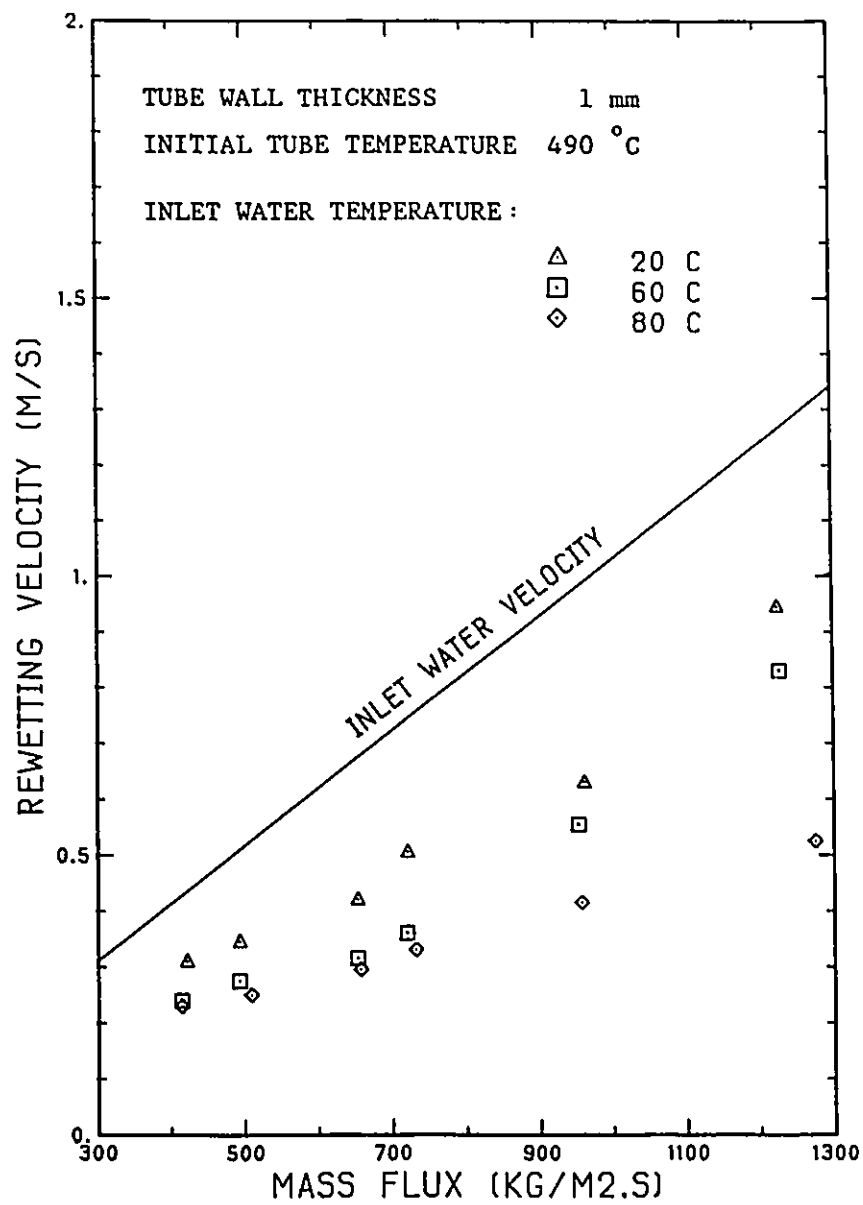


FIGURE 5-3 REWETTING VELOCITY VERSUS MASS FLUX

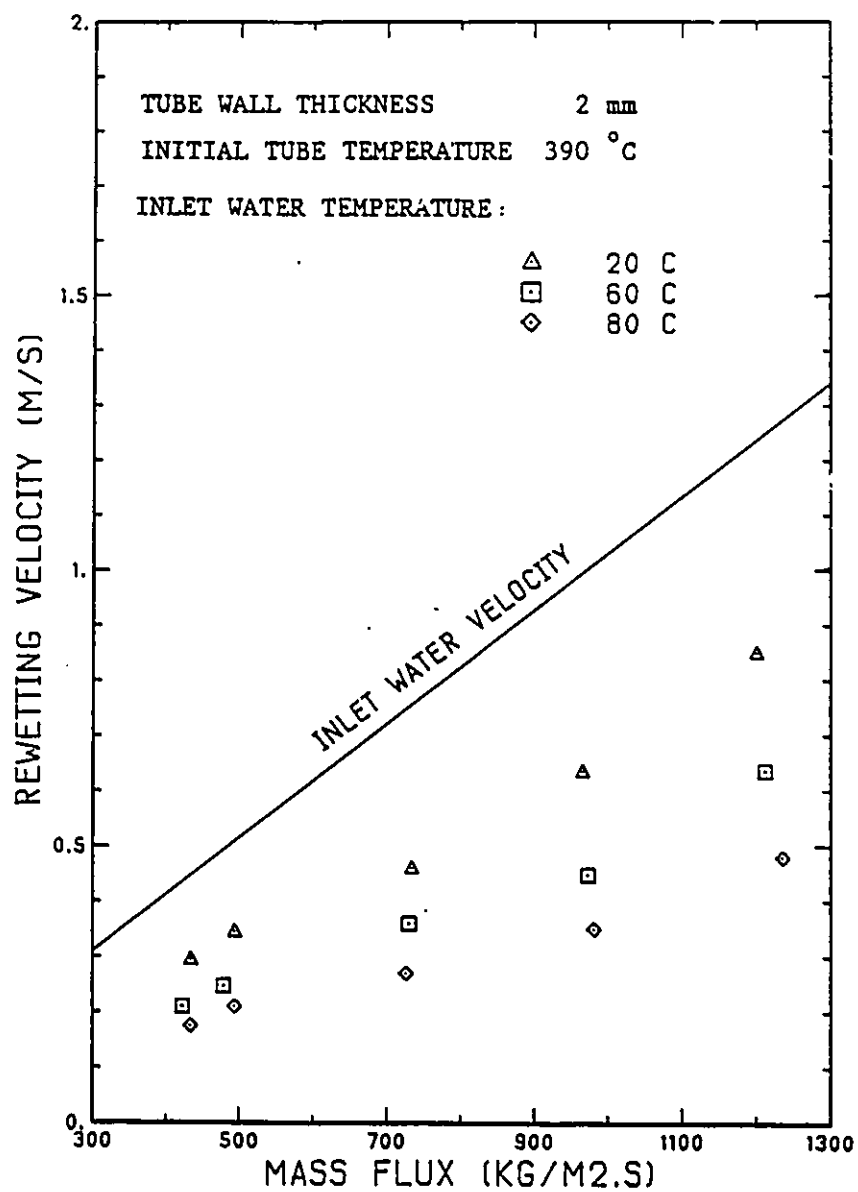


FIGURE 5-4 REWETTING VELOCITY VERSUS MASS FLUX

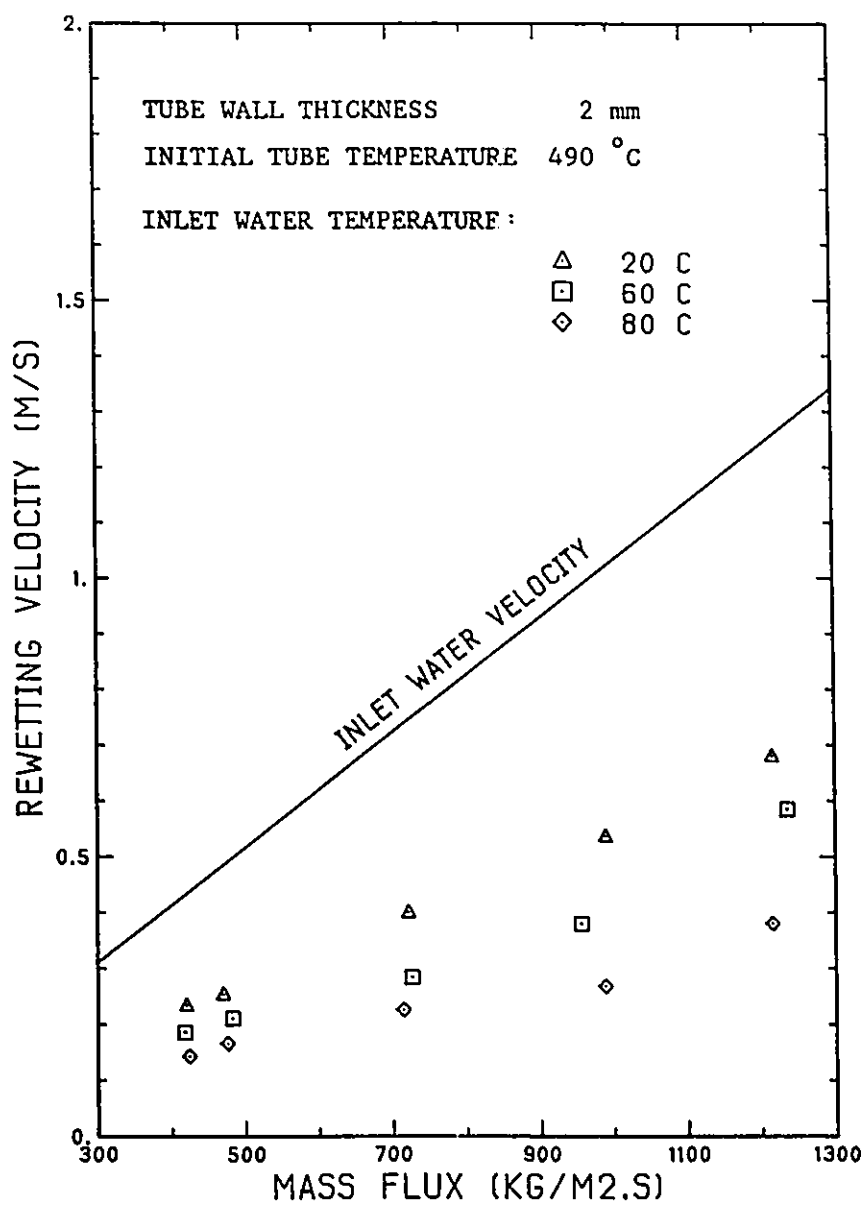


FIGURE 5-5 REWETTING VELOCITY VERSUS MASS FLUX

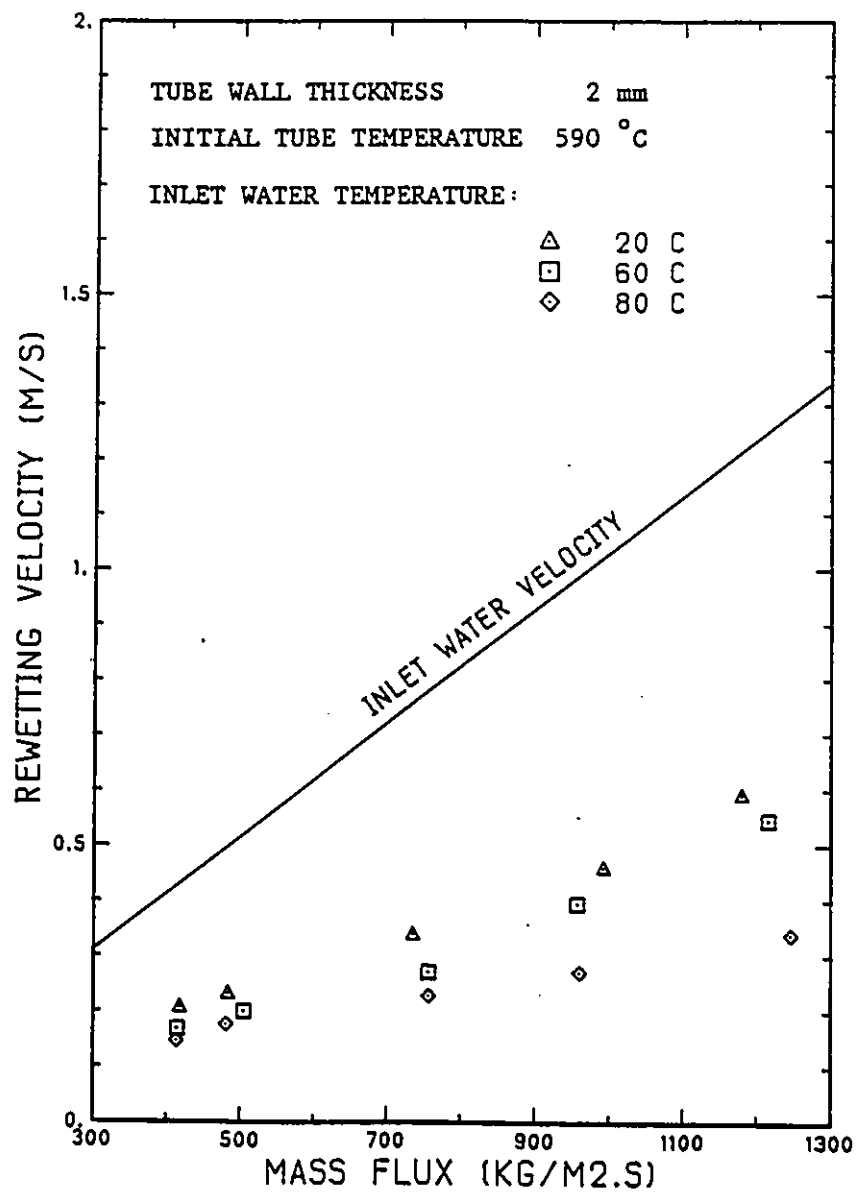


FIGURE 5-6 REWETTING VELOCITY VERSUS MASS FLUX

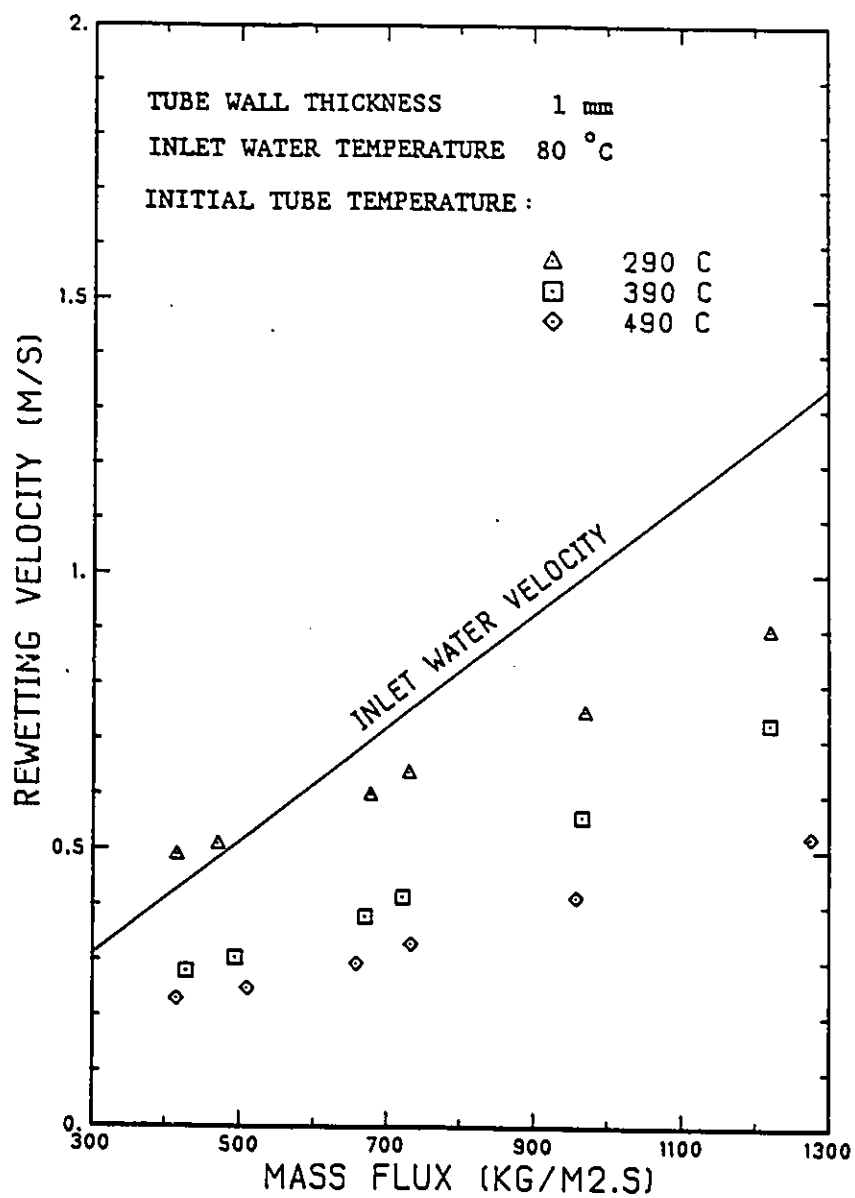


FIGURE 5-7 REWETTING VELOCITY VERSUS MASS FLUX

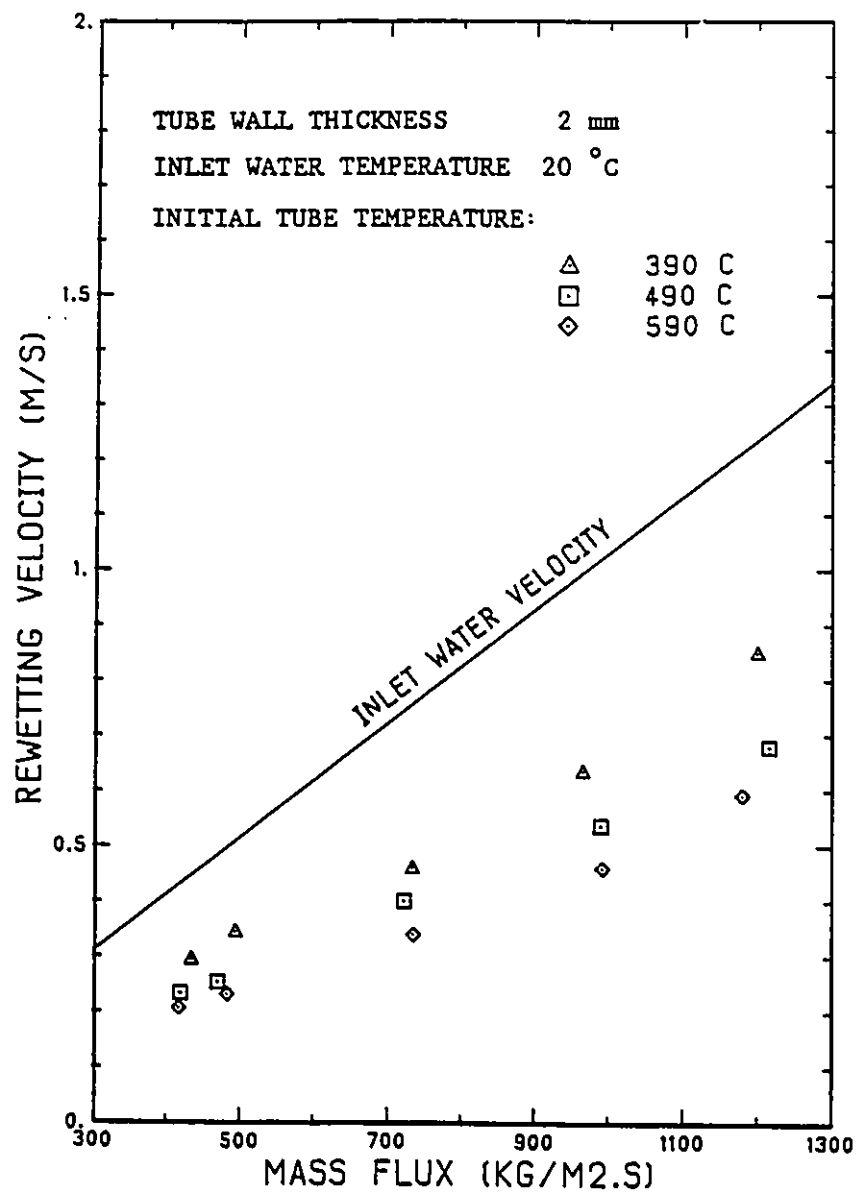


FIGURE 5-8 REWETTING VELOCITY VERSUS MASS FLUX

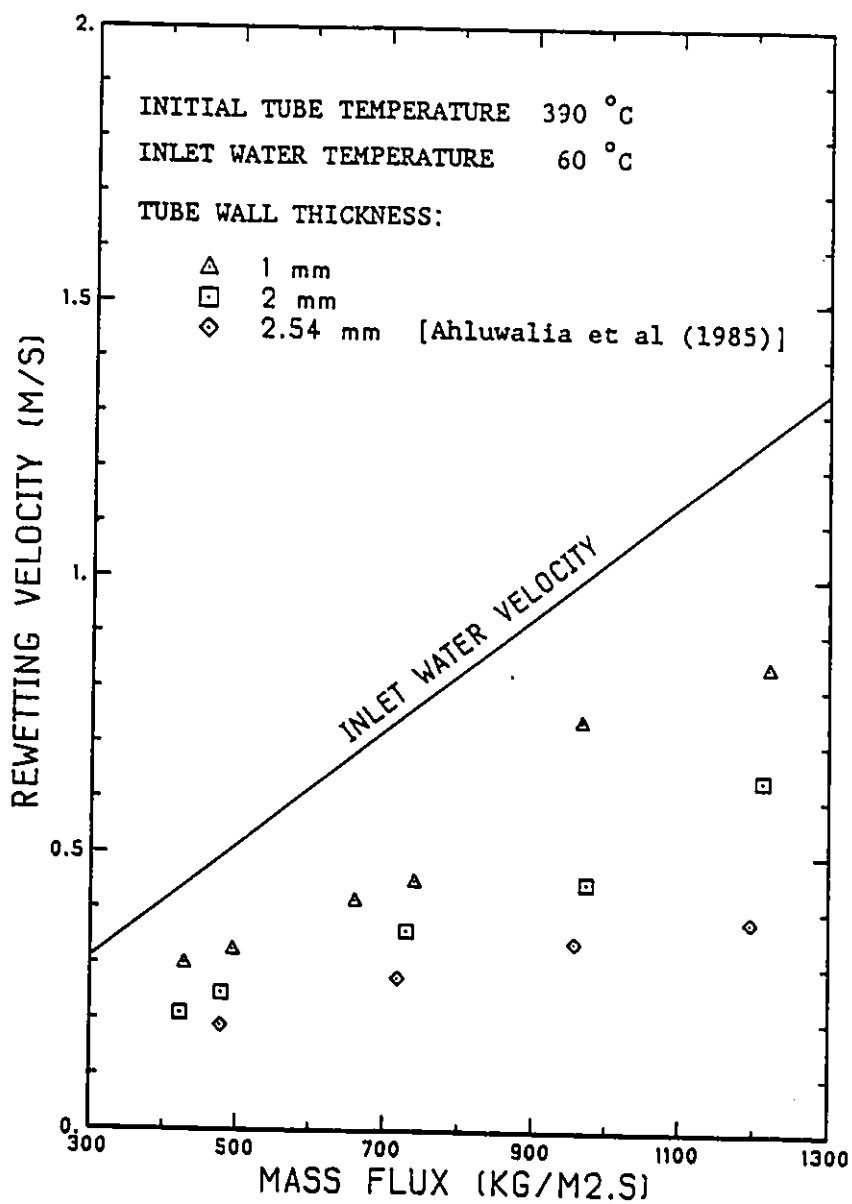


FIGURE 5-9 REWETTING VELOCITY VERSUS MASS FLUX

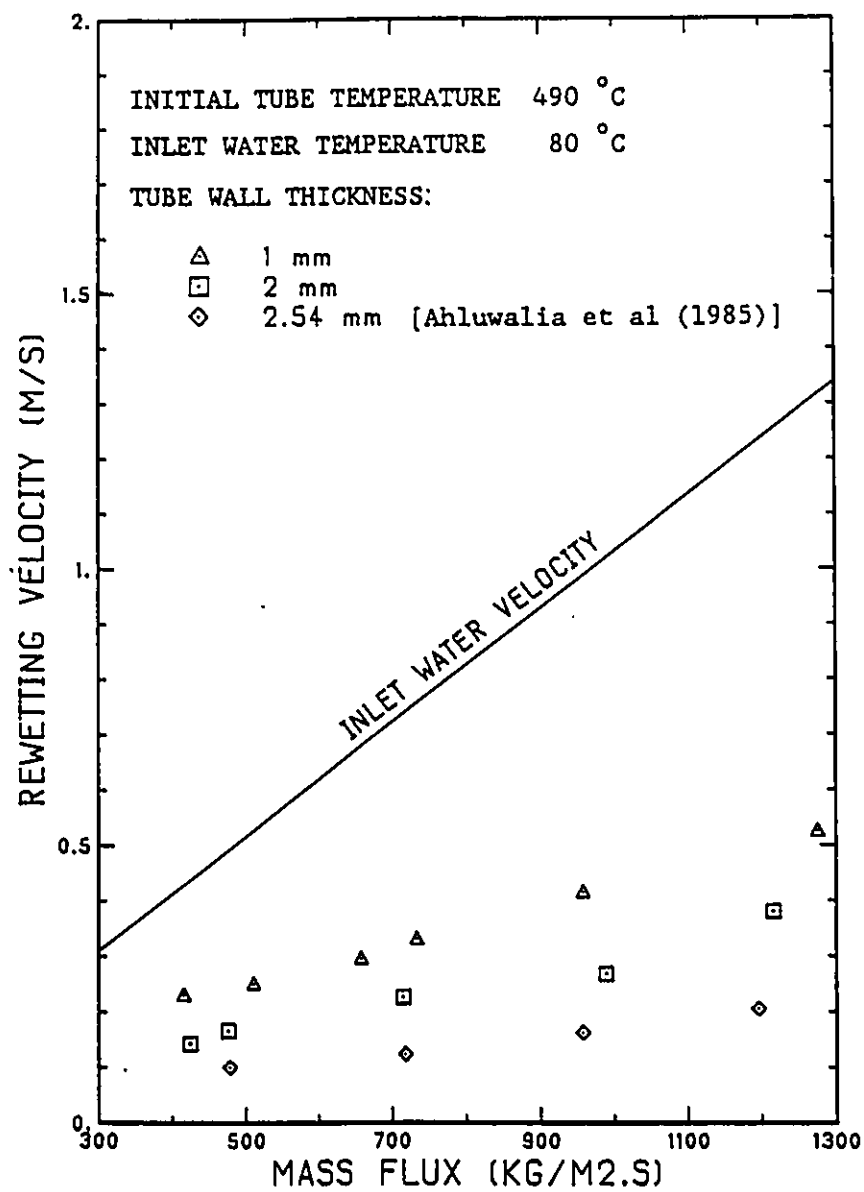


FIGURE 5-10 REWETTING VELOCITY VERSUS MASS FLUX

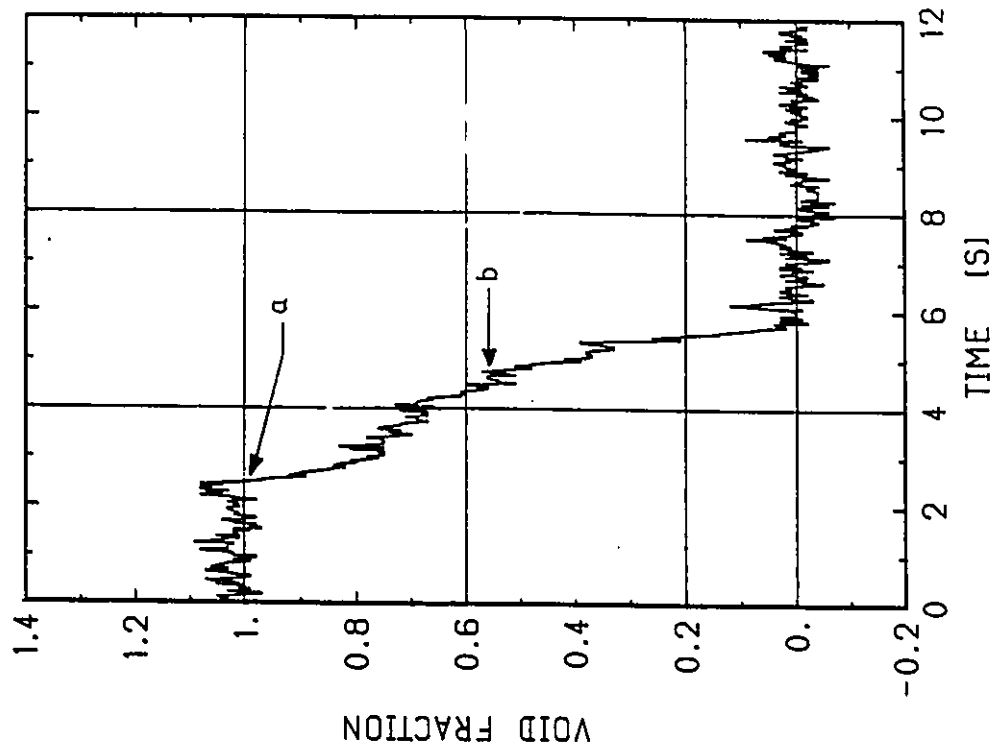


FIGURE 5-11b
TRANSIENT VOID FRACTION AT MODERATE
FLOW RATES.

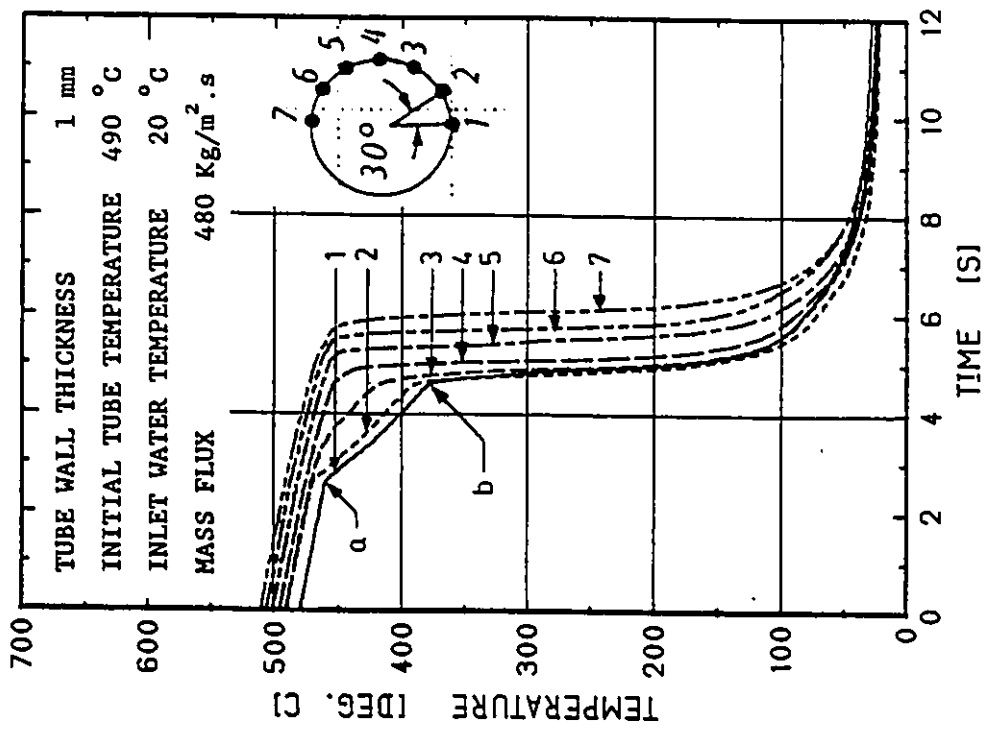


FIGURE 5-11a
TRANSIENT CIRCUMFERENTIAL TEMPERATURE
CURVES AT MODERATE FLOW RATES.

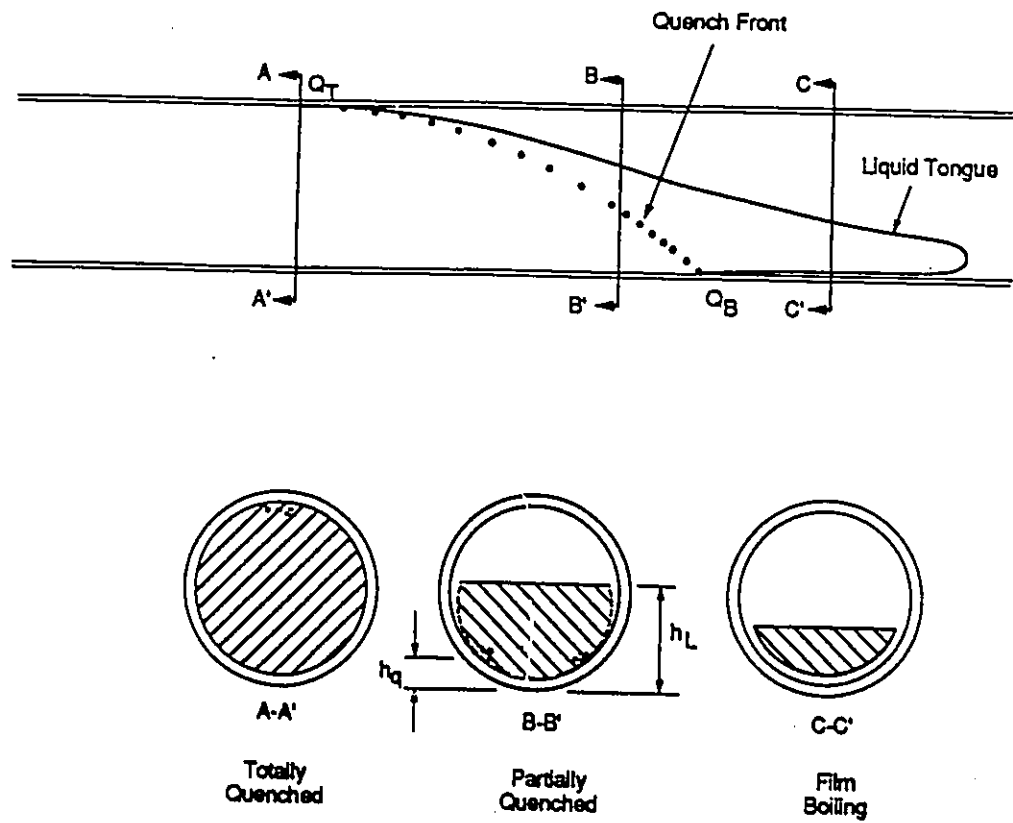


FIGURE 5-12 CHARACTERISTIC OF HORIZONTAL CHANNEL REWETTING AT MODERATE FLOW RATE

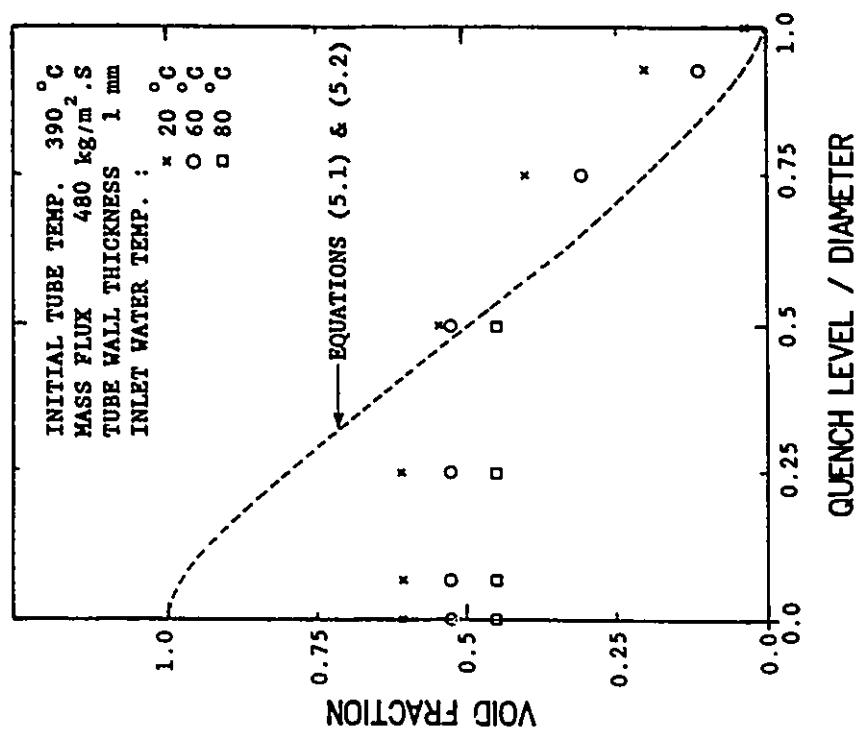


FIGURE 5-13

QUENCH LEVEL - VOID FRACTION VARIATION.

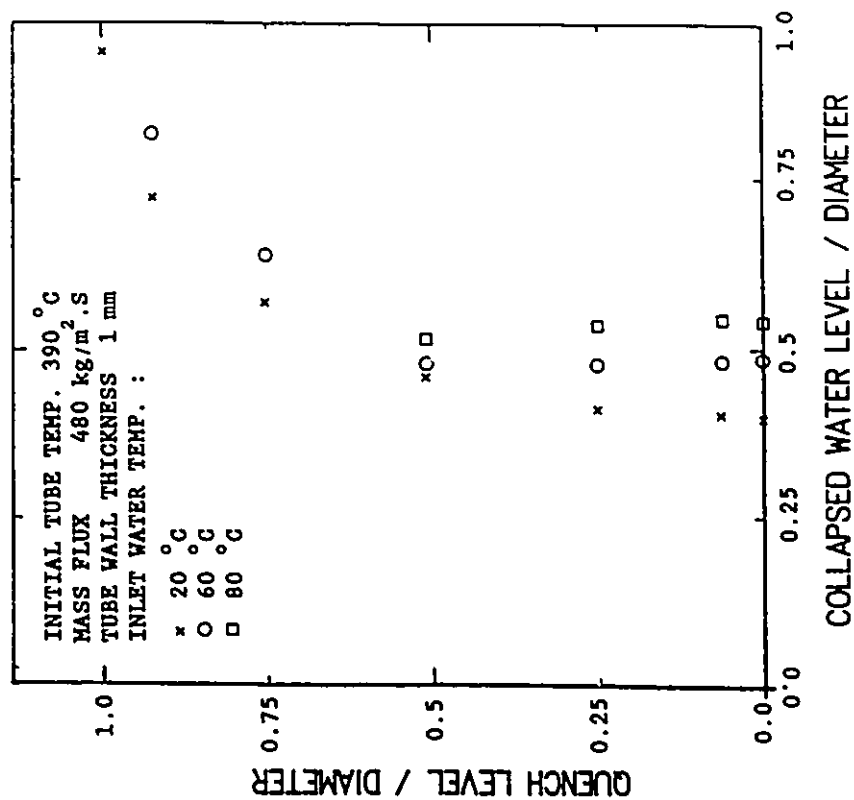


FIGURE 5-14

QUENCH LEVEL - WATER LEVEL VARIATION.

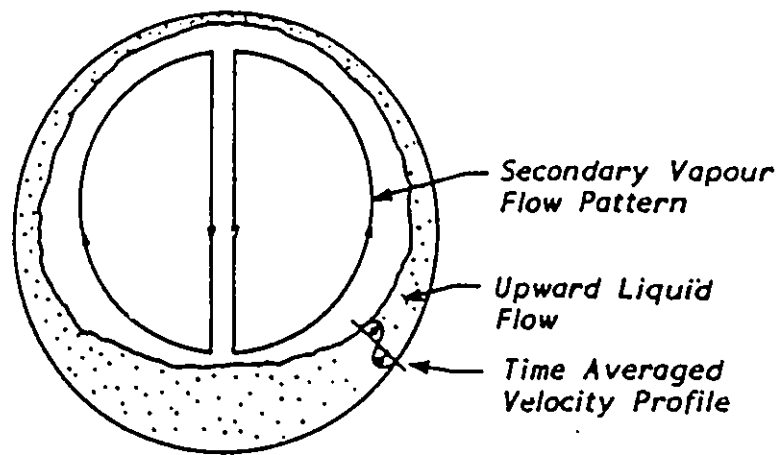
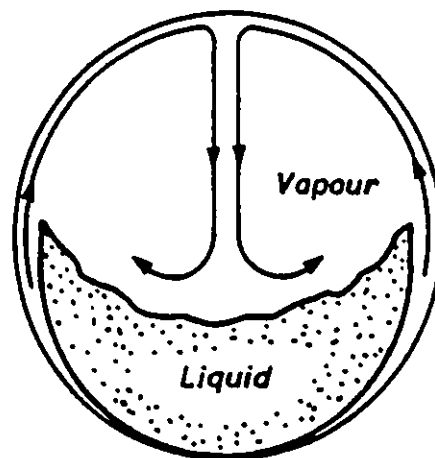


FIGURE 5-15A HORIZONTAL ANNULAR FLOW

FIGURE 5-15B SPECULATED SECONDARY VAPOUR FLOW DURING
REFILLING OF A HOT HORIZONTAL TUBE

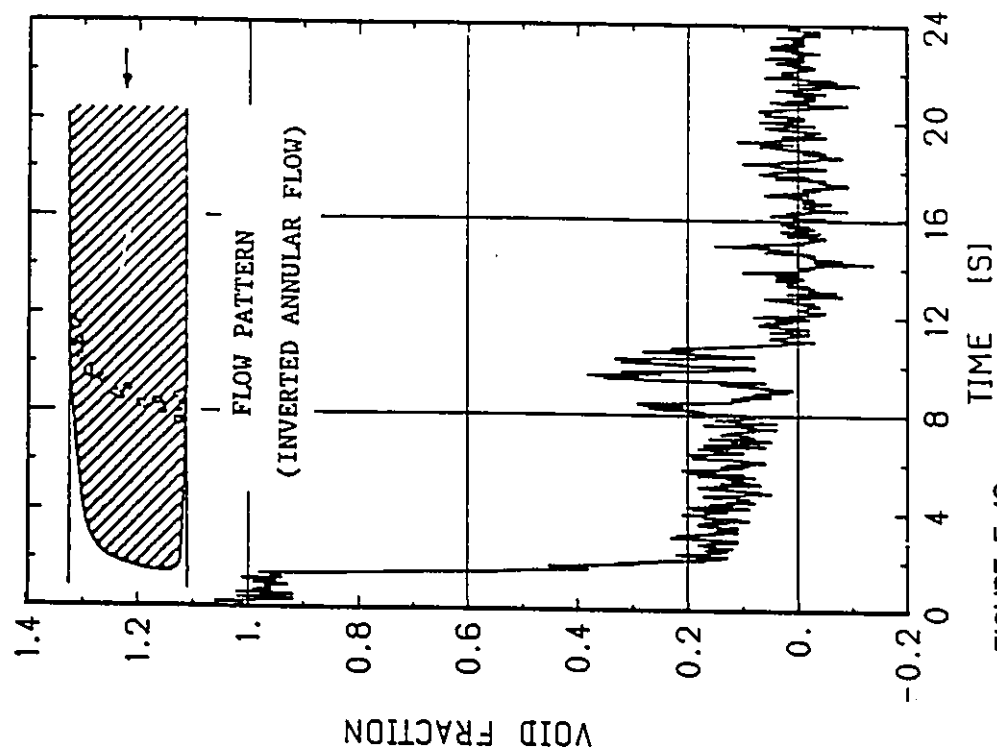


FIGURE 5-16B

TRANSIENT VOID FRACTION AT HIGH FLOW
RATES AND HIGH TUBE HEAT CAPACITY.

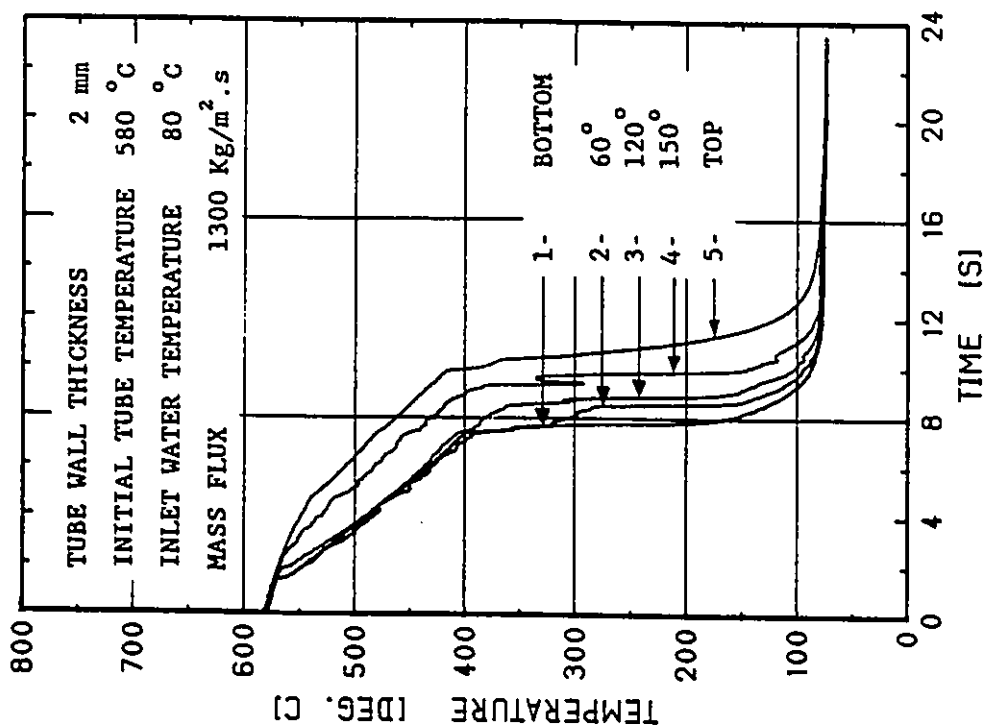


FIGURE 5-16A

TRANSIENT CIRCUMFERENTIAL TEMPERATURE
CURVES AT HIGH FLOW RATES AND HIGH
TUBE HEAT CAPACITY.

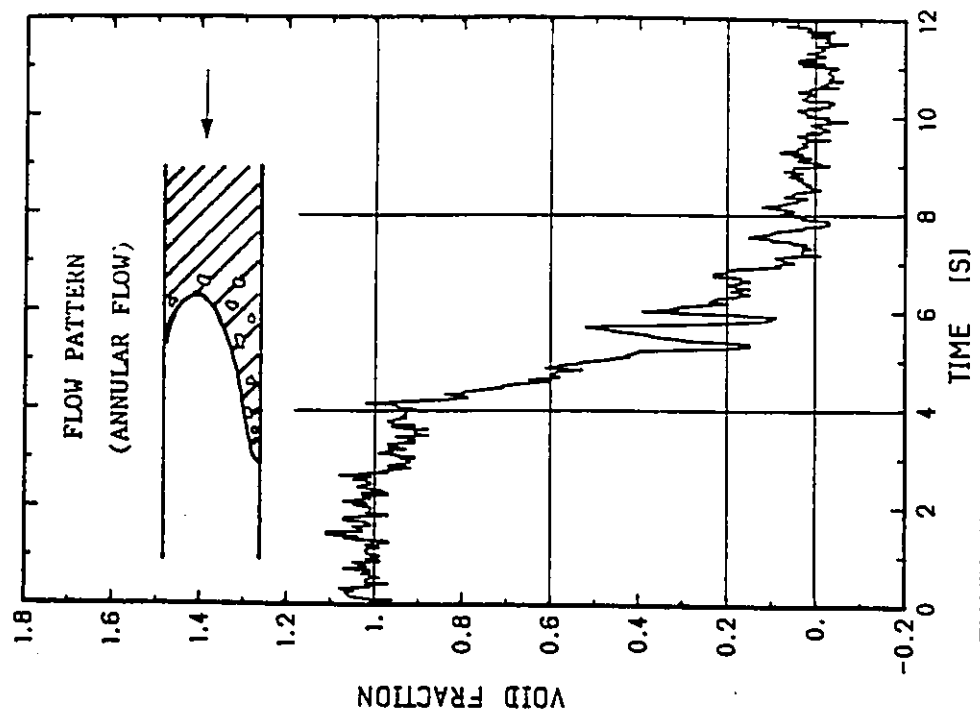


FIGURE 5-17B
TRANSIENT VOID FRACTION AT LOW FLOW
RATES AND LOW TUBE HEAT CAPACITY.

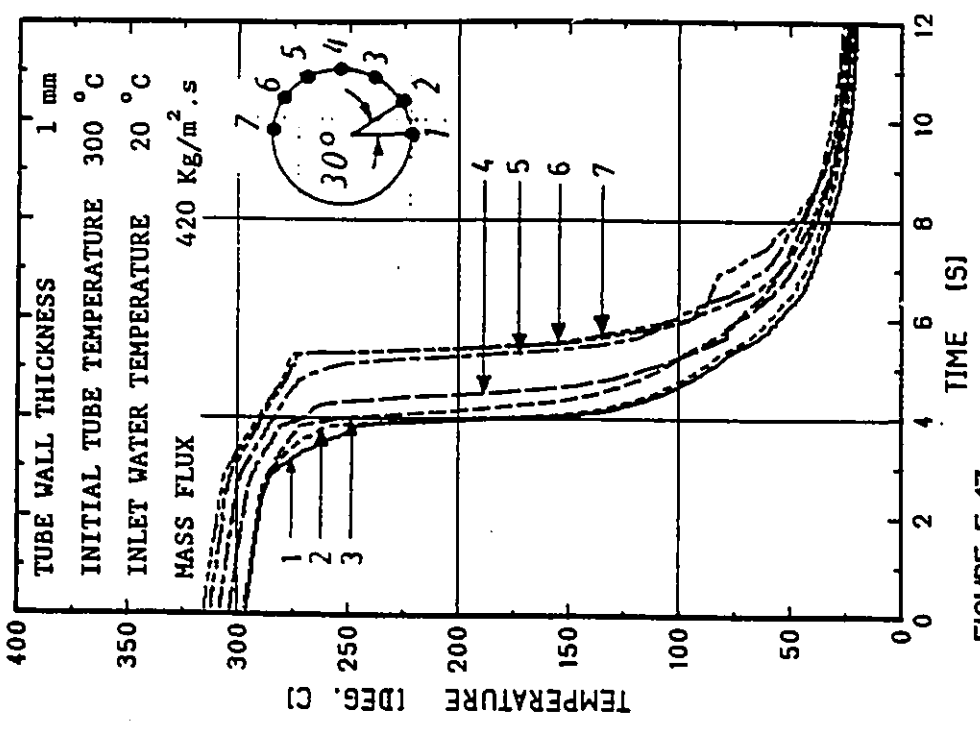


FIGURE 5-17A
TRANSIENT CIRCUMFERENTIAL TEMPERATURE
CURVES AT LOW FLOW RATES AND LOW TUBE
HEAT CAPACITY.

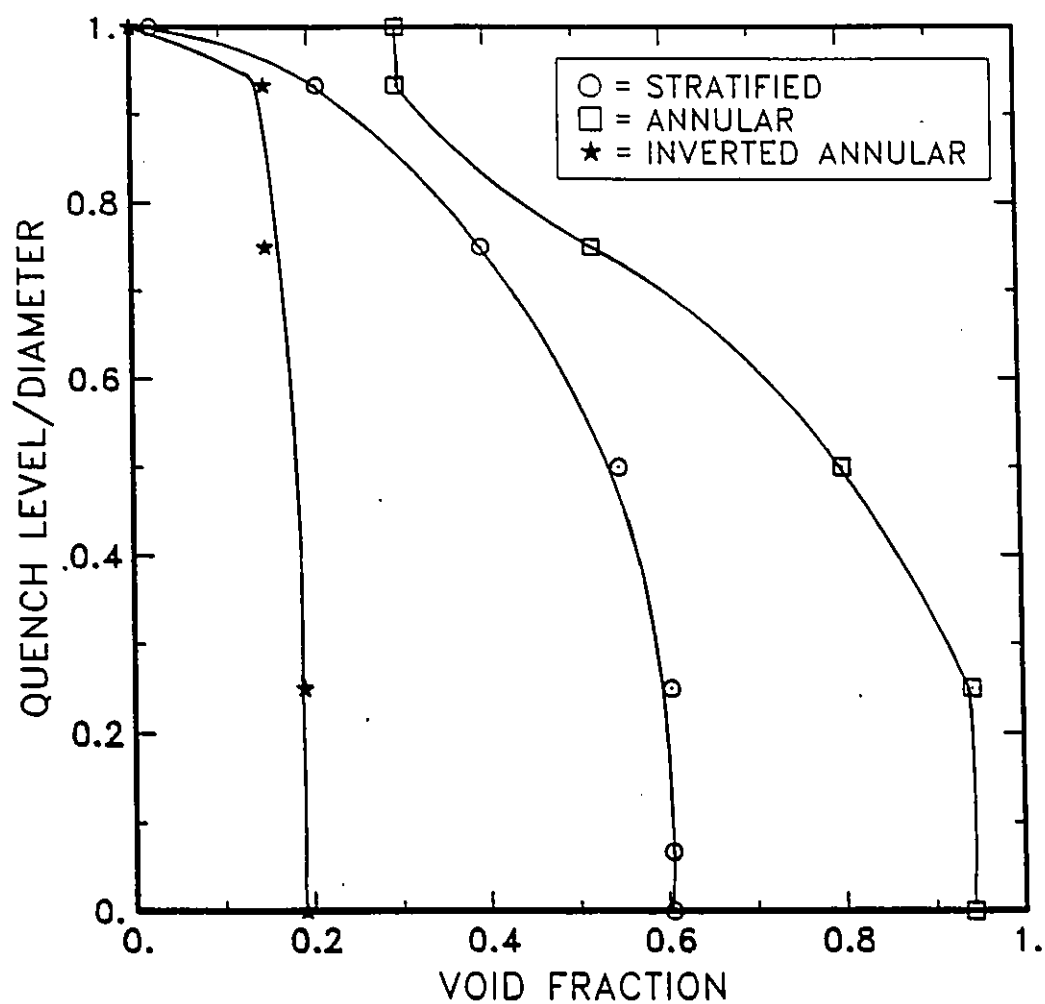


FIGURE 5-18 DIMENSIONLESS QUENCH LEVEL VERSUS VOID FRACTION FOR STRATIFIED, ANNULAR AND INVERTED ANNULAR FLOW REGIMES

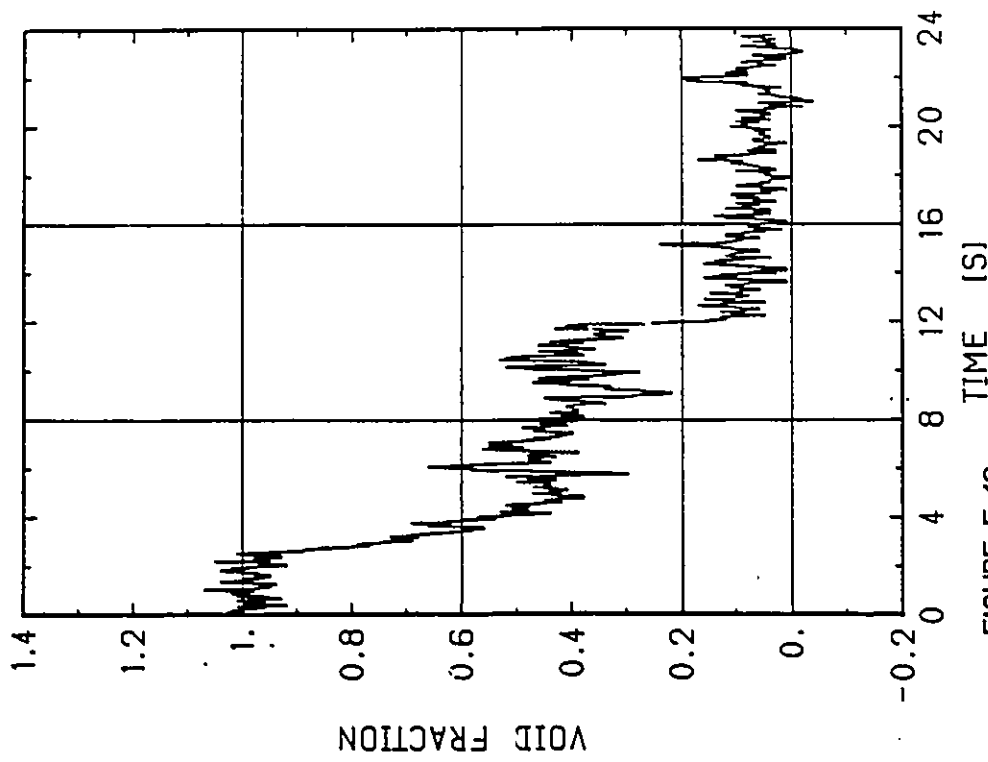


FIGURE 5-19B
TRANSIENT VOID FRACTION FOR THE
THICK TUBE.

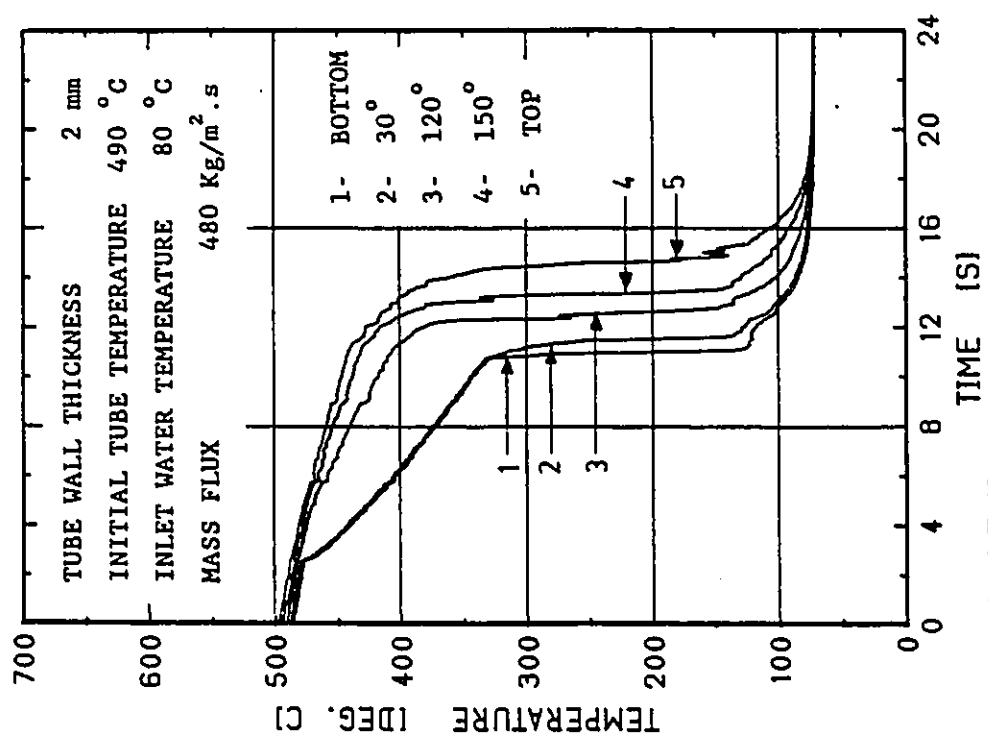


FIGURE 5-19A
TRANSIENT CIRCUMFERENTIAL TEMPERATURE
CURVES FOR THE THICK TUBE.

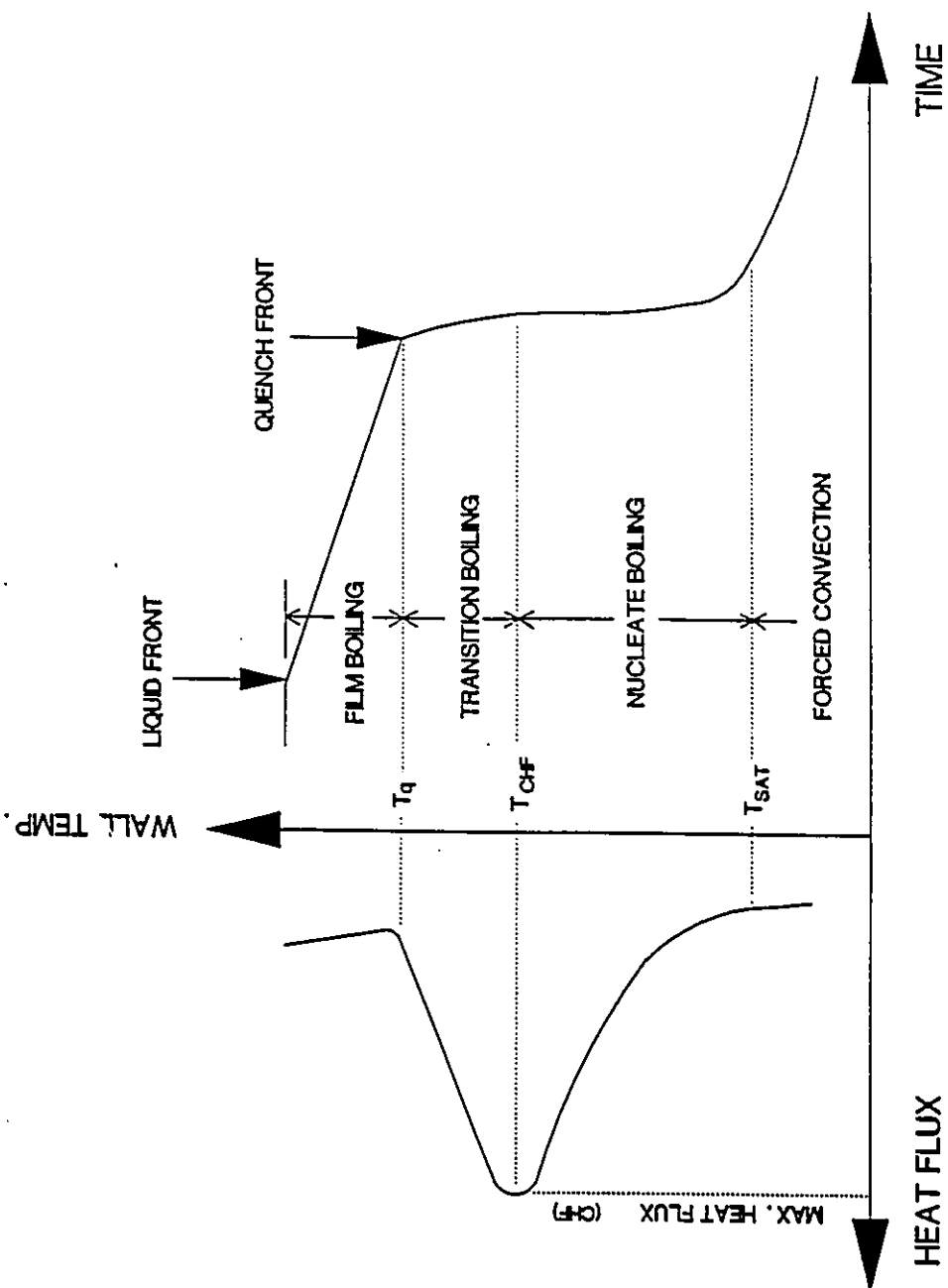


FIGURE 5-20 A TYPICAL QUENCH CURVE AND THE CORRESPONDING
TRANSIENT WALL TEMPERATURE

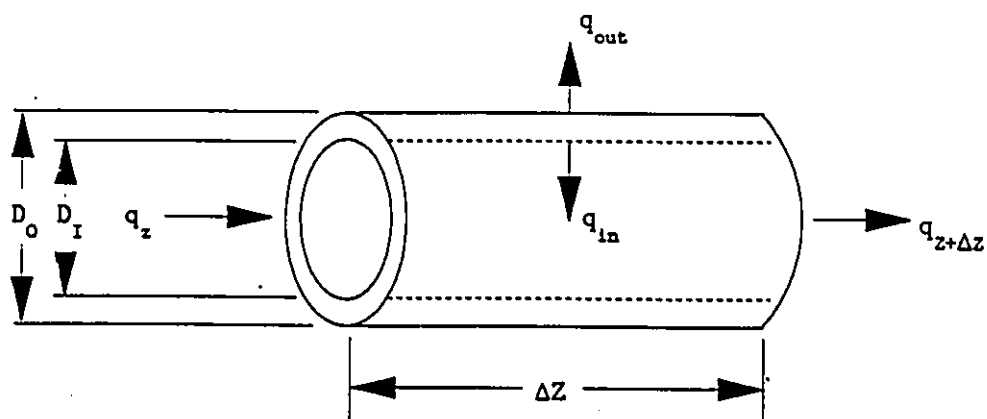


FIGURE 5-21 HEAT BALANCE ON AN ELEMENT OF THE TEST SECTION

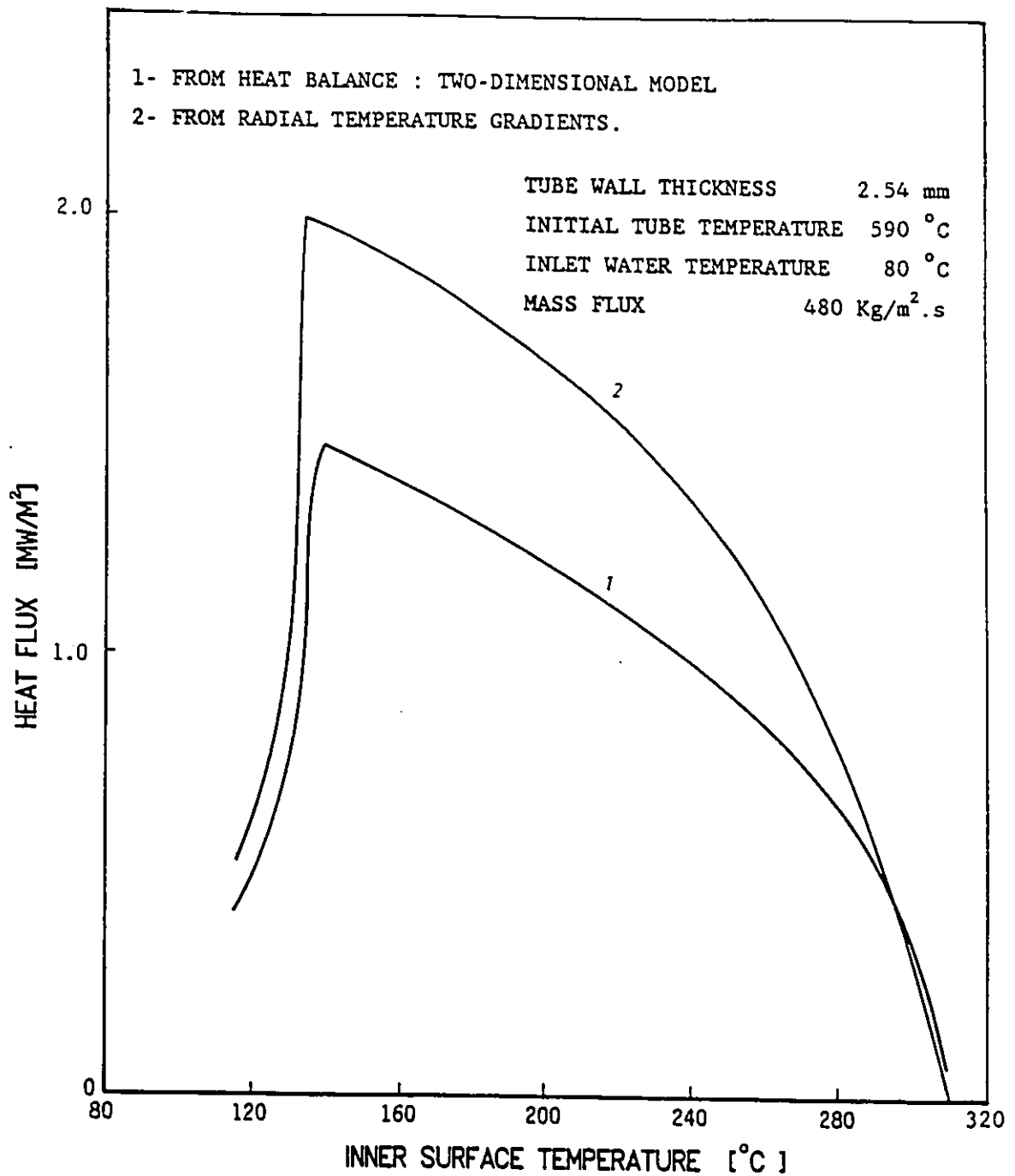


FIGURE 5-22 COMPARISON BETWEEN THE HEAT FLUX OBTAINED FROM HEAT BALANCE AND RADIAL TEMPERATURE GRADIENTS AT THE QUENCHED SURFACE.

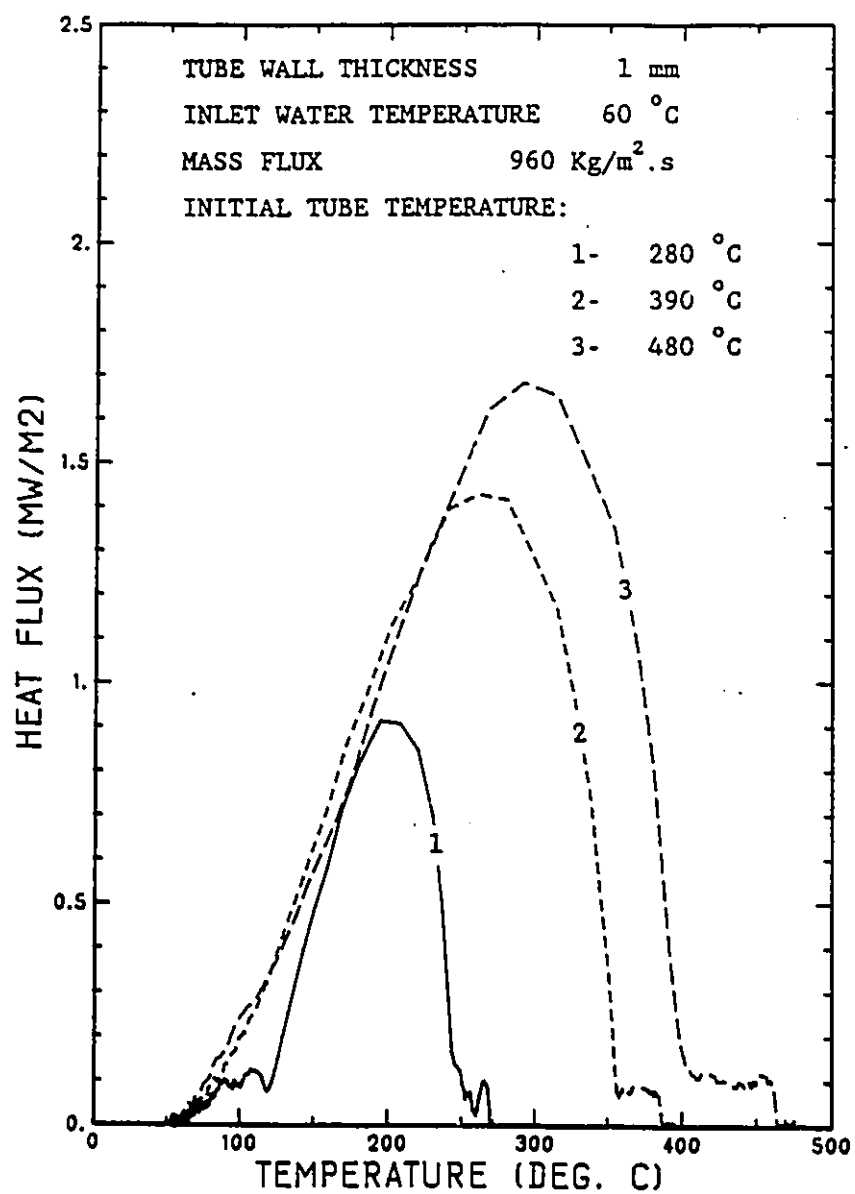


FIGURE 5-23 QUENCH CURVES : EFFECT OF INITIAL TUBE TEMPERATURE

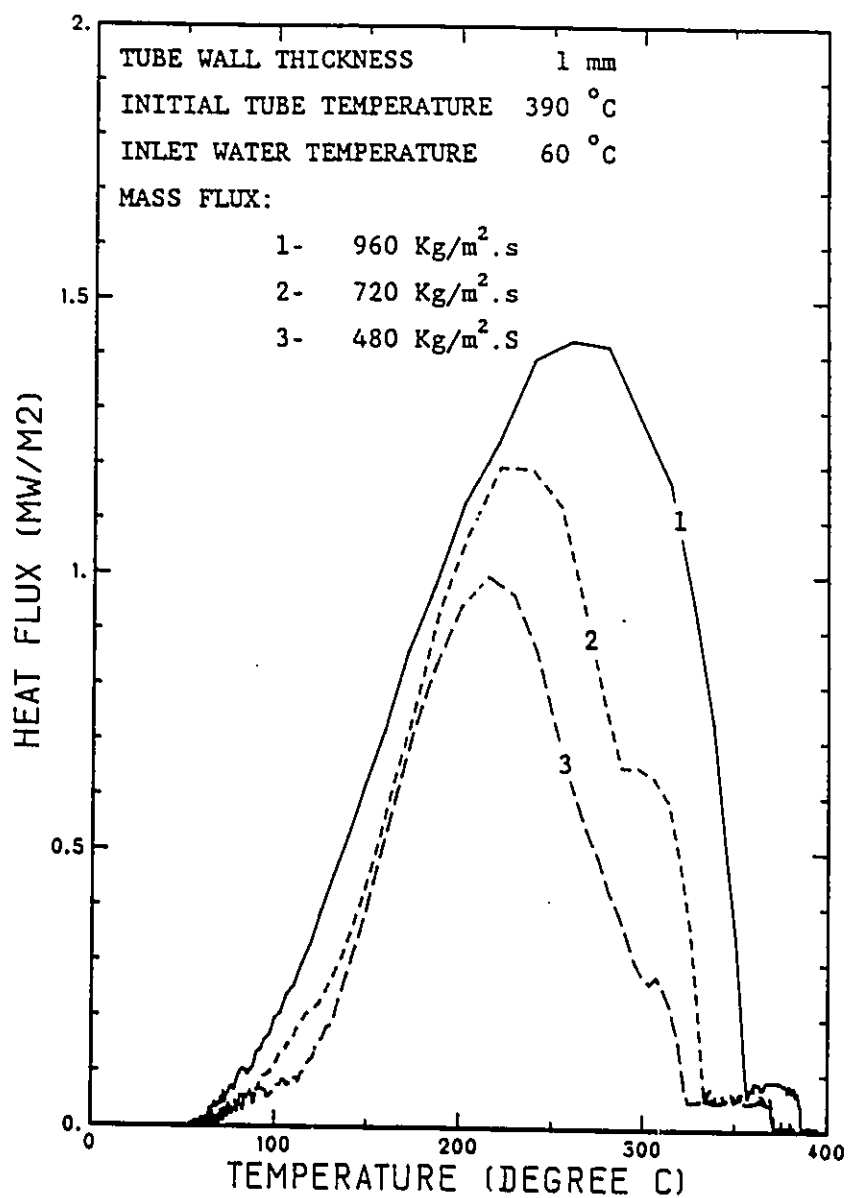


FIGURE 5-24 QUENCH CURVES : EFFECT OF MASS FLUX

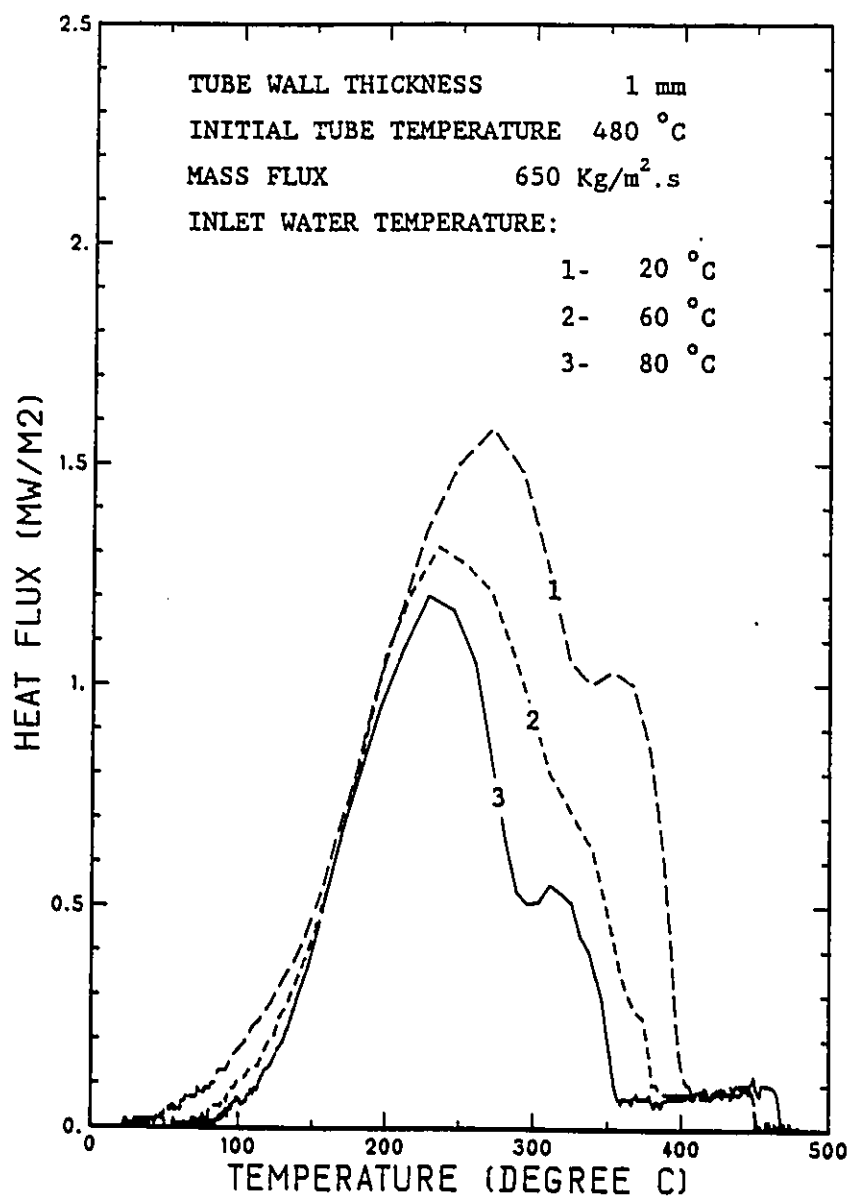


FIGURE 5-25 QUENCH CURVES : EFFECT OF SUBCOOLING

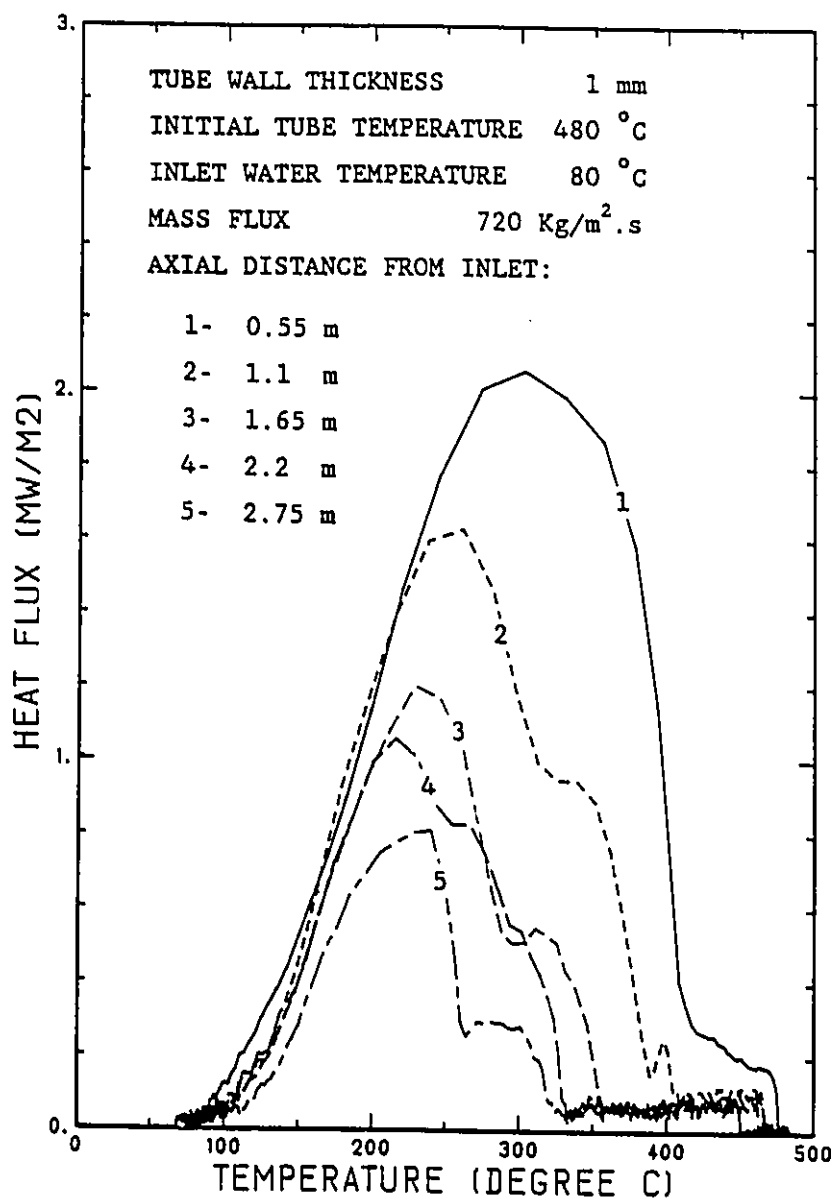


FIGURE 5-26 QUENCH CURVES : EFFECT OF AXIAL LOCATION

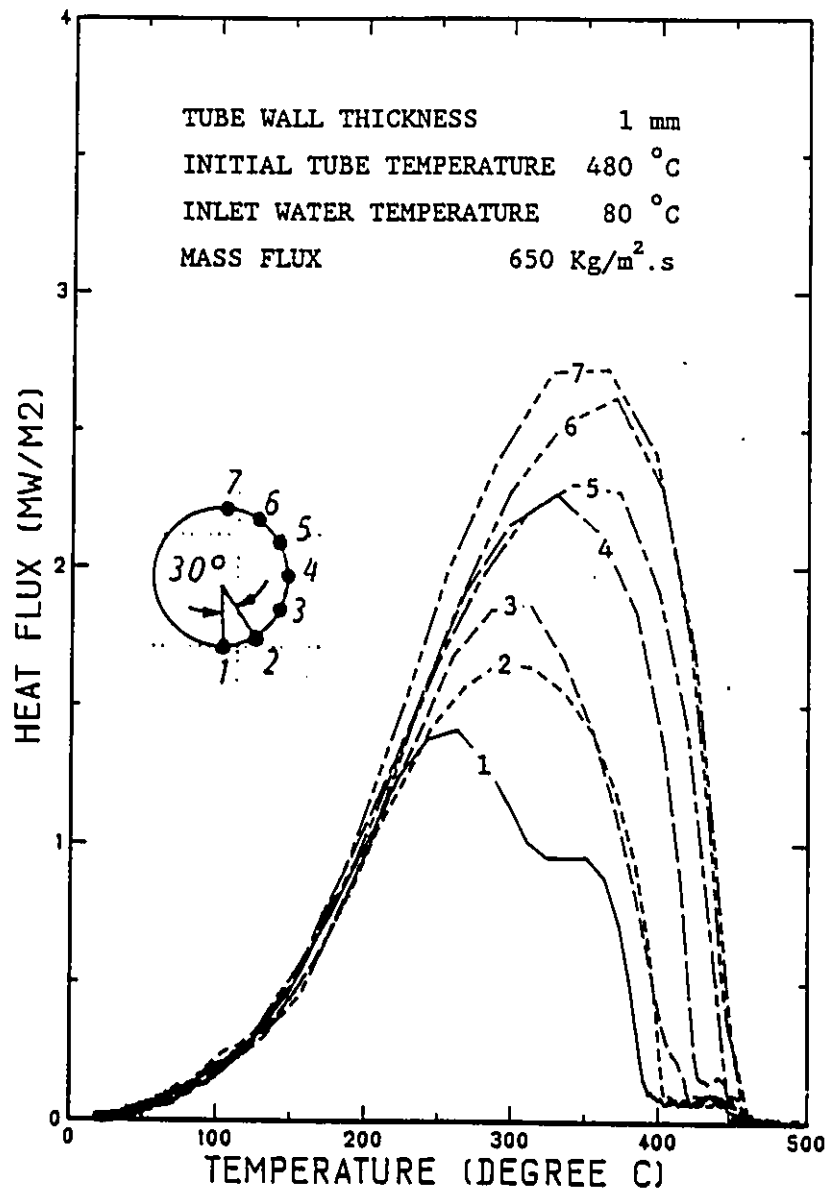


FIGURE 5-27 QUENCH CURVES : EFFECT OF CIRCUMFERENTIAL LOCATION

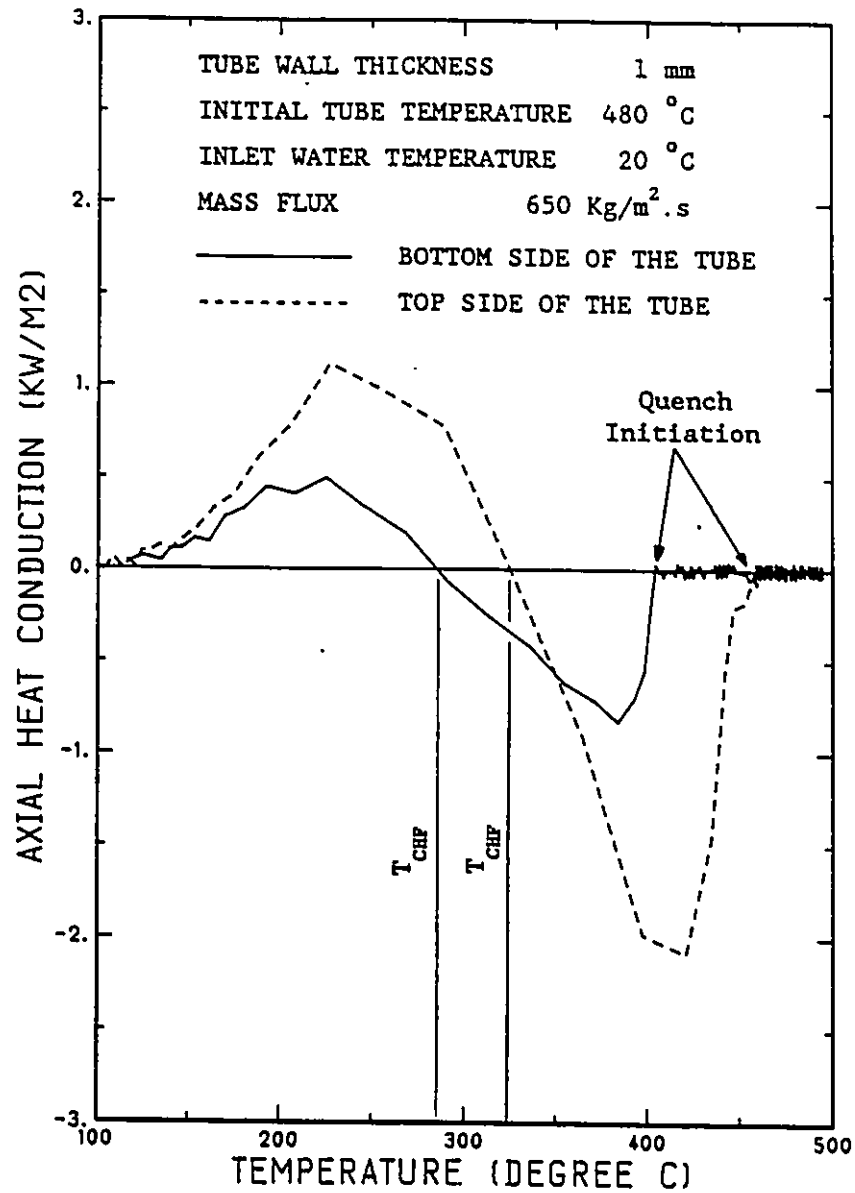


FIGURE 5-28 AXIAL HEAT CONDUCTION

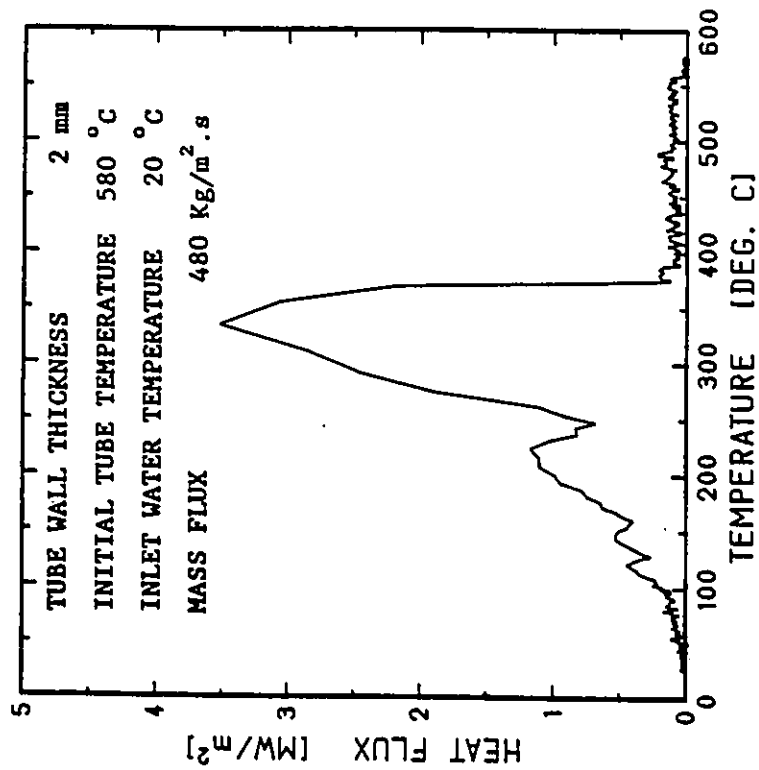


FIGURE 5-29A

QUENCH CURVE FOR THE THICK TUBE : HEAT FLUX
VERSUS TUBE TEMPERATURE.

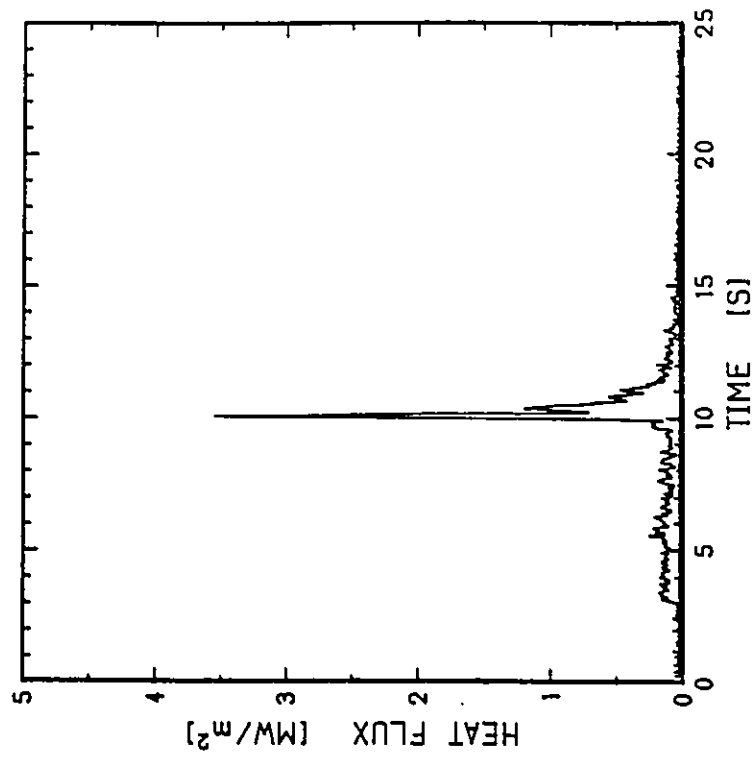


FIGURE 5-29B

QUENCH CURVE FOR THE THICK TUBE : HEAT FLUX
VERSUS TIME.

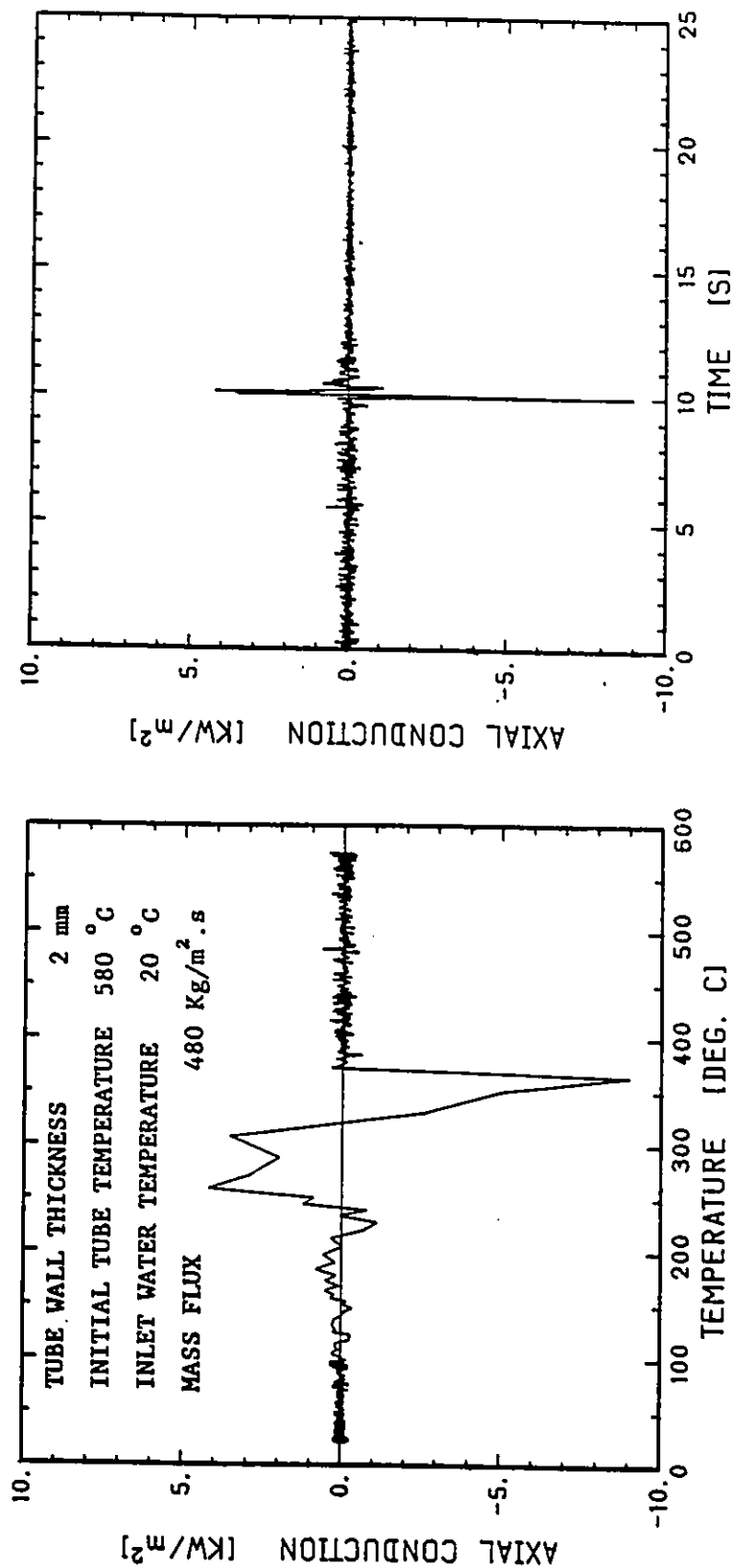


FIGURE 5-30a

AXIAL HEAT CONDUCTION FOR THE THICK TUBE :
HEAT FLUX VERSUS TUBE TEMPERATURE.

FIGURE 5-30b

AXIAL HEAT CONDUCTION FOR THE THICK TUBE :
HEAT FLUX VERSUS TIME.

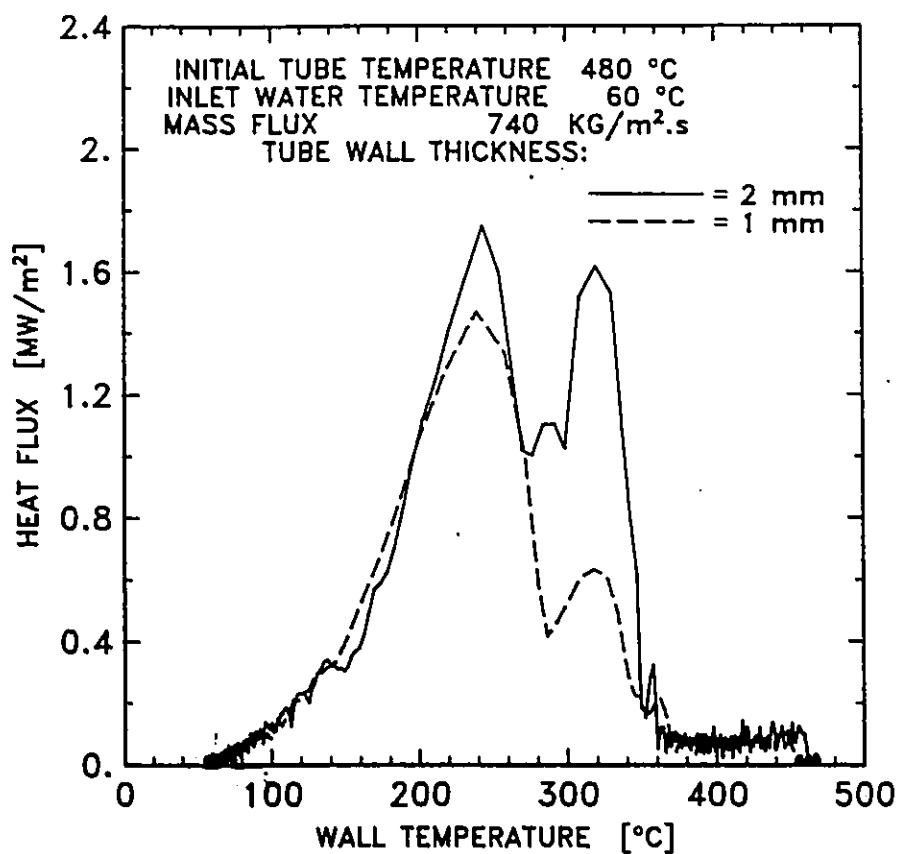


FIGURE 5-31A

EFFECT OF TUBE WALL THICKNESS ON THE QUENCH
CURVE : HEAT FLUX VERSUS TUBE TEMPERATURE.

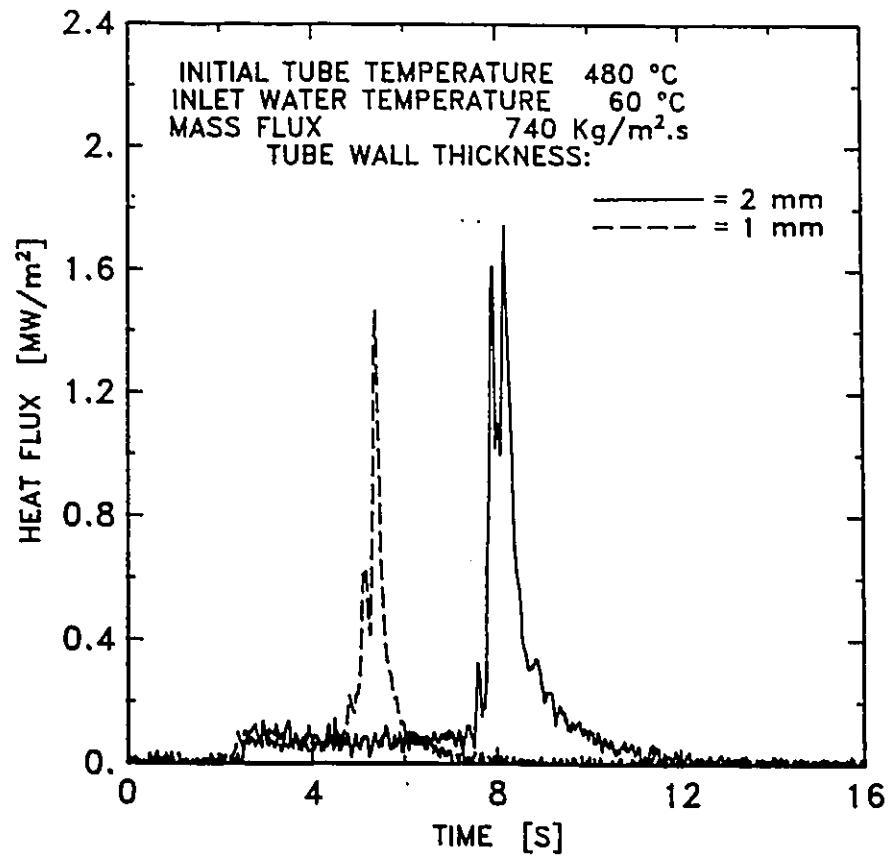


FIGURE 5-31B

EFFECT OF TUBE WALL THICKNESS ON THE QUENCH
CURVE : HEAT FLUX VERSUS TIME.

CHAPTER 6

SURFACE REWETTING

Surface rewetting is the re-establishment of continuous liquid contact with a dry hot surface. This phenomenon is usually identified by the temperature at which surface rewetting occurs. There is no universally accepted definition of the rewetting temperature. This temperature has been called Leidenfrost, sputtering, minimum film boiling or quenching temperature. Surface rewetting is usually associated with high heat transfer rate which results from the transition from stable film boiling to transition and nucleate boiling. Accordingly, it is very important to identify the mechanisms and conditions under which surface rewetting is accomplished.

6-1 BACKGROUND:

Literature on the mechanisms and conditions at which surface rewetting occurs has been reviewed. It can be divided into three categories, namely surface rewetting by i) small mass of liquid (Leidenfrost phenomena) ii) pool of liquid and iii) flowing liquid.

6-1-1 LEIDENFROST TEMPERATURE.

The earliest experimental investigations related to surface rewetting involved measuring the Leidenfrost temperature which is commonly defined as the surface temperature at which a "small" droplet

floating on a vapour film over a hot surface will collapse and come in contact with the wall. More accurately, it is the solid surface temperature corresponding to the maximum evaporation time for a liquid droplet in the spheroidal state. In measuring this temperature, the time needed for the liquid droplet to evaporate is plotted against the corresponding solid surface temperatures as shown in figure 6-1. If the solid surface temperature is below the Leidenfrost temperature, nucleate and transition boiling occur and the droplet vaporization time is very short. For solid surface temperatures greater than the Leidenfrost temperature, film boiling occurs and the droplet vaporization time is longer than that for transition and nucleate boiling.

Bell (1967) conducted a survey on the Leidenfrost phenomena. He reported that for a given liquid the range of Leidenfrost temperatures obtained by various investigators was rather wide depending on their respective experimental conditions.

Baumeister and Simon (1973) reported that the wall property group $(k\rho C)_w$ is an important parameter which affects the Leidenfrost temperature, where k is thermal conductivity, ρ is density and C is specific heat. For a given fluid, the higher the value $(k\rho C)_w$ of the surface, the lower the measured Leidenfrost temperature. For example, the measured Leidenfrost temperature of a saturated 0.032 ml water droplet on a stainless steel surface was 285 °C while it was 500 °C on a pyrex glass surface. The authors also reported that increasing the surface roughness led to higher Leidenfrost temperatures. For example, the measured Leidenfrost temperature of a saturated 6 ml water drop on

aluminum surface was increased from 235 °C to 265 °C by increasing the surface roughness from 3-4 root mean square to 25 root mean square.

Experimental investigations conducted by Baumeister et al (1966) and Wacthers et al (1966) showed that following a very careful procedure to suppress disturbances and using extremely smooth surfaces resulted in very low Leidenfrost temperatures. Baumeister et al (1966) reported Leidenfrost temperatures close to saturation and Wacthers et al (1966) reported Leidenfrost temperatures even lower than saturation temperature.

In a recent study, Avedisian and Koplik (1987) measured the Leidenfrost temperature of methanol droplets on a polished stainless steel surface and three ceramic alumina surfaces of 10%, 25% and 40% porosity. It was found that the Leidenfrost temperature increased as surface porosity increased. The measured Leidenfrost temperatures for the polished stainless steel surface, 10% and 25% porous ceramic alumina surfaces were 170 °C, 297 °C and 372 °C respectively.

6-1-2 MINIMUM FILM BOILING LIMIT IN POOL BOILING:

Extensive experimental and theoretical work has been conducted to define the conditions at which surface rewetting occurs in pool boiling. A hydrodynamic approach to the analysis of the boiling process became popular in the 1950's, where attempts to determine the minimum heat flux in film boiling (q_{\min} in the boiling curve which represents the onset of stable film boiling in temperature controlled systems) by purely hydrodynamic considerations were reported.

Chang (1957) was the first to point out that this phenomenon can be accompanied by waves on the vapour-liquid interface. Zuber (1958) utilized this approach, showed that the shape of the vapour-liquid interface can be described by Taylor's theory of stability and that vapour departs from standing wave nodal points in the form of spherical bubbles. He obtained the relationship

$$q_{\min} = 0.13 h_{fg} \rho_G \left[\frac{\sigma g (\rho_L - \rho_G)}{(\rho_L + \rho_G)^2} \right]^{1/4} \quad (6.1)$$

where σ is surface tension, h_{fg} is the latent heat of evaporation, and ρ_L and ρ_G are density of the liquid and vapour phases respectively.

The first attempt to define not only the minimum heat flux but also the corresponding minimum film temperature, was made by Berenson (1961). He combined the hydrodynamic concepts of Chang (1957) and Zuber (1958) with Bromley's approach for laminar film boiling. As a result, Berenson obtained

$$q_{\min} = 0.09 h_{fg} \rho_G \left[\frac{\sigma g (\rho_L - \rho_G)}{(\rho_L + \rho_G)^2} \right]^{1/4} \quad (6.2)$$

$$\Delta T_{\min} = 0.127 \frac{h_{fg} \rho_G}{k_L} \left[\frac{\sigma}{g(\rho_L - \rho_G)} \right]^{1/2} \left[\frac{\mu_L g(\rho_L - \rho_G)}{(\rho_L + \rho_G)^2} \right]^{1/3} \quad (6.3)$$

where $\Delta T_{\min} = T_{\min} - T_{SAT}$ and the constant 0.09 in equation 6.2 was adopted by the author on the basis of his own experimental data.

Lienhard and Wong (1964) examined q_{\min} and the dominant

length of the instability wave with film boiling on small diameter horizontal cylinder where surface tension affects the hydrodynamics of bubble formation. They obtained an expression that takes into account the influence of a characteristic surface dimension

$$q_{\min} = 0.16 \frac{h_{fg} \rho_G}{D} \left[\frac{\sigma^2}{g(\rho_L + \rho_G)} \right]^{1/4} \left[\frac{g(\rho_L - \rho_G)}{\sigma} + \frac{2}{D^2} \right]^{-1/4} \quad (6.4)$$

where D is the cylinder diameter.

The earliest thermodynamic approach for predicting the minimum film boiling temperature was made by Spiegler et al (1963). They suggested that T_{\min} can be determined by the temperature of the maximum liquid superheat which satisfies Van der Waals equation of state. For low pressures, they obtained the following relationship

$$T_{\min} = \frac{27}{32} T_{cr} \quad (6.5)$$

where T_{cr} is the critical fluid temperature. However, this method of calculating T_{\min} implied that the thermal characteristics of both the surface material and liquid were negligible.

Baumeister and Simon (1973), suggested the use of the thermodynamic approach to evaluate the minimum film boiling temperature. The thermodynamic approach of Spiegler was modified to include the effect of solid-liquid surface energy ratio and the thermal properties of the solid. The correlation obtained is given below

$$T_{\min} = \frac{27/32 T_{cr} \{1 - \exp[-0.52(10^4(\rho/A)^{4/3}/\sigma)^{1/3}]\} - T_L}{\exp(0.00175/\rho C k) \operatorname{erfc}[0.042(1/\rho C k)^{1/2}]} + T_L \quad (6.6)$$

where ρ , C , k and A are density, specific heat capacity, thermal conductivity and the atomic mass of the surface material, respectively and T_L is liquid temperature.

On the other hand, Henry (1974) suggested a modification for Berenson's hydrodynamic model to account for the influence of surface material. He proceeded from the assumption of an existing liquid-wall contact, causing large temporal variations in the wall surface temperature. It was assumed that $\Delta T_{\min, iso}$, i.e., $(T_{\min} - T_{SAT})$, for an isothermal surface can be calculated by Berenson's model (equation 6.3). Correlating experimental data for six fluids, boiling under atmospheric pressure, with one third of the data referring to the boiling of small liquid droplets in spheroidal state, the following relationship was obtained

$$\frac{\Delta T_{\min}}{\Delta T_{\min, iso}} = 1 + 0.42 \left[\left(\frac{\rho C k_L}{\rho C k_W} \right)^{1/2} \frac{h_{fs}}{C_W \Delta T_{\min, iso}} \right]^{0.6} \quad (6.7)$$

where $(\rho C k_L)$ and $(\rho C k_W)$ are property groups for liquid and wall respectively.

It was reported by Klimenko and Snytin (1988) that Berlin et al (1986) used the concept of liquid-wall contact to develop a relationship for T_{\min} from a purely thermodynamic approach. The onset of surface rewetting was defined by the thermodynamic stability of liquid touching the wall. Therefore, the temperature on the boundary of contact at the onset of rewetting was assumed equal to the limiting liquid superheat. The final relation was obtained by correlating experimental data.

$$\frac{\Delta T_{\min}}{T_{cr} - T_L} = \left[0.16 + 2.5 \left\{ \frac{\rho Ck_L}{\rho Ck_W} \right\}^{1/4} + \frac{\rho Ck_L}{\rho Ck_W} \right] (1 + 0.13 \cos \gamma) \frac{1 + \cos \theta}{2} \quad (6.8)$$

The range of parameters included are

$$\rho Ck_L / \rho Ck_W = 10^{-6} - 1, \quad \theta \leq 50^\circ, \quad \gamma = 0 - 180^\circ, \quad D/b > 5, \quad \text{and}$$

$$p/p_{cr} = 0.005 - 0.63$$

where θ is the wetting angle, γ is angle of surface orientation, D is diameter and b is defined as

$$b = \left[\frac{\sigma}{g(\rho_L - \rho_G)} \right]^{1/2}$$

Klimenko and Snytin (1988) conducted boiling experiments on spheres of six different diameters, using six different materials and four different saturated cryogenic liquids in the range of pressures from atmospheric to critical. Their results agreed with existing data by showing clearly the trend of a pronounced increase of ΔT_{\min} and q_{\min} with the decrease of the parameter $(\rho Ck)_W$. This trend was observed in the entire pressure range examined. On the other hand, both ΔT_{\min} and q_{\min} were found to increase slightly with increasing pressure reaching their maximum values in the range of reduced pressure, $p/p_{cr} = 0.08 - 0.15$. This was followed by a decrease of ΔT_{\min} and q_{\min} with further increase in pressure. It was concluded that this experimentally observed dependence of ΔT_{\min} on (P) is hydrodynamic in nature, since the hydrodynamic models (such as the Berenson and Henry models) predict similar trends of having maximum values of ΔT_{\min} and q_{\min} at certain values of pressure. The authors proposed a relation for ΔT_{\min} having

thermodynamic and hydrodynamic dependence in the form of

$$\frac{\Delta T_{\min}}{\Delta T_{\lim}} = f \left(\frac{(\rho Ck)_L}{(\rho Ck)_W}, \frac{\rho_L}{\rho_G} \right) \quad (6.9)$$

where the ratio of liquid and solid thermal effusivities $(\rho Ck)_L/(\rho Ck)_W$ represents the thermodynamic aspects, and the ratio of liquid and vapour densities represents the hydrodynamic aspects. The limiting liquid superheat T_{\lim} was obtained from

$$T_{\lim} = [B + (1-B)(p/p_{cr})]T_{cr} \quad (6.10)$$

where $B = 0.916 - 0.015 A + 0.00038 A^2$ and A is the atomic mass of the surface material.

To generalize the ΔT_{\min} correlation, the authors used 182 experimental points from 36 research groups who used 12 liquids boiling on surfaces of various geometries and sizes. The following relationship for the calculation of ΔT_{\min} with film boiling in a pool of saturated liquid was obtained.

$$\frac{\Delta T_{\min}}{\Delta T_{\lim}} = \left[8.2 + 4 \frac{\rho Ck_L}{\rho Ck_W} + 60 \left(\frac{\rho Ck_L}{\rho Ck_W} \right)^{1/2} \right] f \left(\frac{\rho_L}{\rho_G} \right) \quad (6.11)$$

where the function $f(\rho_L/\rho_G)$ is dependent on range of the liquid-vapour density ratios as given below

$$f \left(\frac{\rho_L}{\rho_G} \right) = \begin{cases} (\rho_L/\rho_G)^{-0.52} & \text{for } \rho_L/\rho_G < 360 \\ 0.047 & \text{for } \rho_L/\rho_G \geq 360 \end{cases}$$

Equation (6.11) was obtained in the range of parameters

$$p/p_{cr} = 9 \times 10^{-4} - 0.95, (\rho Ck)_L / (\rho Ck)_W = 6.7 \times 10^{-5} - 4.9 \text{ and}$$

$$\rho_L / \rho_G = 1.9 - 7550$$

The authors showed that equation 6.11 was capable of predicting the large data base investigated better than the models suggested by Berenson (equation 6.3), Henry (equation 6.7), and Berlin et al (equation 6.8).

Toda and Mori (1982) studied the vapour film behaviour in film boiling from a horizontal platinum wire and a stainless steel sphere to stagnant subcooled water. A laser beam was used to measure the vapour-liquid interface motion. It was found that the minimum film boiling temperature at high subcooling and at atmospheric pressure far exceeds the critical temperature of the liquid. Moreover, the vapour film thickness and vapour film fluctuations decreased as liquid subcooling increased.

Michiyoshi et al (1988) among others, confirmed that coating the solid surface with a thin insulating layer or increasing the subcooling results in high minimum film boiling temperature. It was also reported that increasing the thickness of the coating increases the minimum film boiling temperature significantly, especially for high subcooling.

6-1-3 MINIMUM FILM BOILING TEMPERATURE IN CONVECTIVE FLOW SYSTEMS:

All mechanisms and models for minimum film boiling temperature, discussed in the above two sections, do not include forced convective effects. A great deal of work has been done in recent years on the thermal-hydraulic aspects of film flow boiling particularly on the

subject of rewetting or quenching which marks the transition from stable film boiling to transition and nucleate boiling. Most of the work on this subject was motivated by the need to develop models for the analysis and evaluation of emergency core cooling systems of water cooled nuclear reactors.

Different mechanisms for surface rewetting in convective flow systems were reported in the literature. Iloeje et al (1973) introduced three different controlling mechanisms for forced convective rewetting. These are impulse cooling due to vapour film collapse, axial conduction controlled rewet and dispersed flow rewet.

Groeneveld and Stewart (1982) distinguished four different types of minimum film boiling which have been encountered during flow boiling as shown in figure 6-2. These different mechanisms controlling forced convective rewetting were defined as shown below

- i- Collapse of vapour film (type I in figure 6-2), which occurs in the inverted-annular flow regime where liquid contact with the heated surface is established as a result of a spontaneous collapse of the vapour film following a reduction in surface temperature.
- ii- Axial conduction controlled rewetting, which occurs in top and bottom flooding, is characterized by an advancing quench front (types II and III in figure 6.2). In these cases wall conduction transfers the heat from the film boiling side to the nucleate boiling side and causes the surface temperature to decrease with time. Transition from film boiling to nucleate boiling is assumed to occur when the wall temperature reaches the rewetting temperature.
- iii- Dispersed flow rewetting, which occurs when the heated surface is

precooled by spray of droplets which eventually may lead to the droplets rewetting the surface.

The minimum film boiling temperature measured in the presence of a propagating rewetting front (type II & III in figure 6-2) is usually termed the apparent quench temperature. This temperature has been reported to be higher than the true quench temperature, which represents the minimum film boiling temperature in the absence of advancing rewetting fronts (type I & IV in Fig. 6-2).

The general approach used in the assessment of the low limit of flow film boiling is to derive empirical correlations based directly on minimum flow film boiling data as shown below

Plummer et al (1973) suggested that Berenson's correlation could be modified to account for flow parameters. The modified form of the suggested correlation, shown below, was based on forced convective transient data to predict the apparent quench temperature (T_q).

$$\Delta T_q = 0.29 \Delta T_{Ber} (1 - 0.295 x_*^{2.45}) F_G \quad (6.12)$$

$$\text{where } F_G = 2.41 \quad \text{for } G < 67.8 \text{ kg m}^{-2} \cdot \text{s}^{-1}$$

$$F_G = 3.24 \quad \text{for } G > 135.6 \text{ kg m}^{-2} \cdot \text{s}^{-1}$$

$$F_G = (1 + G/13.56)^{0.49} \quad \text{for } 67.8 < G < 135.6$$

$$\Delta T = T - T_{sat}$$

The data was obtained for $G = 67.8\text{-}137 \text{ kg} \cdot \text{m}^{-2} \cdot \text{s}^{-1}$, $p = 6900 \text{ kPa}$, $x = 0.3, 0.6$ and 0.8 . This correlation suggests that T_q increases as the mass flux (G) increases and the quality (x) decreases.

Kim and Lee (1979) suggested an empirical correlation derived

from dimensional analysis, with the constants obtained from bottom flooding tests, which predicts the apparent quench temperature.

$$\Delta T_q = 19.51 \Delta T_w \left[\frac{\Delta T_{SUB}}{\Delta T_w} \right]^{0.107} \left[\frac{k}{C_p G t} \right]^{0.162} \left[\frac{t G^3}{k \rho^2 \Delta T_w} \right]^{0.989} \left[\frac{t}{z} \right]^{0.163} \quad (6.13)$$

where the thermal and physical properties in the correlation are wall material properties. t is the wall thickness and z is the axial distance from inlet. The correlation was based on data range of $100 < G < 400 \text{ kg.m}^{-2}.\text{s}^{-1}$ and $10^\circ\text{C} < \Delta T_{SUB} < 80^\circ\text{C}$. The pressure was about one atmosphere.

De Slave and Panella (1987) adopted an approach based on a correlation derived by Baumeister and Simon (1973), which gives the temperature of a semi-infinite wall in contact with a water drop of infinite mass as a function of time, to estimate the apparent quench temperature as follows;

$$\frac{T_I - T_L}{T_w - T_L} = \exp(t^*) \operatorname{erf}(\sqrt{t^*}) = a \quad (6.14)$$

where T_L is the local liquid temperature, T_I is the interface temperature, T_w is the wall temperature and $t^* = h^2 t / (\rho C k)_w$ is a dimensionless time in which t is the duration of the wall-liquid interaction phase till the re-establishment of a permanent contact and h is the average heat transfer coefficient during such a phase. By taking T_I equal to the maximum water temperature under metastable conditions (Spiegler et al (1963)) which is equal to 273°C at atmospheric pressure, the corresponding T_w was considered the maximum

wall temperature at which rewetting could occur. Therefore, equation 6.14 was reduced to,

$$T_q = T_L + \frac{1}{a} (273 - T_L) \quad (6.15)$$

It was indicated that a could be a function of many parameters including mass velocity, liquid temperature and the wall temperature. The mass velocity effect was considered by including a term suggested by Plummer et al (1973). Accordingly, equation 6.15 was modified obtaining the following correlation,

$$T_q = T_L + 0.355 (1 + 0.279G^{0.49})(273 - T_L) \quad (6.16)$$

Values of the parameter a between 0.5 and 1 in equation 6.15 correspond to mass velocity G between 50 and 300 kg/m².s. This correlation is limited to the prediction of the apparent quench temperature in flooding analysis when the quench front is upstream of an inverted annular subcooled water flow. However, the authors pointed out that this correlation tends to overpredict the flow rate effect and does not take into account the initial wall temperature effect.

The empirical data that are clearly associated with a sudden collapse of vapour film during stationary inverted-annular flow boiling are available from Groeneveld and Stewart (1982), Fung (1981) and Cheng et al (1985). Using such data, what is called "true" quench temperature correlations were obtained.

Groeneveld and Stewart (1982) obtained high pressure experimental data which indicated that the mass flux did not have significant effect on T_{min} . Moreover, the effect of local quality was

found to be negligible for low subcooling. However, in the subcooled region a large increase in T_{\min} with increasing subcooling was observed. They formulated a "true" quench temperature based on their high pressure experimental data (52 points) and Fung's atmospheric pressure data (12 points). The authors correlated the quench temperature as a function of pressure and quality, as

$$\left. \begin{aligned}
 &\text{for } x \leq 0 \quad \text{and} \quad P \leq 9000 \text{ kPa} \\
 &T_{\min} = 284.7 + 0.0441 P - 3.72 \cdot 10^{-5} P^2 - \frac{x \cdot 10^4}{2.82 + 0.00122 P} \\
 &\text{for } x > 0 \quad \text{and} \quad P \leq 9000 \text{ kPa} \\
 &T_{\min} = 284.7 + 0.0441 P - 3.72 \cdot 10^{-5} P^2 \\
 &\text{for } P > 9000 \text{ kPa} \\
 &T_{\min} = (\Delta T_{\min, 9000 \text{ kPa}}) \left(\frac{\frac{P}{P_{cr}} - P}{\frac{P}{P_{cr}} - 9000} \right) + T_{SAT}
 \end{aligned} \right\} \quad (6.17)$$

Cheng and Poon (1985) compared their data (71 points) with the Groeneveld and Stewart correlation (equation 6.17). They observed good agreement for all negative qualities (subcooled data). However, this correlation (equation 6.17) overpredicted their low pressure data in the positive quality range. In general, the data showed that the true quench temperature increases with mass flux, inlet subcooling and pressure but decreases with increasing quality. Accordingly, a new correlation based on all the available data (143 data points, from Groeneveld and Stewart (1982), Fung (1981) and Cheng et al (1985)) was

obtained. This quench temperature correlation is expressed as follows

$$\left. \begin{aligned}
 &\text{for } x < 0 \quad \text{and} \quad 0.35 \text{ MPa} < P < 9 \text{ MPa} \\
 &T_{\min} = 300.21 + 44.45 P - 3.5 P^2 - \frac{10^4 x}{5.66 P + 1.6} \\
 &\text{for } x > 0 \quad \text{and} \quad 0.35 \text{ MPa} < P < 9 \text{ MPa} \\
 &T_{\min} = 300.21 + 44.45 P - 3.5 P^2 \\
 &\text{for all } x\text{'s} \quad \text{and} \quad P < 0.35 \text{ MPa} \\
 &T_{\min} = 300.21 + 44.45 P - 3.5 P^2 - \frac{10^4 x}{68.83 P - 2.48}
 \end{aligned} \right\} \quad (6.18)$$

Johannsen (1988), attempted to examine the functional dependency of the quench temperature on pressure, quality, mass flux and inlet subcooling. He used the available data base (the above mentioned 143 data points) to produce contour plots with simultaneous variation of two parameters either local quality and pressure or local quality and mass flux. From these contour plots, he concluded that the data base seems both too sparse and inaccurate to draw any definite conclusions regarding the parametric dependencies of quench temperature. However, he stated that the data show a mass flux effect which decreases with pressure and is most pronounced at high subcooling regardless of pressure.

All the empirical correlations discussed in this section were based on data obtained from experiments conducted on vertical systems. However, they were assumed to be applicable for horizontal systems as well.

6-2 COMPARISON WITH THE PRESENT DATA.

Among all of the correlations discussed above, the one suggested by Kim and Lee (1979) for the minimum film boiling temperature in convective systems seems to be most appropriate for comparison with the present data. This is because, this correlation was based on transient convective data collected at atmospheric pressure in keeping with the present experimental work. This correlation considered all the parameters which affect the apparent quench temperature. These parameters are the heat capacity of the tube, inlet subcooling, mass flux, tube temperature and axial distance from the inlet. However, it should be noted that this correlation was based on vertical flooding data obtained for a mass flux range of 100 - 400 $\text{kg/m}^2\text{s}$ while the present data are related to refilling experiments in hot horizontal tubes for a mass flux range of 400 - 1300 $\text{kg/m}^2\text{s}$. Moreover, the present data showed that the apparent quench temperature at the top side of the tubes is considerably higher than that at the bottom side of the tubes while there is no such circumferential variation in flooding vertical tubes. Figures 6-3 and 6-4 show a comparison between the apparent quench temperatures predicted by the correlation suggested by Kim and Lee (1979) with those of the present data. Data for the rewetting of both the bottom and top sides of the tube are included in the present data. In figure 6-3 only data for 400 $\text{kg/m}^2\text{s}$ were considered while all the data obtained in the present experimental work (400 - 1300 $\text{kg/m}^2\text{s}$) are shown in figure 6-4. These figures indicate that the correlation suggested by Kim and Lee (1979) predicted the right parametric effect of tube heat capacity, inlet subcooling, mass

flux, tube temperature and axial distance from inlet on the quench temperature. It is clear in both figures that the correlation is better able to predict the rewetting temperature of the top side of the tube rather than the bottom side where the correlation overpredicts the measured rewetting temperatures. The general level of agreement between the data and the correlation appears to be the same in both figures 6-3 and 6-4 although the data in figure 6-4 was obtained for a mass flux range beyond the range recommended by Kim and Lee (1979).

6-3 THE CONCEPT OF MINIMUM VAPOUR FILM THICKNESS.

It is obvious from the above review that there is no unique temperature at which a hot surface will rewet. The surface rewetting temperature is a function of many thermal, hydrodynamic and geometrical parameters which are pertinent to the system under consideration. However, for convective systems available data, including that obtained in the present work, are consistent in identifying the effect of different operating parameters on the rewetting temperature. It is well established that in a convective rewetting case a hot surface at a given initial temperature rewets at lower temperature with increasing wall heat capacity and with decreasing liquid subcooling or mass flux. It is also interesting to note the correlation between the rewetting temperature and the duration of the film boiling region prior to surface rewet as discussed earlier in chapter 5. It was shown that a decrease in the rewetting temperature was always associated with longer duration of the film boiling regime. Longer film boiling duration resulted not only in lower rewetting temperature but also in lower

maximum heat flux. Increasing the duration of stable film boiling may be attributed to higher initial vapour film thickness, i.e., higher rate of vapour generation. Indeed all the parameters that may lead to lower rewetting temperature, as discussed above, can also cause higher initial vapour film thickness and consequently longer film boiling duration. Decreasing liquid subcooling results in decrease in the sensible portion of the heat transported to the liquid and accordingly higher vapour generation causing longer stable film boiling. Also, decreasing the mass flux in the flow boiling case has a similar effect of decreasing the heat convected to the subcooled liquid and consequently results in higher vapour generation rate and longer duration of the film boiling regime. The effect of initial wall temperature and system heat capacity can be viewed in a similar manner.

The apparent correlation between the initial vapour film thickness or the duration of the film boiling and the resulting rewetting temperature suggests that, for a given system, there is a minimum vapour film thickness below which the vapour film may collapse. Consequently the surface may rewet independent of the surface temperature. For example, having higher initial vapour film thickness caused by any of the system parameters, will require longer duration for the film thickness to reach this minimum value, i.e., longer film boiling regime, and accordingly a lower rewetting temperature is attained.

Also in support of the concept of a minimum vapour film thickness, it is shown in the literature that using surface materials with low thermal conductivity, or coating a surface with insulating

materials (surfaces of lower heat capacity) resulted in higher minimum film boiling temperature. This could be explained by the fact that the low thermal conductivity prevents the inflow of heat from the hot solid to the locally cooled surface. As a result, lower vapour generation rate is encountered and consequently, thinner initial vapour film is formed. Shorter duration of film boiling will be needed to reach the minimum vapour film thickness resulting in higher surface temperature at rewetting.

It should be noted that the value of this minimum (or critical) vapour film thickness at which vapour film collapse may take place is expected to be system dependent. Systems that are free of perturbations may sustain film boiling for long periods, i.e., lower minimum vapour film thickness, and therefore lower rewetting temperatures may result. This is also supported by experimental data obtained from the literature. It has been observed that the suppression of liquid-vapour interface fluctuations results in lower rewetting temperatures. This is consistent with the proposed criterion in as much as the suppression of the interface fluctuation would result in a thinner vapour film, i.e., reduction of the critical vapour film thickness for such a system.

Studies on the Leidenfrost temperature and minimum film boiling temperature in pool boiling showed similar trends suggesting the applicability of the minimum vapour film thickness concept in these cases as well. As mentioned earlier, it was shown that having extremely smooth surfaces and carefully suppressing disturbances result in a very low Leidenfrost temperatures. This can be explained by realizing that suppressing disturbances leads to smooth liquid-vapour interface and as

such allows the film boiling process to continue for a longer duration, thereby lowering the value of the minimum film boiling temperature. In the case of the Leidenfrost phenomenon, the vapour film would exist as long as the solid surface is superheated and the vapour ventilation rate from underneath the liquid droplet is lower than or equal to the vapour generation rate. Consequently, very low Leidenfrost temperatures could be obtained. On the other hand, increasing the porosity of the solid surface has an opposite effect since increasing porosity will increase the vapour ventilation rate through the solid. Accordingly, a thinner vapour film is involved which could collapse at high surface temperature.

A proposed rewetting criterion based on the above discussion is presented in more details in section 6-5.

6-4 EVALUATING THE AVAILABLE REWETTING CRITERIA IN REFILLING OF HOT HORIZONTAL TUBES.

It seems that the study reported by Chan and Banerjee (1981) is the only attempt conducted, so far, to develop a quench criterion for the rewetting and refilling of hot horizontal tubes based on hydrodynamic considerations. The criterion was based on the occurrence of a Kelvin-Helmholtz instability at the vapour-liquid interface in the film boiling. The initiation of instability was related to the height of the stratified water level by a simple model. The water level necessary to initiate the interfacial instability and consequently initiate tube quenching, was called the critical water level. Speculating that vapour is venting circumferentially upward in the film

boiling region, the vapour velocity was obtained by solving the mass and momentum equations assuming, i) constant vapour density, ii) heat transfer across the vapour film by conduction only, and iii) negligible transient terms. The Kelvin-Helmholtz instability condition was reduced to

$$U_G \geq \left[\frac{2 \pi \sigma}{\rho_G \lambda} \right]^{1/2} \quad (6.19)$$

where U_G is the critical vapour velocity, σ is the surface tension and λ is the wave length of the instability. Assuming the wave length equal to the vapour channel length, the critical vapour velocity for the onset of instability was calculated using the above equation. Results for the fundamental mode and its first harmonic are plotted in figure 6-5 for different water levels (h_L). The mean value of the vapour velocity, obtained by solving the simplified momentum and continuity equation as mentioned earlier, for different wall superheats are also plotted in figure 6-5. Accordingly, the suggested critical water level for the onset of instability is the water level at which the mean vapour velocity equals the critical velocity.

In the present study of refilling and rewetting of hot horizontal tubes, it is important to investigate the applicability of the quench initiation model of Chan and Banerjee (1981) under a wide range of initial and boundary conditions. An implication of this model (Chan and Banerjee (1981)) was that the critical water level increases as vapour velocity decreases, as shown in figure 6-5. This suggests that the critical water level would increase with increasing liquid

subcooling and decreasing initial wall temperature, since both result in reducing vapour generation rate and consequently decreasing vapour velocity. Moreover, this model implies that the critical water level is independent of the flow rate.

The detailed measurements carried out in the present work allow the evaluation of the above parametric trends. The critical water level was evaluated from the transient void fraction measurement at the time of quench initiation. The effects of initial wall temperature and water subcooling on the critical water level for the present experiments are presented in figure 6-6a which shows clearly that increasing the initial tube temperature and the inlet water temperature will increase the water level at quench initiation. Figure 6-6b also shows that the critical water level is dependent on the flow rate. These trends are obviously opposite to the implications of the quench initiation model proposed by Chan and Banerjee (1981). Moreover, in using their two-fluid model to predict the rewetting of hot horizontal tubes, Chan and Banerjee (1981) did not use the proposed quench initiation model to predict the critical water level. Instead, the critical water level was adjusted numerically to agree with the corresponding experimental runs. Accordingly, a more reliable model, capable of explaining the parametric trends is needed.

Although, the author agrees that vapour-liquid interface behaviour and its instability is responsible for the onset of rewetting, it is clear from the above data trends that this can not be described in terms of a critical water level as proposed by Chan and Banerjee (1981). Evidence seems to suggest that it may be possible to

describe it in terms of a critical vapour film thickness. For example, the observed trends in figure 6-6a and 6-6b can be explained in terms of a system minimum (or critical) vapour film thickness. Increasing the initial tube temperature and or inlet water temperature will result in increase in vapour generation rate, i.e., greater initial vapour film thickness in film boiling. This can result in longer film boiling duration so that the vapour film thickness may be reduced to its minimum value before quenching. A longer duration of the film boiling regime prior to quenching will allow the increase in water inventory, i.e., higher water level at quench initiation. The preceding description is consistent with the data in figures 6-6a and 6-6b.

6-5 THE PROPOSED GENERAL REWETTING CRITERION.

The literature review and the trends of the present experimental results suggest that the physics of ending film boiling and establishing transition and nucleate boiling is the same for the three categories of surface rewetting discussed previously. It is concluded that the thickness of the vapour film and the dynamic behaviour of the liquid-vapour interface in the film boiling region are the controlling parameters which define the boundary between film boiling and transition and nucleate boiling, i.e.,

The proposed general criterion for rewetting is that, there is a minimum vapour film thickness at which rewetting may be initiated. The critical value of the vapour film thickness is defined by the magnitude of liquid-vapour interface fluctuations

and solid surface roughness such that surface rewetting occurs only if the vapour film thickness decreases down to a value equal to the sum of the amplitude of the vapour-liquid interface fluctuations and solid surface roughness.

The present experimental results support the proposed general criterion for rewetting in showing a systematic trend of increase in the duration of the film boiling regime, and the corresponding increase in liquid inventory prior to quenching, with increasing wall temperature, inlet water temperature and tube wall thickness. This can be explained qualitatively in terms of a minimum vapor film thickness as follows:

i) The component of the total heat transfer rate that causes vapour generation increases with increasing tube wall heat capacity, initial tube temperature, and inlet water temperature. Increasing the vapour generation rate results in higher initial vapour film thickness which in turn will result in longer film boiling duration since longer time will be required to dissipate the heat accumulated in the wall and to bring the initial vapour film thickness down to the "critical" value causing quenching.

ii) It is clear that for any given test run the length of the film boiling period increased as the refilling front advanced axially. This is believed to be related to the decrease of local liquid subcooling along the tube resulting again in a higher vapour generation rate downstream. As above this can be related to a minimum vapour film

thickness.

iii) In all tests, tube quenching was always initiated at the bottom of the tube where the vapour film thickness is minimum.

6-6 LIQUID-VAPOUR INTERFACE BEHAVIOUR IN FILM BOILING:

6-6-1 REVIEW:

The liquid-vapour interface fluctuation is expected to be highly dependent on system disturbances. This in turn depends on the source of such disturbances. For example, in pool boiling on flat horizontal surfaces, bubble formation and subsequent release could be the most dominant source of disturbances leading to interface fluctuations while in flow boiling systems, hydraulic disturbances such as system pressure fluctuations could be the dominant source.

Experimental investigation reported by Bradfield (1965) and Sheppard and Bradfield (1972) showed that the laminar film boiling regime during pool boiling around the forward stagnation point on a vertically oriented cylinder with a hemispherical lower end exhibits a continuously wavy interface for fluids near their saturation temperature and these waves emanate from the stagnation point region. The same authors developed an analytical solution for the liquid-vapour interface oscillations during saturated film boiling at a stagnation interface element. They also obtained expressions for the mean vapour film thickness, the oscillation frequency and the average heat flux.

Orozco et al (1987) and Orozco and Stellman (1988) extended the theoretical analysis developed by Sheppard and Bradfield (1972) to

treat the stagnation point of flow film boiling on a sphere immersed in a subcooled liquid. The effect of system parameters on the dynamic behaviour of the liquid-vapour interface as well as the response to step changes in the temperature and velocity fields were investigated.

Naylor and Patrick (1986) reported a study on film boiling destabilization both experimentally and theoretically. The experiments were also conducted on a heated rod with a hemispherical lower end. Both untriggered and triggered (by the use of pressure pulses) film boiling collapse were investigated. They concluded that untriggered film boiling collapse is dependent on various inherent perturbations, for example: surface roughness, vapour-liquid interface instabilities and interface disturbances following bubble departure. Their results suggested that untriggered film boiling collapse occurred when the average vapour film thickness at the stagnation point became less than the sum of surface roughness plus the amplitude of the interface ripples and waves. They also observed that following triggered film collapse film boiling was re-established again when the metal and water temperatures were above a "thermal threshold".

6-6-2 EXPERIMENTAL RESULTS.

Assuming that during film boiling, heat is transferred by conduction and radiation across the vapour film, the minimum vapour film thickness, for the present experiments, was obtained by using the value for the local heat flux at quenching (i.e., corresponding to the apparent quench temperature). The heat flux was estimated by utilizing the measured transient temperature distribution in the tube wall as

discussed in chapter 5. Figure 6-7 shows the estimated critical vapour film thickness at the bottom of the tube versus the apparent quench temperature for the two tube wall thicknesses (1 and 2 mm) and different subcoolings. As shown in this figure, the estimated critical vapour film thickness appear to be reasonably constant (about 0.11 mm) independent of the surface temperature at rewetting, wall thickness, inlet subcooling, and inlet mass flux.

Since it is speculated that this minimum vapour film thickness is related to the order of magnitude of the liquid-vapour interface fluctuations leading to vapour film collapse, the analysis is focused on the dynamic behaviour of the liquid-vapour interface in the film boiling region at the bottom of a hot horizontal tube near the quench front.

6-7 DYNAMIC BEHAVIOUR OF THE LIQUID-VAPOUR INTERFACE OF FILM

BOILING DURING REFILLING OF A HOT HORIZONTAL TUBE.

6-7-1 THE MODEL.

The typical flow pattern observed during the refilling and rewetting of hot horizontal tubes which was discussed previously is characterized by a stratified liquid tongue moving on top of a vapour layer downstream of the quench front as shown in figure 6-8a. The geometry of a cross section of the tube in the film boiling region is shown in figure 6-8b. It is postulated that the vapour in the film boiling is vented circumferentially upward. Moreover, the following assumptions are made, i) incompressible liquid and vapour, ii) the vapour film is thin compared to the tube radius, iii) heat transfer from the tube wall to the interface is only by conduction. Following the suggestion by Bradfield (1965), the equation of motion for the liquid-vapour interface is :

$$\frac{P_L}{g} \ddot{\delta} = P_G - P_L \quad (6.20)$$

where P_L is the hydrostatic liquid pressure at the interface, P_G is the vapour pressure and $\ddot{\delta}$ is the acceleration of the interface. In equation 6.20, the vibrating mass is represented by the mass of the liquid column per unit area while the forces acting on the interface per unit area is represented by vapour pressure from the vapour side and the hydrostatic liquid pressure from the liquid side.

Referring to figure 6-8c, the hydrostatic liquid pressure at

angle θ is given by

$$P_L = (h_L - \delta - \Delta h) \rho_L g \quad (6.21)$$

where h_L is the liquid level above the bottom of the tube, δ is the vapour film thickness and ρ_L is liquid density.

$$\text{But } \Delta h = (R - \delta)(1 - \cos\theta) = (R - \delta) \sin^2\theta / (1 + \cos\theta)$$

Therefore, for $R \gg \delta$ and very small θ , Δh could be approximated by

$$\Delta h = \frac{R \theta^2}{2} \quad (6.22)$$

Substituting equation 6.22 into equation 6.21 we get

$$P_L = (h_L - \delta - 0.5 R \theta^2) \rho_L g \quad (6.23)$$

In order to investigate the dynamic behaviour of the interface by solving equation 6.20, a solution for the vapour pressure in the film boiling region is required. To achieve this a one-dimensional treatment for the vapour flow in the film boiling region is considered. Choosing the coordinates as shown in figure 6-8c, the continuity equation is given by

$$\frac{\partial \delta}{\partial t} + \frac{\partial}{\partial x} (\delta u_g) = V \quad (6.24)$$

where V is the velocity of vapourization defined as

$$V = \frac{\beta k_g \Delta T_{SAT}}{\rho_g h_{fg} \delta} \quad (6.25)$$

where ΔT_{SAT} is the surface superheat, β is a partition factor

representing the portion of the heat transfer used in vapour generation, u_g is the vapour velocity and k_g , ρ_g , and h_{fg} are the vapour thermal conductivity, vapour density and latent heat of vapourization, respectively.

For small θ , δ is almost constant. Therefore equation 6.24 could be simplified to

$$\delta \frac{\partial}{\partial x} (u_g) = (V - \dot{\delta}) \quad (6.26)$$

where $\dot{\delta}$ is the interface velocity ($\partial\delta/\partial t$).

Integrating equation 6.26 with respect to x we get

$$u_g = \left(\frac{V - \dot{\delta}}{\delta} \right) x + F(t) \quad (6.27)$$

where $F(t)$ is function of time. However, from the boundary condition at the bottom of the tube where the symmetry of the flow provide $u_g = 0.0$ at $x = 0$ we get $F(t) = 0$.

Accordingly, equation 6.27 is reduced to

$$u_g = \left(\frac{V - \dot{\delta}}{\delta} \right) x \quad (6.28)$$

The momentum equation of the vapour flow in the film boiling region is

$$\frac{\partial}{\partial t} (\delta u_g) + \frac{\partial}{\partial x} (\delta u_g^2) = - \frac{1}{\rho_g} \frac{\partial}{\partial x} (\delta P_g) - \frac{1}{\rho_g} (\tau_w + \tau_i) \quad (6.29)$$

where τ_w is the wall shear stress and τ_i is the interfacial shear stress.

In order to obtain an approximate simple analytical solution for the vapour pressure, the unsteady term in the momentum equation is ignored. Furthermore, the interfacial shear stress is neglected. The effect of τ_i was later examined and found to be insignificant. Accordingly, equation 6.29 is reduced to

$$\frac{\partial}{\partial x} (\delta u_G^2) = - \frac{1}{\rho_G} \frac{\partial}{\partial x} (\delta P_G) - \frac{\tau_w}{\rho_G} \quad (6.30)$$

The wall shear stress is given by

$$\tau_w = \frac{1}{2} f \rho_G u_G^2 \quad (6.31)$$

where f is the wall friction factor. The friction factor is approximated by a value derived for fully developed laminar flow between two parallel flat plates separated by a distance δ with no slip condition at the wall and zero shear stress at the liquid-vapour interface.

Based on the above, the friction factor is given by

$$f = \frac{6 \mu_G}{\rho_G \delta u_G} \quad (6.32)$$

where μ_G is the vapour dynamic viscosity.

Utilizing equations 6.28, 6.31 and 6.32, equation 6.30 becomes

$$\frac{\partial}{\partial x} \left[\delta \left(\frac{V - \delta}{\delta} \right)^2 x^2 + \frac{1}{\rho_G} \delta P_G \right] = - \frac{3 \mu_G}{\rho_G \delta^2} (V - \delta) x \quad (6.33)$$

Integrating equation 6.33 with respect to x gives

$$P_G = - \left[\frac{3 \mu_G}{2} \left(\frac{V - \delta}{\delta^3} \right) + \rho_G \left(\frac{V - \delta}{\delta} \right)^2 \right] x^2 + E(t) \quad (6.34)$$

Substituting equations 6.23 and 6.34 into equation 6.20 and substituting for x by $R\theta$ we get

$$\rho_L g (h_L - \delta - 0.5R\theta^2) \left(\frac{\ddot{\delta}}{g} + 1 \right) = - \left[\frac{3 \mu_G}{2} \left(\frac{V - \dot{\delta}}{\delta^3} \right) + \rho_G \left(\frac{V - \dot{\delta}}{\delta} \right)^2 \right] R^2 \theta^2 + E(t) \quad (6.35)$$

Since the interest in interface dynamics is focused at the bottom of the tube where surface rewetting first occurs, $E(t)$ is calculated at $\theta = 0$ as

$$E(t) = \rho_L g (h_L - \delta) \left(\frac{\ddot{\delta}}{g} + 1 \right) \quad (6.36)$$

Substituting for $E(t)$ from equation 6.36 and V from equation 6.25 into equation 6.35 we get the following governing equation

$$\ddot{\delta} = C_1 \left(\frac{\dot{\delta}}{\delta} \right)^2 + C_2 \frac{\dot{\delta}}{\delta^3} + C_3 \frac{1}{\delta^4} + C_4 \quad (6.37)$$

where

$$\left. \begin{aligned} C_1 &= 2\rho_G R / \rho_L \\ C_2 &= - (4R/\rho_L) [a\beta + 0.75 \mu_G] \\ C_3 &= (2R/\rho_G \rho_L) [a^2 \beta^2 + 1.5a\beta \mu_G] \\ a &= k_G \Delta T_{SAT} / h_{fg} \\ C_4 &= -g \end{aligned} \right\} \quad (6.38)$$

The steady state solution of equation 6.37 gives the equilibrium vapour film thickness. Therefore, the equilibrium vapour film thickness

at the bottom of the tube is given by

$$\delta_{eq} = [(2R/\rho_L \rho_G g)(a^2 \beta^2 + 1.5a\beta\mu_G)]^{1/4} \quad (6.39)$$

It should be noted that using equations 6.37 and 6.39 requires estimating the partition factor β . A simple model for β is developed in section 6-8.

6-7-2 ANALYSIS AND DISCUSSION.

6-7-2-1 EQUILIBRIUM VAPOUR FILM THICKNESS.

Equation 6.39 was verified using the experimental results discussed earlier. To eliminate any uncertainties related to the value of β , the low subcooling experiments were considered. For these experiments, the wall temperature transients during stable film boiling at the most downstream measuring stations, where the liquid is assumed to be almost saturated, was used to calculate the wall heat flux and subsequently the average stable vapour film thickness. The values calculated from these experiments are compared with the predictions of equation 6.39, with $\beta=1$, in figure 6-9. Very good agreement is shown suggesting the validity of using equation 6.39 to predict the equilibrium vapour film thickness in film boiling in the present model.

6-7-2-2 DYNAMIC INTERFACIAL ANALYSIS:

Equations 6.37 was solved numerically, using the fourth order Runge-Kutta Nyström method, given by Kreyszig (1983), to investigate

the dynamic response of the interface due to thermal and hydraulic perturbations. Thermal disturbances could result from the sudden tube wall temperature drop associated with the arrival of the quench front. This can be represented by a step change in tube wall temperature implemented by changing ΔT_{SAT} in C_2 and C_3 in equation 6.38. The hydraulic disturbances are system pressure fluctuations which are the characteristics of the two-phase flow as a result of the interaction between the two phases during the quenching process. These hydraulic disturbances are modeled by a pressure square pulse forcing function implemented on the equation of motion by adding the term $\Delta P/(\rho_L R)$ to equations 6.37, where ΔP is the magnitude of the pressure pulse selected to be within the order of magnitude of the system pressure fluctuations as experimentally observed and R is the tube radius.

Figure 6-10 illustrate the dynamic response of the liquid-vapour interface to a sudden step in the tube surface temperature, for saturated water ($\beta=1$). It shows a damped oscillatory behaviour around a new equilibrium vapour film thickness. As shown, increasing the temperature step increases the fluctuation amplitude. Temperature drop of up to 200°C were tried. However, the fluctuation amplitudes were small compared to the observed equilibrium vapour film thickness. This suggests that the thermal disturbances, as represented by a sudden surface temperature drop, could not be responsible for the collapse of the vapour film for the system under investigation.

The effect of liquid subcooling and liquid velocity was investigated by changing the value of β in the equations of motion.

Figures 6-11a and 6-12b show that increasing subcooling and/or liquid velocity (i.e., reducing β) will result in smaller amplitudes of fluctuation. This agrees with previous results obtained by Bradfield (1965), Orozco et al (1987) and Naylor and Patrick (1986).

To investigate the dynamic response of the interface due to pressure disturbances, a square pulse was used to model the system pressure fluctuations as previously indicated. The transient system pressure was recorded during the refilling and rewetting experiments by two pressure transducers installed at the inlet and outlet of the 3 m test sections. They showed pressure fluctuations with amplitudes up to 80 kPa depending on the initial and boundary conditions tested. However, typical values were in the range of 30-50 kPa.

Figure 6-12a illustrates the response of the interface to a 4kPa pulse. This indicates a relatively big amplitude of fluctuation which is eventually damped to retain the initial equilibrium vapour film thickness. Unless very small time period (less than 0.1 millisec) is used for the pressure pulse, no effect on the fluctuation amplitudes were detected.

Implementing an average pressure pulse of 40 kPa, gives a fluctuation amplitude higher than 80% of the equilibrium vapour film thickness as shown in figure 6.12b. It should be noted that the present analysis would underpredict the fluctuations amplitude since the vapour was considered incompressible. Moreover, surface roughness could result in a thinner net vapour film.

The above analysis suggests that liquid-wall contact could be established due to system pressure fluctuations. These pressure

fluctuations were sufficient to cause liquid-vapour interface fluctuations capable of initiating surface rewetting. Liquid-wall contact could have been established when the sum of the magnitude of the interface fluctuations and surface roughness equaled the equilibrium vapour film thickness.

It should be noted that the above model represents a necessary but not sufficient condition for rewetting. If the wall heat capacity is low enough the liquid-wall contact will initiate a sustained surface rewetting. However, for high heat capacity, film boiling may be reestablished. It is speculated, accordingly, that under the present situation, the system heat capacity was not enough to reestablish film boiling again. Therefore, this would define the end of the film boiling.

6-7-2-3 THE EFFECT OF SYSTEM PRESSURE FLUCTUATION ON

THE CRITICAL VAPOUR FILM THICKNESS.

The above analysis shows that the critical vapour film thickness is dependent on the system hydraulic perturbations as represented by the system pressure fluctuations. It is obvious that higher system pressure fluctuation can cause early rewetting as it would be sufficient to initiate liquid-wall contact while the vapour film is still relatively thick, i.e., higher critical vapour film thickness.

The relationship between the maximum amplitude of the interface fluctuations and the magnitude of pressure fluctuation is given in

figure 6.13. It is clear that the higher the pressure fluctuations, the higher the fluctuations amplitude of the interface. However, the rate of increase in the amplitude of the interface fluctuations with pressure fluctuations decreases significantly as the pressure fluctuations increases.

6-8 A SIMPLE MODEL FOR EVALUATING THE PARTITION FACTOR β .

It is clear that the solutions for equations 6.37 and 6.39 cannot be obtained unless the fraction of heat transfer used for evaporation (β) is known. This in turn requires the knowledge of the fraction of heat conducted to the liquid, since the total heat transfer to the interface will be consumed in both heating the subcooled liquid and generating vapour. It is postulated that the convection heat transfer from the liquid-vapour interface to the subcooled liquid during refilling and rewetting of hot tubes is governed by the developing thermal boundary layer in the subcooled liquid phase. An approximate solution for the thermal boundary layer in the liquid phase is obtained by assuming that the liquid temperature is uniform at the quench front and that the liquid phase moves with uniform velocity on top of flat liquid-vapour interface. Using the integral formulation technique, an energy balance on the control volume shown in figure 6.14 gives

$$-\frac{d}{dz} \left(\int_0^{\delta_t} \rho_L C_{P_L} T_L U_L dy \right) dz - G_y C_{P_L} T_0 dz + \dot{q} dz = 0 \quad (6.40)$$

where T_0 is the liquid bulk temperature and G_y is the mass flux out of

the boundary layer

$$G_y = - \frac{d}{dz} \int_0^{\delta_t} \rho_L U_L dy$$

and $q'' = - k_L \frac{\partial T}{\partial y} \big|_{y=0}$

Therefore, equation 6.40 reduces to

$$\frac{d}{dz} \left(\int_0^{\delta_t} (T_0 - T) U_L dy \right) = \frac{k_L}{\rho_L C_{P_L}} \frac{\partial T}{\partial y} \big|_{y=0} \quad (6.41)$$

An assumed temperature profile is needed to solve equation 6.41. The velocity has already been assumed constant. The temperature distribution in the liquid interfacial boundary layer near the bottom of the tube, i.e., small angle θ , is assumed to be independent of z and to have a distribution in the form :

$$\phi = T - T_{SAT} = a_1 y^2 + a_2 y + a_3 \quad (6.42)$$

The coefficients of equation 6.42 are obtained from the following boundary conditions

$$\phi \big|_{y=0} = 0, \quad \frac{d\phi}{dy} \big|_{y=\delta_t} = 0$$

and

$$\phi \big|_{y=\delta_t} = \phi_0 = T_0 - T_{SAT}$$

which give the distribution

$$\frac{\phi}{\phi_0} = 2 \left(\frac{y}{\delta_t} \right) - \left(\frac{y}{\delta_t} \right)^2 \quad (6.43)$$

where T_0 is the liquid bulk temperature.

Substituting the above temperature profile in equation 6.41

gives

$$U_L \frac{d}{dz} \int_0^{\delta_t} \left(1 - 2 \frac{y}{\delta_t} + \frac{y^2}{\delta_t^2} \right) dy = \frac{2 k_L}{\rho_L C_{P_L}} \frac{1}{\delta_t} \quad (6.44)$$

which yields

$$\delta_t = \left[\frac{12 k_L z}{\rho_L C_{P_L} U_L} \right]^{1/2} \quad (6.45)$$

where the constant of integration is zero since uniform temperature at the quench front is assumed, i.e., $\delta_t = 0$ at $z = 0$.

Substituting equation 6.45 back into the assumed temperature profile (equation 6.43) gives

$$\frac{\phi}{\phi_0} = \left[\left(\frac{\rho_L C_{P_L} U_L}{3 k_L} \right)^{1/2} \frac{y}{z^{1/2}} - \left(\frac{\rho_L C_{P_L} U_L}{12 k_L} \right) \frac{y^2}{z} \right] \quad (6.46)$$

The heat convected to the liquid is obtained from

$$q_{\text{conv.}} = - k_L \left. \frac{\partial T}{\partial y} \right|_{y=0}$$

$$q_{\text{conv.}} = \left(\frac{\rho_L C_{P_L} k_L U_L}{3 z} \right)^{1/2} (T_{\text{SAT}} - T_0) \quad (6.47)$$

The partition factor (β) is defined by

$$\beta = 1 - \frac{q_{\text{conv.}}}{q} \quad (6.48)$$

where the total heat transfer rate (q) is given by

$$q = k_G \left(\frac{T_W - T_{SAT}}{\delta} \right) \quad (6.49)$$

where T_W is the wall temperature.

After substituting for δ from equation 6.39 and utilizing equations 6.47 and 6.49, equation 6.48 will give the following implicit β relation.

$$\beta = 1 - J [a^2 \beta^2 + 1.5 a \beta \mu_G]^{1/4} \quad (6.50)$$

$$\text{where } J = \left[\frac{\Delta T_{SUB}}{k_G \Delta T_{SAT}} \right] \left[\frac{C_P k_L U_L}{3 z} \right]^{1/2} \left[\frac{2 R \rho_L}{g \rho_G} \right]^{1/4}$$

in which ΔT_{SUB} is the liquid subcooling.

The effect of initial wall temperature, liquid velocity and liquid subcooling at the quench front on the partition factor β is shown in figures 6-15, 6-16 and 6-17 respectively. Since the thermal boundary layer is assumed to develop from the location of the quench front along the advancing liquid downstream of the quench front, the partition factor was evaluated as a function of the axial distance downstream of the quench front. It is clear that the partition factor increases downstream from the quench front. This is because the thermal boundary layer thickness and accordingly the latent heat portion of the total heat transfer rate increases with distance from the quench front. As shown, increasing surface wall temperature, decreasing mass flux and subcooling at the quench front results in higher values of the partition factor, i.e., increasing the latent heat

portion of the total heat transfer rate. However, the effect of subcooling at the quench front is more significant than that of surface wall temperature and mass flux.

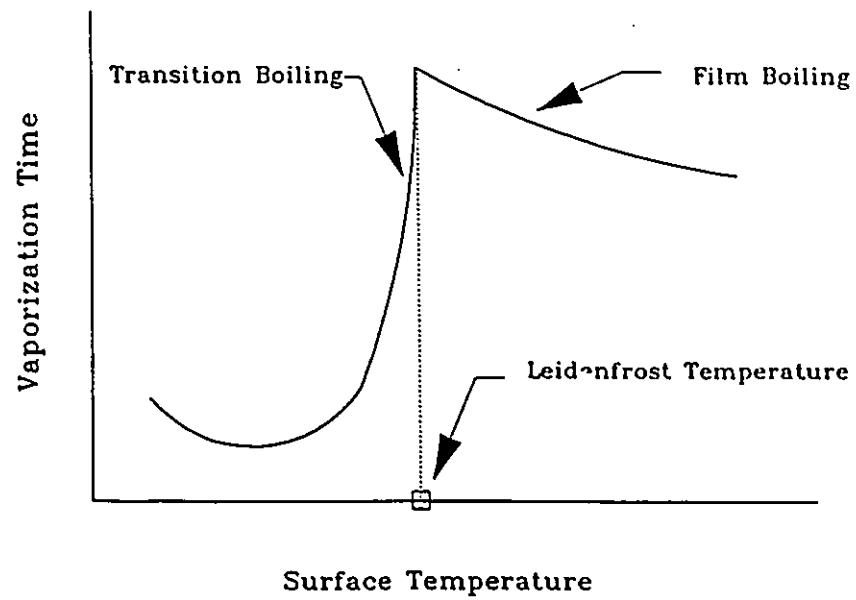


FIGURE 6-1 LEIDENFROST TEMPERATURE

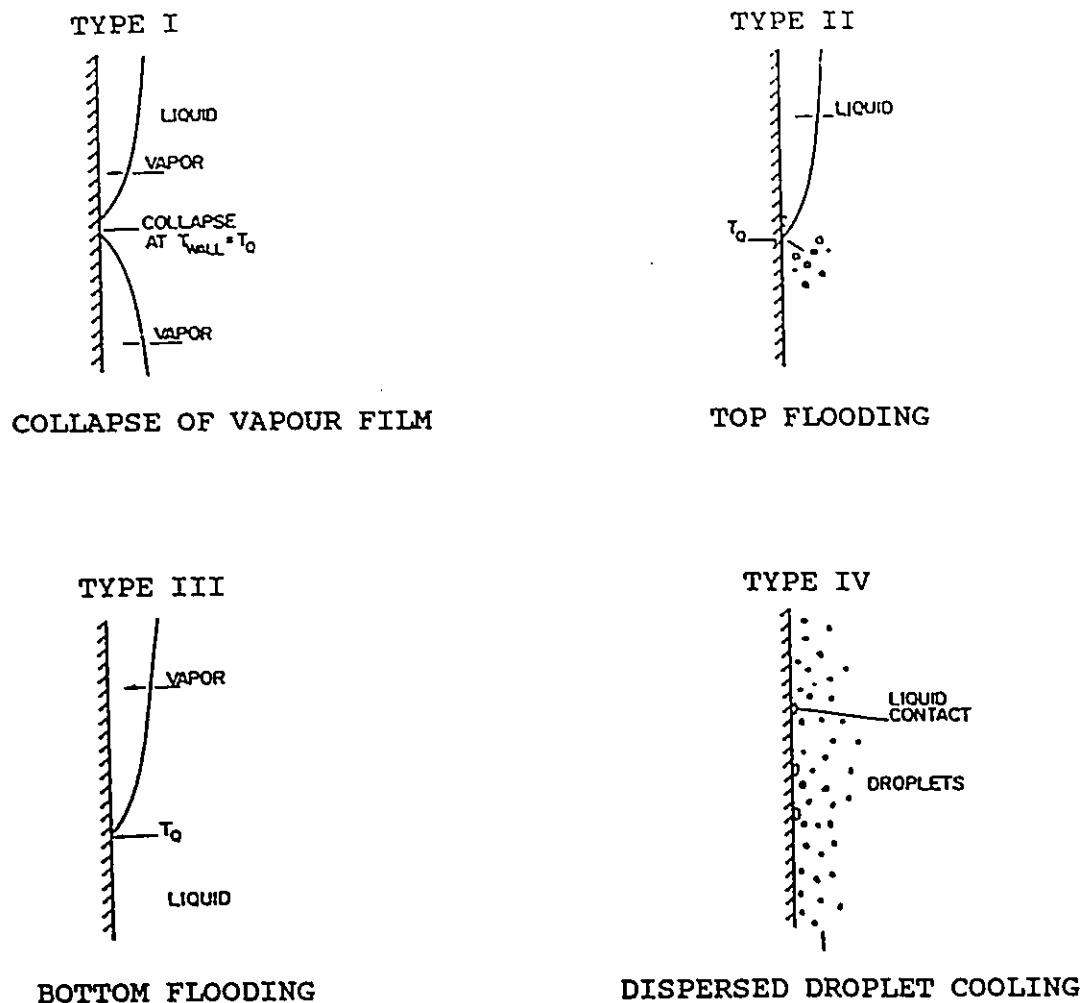


FIGURE 6-2 FILM BOILING TERMINATION MECHANISMS

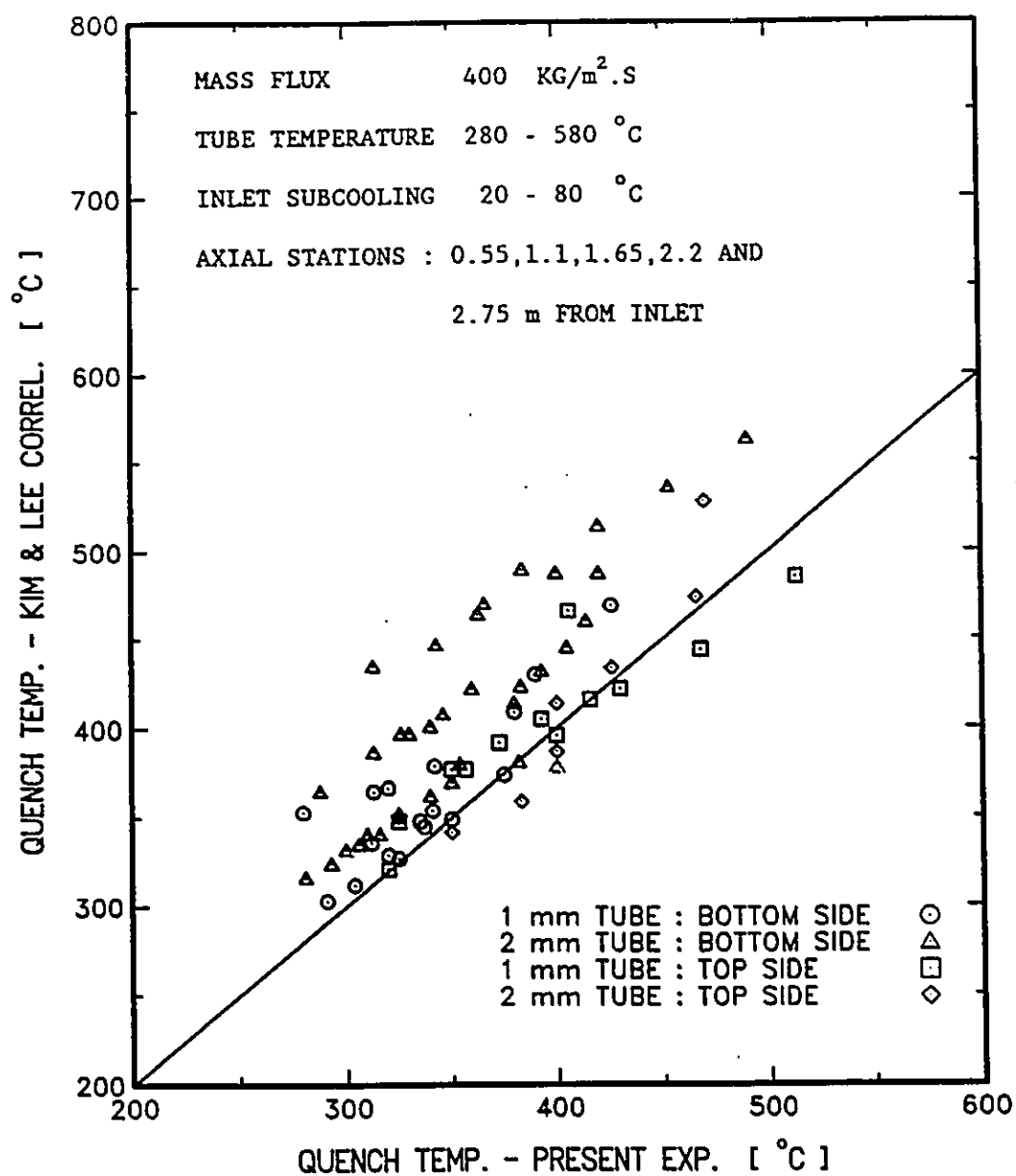


FIGURE 6-3 COMPARISON BETWEEN THE APPARENT QUENCH TEMPERATURE OF THE PRESENT EXPERIMENTS WITH THAT PREDICTED BY CORRELATION [KIM AND LEE (1979)]

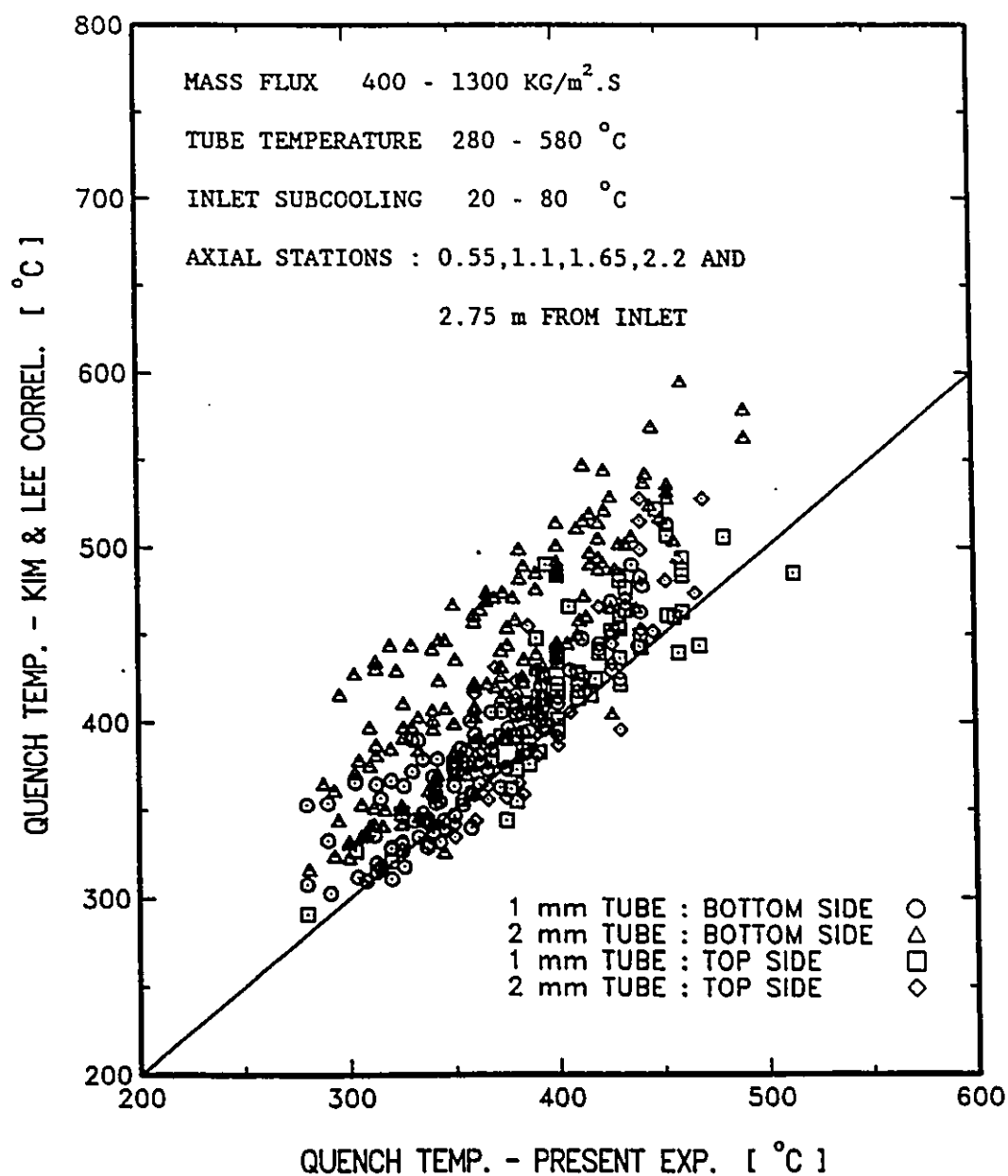


FIGURE 6-4 COMPARISON BETWEEN THE APPARENT QUENCH TEMPERATURE OF THE PRESENT EXPERIMENTS WITH THAT PREDICTED BY CORRELATION [KIM AND LEE (1979)]

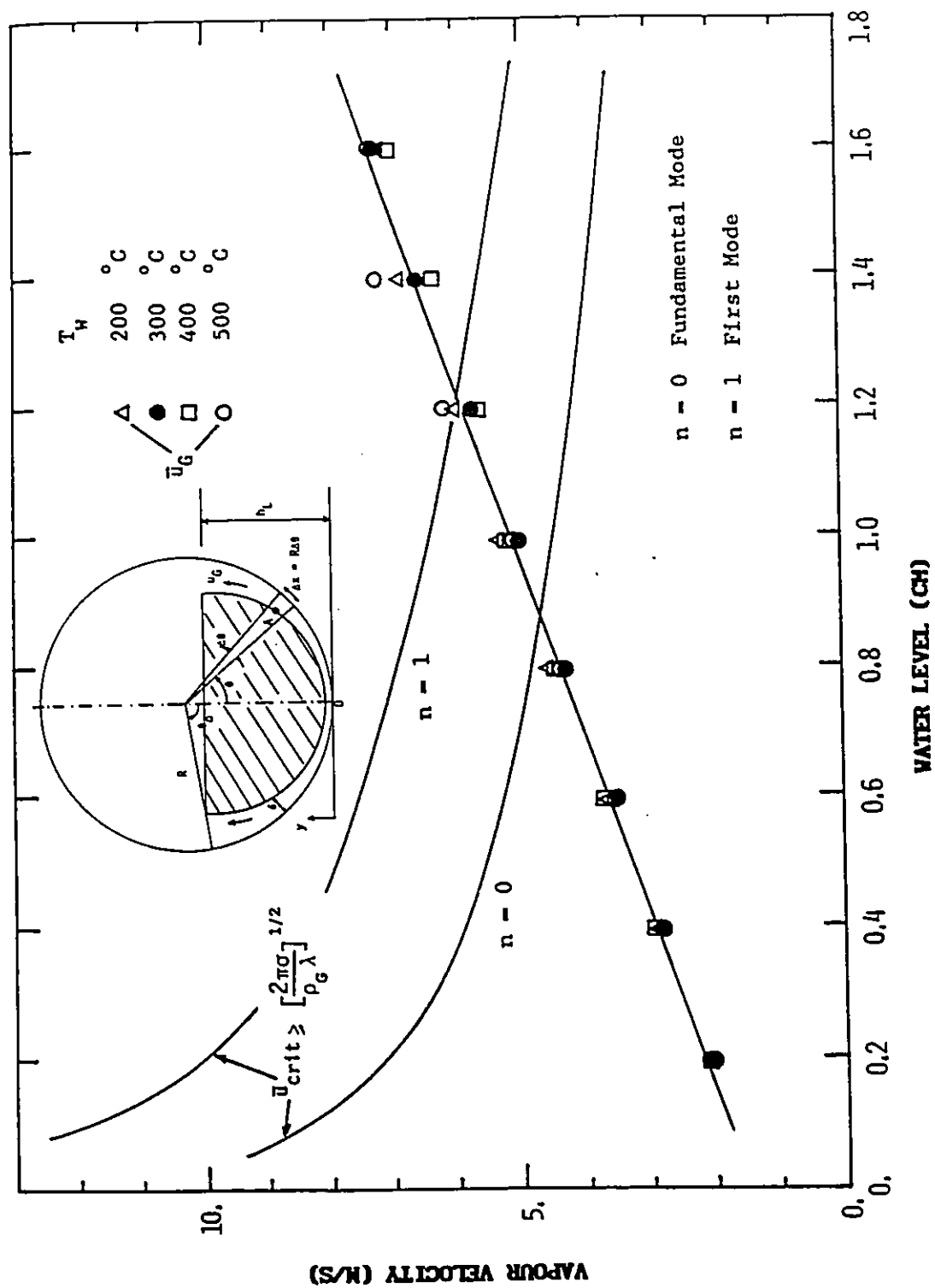


FIGURE 8-5 CRITICAL AND AVERAGE VAPOUR VELOCITIES VERSUS WATER LEVEL [CHAN AND BANERJEE (1981)]

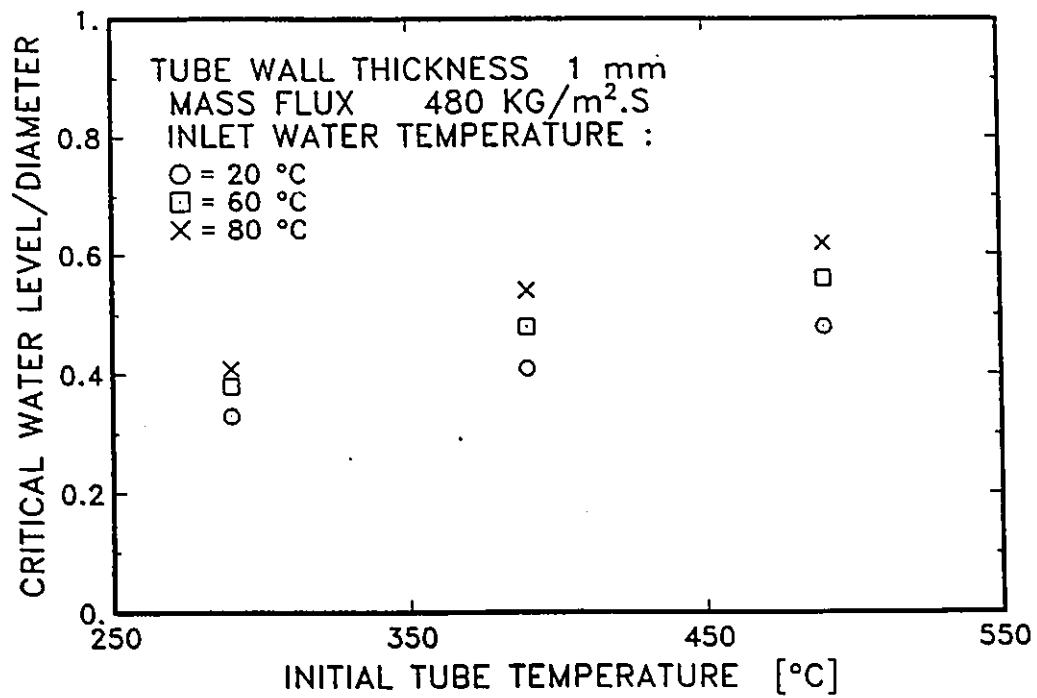


FIGURE 6-6a EFFECT OF INITIAL TUBE TEMPERATURE
AND WATER SUBCOOLING ON THE CRITICAL
WATER LEVEL

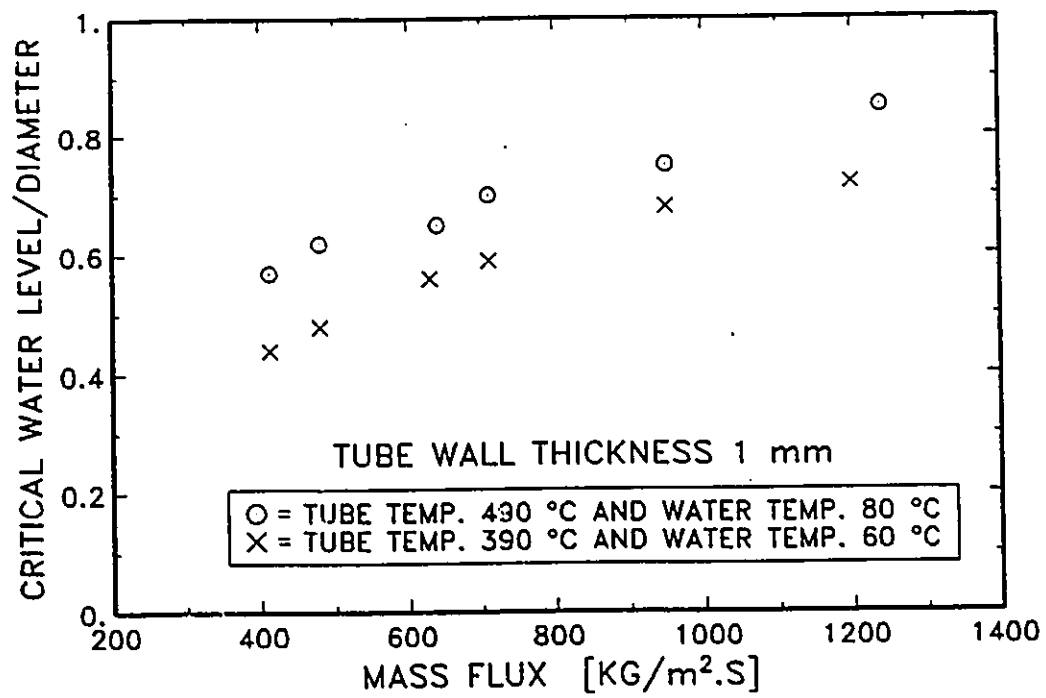


FIGURE 6-6b EFFECT OF MASS FLUX ON THE CRITICAL WATER LEVEL

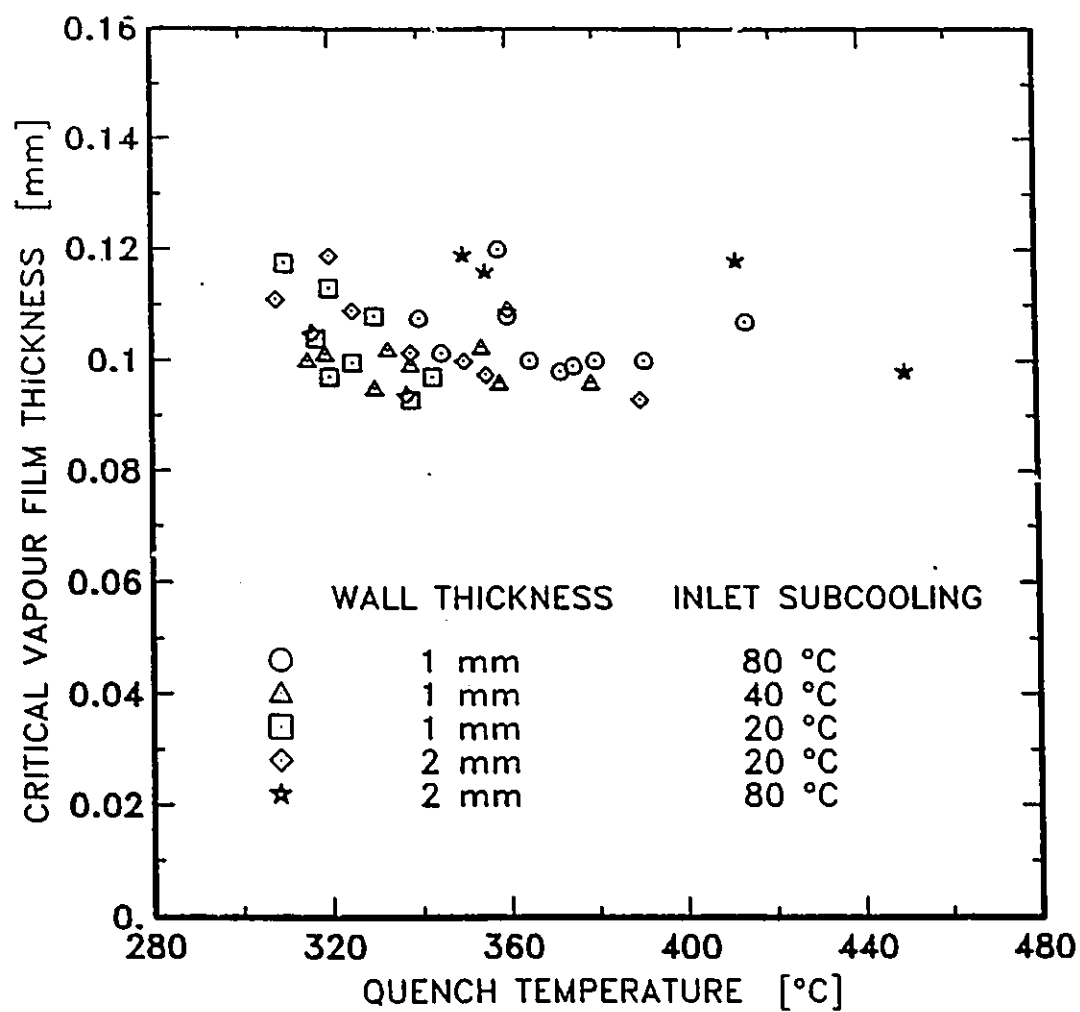
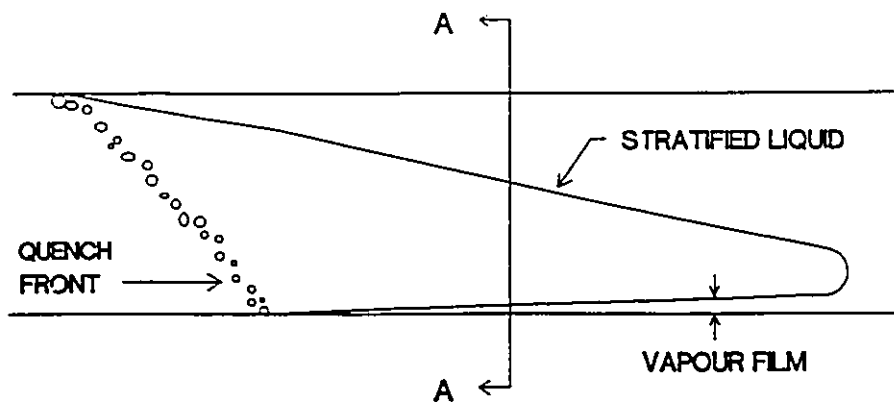
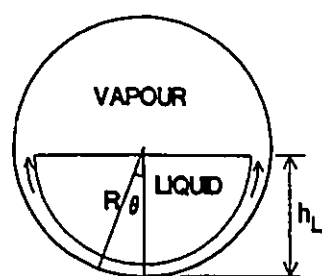


FIGURE 6-7 CRITICAL VAPOUR FILM THICKNESS
VERSUS QUENCH TEMPERATURE

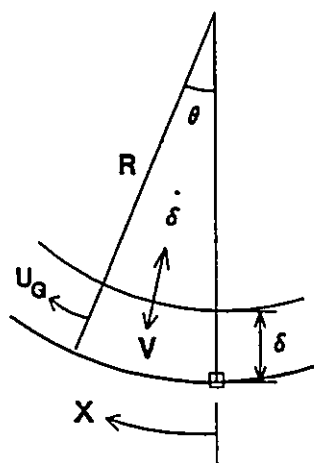


6-8a



SECTION A-A

6-8b



6-8c

FIGURE 6-8 OVERALL GEOMETRY AND PROPOSED MODEL

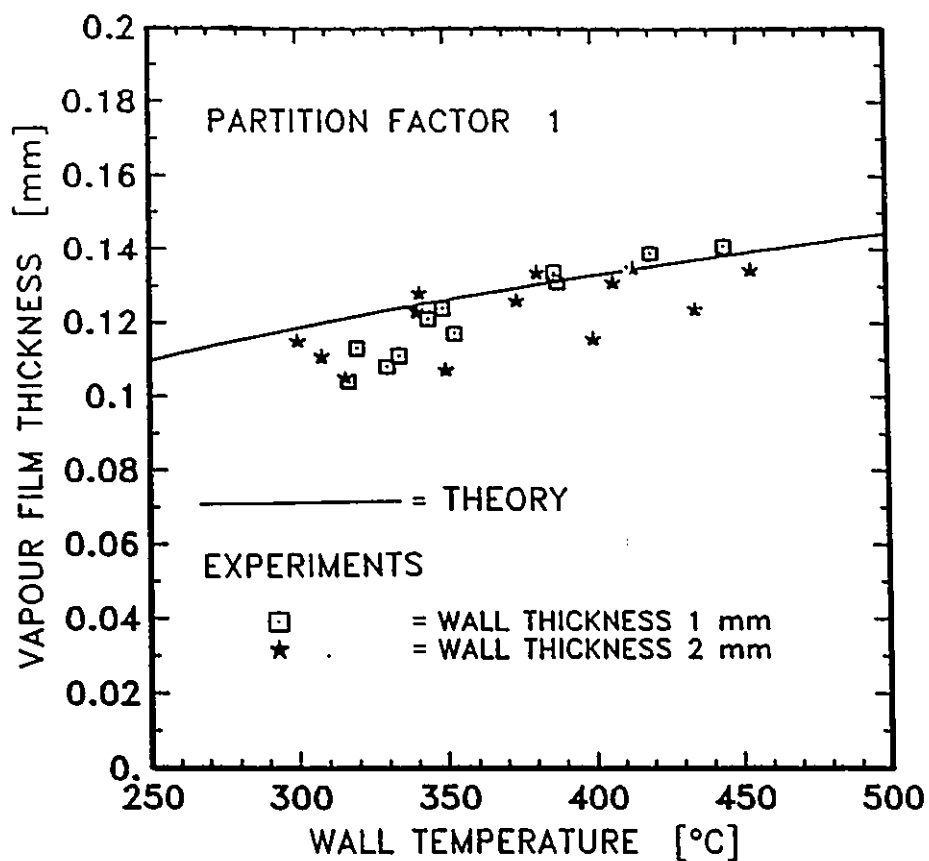


FIGURE 6-9 EQUILIBRIUM VAPOUR FILM THICKNESS
VERSUS TUBE WALL TEMPERATURE.
THEORY AND EXPERIMENTS

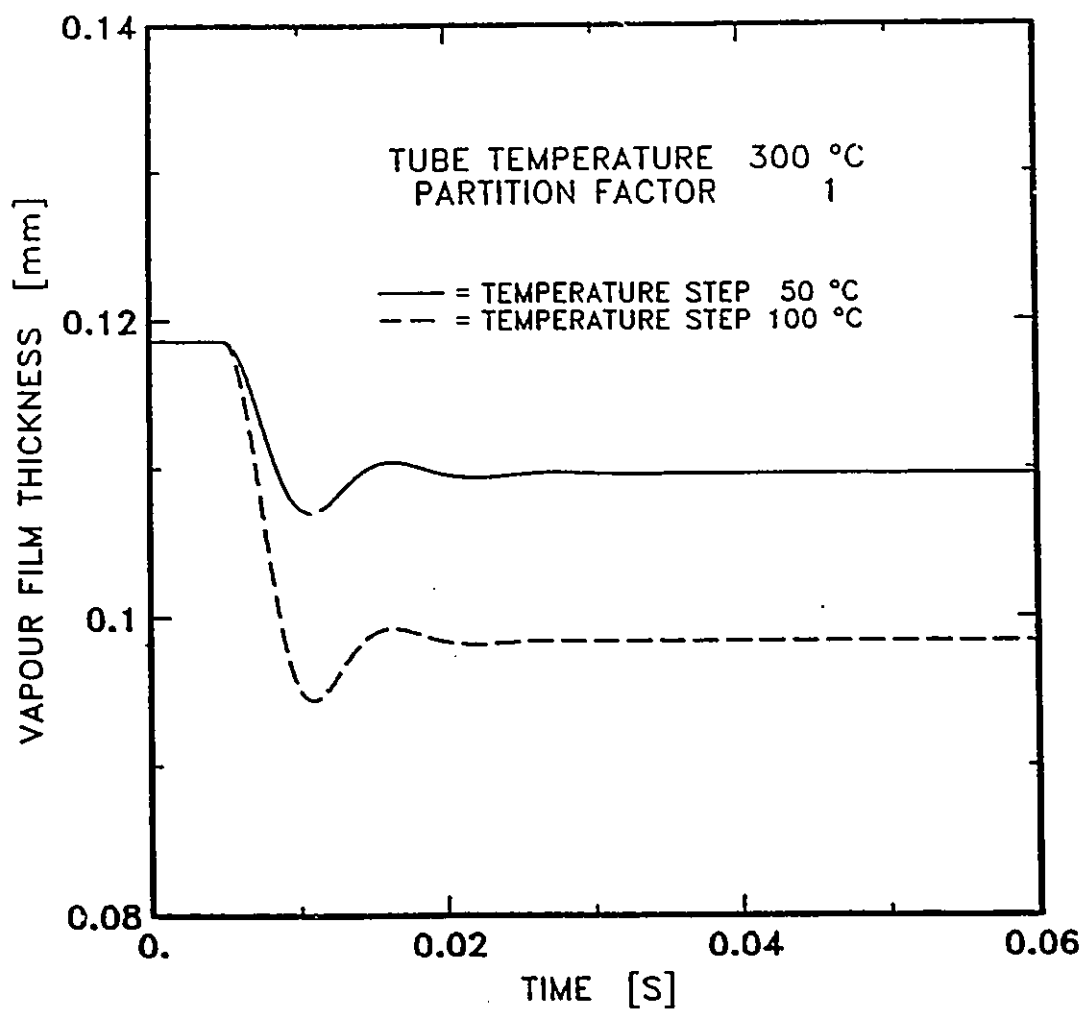


FIGURE 6-10 DYNAMIC RESPONSE OF LIQUID-VAPOUR INTERFACE TRIGGERED BY STEP CHANGE IN TUBE TEMPERATURE

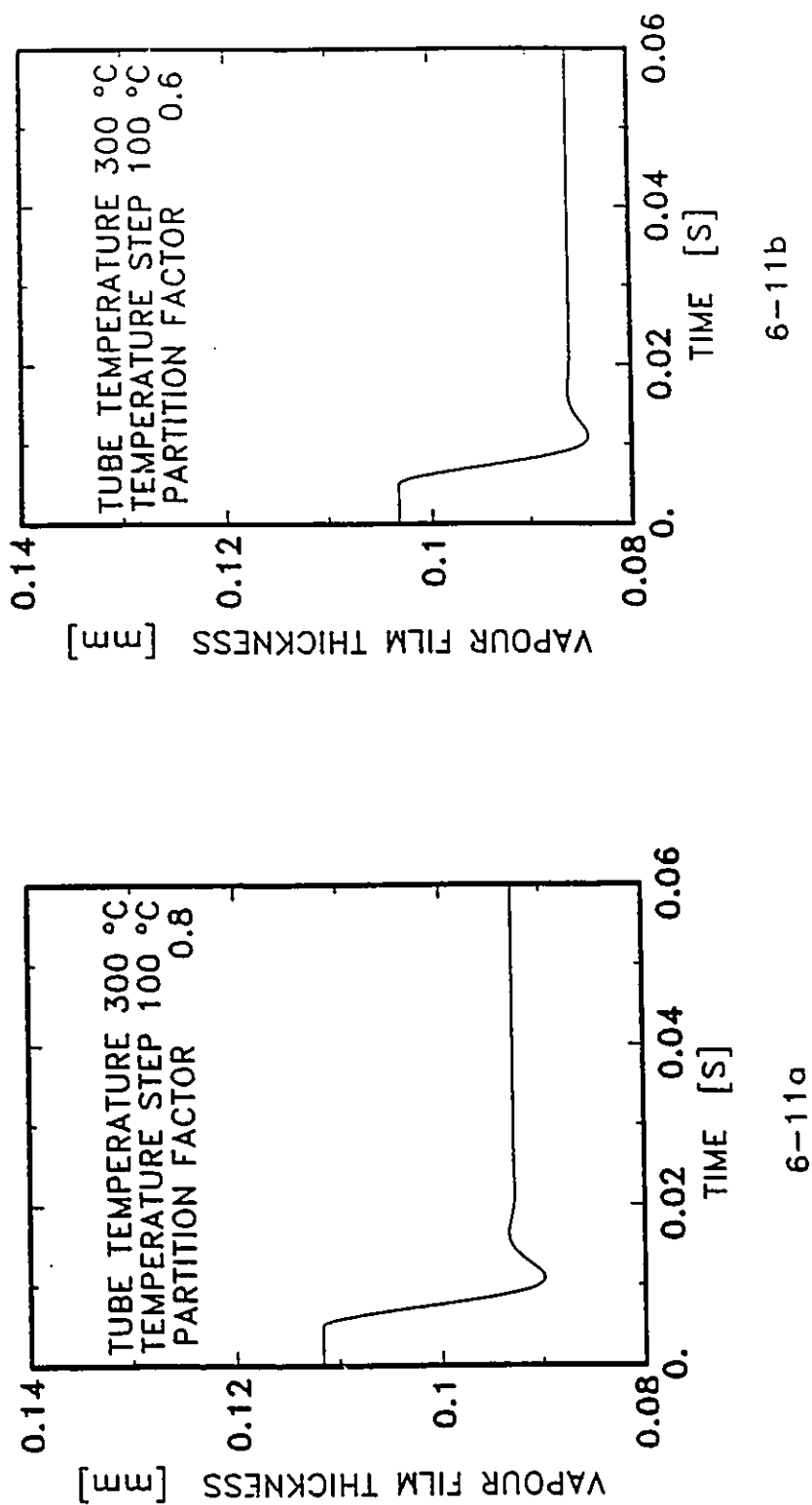


FIGURE 6-11 EFFECT OF SUBCOOLING AND LIQUID VELOCITY ON
THE DYNAMIC RESPONSE OF THE LIQUID-VAPOUR INTERFACE

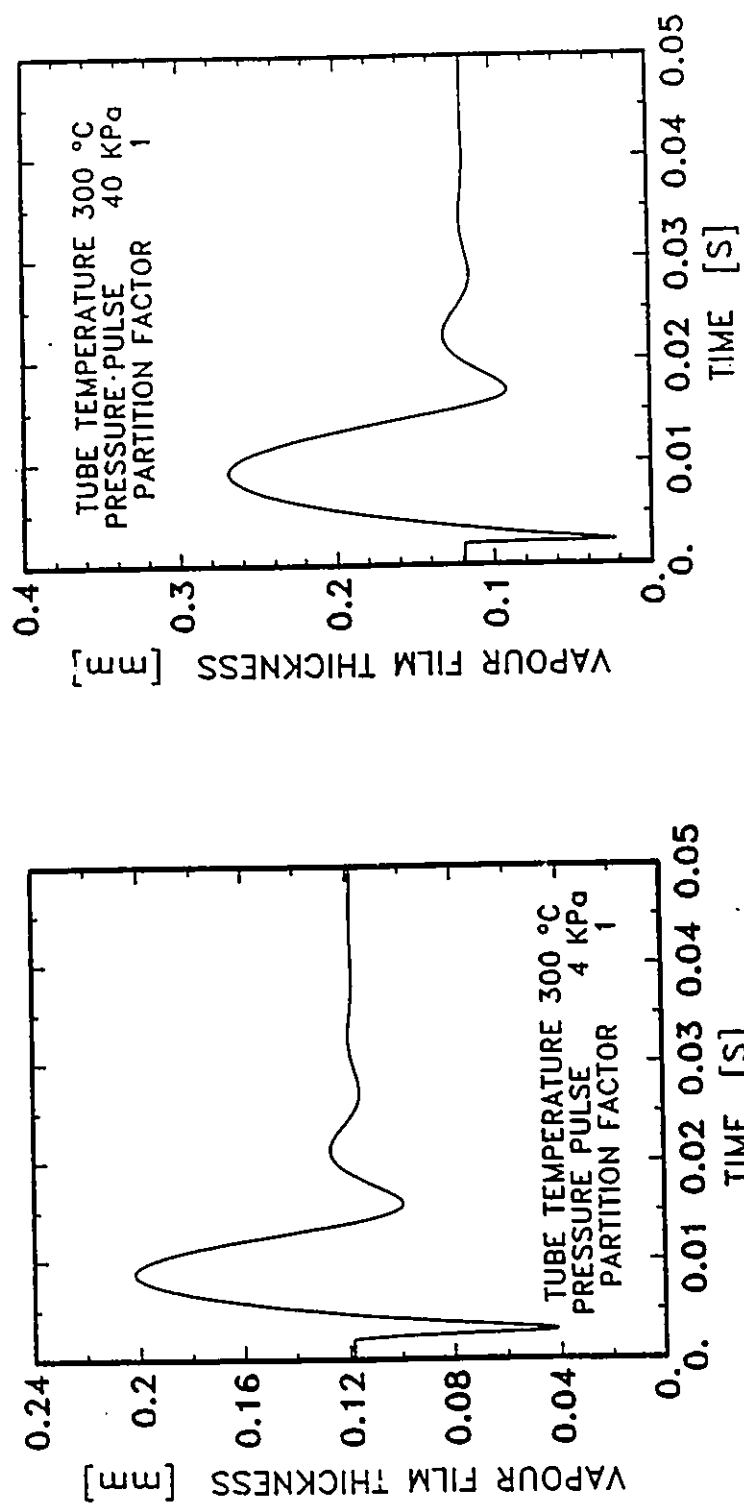


FIGURE 6-12 DYNAMIC RESPONSE OF LIQUID-VAPOUR INTERFACE TRIGGERED BY A PRESSURE PULSE

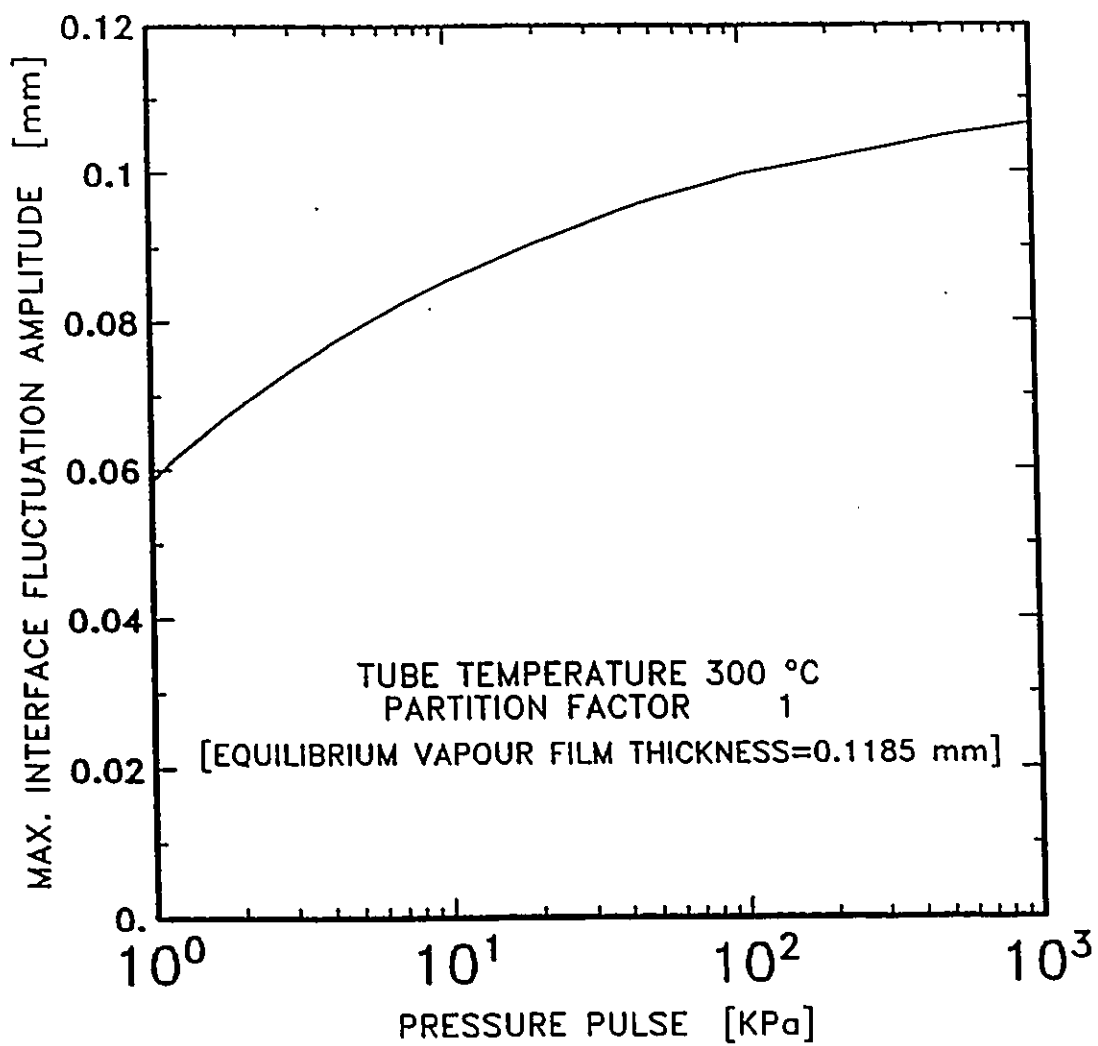


FIGURE 6-13 PRESSURE PULSE VERSUS MAXIMUM AMPLITUDE OF INTERFACE FLUCTUATIONS

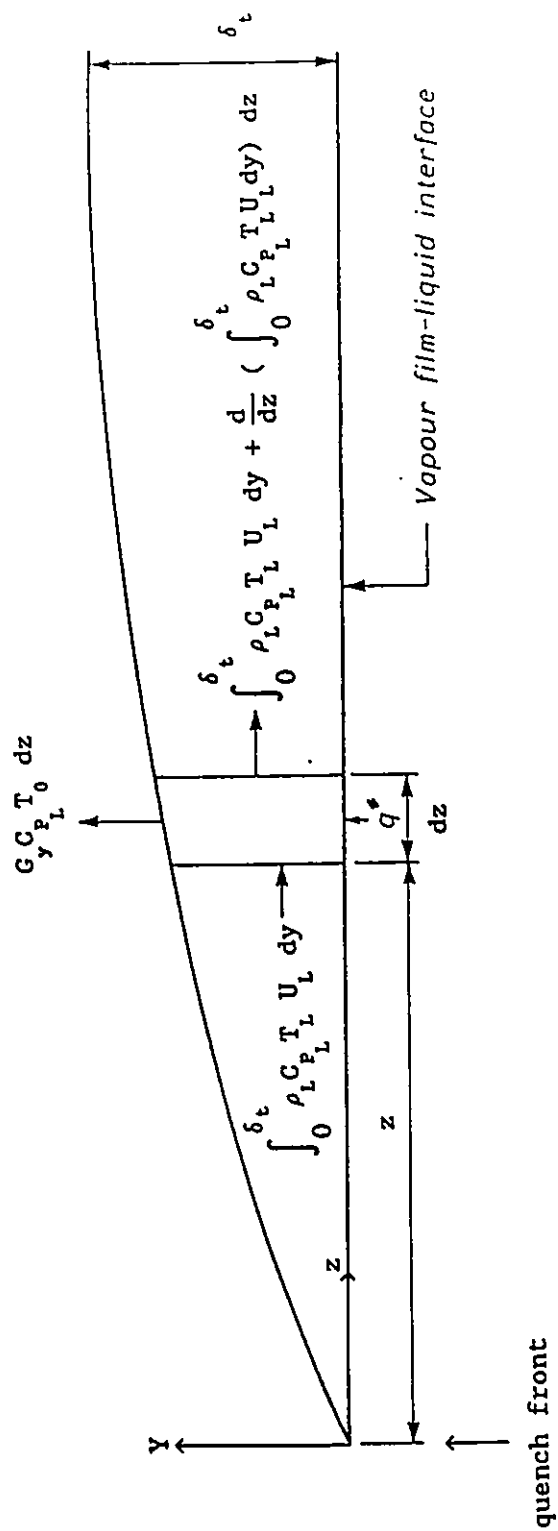


FIGURE 6-14: INTEGRAL FORMULATION OF THE THERMAL BOUNDARY LAYER
IN THE LIQUID PHASE

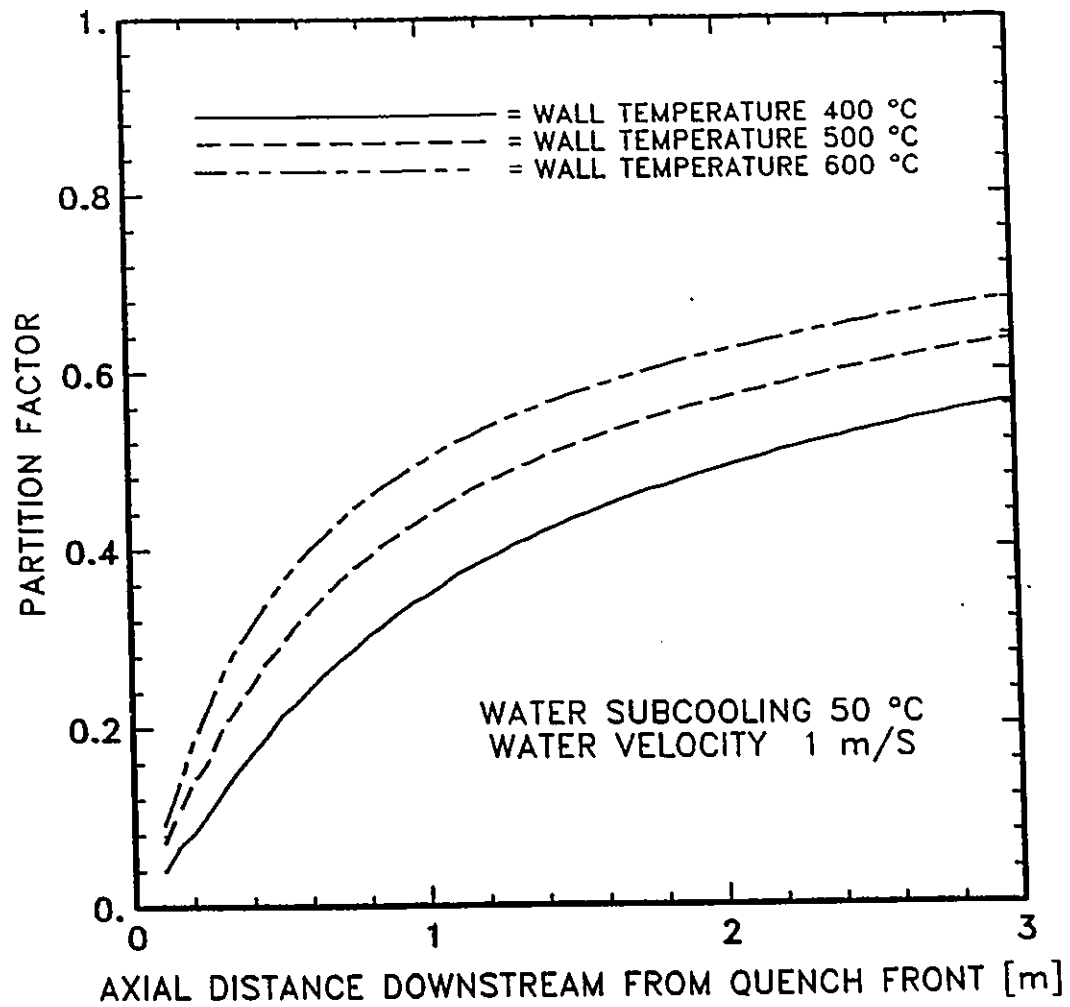


FIGURE 6-15 PARTITION FACTOR AT DIFFERENT TUBE WALL TEMPERATURES

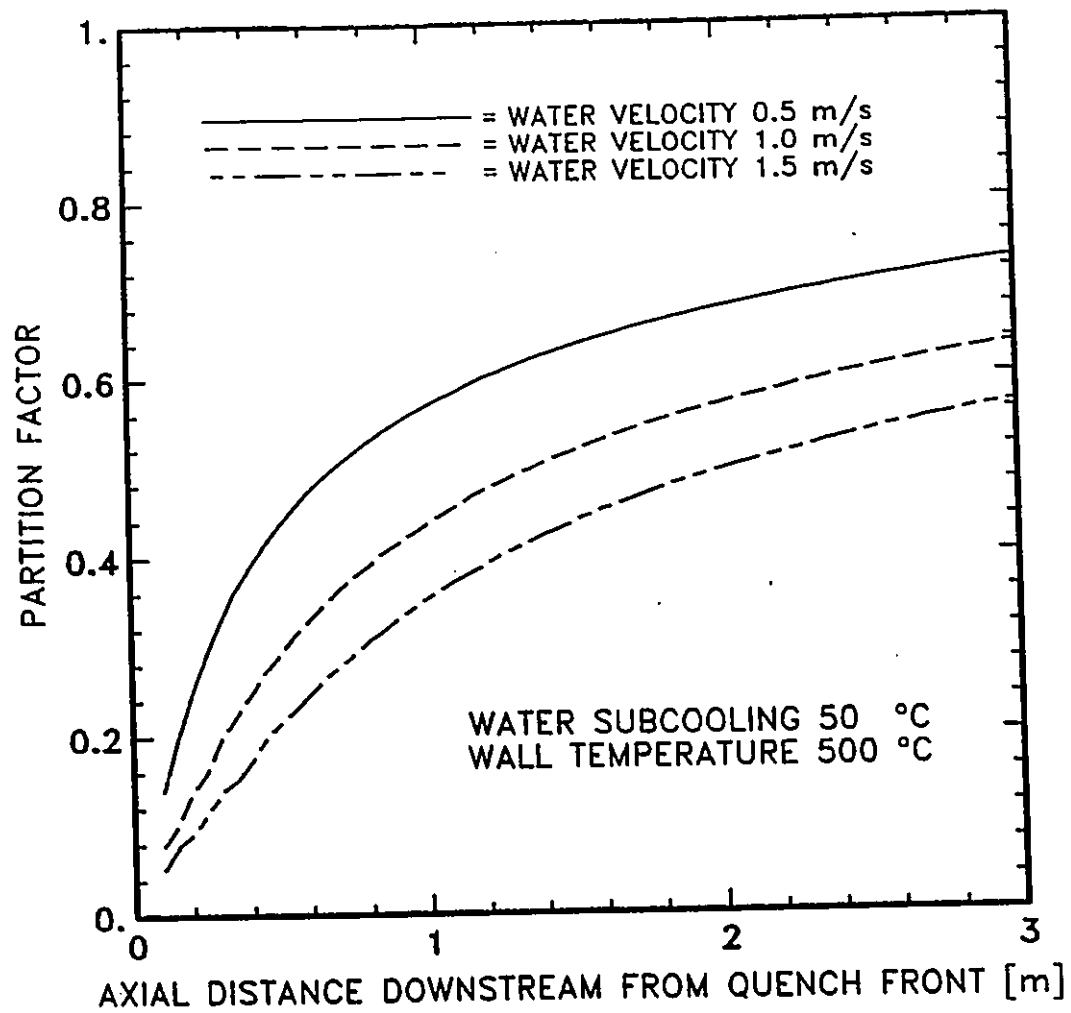


FIGURE 6-16 PARTITION FACTOR AT DIFFERENT WATER VELOCITIES

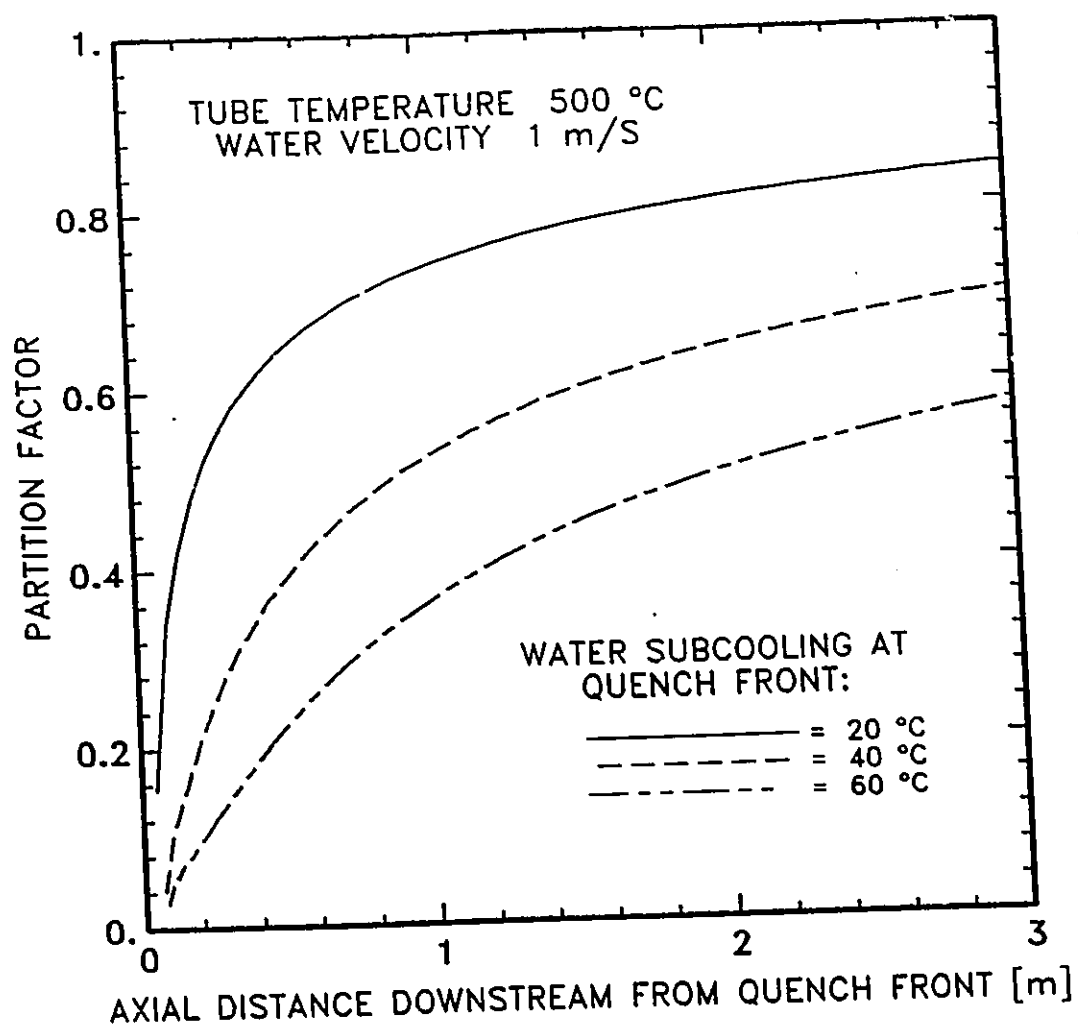


FIGURE 6-17 PARTITION FACTOR AT DIFFERENT SUBCOOLINGS

CHAPTER 7

TWO-FLUID MODEL

7-1 INTRODUCTION.

A well known approach in modelling the rewetting process, which has appeared extensively in the literature, is conduction controlled modelling. In conduction controlled models, it is assumed that the quench velocity is determined by the rate at which heat can be conducted from the dry hot side to the cooler wetted side of the wall where it is removed by boiling. In these models, all thermal and hydraulic processes associated with the quench process are frozen by assuming a constant quench velocity and using a moving coordinate system which moves with a speed equal to the quench velocity. This approach can be justified for the case of vertical systems rewetted by falling liquid films since the flow and heat transfer parameters in the vicinity of the quench front remain almost unchanged as the quench front propagates down along the hot surface. This approach may not be valid for bottom reflooding in vertical systems since the flow patterns and heat transfer regimes associated with the quench front may change as the quench front propagates upward. In the case of horizontal systems, the problem is more complicated due to possible flow stratification caused by gravitational effects. Therefore, it is essential to use a two-fluid model to incorporate all the important thermohydraulic aspects associated with the process.

The general approach in developing the two-fluid model presented by Chan and Banerjee (1981) has been followed in the present study. However, the main features of the present work are:

- i- A different numerical scheme for solving the hydraulic equations is used which showed a very good ability to predict the hydrodynamics under a wide range of mass flux.
- ii- The rewetting criterion developed in the present work was incorporated in the two-fluid model. The rewetting criterion is a key factor in predicting the propagation of the quench front.
- iii- The newly derived theoretical models for the partition factor (fraction of heat used in evaporation), and the film boiling heat transfer coefficient are used in the present model.
- iv- The model is extended to handle the inverted annular flow which was found to exist under certain conditions namely, high coolant mass flux and high tube heat capacity.

7-2 MODELLING OF MULTI-PHASE SYSTEMS.

Generally, a multi-phase flow system can be considered as a field subdivided into single phase regions separated by moving boundaries. The formulation of a mathematical model for such flow system is more complicated than for single phase flow due to the changing phase distribution and shape of the interface. Accordingly, local instantaneous conservation equations for each phase and the corresponding jump conditions at the interfaces are required. Normally these equations are simplified by means of an appropriate averaging procedure to yield field averaged balance equations describing the

macroscopic behaviour of the multi-phase flow system.

7-2-1 LOCAL INSTANTANEOUS CONSERVATION EQUATIONS:

The details of deriving the local instantaneous conservation equations have been studied by Vernier and Delhay (1968) and Ishii (1975) among others. The fundamental conservation laws are expressed by integral balance equations written for a fixed finite control volume containing both phases as shown in figure 7-1 . They are the balances of mass, momentum, and energy.

The generalized form is:

$$\begin{aligned} \sum_{k=1,2} \frac{d}{dt} \int_{V_k(t)} \rho_k \psi_k dV - \sum_{k=1,2} \int_{a_k(t)} \rho_k \psi_k (\bar{U}_k \cdot \bar{n}_k) da \\ + \sum_{k=1,2} \int_{V_k(t)} \rho_k \phi_k dV - \sum_{k=1,2} \int_{a_k(t)} \bar{n}_k \cdot \bar{J}_k da \end{aligned} \quad (7.1)$$

For a material volume $V(t)$, the expressions of ψ_k , J_k , and ϕ_k for mass, momentum, and energy conservation are given in the following table.

Balance	ψ_k	\bar{J}_k	ϕ_k
Mass	1	0	0
Momentum	\bar{U}_k	$-\bar{\sigma}_k$	\bar{g}
Energy	$e_k + \frac{1}{2} U_k^2$	$\bar{q}_k - \bar{\sigma}_k \cdot \bar{U}_k$	$\bar{g} \cdot \bar{U}_k + Q_k$

where \bar{U}_k is the velocity field of the fluid, $\bar{\sigma}_k$ is the stress tensor, e_k is the internal energy, \bar{q}_k is the heat flux, and Q_k is the heat generation term.

The integral balance equation, is transformed by using the Leibnitz rule and the Gauss theorem into the following form:

$$\sum_{k=1,2} \int_{V_k(t)} \left[\frac{\partial}{\partial t} (\rho_k \phi_k) + \nabla \cdot (\rho_k \phi_k \bar{U}_k) + \nabla \cdot \bar{J}_k - \rho_k \phi_k \right] dV - \int_{a_1(t)} \left[\sum_{k=1,2} \rho_k \phi_k (\bar{U}_k - \bar{U}_1) \cdot \bar{n}_k + \bar{n}_k \cdot \bar{J}_k \right] da = 0 \quad (7.2)$$

where \bar{U}_1 is the interface velocity.

Equation 7.2 has to be satisfied for all values of \bar{U}_k and $a_1(t)$. Therefore, the local instantaneous phase equations can be written as:

$$\frac{\partial}{\partial t} (\rho_k \phi_k) + \nabla \cdot (\rho_k \phi_k \bar{U}_k) + \nabla \cdot \bar{J}_k - \rho_k \phi_k = 0 \quad (7.3)$$

and the local instantaneous jump conditions as:

$$\sum_{k=1,2} \left[\rho_k \phi_k (\bar{U}_k - \bar{U}_1) \cdot \bar{n}_k + \bar{n}_k \cdot \bar{J}_k \right] = 0 \quad (7.4)$$

$$\text{where } \rho_k \bar{n}_k \cdot (\bar{U}_k - \bar{U}_1) = \dot{m}_k = \text{rate of mass leaving phase } k \quad (7.5)$$

7-2-2 AVERAGING PROCEDURES

Since for many engineering applications averaged flow quantities are sufficient, one of the main approaches in multi-phase flow modelling has been to develop an averaged set of field equations

based on the local instantaneous conservation equations (Ishii (1975), Delhayé and Achard (1976), Agee et al (1978) and Banerjee and Chan (1980)). Accordingly, much simpler mathematical models could be generated describing the macroscopic behaviour of the system. However, some information will be lost in the averaging process and should be supplied in the form of constitutive equations.

Various forms of averaging applicable to the two-phase flow equations have been discussed by Ishii (1975), Delhayé and Achard (1976) and Banerjee and Chan (1980). However, the widely used averaging procedures are:

- i- Space averaging (volume or area).
- ii- Time averaging.
- iii- Ensemble-space averaging.
- iv- Time-space averaging.

It is important to note that any averaging procedure adopted should lead to mean flow parameters that are continuous and have continuous first derivatives. Accordingly, double averaging is normally required to avoid any discontinuity in the first derivatives of the flow parameters which could happen using area or time averaging only.

7-2-2-1 THE AVERAGED EQUATIONS.

The time-volume averaged equations are the most convenient and appropriate form for one dimensional approximation. This could be achieved by any order since time and volume averaging operations are commutative (Delhayé and Achard (1976)).

To derive the one-dimensional volume-averaged form of the

conservation equations, consider figure 7.2 where V_k represents the volume of phase k enclosed between the walls and the cross-sectional plane spaced a distance z apart. If we integrate the local instantaneous balance equations for phase k over a volume $V_k(t,z)$ and using Gauss' theorem and Leibnitz' rule, the generalized volume-averaged one-dimensional conservation equation could be shown as (Banerjee and Chan(1980)):

$$\begin{aligned} \frac{\partial}{\partial t} \alpha_k \langle \rho_k \psi_k \rangle + \frac{\partial}{\partial z} \alpha_k \langle \bar{n}_z \cdot (\rho_k \psi_k \bar{U}_k + \bar{J}_k) \rangle - \alpha_k \langle \rho_k \phi_k \rangle \\ = - \frac{1}{V} \int_{a_1} (\dot{m}_k \psi_k + \bar{J}_k \cdot \bar{n}_k) da - \frac{1}{V} \int_{a_{kw}} \bar{n}_{kw} \cdot \bar{J}_k da \end{aligned} \quad (7.6)$$

where the definitions

$$\langle f_k \rangle = \frac{1}{V_k} \int_{V_k} f_k dV \quad (7.7)$$

$$\langle f_k \rangle_i = \frac{1}{V} \int_{a_1} f_k da \quad (7.8)$$

$$V = \sum_{k=1,2} V_k \quad (7.9)$$

$$\alpha_k = \frac{V_k}{V} \quad (7.10)$$

and \dot{m}_k is the mass transfer rate out of phase k .

The forms of mass, momentum, and energy conservation equations will now be considered.

Mass Conservation:

For this case, $\psi_k = 1$, $\bar{J}_k = 0$, and $\phi_k = 0$. Equation 7.6 becomes

$$\frac{\partial}{\partial t} \alpha_k \langle \rho_k \rangle + \frac{\partial}{\partial z} \alpha_k \langle \rho_k u_k \rangle = - \langle \dot{m}_k \rangle_i \quad (7.11)$$

where u_k is the velocity component in z direction.

Momentum Conservation:

For this case, $\psi_k = \bar{U}_k$, $\bar{J}_k = -\bar{\sigma}_k = \delta_{1j} p_k = \bar{\tau}_k$, and $\phi_k = \bar{g}$. Taking the dot product of equation 7.6 with \bar{n}_z (the unit z-direction vector), the z-direction momentum conservation equation is obtained

$$\begin{aligned} & \frac{\partial}{\partial t} \alpha_k \langle \rho_k u_k \rangle + \frac{\partial}{\partial z} \alpha_k \langle \rho_k u_k^2 \rangle + \frac{\partial}{\partial z} \alpha_k \langle p_k \rangle \\ & - \frac{\partial}{\partial z} \alpha_k \langle \bar{n}_k \cdot (\bar{\tau}_k \cdot \bar{n}_z) \rangle = \alpha_k \langle \rho_k g_z \rangle \\ & = -\frac{1}{V} \int_{a_i} [\dot{m}_k u_k + \bar{n}_z \cdot \bar{n}_k p_k - \bar{n}_z \cdot (\bar{n}_z \cdot \bar{\tau}_k)] da \\ & + \frac{1}{V} \int_{a_{kw}} \bar{n}_z \cdot (\bar{n}_{kw} \cdot \bar{\tau}_k) da \end{aligned} \quad (7.12)$$

where the relationship $\bar{n}_{kw} \cdot \bar{n}_z p_k = 0$, has been used, since $\bar{n}_{kw} \cdot \bar{n}_z = 0$ for constant cross section.

The pressure term on the right hand side can be made more explicit by considering an average and a fluctuating part (Chan and Banerjee (1981)). Consider

$$\int_{a_1} \bar{n}_k \cdot (\bar{n}_z p_k) da = \int_{a_1} \bar{n}_k \cdot [\bar{n}_z (\langle p_k \rangle + \Delta p_{k1} + \Delta p_{k1}^1)] da \quad (7.13)$$

where $\Delta p_{k1} = \langle p_{k1} \rangle - \langle p_k \rangle$ is the difference between the average interfacial and averaged phase pressures, and $\Delta p_{k1}^1 = p_{k1} - \langle p_{k1} \rangle$ is the difference between the local and average interfacial pressures.

Using Gauss' theorem

$$\begin{aligned} \frac{1}{V} \int_{a_1} \bar{n}_k \cdot (\bar{n}_z p_k) da = & - \left[\langle p_k \rangle + \Delta p_{k1} \right] \frac{\partial \alpha_k}{\partial z} \\ & + \frac{1}{V} \int_{a_1} \bar{n}_k \cdot (\bar{n}_z \Delta p_{k1}^1) da \end{aligned} \quad (7.14)$$

Substituting equation 7.14 into equation 7.12 we get

$$\begin{aligned} \frac{\partial}{\partial t} \alpha_k \langle \rho_k u_k \rangle + \frac{\partial}{\partial z} \alpha_k \langle \rho_k u_k^2 \rangle + \alpha_k \frac{\partial \langle p_k \rangle}{\partial z} - \frac{\partial}{\partial z} \alpha_k \langle r_{zz,k} \rangle - \Delta p_{k1} \frac{\partial \alpha_k}{\partial z} \\ = \alpha_k \langle \rho_k g_z \rangle - \langle \dot{m}_k \dot{u}_k \rangle_i - \langle \Delta p_{k1}^1 \rangle_i \\ + \langle (\bar{n}_z \cdot \bar{r}_z) \rangle_i + \langle (\bar{n}_{kw} \cdot \bar{r}_z) \rangle_w \end{aligned} \quad (7.15)$$

For most cases, equation 7.15 reduces to the usual constant phase pressures by letting $\Delta p_{k1} = \Delta p_{k1}^1 = 0$. However, in many cases, this assumption is not appropriate. For example, in the present case stratification in the horizontal system is governed by the term Δp_{k1} . However, assuming a smooth surface interface leads to the absence of interface pressure fluctuations ($\Delta p_{k1}^1 = 0$).

Energy Conservation:

For this case, $\phi_k = e_k + \frac{u_k^2}{2} = E_k$, $\bar{J}_k = \bar{q}_k \cdot (\bar{p}_k \delta_{ij} - \bar{r}_k) \cdot \bar{U}_k$, and $\phi_k = \bar{g}_k \cdot \bar{U}_k$

Equation 7.6 becomes

$$\begin{aligned} & \frac{\partial}{\partial t} \alpha_k \langle \rho_k E_k \rangle + \frac{\partial}{\partial z} \alpha_k \langle \rho_k E_k u_k \rangle + \frac{\partial}{\partial z} \alpha_k \langle q_{z,k} \rangle \\ & + \frac{\partial}{\partial z} \alpha_k \langle \rho_k u_k \rangle - \frac{\partial}{\partial z} \alpha_k \langle \bar{n}_k \cdot (\bar{r}_k \cdot \bar{U}_k) \rangle \\ & = - \frac{1}{V} \int_{a_1} \left[\dot{m}_k E_k + \bar{n}_k \cdot (\bar{q}_k + p_k \bar{U}_k - \bar{r}_k \cdot \bar{U}_k) \right] da \\ & - \frac{1}{V} \int_{a_{kw}} n_{kw} \cdot \bar{q}_k da + \alpha_k \langle \rho_k (\bar{g} \cdot \bar{U}_k) \rangle \end{aligned} \quad (7.16)$$

But

$$\begin{aligned} & - \frac{1}{V} \int_{a_1} (\dot{m}_k E_k + \bar{n}_k \cdot p_k \bar{U}_k) da = - \frac{1}{V} \int_{a_1} \left[\dot{m}_k \left(h_k + \frac{u_k^2}{2} - \frac{p_k}{\rho_k} \right) + \frac{p_k}{\rho_k} \dot{m}_k + p_k \bar{n}_k \cdot \bar{U}_k \right] da \\ & = - \frac{1}{V} \int_{a_1} \left[\dot{m}_k \left(h_k + \frac{u_k^2}{2} \right) + p_k (\bar{n}_k \cdot \bar{U}_k) \right] da \end{aligned} \quad (7.17)$$

where the relation $E_k = h_k + \frac{u_k^2}{2} - \frac{p_k}{\rho_k}$ has been used in which h_k is the enthalpy of phase k .

Treating the pressure term as in the momentum equation and using Leibnitz' rule we could write

$$\begin{aligned}
\frac{1}{V} \int_{a_1} p_k (\bar{n}_k \cdot \bar{U}_1) da - \left[\langle p_k \rangle + \Delta p_{k1} \right] \frac{\partial \alpha_k}{\partial t} \\
+ \frac{1}{V} \int_{a_1} \Delta p_{k1} (\bar{n}_k \cdot \bar{U}_1) da
\end{aligned} \quad (7.18)$$

Using equations 7.17 and 7.18, the volume averaged energy equation 7.16, can be written as

$$\begin{aligned}
\frac{\partial}{\partial t} \alpha_k \left\langle \rho_k \left(h_k + \frac{u_k^2}{2} \right) \right\rangle + \frac{\partial}{\partial z} \alpha_k \left\langle \rho_k u_k \left(h_k + \frac{u_k^2}{2} \right) \right\rangle - \alpha_k \frac{\partial \langle p_k \rangle}{\partial t} \\
+ \Delta p_{k1} \frac{\partial \alpha_k}{\partial t} + \frac{\partial}{\partial z} \alpha_k \langle q_{z,k} \rangle - \frac{\partial}{\partial z} \alpha_k \langle \bar{n}_k \cdot (\bar{r}_k \cdot \bar{U}_k) \rangle \\
= - \left\langle \left[\dot{m}_k \left(h_k + \frac{u_k^2}{2} \right) + \bar{n}_k \cdot \bar{U}_1 \Delta p_{k1} + \bar{n}_k \cdot \bar{q}_k - \frac{\partial}{\partial t} (\bar{n}_k \cdot \bar{U}_k \cdot \bar{r}_k) \right] \right\rangle_1 \\
- \langle (\bar{n}_{kw} \cdot \bar{q}_k) \rangle_w + \alpha_k \langle (\rho_k \bar{U}_k \cdot \bar{g}) \rangle
\end{aligned} \quad (7.19)$$

The local instantaneous form of the generalized conservation equation across the interface (equation 7.4) can be volume averaged in the same way as follows:

Interface Mass:

$$\psi_k = 1, J_k = 0$$

$$\sum_{k=1}^2 \frac{1}{V} \int_{a_i} \dot{m}_k dV = 0$$

or

$$\langle \dot{m}_1 \rangle_1 = - \langle \dot{m}_2 \rangle_1 \quad (7.20)$$

Interface Momentum:

$$\psi_k = \bar{U}_k, \quad \bar{J}_k = - \bar{\sigma}_k = p_k \delta_{ij} - \bar{r}_k$$

Taking the z-component only

$$\sum_{k=1}^2 \frac{1}{V} \int_{a_i} \left[\dot{m}_k \bar{U}_k + \bar{n}_z \cdot (\bar{n}_k p_k) - \bar{n}_z \cdot (\bar{n}_k \bar{r}_k) \right] da = 0 \quad (7.21)$$

Using equation 7.13 and 7.20, and knowing that $\bar{n}_1 = - \bar{n}_2$ we get

$$\begin{aligned} \left[\langle p_{11} \rangle - \langle p_{21} \rangle \right] \frac{\partial \alpha}{\partial z} &= \langle \dot{m}_1 (u_1 - u_2) + (\Delta p_{11} - \Delta p_{21}) \\ &\quad - \bar{n}_1 \cdot (\bar{r}_{1,z} - \bar{r}_{2,z}) \rangle_1 \end{aligned} \quad (7.22)$$

Interface Energy:

$$\psi_k = e_k + \frac{U_k^2}{2}, \quad \bar{J}_k = q_k + (p_k \delta_{ij} - \bar{r}_k) \cdot \bar{U}_k$$

$$\sum_{k=1}^2 \int_{a_i} \left[\dot{m}_k \left(h_k + \frac{U_k^2}{2} \right) + p_k (\bar{n}_k \cdot \bar{U}_k) + \bar{n}_k \cdot (\bar{q}_k - \bar{r}_k \cdot \bar{U}_k) \right] da = 0 \quad (7.23)$$

Using equations 7.18, and 7.20 we get

$$\begin{aligned}
[\langle p_{11} \rangle - \langle p_{21} \rangle] \frac{\partial \alpha}{\partial t} = & \langle \bar{n}_1 \cdot [(\bar{U}_1 \cdot \bar{r}_1) - (\bar{U}_2 \cdot \bar{r}_2)] - \bar{n}_1 \cdot (\bar{q}_1 - \bar{q}_2) \\
& - \bar{n}_1 \cdot \bar{U}_1 (\Delta p_{11}^1 - \Delta p_{21}^1) - \dot{m}_1 [(h_1 + \frac{u_1^2}{2}) - (h_2 + \frac{u_2^2}{2})] \rangle_1
\end{aligned} \quad (7.24)$$

The above derived phasic equations (equations 7.11, 7.15, and 7.19) and the jump condition equations (equations 7.20, 7.22 and 7.24) are in the instantaneous volume averaged form. If they are further time averaged, the form remains exactly the same. Terms such as $\frac{\partial}{\partial t} \alpha_k \langle \rho_k \rangle$ become $\overline{\frac{\partial}{\partial t} \alpha_k \langle \rho_k \rangle}$ where the over bar indicates time averaging. However, for simplicity, the averaged notation will not be used and all variables will be considered to be time and volume averaged.

7-2-3 AUXILIARY RELATIONSHIPS:

As it was explained previously, during the averaging processes information is usually lost. Therefore, auxiliary relationships are needed. These relationships include interfacial and wall mass, momentum, and energy transfer, as well as interfacial area per unit volume, and intraphase distribution coefficients. The intraphase distribution coefficients are needed to relate the averages of products of the dependent variables to the products of averages. However, due mainly to lack of information, an assumption is generally made that phase density variations within the averaging volume are negligible, and the averages of products of the dependent variables could be substituted by the products of the averages. This procedure is justified when the averaging volume is small.

7-3 SIMPLIFIED TWO FLUID MODEL FOR THE REFILLING AND REWETTING OF HOT HORIZONTAL CHANNELS.

The generalized forms of time-volume averaged one dimensional conservation equations are represented by the set of equations 7.11, 7.15 and 7.19. These phasic equations must be supplemented by auxiliary interfacial transfer relationships. However, these interfacial transfer relationships should satisfy the jump boundary conditions (i.e., equations 7.20, 7.22 and 7.24).

Generally, starting with the identification of the most dominant phenomena in a given two phase flow situation, and depending on physical insight, a considerable simplification can be achieved in the mathematical model. It is understood that the flow patterns involved should be known prior to reducing the mathematical model and selecting the appropriate auxiliary relationships for such situation.

In the refilling of horizontal systems, gravitational effects may lead to flow stratification. Therefore, the stratified flow pattern is used as the basis for model development. This is supported by the present experimental work which shows that the stratified flow pattern is the most common flow pattern during refilling and rewetting of hot horizontal tubes. However, other flow regimes observed experimentally such as the inverted annular flow are treated as a further development from stratified flow.

Therefore, the general procedure for reducing the mathematical model which was applied by Chan and Banerjee (1981) is followed in the present model.

This approach is capable of solving for only four dependent

variables, namely, liquid velocity, liquid level, liquid temperature, and vapour velocity. It is assumed that the vapour is saturated and that both phases are incompressible.

In deriving the simplified set of hydraulic equations, the momentum and continuity equations of both phases are considered first. The liquid continuity equation reduces to

$$\rho_L \frac{\partial \alpha_L}{\partial t} + \rho_L \frac{\partial (\alpha_L u_L)}{\partial z} = - \dot{m}_L \quad (7.25)$$

The liquid momentum equation reduces to

$$\begin{aligned} \rho_L \frac{\partial (\alpha_L u_L)}{\partial t} + \rho_L \frac{\partial (\alpha_L u_L^2)}{\partial z} = & - r_L a_L + r_i a_i - \alpha_L \frac{\partial p_L}{\partial z} \\ & + \Delta p_{Li} \frac{\partial \alpha_L}{\partial z} - \dot{m}_L u_i \end{aligned} \quad (7.26)$$

where smooth stratified flow is assumed by neglecting the interface pressure fluctuation term.

The subscripts L and i denote the liquid phase and interface respectively and p_L is the bulk liquid pressure defined as

$$p_L = \frac{1}{A_L} \int_{A_L} p_L dA \quad (7.27)$$

where the local liquid pressure at any height y from the bottom of the tube is

$$p_L = \rho_L g (H_L - y) \quad (7.28)$$

$$\text{and } \Delta p_{Li} = p_L - p_i \quad (7.29)$$

A_L is the liquid cross-sectional area, a_L is the wall surface area in

contact with the liquid phase per unit volume, a_i is the interface area per unit volume and H_L is the liquid level in the tube.

Both α_L and Δp_{Li} are functions of the liquid level H_L . $\partial \alpha_L = (\partial \alpha_L / \partial H_L) \partial H_L$ and $\partial \Delta p_{Li} = (\partial \Delta p_{Li} / \partial H_L) \partial H_L$. Therefore, equation 7.25 could be written as

$$\frac{\partial H_L}{\partial t} + u_L \frac{\partial H_L}{\partial z} + \frac{\alpha_L}{(\partial \alpha_L / \partial H_L)} \frac{\partial u_L}{\partial z} = - \frac{\dot{m}_L}{\rho_L (\partial \alpha_L / \partial H_L)} \quad (7.30)$$

By using equations 7.25 and 7.29, equation 7.26 could be reduced to

$$\begin{aligned} \frac{\partial u_L}{\partial t} + u_L \frac{\partial u_L}{\partial z} + \frac{1}{\rho_L \alpha_L} \left(\alpha_L \frac{\partial}{\partial H_L} \Delta p_{Li} + \Delta p_{Li} \frac{\partial \alpha_L}{\partial H_L} \right) \frac{\partial H_L}{\partial z} \\ = - \frac{r_L a_L}{\rho_L \alpha_L} + \frac{r_i a_i}{\rho_L \alpha_L} - \frac{1}{\rho_L} \frac{\partial p_i}{\partial z} + \frac{\dot{m}_L}{\rho_L \alpha_L} (u_L - u_i) \end{aligned} \quad (7.31)$$

By using the geometrical relations of α_L and Δp_{Li} in terms of H_L for a circular channel, and obtaining their derivatives with respect to H_L ($(\partial \alpha_L / \partial H_L)$, and $(\partial \Delta p_{Li} / \partial H_L)$), it is shown by Chan and Banerjee (1981) that

$$\frac{1}{\rho_L \alpha_L} \left(\alpha_L \frac{\partial}{\partial H_L} \Delta p_{Li} + \Delta p_{Li} \frac{\partial \alpha_L}{\partial H_L} \right) = g \quad (7.32)$$

and

$$\frac{\alpha_L}{(\partial \alpha_L / \partial H_L)} = \frac{A_L}{2(2RH_L - H_L^2)^{1/2}} = y_h \quad (7.33)$$

where y_h is defined as the hydraulic depth, which is the ratio between liquid cross-sectional area and the liquid free surface width.

The continuity equation of the vapour phase is given by

$$\rho_G \frac{\partial \alpha_G}{\partial t} + \rho_G \frac{\partial (\alpha_G u_G)}{\partial z} = \dot{m}_L \quad (7.34)$$

The momentum equation of the vapour phase is given by

$$\begin{aligned} \rho_G \frac{\partial}{\partial t} (\alpha_G u_G) + \rho_G \frac{\partial (\alpha_G u_G^2)}{\partial z} = & - r_G a_G - r_i a_i - \alpha_G \frac{\partial p_G}{\partial z} \\ & + \Delta p_{Gi} \frac{\partial \alpha_G}{\partial z} + \dot{m}_L u_i \end{aligned} \quad (7.35)$$

By using equation 7.34, equation 7.35 could be rewritten as

$$\begin{aligned} - \frac{\partial p_G}{\partial z} = & \rho_G \left[\frac{\partial u_G}{\partial t} + u_G \frac{\partial u_G}{\partial z} \right] \\ & + \frac{1}{\alpha_G} \left[r_G a_G + r_i a_i + \dot{m}_L (u_G - u_i) - \Delta p_{Gi} \frac{\partial \alpha_G}{\partial z} \right] \end{aligned} \quad (7.36)$$

Now assuming that $p_G = p_i$ and substituting equations 7.32 and 7.36 into equation 7.31 we get

$$\begin{aligned} \frac{\partial u_L}{\partial t} + u_L \frac{\partial u_L}{\partial z} + g \frac{\partial H_L}{\partial z} = & - \frac{r_L a_L}{\rho_L \alpha_L} + \frac{r_G a_G}{\rho_L \alpha_G} + \frac{r_i a_i}{\rho_L} \left[\frac{1}{\alpha_L} + \frac{1}{\alpha_G} \right] \\ & + \frac{\dot{m}_L}{\rho_L} \left[\frac{u_L - u_i}{\alpha_L} + \frac{u_G - u_i}{\alpha_G} \right] \\ & + \frac{\rho_G}{\rho_L} \left[\frac{\partial u_G}{\partial t} + u_G \frac{\partial u_G}{\partial z} \right] \end{aligned} \quad (7.37)$$

Recalling that $\alpha_G = 1 - \alpha_L$ and utilizing the relationship between H_L and α_L , i.e., equation 7.33, equations 7.30, 7.34, and 7.37 should be solved

for the three dependent variables u_L , H_L , and u_g for a given rate of vapour generation \dot{m}_L . However, further simplification suggested by Chan and Banerjee (1981) is adopted here also, namely, neglecting the time derivatives of the gas phase, permitting the integration of the steady state continuity equation for the gas and the solution of the vapour phase velocity. This was justified by the relatively slow transient nature of the transient refilling and rewetting of horizontal tubes. This would lead to the overprediction of vapour velocity. Accordingly, the interfacial terms e.g interfacial shear, would be overpredicted as well. However, in the present situation, the interfacial terms play a relatively minor role because the coupling between the liquid and vapour phases is rather weak. This poor phasic coupling is more pronounced for high liquid flow with high subcooling, since a low evaporation rate leads to smaller interfacial terms.

By solving the continuity equation of the vapour phase for the vapour velocity, the two remaining hydraulic equations 7.30, and 7.37 could be solved for the two dependent variables, u_L , and H_L . The details of the scheme will be discussed later.

The energy equation for the liquid phase is simplified to be

$$\frac{\partial}{\partial t} (\alpha_L T_L) + \frac{\partial}{\partial z} (\alpha_L u_L T_L) = \left(\frac{1}{\rho C_p}\right)_L (1 - \beta) \bar{q} \quad (7.38)$$

where T_L is the liquid temperature, and \bar{q} is the total heat transfer per unit volume where \bar{q} is given by

$$\bar{q} = \frac{1}{V} \int_0^{2\pi} h(\theta, z) [(T_w(\theta, z) - T_f(\theta, z))] d\theta \quad (7.39)$$

where $h(\theta, z)$ is an appropriate heat transfer coefficient, T_f is an appropriate fluid temperature, and β is the fraction of energy used in evaporation and $(1-\beta)$ represents the fraction of heat transferred to the liquid phase.

The transient temperature distribution in the tube wall is required as a boundary condition to introduce the heat flux into the system. However, an appropriate heat transfer coefficient should be used. Since the film boiling region appears to be the most dominant region in the rewetting process, a theoretical model was derived in chapter 6 for this region, while appropriate empirical correlations are used for the other heat transfer modes as will be discussed later.

The temperature of the wall can be obtained using the three dimensional transient heat conduction equation in cylindrical coordinates. When there is no heat source the equation is

$$\frac{1}{\alpha_w} \frac{\partial T_w}{\partial t} = \frac{1}{r} \frac{\partial T_w}{\partial r} + \frac{\partial^2 T_w}{\partial r^2} + \frac{\partial^2 T_w}{\partial z^2} + \frac{1}{r^2} \frac{\partial^2 T_w}{\partial \theta^2} \quad (7.40)$$

where α_w is the thermal diffusivity of the tube wall.

7-4 NUMERICAL COMPUTATION:

A uniform mesh size is used. The heated test section is represented by thirty cells, while the inlet and outlet tubing are simulated by nine and two cells respectively. Temperatures are defined

at cell centers while velocities, voids and liquid level are defined at cell boundaries. The numerical schemes used for the hydraulic and thermal equations are discussed below

7-4-1 THE HYDRAULIC EQUATIONS:

The hydraulic equations of the liquid phase, i.e., equations 7.30 and 7.37 are reproduced here:

$$\frac{\partial H_L}{\partial t} + u_L \frac{\partial H_L}{\partial z} + y_h \frac{\partial u_L}{\partial z} + E_1 = 0 \quad (7.41)$$

$$\frac{\partial u_L}{\partial t} + u_L \frac{\partial u_L}{\partial z} + g \frac{\partial H_L}{\partial z} - E_2 = 0 \quad (7.42)$$

where

$$E_1 = \frac{\dot{m}_L}{\rho_L (\partial \alpha_L / \partial H_L)} \quad (7.43)$$

and

$$\begin{aligned} E_2 = & - \frac{r_L a_L}{\rho_L \alpha_L} + \frac{r_i a_i}{\rho_L} \left[\frac{1}{\alpha_L} + \frac{1}{\alpha_G} \right] + \frac{r_G a_G}{\rho_L \alpha_G} \\ & + \frac{\dot{m}_L}{\rho_L} \left[\frac{u_L - u_i}{\alpha_L} + \frac{u_G - u_i}{\alpha_G} \right] + \frac{\rho_G}{\rho_L} u_G \frac{\partial u_G}{\partial z} \end{aligned} \quad (7.44)$$

A scheme proposed by Keller and Lax as given by Stoker (1957) for unsteady flows in open channels is adopted here to solve equations 7.41 and 7.42 for the liquid velocity u_L , and liquid level H_L . It is a finite difference technique implementing a staggered rectangular net as indicated in figure 7.3. The values $u_{L(M)}$ and $H_{L(M)}$ at the midpoint M of the segment LR are defined by the averages :

$$\left. \begin{aligned} u_{L(M)} &= \frac{u_{L(L)} + u_{L(R)}}{2} \\ H_{L(M)} &= \frac{H_{L(L)} + H_{L(R)}}{2} \end{aligned} \right\} \quad (7.45)$$

Accordingly, the derivatives at M are approximated by the difference quotients as:

$$\left. \begin{aligned} \frac{\partial u_L}{\partial z} &= \frac{u_{L(R)} - u_{L(L)}}{\Delta z}, & \frac{\partial H_L}{\partial z} &= \frac{H_{L(R)} - H_{L(L)}}{\Delta z} \\ \frac{\partial u_L}{\partial t} &= \frac{u_{L(P)} - u_{L(M)}}{\Delta t}, & \frac{\partial H_L}{\partial t} &= \frac{H_{L(P)} - H_{L(M)}}{\Delta t} \end{aligned} \right\} \quad (7.46)$$

Upon the substitution of these quantities into equations 7.41 and 7.42, H_L, u_L, y_h, E_1 , and E_2 at point M are evaluated, and subsequently solution of the two equations for $H_{L(P)}$ and $u_{L(P)}$ at point P, which is located in the center between L and R at the advanced time step $t+\Delta t$, is obtained as

$$\begin{aligned} H_{L(P)} = H_{L(M)} - \frac{\Delta t}{\Delta z} \left[u_{L(M)} (H_{L(R)} - H_{L(L)}) \right. \\ \left. + y_{h(M)} (u_{L(R)} - u_{L(L)}) + E_1 \Delta z \right] \end{aligned} \quad (7.47)$$

$$\begin{aligned} u_{L(P)} = u_{L(M)} - \frac{\Delta t}{\Delta z} \left[u_{L(M)} (u_{L(R)} - u_{L(L)}) \right. \\ \left. + g (H_{L(R)} - H_{L(L)}) - E_2 \Delta z \right] \end{aligned} \quad (7.48)$$

Accordingly, u_L and H_L are obtained at the mesh centers at an advanced

time equal to $t_{in} + \Delta t$. Then, H_L , u_L , y_h , E_1 and E_2 are evaluated at the mesh sides, i.e., the original spatial mesh, to be used this time in solving equations 7.41 and 7.42 for u_L and H_L at the mesh sides at an advanced time equal to $t_{in} + 2\Delta t$, i.e., points X and Y in figure 7-3. Therefore the solution of u_L and H_L for the original mesh is obtained at time step of $2\Delta t$.

The criterion for convergence is that point P should lie within a triangle formed by the segment LR and the two characteristics issuing from its ends. The two characteristics lines are defined by $\frac{dz}{dt} = u_L \pm c$ where c is the wave propagation velocity and equal to $\sqrt{gy_h}$. In other words, the time step Δt should be small enough to ensure that point P lies within the domain enclosed by the segment LR, the positive characteristic line $u_L + c$ emerging from point L and the negative characteristic line $u_L - c$ emerging from point R.

7-4-2 VAPOUR PHASE VELOCITY.

Assuming that the vapour phase is in quasi-steady state, the vapour velocity is calculated by integrating the steady vapour continuity equation. Therefore, equation 7.34 reduces to the finite difference form

$$u_{G(j)} = \frac{1}{\alpha_{G(j)}} \left[u_{G(j-1)} \alpha_{G(j-1)} + \frac{\dot{m}_{L(j)}}{\rho_G} \Delta z \right] \quad (7.49)$$

where

$$\dot{m}_{L(j)} = (1 - \beta_{(j)}) \frac{\bar{q}_{(j)} + \bar{q}_{(j-1)}}{2 h_{fg}} \quad (7.50)$$

where h_{fg} is the enthalpy of evaporation, and \bar{q} is calculated from equation 7.39.

Equation 7.49 is solved for u_g at the mesh centers and mesh sides alternatively, in the same sequence in which the hydraulic equations 7.41 and 7.42 were solved. This is required to calculate the appropriate values of the coupling terms E_1 and E_2 in equations 7.41 and 7.42.

7-4-3 THE ENERGY EQUATION OF THE LIQUID PHASE.

The energy equation of the liquid phase (equation 7.38) is simplified by neglecting the axial conduction term since it is very small compared to the other terms.

An explicit upwind finite difference technique is used. The liquid velocity and liquid levels used are the average of the previous and new time step values. The finite difference grid is shown in figure 7.4. The finite difference form of the liquid energy equation is

$$\begin{aligned}
& \frac{\alpha_{L(j+1/2)}^{n+1} T_{L(j)}^{n+1} - \alpha_{L(j+1/2)}^n T_{L(j)}^n}{\Delta t} = \\
& - \frac{\alpha_{L(j+1)}^{n+1/2} u_{L(j+1)}^{n+1/2} T_{L(j)}^n - \alpha_{L(j)}^{n+1/2} u_{L(j)}^{n+1/2} T_{L(j-1)}^n}{\Delta z} \\
& + \left(\frac{1}{\rho C_p} \right)_j^n (1-\beta)_j \bar{q}_j^n \quad (7.51)
\end{aligned}$$

Equation 7.51 can be solved for $T_{L(j)}^{n+1}$ where \bar{q}_j^n is calculated by equation 7.39 and $\alpha_{L(j+1/2)}^{n+1}$ can be estimated from simplifying the liquid continuity equation such that

$$\alpha_{L(j+1/2)}^{n+1} = \alpha_{L(j+1/2)}^n + \frac{\Delta t}{\Delta z} \left[\alpha_{(j)} u_{L(j)} - \alpha_{L(j+1)} u_{L(j+1)} \right]^n \quad (7.52)$$

The stability requirement for the solution scheme is governed by the Courant criterion where $\Delta t \leq \frac{\Delta z}{u_L}$.

7-4-4 WALL TEMPERATURE:

The transient heat conduction equation 7.40 is solved numerically using an explicit finite difference method. The equation can be reduced to the two dimensional form to be used for the case of thin tubes when the wall temperature is assumed uniform across its thickness.

The channel is divided into twelve cells azimuthally. Since the solution is expected to be symmetric with respect to the vertical axis, the energy equation is solved only for half of the channel. Three or five radial cells are used.

The Three-Dimensional Form.

Using the notations i for r , j for z , and k for θ , the energy equation for the interior nodes can be written in finite difference form

$$\begin{aligned}
 \frac{1}{\alpha_{i,j,k}^n} \frac{T_{i,j,k}^{n+1} - T_{i,j,k}^n}{\Delta t} = & \frac{1}{R_i} \frac{T_{i+1,j,k}^n - T_{i-1,j,k}^n}{2\Delta r} \\
 & + \frac{T_{i+1,j,k}^n + T_{i-1,j,k}^n - 2T_{i,j,k}^n}{(\Delta r)^2} \\
 & + \frac{T_{i,j,k+1}^n + T_{i,j,k-1}^n - 2T_{i,j,k}^n}{(R_i \Delta \theta)^2} \\
 & + \frac{T_{i,j+1,k}^n + T_{i,j-1,k}^n - 2T_{i,j,k}^n}{(\Delta z)^2}
 \end{aligned} \tag{7.53}$$

Equation 7.53 is solved for $T_{i,j,k}^{n+1}$ since all other terms are known explicitly.

For the radial boundary nodes, the convective boundary condition is considered. Taking the inner surface of the tube as an example, the finite difference grid is shown in figure 7.5. An energy balance on the control volume ABCD results in the following equation

$$\begin{aligned}
\frac{1}{\alpha_{1,j,k}^n} \frac{T_{1,j,k}^{n+1} - T_{1,j,k}^n}{\Delta \tau} = & \frac{T_{1,j,k+1}^n + T_{1,j,k-1}^n - 2T_{1,j,k}^n}{(R_1 \Delta \theta)^2} \\
& + \frac{T_{1,j+1,k}^n + T_{1,j-1,k}^n - 2T_{1,j,k}^n}{(\Delta z)^2} \\
& + \frac{2(T_{2,j,k}^n - T_{1,j,k}^n)}{(\Delta r)^2} \\
& - \frac{2 h_{1,j,k}^n}{\Delta r K_{1,j,k}^n} (T_{1,j,k}^n - T_{Fj}^n) \quad (7.54)
\end{aligned}$$

Equation 7.54 is able to predict the surface node temperatures in the three dimensional formulation. Therefore, equations 7.53 and 7.54 can be used to give detailed three dimensional temperature variations along the channel. The stability requirement is

$$\Delta \tau \leq \min \left[\frac{(\Delta r)^2}{6\alpha}, \frac{(r\Delta \theta)^2}{6\alpha}, \frac{(\Delta z)^2}{6\alpha} \right] \quad (7.55)$$

Equation 7.55 shows that $\Delta \tau$ is limited by Δr for the present case.

The Two-Dimensional Form.

For two dimensional formulation, the temperature is assumed uniform across the wall. A heat balance on the control volume ABCD of figure 7.6 results in the finite difference equation shown below.

$$\begin{aligned}
\frac{1}{\alpha_{j,k}^n} \frac{T_{j,k}^{n+1} - T_{j,k}^n}{\Delta t} = & \frac{T_{j,k+1}^n + T_{j,k-1}^n - 2T_{j,k}^n}{(R\Delta\theta)^2} \\
& + \frac{T_{j+1,k}^n + T_{j-1,k}^n - 2T_{j,k}^n}{(\Delta z)^2} \\
& - \frac{h_{1,j,k}^n R_I}{K_{j,k}^n \delta_t R_M} (T_{j,k}^n - T_{F1}) \\
& - \frac{h_{2,j,k}^n R_O}{K_{j,k}^n \delta_t R_M} (T_{j,k}^n - T_{F2})
\end{aligned} \tag{7.56}$$

where δ_t is the tube wall thickness, h_1 and h_2 are the heat transfer coefficients at the inner and outer surfaces of the tube respectively and R_I , R_O and R_M are the inner, outer and mean radius of the tube respectively.

The stability requirement becomes

$$\Delta t \leq \min \left[\frac{(R\Delta\theta)^2}{4\alpha}, \frac{(\Delta z)^2}{4\alpha} \right] \tag{7.57}$$

It is expected that tube temperature is almost uniform across the wall in the dry region, because heat transfer is relatively slow in this region. Accordingly, the two dimensional formulation would be used even for thick tubes, since the most important criteria in the present study is surface rewetting, and this is governed by the end of film boiling mode. However, the two-dimensional formulation would result in

slower propagation of the quench front since the entire tube wall thickness is required to cool down prior to quenching.

7-5 INITIAL AND BOUNDARY CONDITIONS:

7-5-1 INITIAL CONDITIONS:

The Hydraulic Initial Conditions:

$$\left. \begin{array}{l} H_{L(j)} = D \\ u_{L(j)} = u_{L,in} \end{array} \right\} \quad \text{for } 1 \leq j \leq 5 \quad (7.58)$$

and

$$u_{L(j)} = u_{G(j)} = H_{L(j)} = 0 \quad \text{for } 6 \leq j \leq 42 \quad (7.59)$$

where $u_{L,in}$ is the inlet coolant velocity and D is the tube diameter. This full tube condition for certain length is implemented to allow for the stratification wave to propagate backward at the beginning of the refilling process which is expected to occur under low mass flux conditions.

The Thermal Initial Conditions:

$$\left. \begin{array}{ll} T_{L(j)} = T_{L,in} & \text{for } 1 \leq j \leq 5 \\ T_{L(j)} = 0.0 & \text{for } 6 \leq j \leq 42 \end{array} \right\} \quad (7.60)$$

$$\left. \begin{array}{ll} T_{W(j)} = T_{WO} & \text{for } 11 \leq j \leq 40 \\ T_{W(j)} = T_R & \text{for } j \leq 10 \text{ and } j \geq 41 \end{array} \right\} \quad (7.61)$$

where T_{WO} is the initial tube temperature, and T_R is the room temperature.

7-5-2 BOUNDARY CONDITIONS:

The Hydraulic Boundary Conditions:

For the inlet:

constant flow boundary

$$\left. \begin{array}{l} u_{L(1)} = u_{L,in} \\ H_{L(1)} = D \end{array} \right\} \quad (7.62)$$

For the exit:

$$\left. \begin{array}{l} u_{L(42)} = u_{L(41)} \\ H_{L(42)} = H_{L(41)} \end{array} \right\} \quad (7.63)$$

The Thermal Boundary Conditions:

Liquid Temperature:

$$\left. \begin{array}{l} T_{L(1)} = T_{L,in} \\ T_{L(42)} = T_{L(41)} \end{array} \right\} \quad (7.64)$$

Wall temperature:

z - direction:

$$\left. \begin{array}{l} T_{1,1,k} = T_{1,2,k} \\ T_{1,42,k} = T_{1,41,k} \end{array} \right\} \quad (7.65)$$

θ - direction:

imposing symmetry around the vertical diameter

$$\left. \begin{array}{l} T_{1,j,1} = T_{1,j,3} \\ T_{1,j,7} = T_{1,j,9} \end{array} \right\} \quad (7.66)$$

r - direction.

$$K_w \left(\frac{\partial T_w}{\partial r} \right)_{r_I} = h_I (T_w - T_F) \quad (7.67)$$

$$K_w \left(\frac{\partial T_w}{\partial r} \right)_{r_o} = h_o (T_w - T_R) \quad (7.68)$$

7-6 AUXILIARY EQUATIONS FOR THE HYDRAULIC MODEL.

To solve the derived finite difference forms of the hydraulic and thermal equations, appropriate auxiliary relationships are needed. These relationships include interfacial and wall mass, momentum, and energy transfer, as well as interfacial area per unit volume. These are discussed below.

7-6-1 WALL TO LIQUID FRICTION.

The liquid to wall shear force per unit volume can be written as

$$F_{wL} = \frac{\tau_L a_L}{\alpha_L} = \frac{1}{2} f_L u_L |u_L| \rho_L \frac{a_L}{\alpha_L} \quad (7.69)$$

where a_L is the liquid to wall contact area per unit volume. For the stratified flow pattern, a_L is given by

$$\left. \begin{aligned} a_L &= \frac{2}{\pi R} \cos^{-1} \left(\frac{R-H_L}{R} \right) & \text{for } H_L \leq R \\ a_L &= \frac{2}{\pi R} \left[\pi - \cos^{-1} \left(\frac{H_L-R}{R} \right) \right] & \text{for } H_L \geq R \end{aligned} \right\} \quad (7.70)$$

and f_L is calculated by the Blasius equation

$$f_L = \frac{0.0791}{Re^{0.25}} \quad (7.71)$$

where the characteristic dimension in the Reynolds number is the liquid hydraulic diameter. In the film boiling region, the liquid phase is separated from the channel wall by a vapour film. Accordingly, there is no wall to liquid shear in this region ($f_L = 0$).

7-6-2 WALL TO VAPOUR FRICTION:

The vapour to wall shear force per unit volume is given by

$$F_{WG} = \frac{\tau_G a_G}{\alpha_L} = \frac{1}{2} f_G u_G |u_G| \rho_G \frac{a_G}{\alpha_G} \quad (7.72)$$

where a_G is the vapour to wall contact area per unit volume, which is given by

$$\left. \begin{aligned} a_G &= \frac{2}{\pi R} \left[\pi - \cos^{-1} \left(\frac{R-H_L}{R} \right) \right] && \text{for } H_L \leq R \\ a_G &= \frac{2}{\pi R} \cos^{-1} \left(\frac{H_L-R}{R} \right) && \text{for } H_L \geq R \end{aligned} \right\} \quad (7.73)$$

Various relations could be used for f_G . However, a simple constant value is used, since it is found that the solution is rather insensitive to variations in f_G as shown in table 7-1. A value of 0.005 is considered for the present calculations as suggested by Wallis (1969).

7-6-3 INTERFACIAL SHEAR:

In calculating the interfacial shear term, the interfacial shear stress is given by

$$\tau_i = \frac{1}{2} f_i \rho_G u_r |u_r| \quad (7.74)$$

where $u_r = u_G - u_L$ and the interfacial surface area per unit volume is given by

$$a_i = \frac{2}{\pi R^2} (2RH_L - H_L^2)^{1/2} \quad (7.75)$$

where f_i is the interfacial friction factor. Again, for simplicity, a constant value of 0.005 is considered since no significant effect is found by varying f_i as shown in table 7-1.

7-6-4 INTERFACIAL MASS TRANSFER:

The interfacial mass transfer per unit volume is given by

$$\dot{m}_L = \frac{\beta \bar{q}}{h_{fg}} \quad (7.76)$$

where \bar{q} is the total heat input per unit volume.

A model for evaluating the partition factor (β) in the film boiling region was developed. The details of this model was given in chapter 6. In the other regions of heat transfer, the partition factor is assumed negligible ($\beta = 0$).

7-6-5 INTERFACIAL MOMENTUM TRANSFER:

The momentum transferred to a phase related to the mass transfer, could be represented by

$$T_m = \dot{m}_L u_i \quad (7.77)$$

where \dot{m}_L is the net mass transfer across the interface and is given by equation 7.76 and u_i is the interface velocity, which is taken as

$$u_i = \frac{u_L + u_G}{2} \quad (7.78)$$

7-6-6 VAPOUR INERTIA:

The vapour inertia force per unit volume is

$$F_{int} = \rho_G u_G \frac{\Delta u_G}{\Delta z} \quad (7.79)$$

7-7 HEAT TRANSFER REGIMES:

A wide range of heat transfer modes are involved in the refilling and rewetting of hot horizontal tubes due to the variation of the thermohydraulic characteristics locally and temporally. Generally, all the heat transfer modes in the typical convective boiling curve are expected to exist at different axial locations. Moreover, different modes of heat transfer could exist at different circumferential locations due to flow stratification. The heat transfer modes which are most likely to exist at different axial and circumferential locations are shown in figure 7.7, which shows that the quench front is lagging behind a stratified refilling liquid front. The four regions identified by the letters A, B, C, and D are discussed below.

Region A.

This region represents the dry wall region downstream of the refilling front. Vapour flow with possible entrained water droplets exists. The heat transfer coefficient in this region is estimated by considering vapour flow convection and radiation.

$$h = h_{\text{vap. conv.}} + h_{\text{rad.}} \quad (7.80)$$

where $h_{\text{vap. conv.}}$ is calculated by using Dittus Boelter equation

$$h_{\text{vap. conv.}} = 0.023 \left(\frac{\rho_G u_G D}{\mu_G} \right)^{0.8} \left(\frac{C_{P_G} \mu_G}{K_G} \right)^{0.4} \frac{K_G}{D} \quad (7.81)$$

and the radiation heat transfer coefficient is defined as

$$h_{\text{rad.}} = \sigma \epsilon \frac{(T_W^4 - T_F^4)}{(T_W - T_F)} \quad (7.82)$$

where σ is the Stefan Boltzman constant, and ϵ is the emissivity of the tube.

Region B.

This region is divided into two subregions. In the first subregion ($y \leq H_L$), stable film boiling is assumed and the model for vapour film thickness at the bottom of the tube, developed earlier where it is proposed that vapour vents circumferentially upward was used. The details of this model are given in chapter 6. In this subregion, the heat transfer coefficient is defined as

$$h = \frac{K_G}{\delta} + h_{\text{rad}} \quad (7.83)$$

where δ is the vapour film thickness which was found in chapter 6 as

$$\delta = [(2R/\rho_L \rho_G g)(a^2 \beta^2 + 1.5a\beta\mu_G)]^{1/4} \quad (7.84)$$

$$a = k_G \Delta T_{\text{SAT}} / h_{\text{fs}}$$

where ΔT_{SAT} is the wall superheat and h_{rad} is calculated by equation 7.82. The partition factor β is given by equation 6.50. The circumferential variation of the vapour film thickness is assumed linear such that if the film boiling is extended to the top side of the tube, the vapour film thickness at the top side is twice its value at the bottom of the tube. In the second subregion ($y > H_L$) equation 7.80 is used where the hydraulic diameter of the vapour channel is used in calculating the vapour flow convection.

Region C.

This region includes the quench front indicated by the dashed line in figure 7.7. In this region, three different subregions exist. They are: i) quenched subregion (below the quench front (H_q)), ii) film boiling subregion (above the quenched front and below the collapsed liquid level (H_L)) and iii) dry subregion (above the collapsed liquid level). In the quenched subregion, transition boiling is assumed to exist until the tube wall temperature is decreased to a value corresponding to the critical heat flux (T_{CHF}). Therefore, the heat transfer coefficient is defined as

$$h = h_{\text{trans. boi.}} \quad (7.85)$$

where T_{CHF} is assumed to be 250°C , and a correlation suggested by Tong (1972) is used for calculating the transition boiling heat transfer coefficient.

$$h_{\text{trans.boi.}} = 9000 \text{ EXP} (- 0.0054 \Delta T_{\text{SAT}}) \quad (7.86)$$

where ΔT_{SAT} is in $^\circ\text{F}$ and h is in $\text{Btu/hr.ft}^2.^\circ\text{F}$.

For tube temperatures below T_{CHF} and higher than saturation temperature, the heat transfer coefficient is considered to be the highest value of nucleate boiling and liquid convection when both are based on $T_W - T_L$ instead of $T_W - T_{\text{SAT}}$. This is represented by

$$h = \text{maximum} (h_{\text{nucl.boi.}}, h_{\text{L.conv.}}) \quad (7.87)$$

This approach was suggested by Groeneveld and Snoek (1986) where $h_{\text{nucl.boi.}}$ is calculated by a correlation suggested by Jens and Lottes (1951). For atmospheric pressure, this correlation is

$$h_{\text{nucl.boi.}} = 0.00271 (\Delta T_W)^3 \quad (7.88)$$

where $\Delta T_W = T_W - T_L$, temperature in $^\circ\text{C}$, and h in $\text{W/m}^2.^\circ\text{C}$ and $h_{\text{Liq.Conv.}}$ is calculated by Dittus Boelter equation

$$h_{\text{Liq. conv.}} = 0.023 \left(\frac{\rho_L u_L D}{\mu_L} \right)^{0.8} \left(\frac{C_{P_L} \mu_L}{K_L} \right)^{0.4} \frac{K_L}{D} \quad (7.89)$$

For the film boiling subregion ($H_q \leq y \leq H_L$), equation 7.83 is used, and in the dry subregion ($y \geq H_L$) equation 7.80 is used.

Region D.

In this region liquid has filled the tube. Treatment similar to that of the quenched subregion of region C is used. Namely, equation 7.85 for $T_w > T_{CHF}$ and equation 7.87 for $T_{SAT} < T_w < T_{CHF}$ are used. When the wall temperature decreases below saturation temperature, liquid convection is considered using equation 7.89.

7-7-1 TRANSITION TO INVERTED ANNULAR FLOW REGIME.

The axial propagation of the quench front could be significantly slower than the refilling front. This is because the quench front could be delayed by the high heat capacity of the tube (high initial temperature and/or large tube thickness), especially for low subcooling. Also, the shape of the refilling front is governed by the inlet flow rate where increasing flow rate reduces flow stratification. Accordingly, for high flow rates and high tube heat capacity, quenching is delayed and the tube is almost filled with water downstream of the quench front forming an inverted annular flow pattern. This flow regime was observed experimentally and discussed in chapter 5. Accordingly, a transition to inverted annular flow pattern was assumed if the quench front is found to be located upstream of an axial location where water inventory is almost filling the entire cross section.

In this flow regime five distinct heat transfer regions (A, B, C, D and E) are indicated as shown in figure 7.8. Regions A, B, E in figure 7.8 are similar to regions A, B, and D respectively of figure 7.7. Accordingly, the same appropriate heat transfer correlations are

considered. In region C, only the film boiling mode would exist where equation 7.83 is used. However, the vapour film thickness would not be uniform around the circumference. It is minimum at the bottom and maximum at the top of the tube. In the inverted annular flow pattern vapour would vent axially. However, due to the imposed circumferential pressure gradient caused by the liquid weight in the present case (refilling of hot horizontal tube) vapour would tend to vent circumferentially upward as well. In theory, a solution for the vapour flow parameters (vapour film thickness and vapour velocity) should be obtained for the asymmetric vapour channel in this region. However, this is complicated since the axial pressure gradient in the vapour channel is unknown. Therefore, if we assume that the circumferential pressure gradient in the vapour channel is still dominant, equation 7.84 could be used for calculating the vapour film thickness at the bottom of the tube in this region as well. Moreover, the circumferential variation of the vapour film thickness is assumed linear such that the vapour film thickness at the top of the tube is twice its value at the bottom of the tube.

7-8 QUENCH MODEL.

It is clear that the criterion of surface quenching which marks the end of stable film boiling and the beginning of the transition boiling is very important in predicting the right quenching times at different axial locations.

It was shown in chapter 6 that surface rewetting is linked to the dynamic fluctuation of the liquid-vapour interface. It was found

that the hydraulic disturbances represented by typical system pressure fluctuations applied to an equilibrium vapour film of thickness equal to the experimentally determined minimum vapour film thickness (0.11 mm) are capable of rewetting the bottom of the tube. This typical pressure fluctuation induces an interface disturbances at which the equilibrium vapour film thickness would equal the sum of the interface fluctuation amplitude and the surface roughness. The details of this study was presented in chapter 6. Accordingly, a constant value of minimum vapour film thickness of 0.11 mm at the bottom of the tube is used in the computer code. The film boiling model developed earlier (section 7-7) was used to calculate the decrease in the equilibrium vapour film thickness upstream of the advancing liquid front. When the equilibrium vapour film thickness at the bottom of the channels reaches 0.11 mm, rewetting initiation was assumed.

The above quenching model defines the conditions at which the bottom of the tube quenches. The circumferential propagation of the quench front is more complicated. However, the following characteristics were observed in the present experiments:

i- When the quench front at the bottom of the tube is established under a stratified liquid tongue, fast circumferential propagation is followed such that after filling more than half the tube, the quench level could be even higher than the average water level. This was discussed in chapter 5. Accordingly, a simple second order polynomial relation is used to predict the circumferential quench propagation. The relation is

$$H_q = D \left(\frac{H_L - H_c}{D - H_c} \right)^{1/2} \quad (7.90)$$

where H_c is the liquid level at which quench initiates at the bottom of the tube.

ii- When quench front at the bottom of the tube is established under a full tube (inverted annular flow region), the circumferential propagation is more uniform leading to a film boiling period at the top which is longer than the film boiling period at the bottom (thicker vapour film thickness at the top). This delay time between quenching the bottom and the top sides of the tube seems to be a function of flow rate, and subcooling. However, this case was simplified by imposing the experimentally observed delay time between quenching the bottom and the top sides of the tube. Moreover, the circumferential quench propagation rate was assumed linear.

7-9 NUMERICAL PROCEDURE

A computer code is developed to predict the transients of the process, starting from injecting the coolant at the inlet until complete quenching of the test tube is achieved. The computational procedure is summarized by the following steps:

- 1- The initial and boundary conditions are defined and the two-dimensional or three-dimensional formulation of the tube wall heat conduction equation is selected.
- 2- An appropriate time step (Δt), which satisfies the hydraulic

convergence criterion, is selected. If the stability criterion of the tube wall heat conduction equation is not satisfied by this time step (Δt), a smaller time step is used in solving the heat conduction equation.

3- The partition factor and the vapour film thickness in the film boiling region is calculated..

4- The new quench front location is marked according to the quench criterion (minimum vapour film thickness).

5- The appropriate local heat transfer coefficients for all the computational cells, based on the identified heat transfer modes involved at each cell, are evaluated.

6- The heat conduction equation of the tube wall is solved to calculate the new time step temperature distribution throughout the tube.

7- The energy equation of the liquid is solved to calculate the new time step values of the liquid temperature.

8- The vapour velocity, the hydraulic depth, and mass and momentum transfer terms (E_1 and E_2 in equations 7.43, and 7.44) at the mesh centers are evaluated.

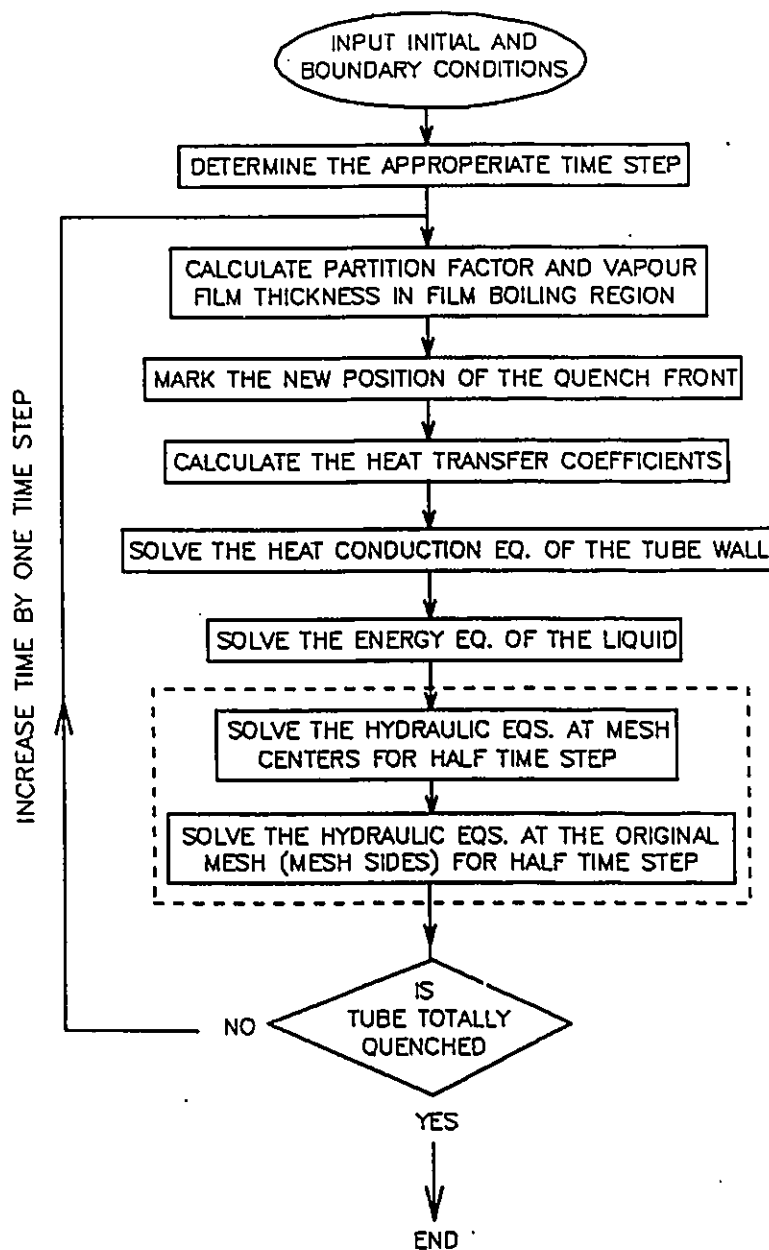
9- Using half the time step ($\Delta t/2$), the hydraulic equations are solved to evaluate liquid velocity and liquid level at the mesh centers.

10- The vapour velocity, the hydraulic depth, and mass and momentum transfer terms at the original mesh (mesh boundaries) are evaluated.

11- Using half the time step ($\Delta t/2$), the hydraulic equations are solved to evaluate liquid velocity and liquid level at the original mesh (mesh boundaries).

12- Repeat step 3 to 11 until the tube is totally quenched.

A flow diagram for the computer code is shown below.



7-10 NUMERICAL PREDICTIONS AND COMPARISON WITH EXPERIMENTAL RESULTS:

The transient behaviour of the refilling and rewetting of hot horizontal tubes was analyzed numerically using the computer code developed based on the mathematical model and the auxiliary relations discussed in previous sections.

The most important phenomenon which governs the process is quench initiation. It is evident from experimental data that quenching is always initiated at the bottom first and then propagates circumferentially upwards. Therefore, the focus was to develop a quench initiation model at the bottom of the tube (chapter 6) where the concept of minimum vapour film thickness was utilized. In order to calculate the axial variation in the equilibrium vapour film thickness, the variation of the partition factor β (the fraction of heat used in vapour generation) is required. Therefore a theoretical model for β in the film boiling region was derived in chapter 6. This is important since vapour generation defines the vapour film thickness and this in turn defines quench propagation at the critical vapour film thickness defined by the quench initiation model. Moreover, vapour generation will define the vapour velocity which in turn defines the interfacial terms coupling the two phases.

7-10-1 REFILLING AND REWETTING FRONTS:

The shape of the refilling and rewetting fronts are obtainable from the numerical calculations. An example of the propagation of the refilling and rewetting fronts along the tube for relatively low mass flux is shown in figure 7.9. Starting with water injection at $t=0$ this

figure shows the locations and shape of the refilling front at three subsequent time frames. This indicates clearly that stratification increases as the refilling front advances downstream. The location of the quench front at the bottom of the tube for these time frames are marked by the letters A, B and C respectively. It is clear that the advancing liquid front propagates downstream at a faster rate than the quench front resulting in longer film boiling region as the refilling front advances along the tube. Although the increase in stratification as the refilling front moves downstream is mainly due to the gravitational effect, this phenomenon is enhanced by the absence of wall-liquid shear in the film boiling region separating the stratified liquid from the tube.

The effect of mass flux on liquid stratification is shown in figure 7.10 where a cold tube was considered to exclude any thermal and interfacial parameters which could affect the stratification. As expected, it is shown that the gravitational force is more dominant at low mass flux because the Froude number, defined as the ratio between the inertia force and the gravitational force, is small. Increasing the mass flux results in higher Froude number. Accordingly, increasing the mass flux will decrease stratification since the inertia force becomes more dominant.

All the above numerical findings are supported by the various experimental results discussed in chapters 4 and 5.

7-10-2 TRANSIENT WALL TEMPERATURE

The transient wall temperatures were obtained numerically by solving the transient heat conduction equation. The two and three-dimensional formulations of the heat conduction equation were used for the thin tube (1 mm thickness) and thick tube (2 mm) respectively. The local heat transfer coefficients at any time are governed by the local thermohydraulic conditions. Accordingly, the transient wall temperatures would represent the outcome of the overall sequence of events involved in the refilling and rewetting process. The transient temperature curves at axial and circumferential locations identical to the experimental measuring stations were produced for comparison with the corresponding experimental curves. Two examples showing two extreme conditions are presented below. One is for low flow rate and moderate wall heat capacity, and the second for high flow rate and high wall heat capacity.

In the first example, the axial wall temperature transients and the corresponding experimental results are shown in figure 7.11, while the circumferential temperature transients and the corresponding experimental curves are shown in figure 7.12. This example represents the initial and boundary conditions for which the initiation of quench at the bottom of the tube occurs under an advancing stratified liquid flow. Figures 7.11 and 7.12 show a good agreement between code predictions and the experimental results except at the last two bottom curves in figure 7.11 where the experimental curves indicate longer film boiling periods and stratified lengths. This could be explained by the fact that in the two-fluid model, the vapour-liquid interfacial

shear in the film boiling region was assumed to have a zero axial component since the proposed physical model assumes that vapour flows circumferentially upwards while in the experiments, vapour velocity in the film boiling region would have a downstream axial component which may increase flow stratification especially for low coolant flow rate.

In the second example, the axial temperature transients and the corresponding experimental results are shown in figure 7.13 , while the circumferential temperature transients and the corresponding experimental curves are shown in figure 7.14. This example represents a typical condition for which the initiation of quench at the bottom of the tube occurs well behind the refilling front where the tube is almost filled with water. This is a result of the combined effect of a steep and short refilling front for high mass flux and a long film boiling period due to high heat capacity of the tube. Accordingly, the quench front is upstream of an inverted annular flow region. Figures 7.13 and 7.14 show a good general agreement between code predictions and experimental results. As mentioned earlier (chapter 4) for the high heat capacity tube results, evidence of surface rewetting followed by temporary dryout was observed. As shown in figure 7-14, the code at the present time cannot capture this phenomenon.

7-11 CONVERGENCE STUDIES

The numerical scheme was tested for spatial and temporal convergence. The results of such study on a case of 480 °C initial tube wall temperature, 60 °C inlet water temperature, 650 kg/m².s mass flux and tube wall thickness of 1 mm is shown in table 7-2. The constitutive

relations outlined in section 7-6 were used. The average rewetting velocities, mass conservation ($|\Delta M|/M$) and energy conservation ($|\Delta Q|/Q$) were compared in these tests. ΔM is the difference between the injected and the calculated mass inventory of the water. ΔQ is the difference between the total energy transferred from the tube (inside & outside surfaces) and the reduction in tube thermal capacity due to the decrease in wall temperature. Based on the results in table 7-2, it is assumed that converged results are obtained using 30 nodes and a time step of 0.03 second.

7-12 PARAMETRIC STUDIES:

The same case of initial and boundary conditions used in the convergence studies was also used to study the sensitivity of the numerical predictions to different interfacial terms. The effect of changing each of the interfacial shear friction coefficient (f_i), the wall-gas friction coefficient (f_g) and the wall-liquid friction coefficient (f_l) is shown in table 7-1 where their effects on the stratified length are also included. The sensitivity of the numerical predictions to any one of the above parameters is tested by changing this particular parameter while keeping the rest of the interfacial terms as proposed in section 7-6.

Table 7-1 shows that doubling the interfacial shear or the wall-gas shear would increase the stratified length slightly, but would have a very little effect on the quench velocity. Accordingly, it appears that the results are rather insensitive to the interfacial and vapour-wall friction effects.

In the film boiling region, the liquid is not in contact with the wall and accordingly assuming the liquid to wall friction factor f_L to be zero is quite justified. It is interesting to examine the effect of imposing a finite value of f_L in that region since it would simulate the case of cold tube refilling. As shown in table 7-1, imposing a liquid to wall friction factor f_L defined by equation 7-71 resulted in a significant reduction of the stratified length. This is consistent with the observed trends of the present experimental results where, for the same inlet flow rate, the level of stratification decreased as the tube heat capacity (initial tube temperature and/or tube wall thickness) and inlet water temperature were decreased since both resulted in shorter film boiling region.

The sensitivity of the numerical solution to the critical vapour film thickness proposed in the quench criterion was tested. This was done by investigating the effect of both reducing and increasing the critical vapour film thickness by 10% on the quenching time required to rewet the entire tube. The results of the study of the case of 1 mm tube wall thickness, 480 °C initial tube temperature, 20 °C inlet water temperature and 480 kg/m².s are shown in table 7-3. As expected, this indicates that increasing the critical vapour film thickness decreases the quenching time and vice versa.

Finally, the effect of using the two or three-dimensional formulation of the tube wall heat conduction equation was also investigated. This was done by using the two formulations of the heat conduction equation for both thin and thick tube cases. As expected, it was found that using the two-dimensional formulation resulted in longer

quench times since the entire tube wall thickness is required to cool down prior to quenching. However, this delay of quench times was less than 1.1% for the thin tube while it was more than 5% for the thick tube. This justifies the use of the two-dimensional formulation of the heat conduction equation for the thin tube.

TABLE 7-1 PARAMETRIC STUDIES

Numerical Test	Quench Velocity (m/s)	$ \Delta M/M $	$ \Delta Q/Q $	Stratified Length (cm) (after 5 s)
1- normal values	0.481	3.1 %	4.1 %	110
2- f_i doubled	0.495	3.2 %	3 %	120
3- f_g doubled	0.492	3.1 %	3.3 %	120
4- f_L imposed on film boiling region	0.491	2.1 %	4.7 %	70

TABLE 7-2 CONVERGENCE STUDIES

Numerical Test	Quench Velocity (m/s)	$ \Delta M/M $	$ \Delta Q/Q $
1- $\begin{cases} 30 \text{ nodes} \\ \Delta t = 0.03 \text{ s} \end{cases}$	0.481	3.1 %	4.1 %
2- $\begin{cases} 60 \text{ nodes} \\ \Delta t = 0.03 \text{ s} \end{cases}$	0.464	3.6 %	2.1 %
3- $\begin{cases} 30 \text{ nodes} \\ \Delta t = 0.02 \text{ s} \end{cases}$	0.488	1.9 %	3.9 %
4- $\begin{cases} 60 \text{ nodes} \\ \Delta t = 0.02 \text{ s} \end{cases}$	0.465	2.1 %	3.7 %

TABLE 7-3 SENSITIVITY TO CRITICAL VAPOUR
FILM THICKNESS

Critical Vapour Film Thickness (mm)	Quenching Time (s)
0.110	8.55
0.121	8.10
0.099	8.82

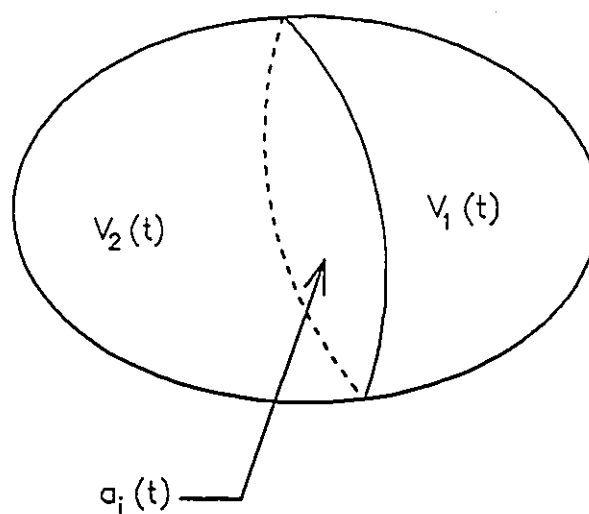


FIGURE 7-1 GENERAL TWO-PHASE CONTROL VOLUME

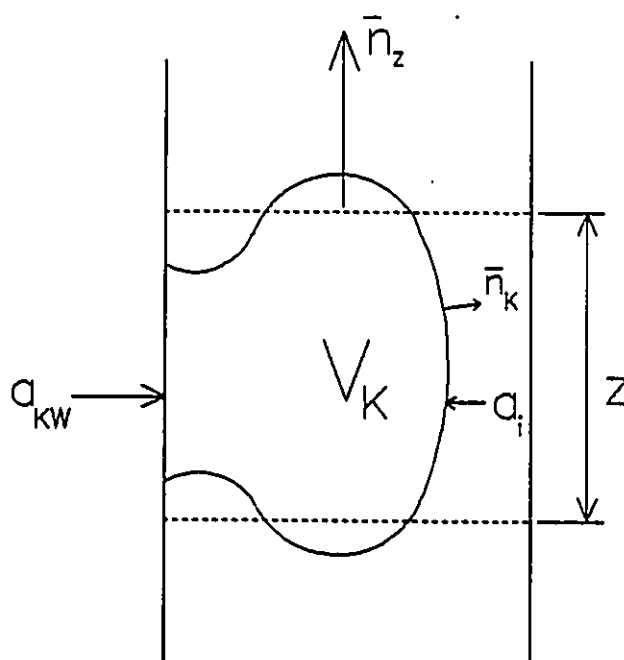


FIGURE 7-2 CONTROL VOLUME FOR THE AVERAGING PROCESS

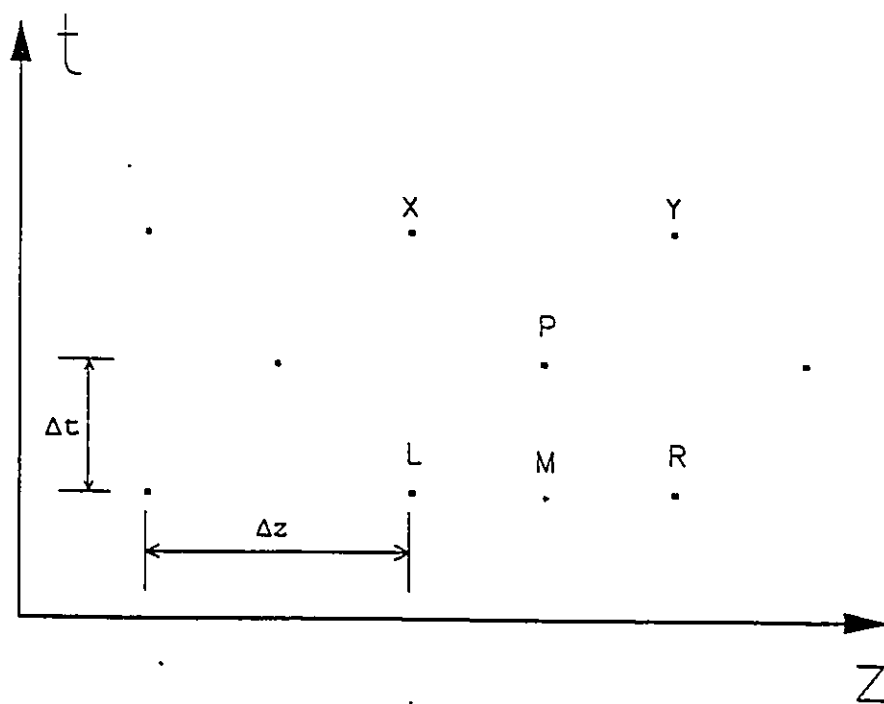


FIGURE 7-3 STAGGERED NET USED FOR THE HYDRAULIC EQUATIONS

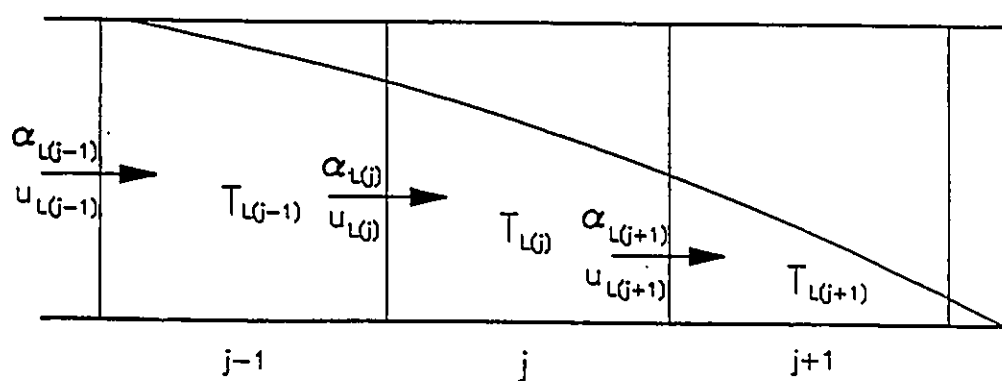


FIGURE 7-4 FINITE DIFFERENCE GRID USED FOR LIQUID TEMPERATURE CALCULATIONS

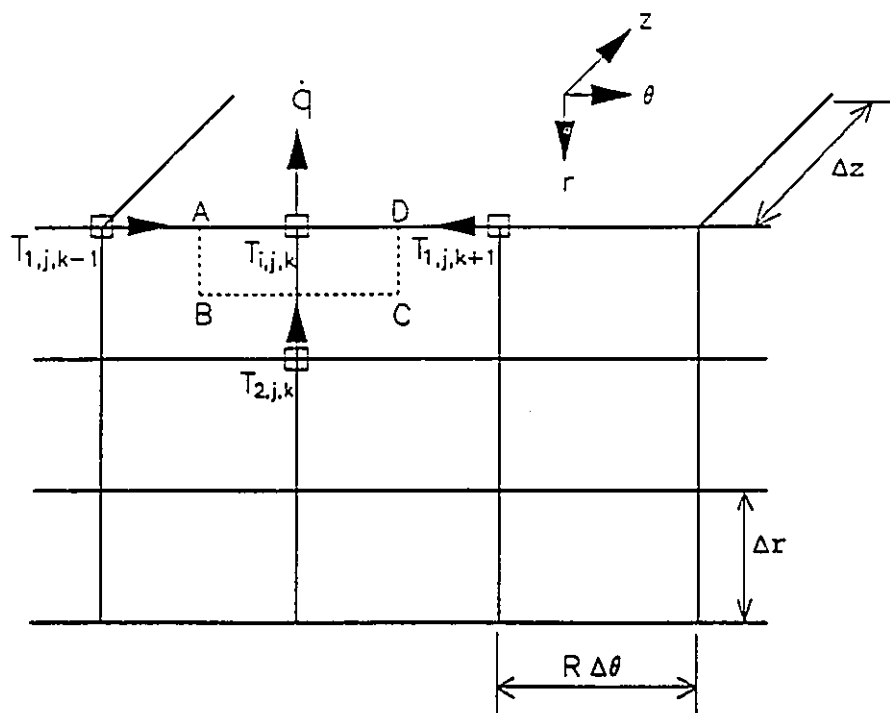


FIGURE 7-5 CONVECTIVE BOUNDARY CONDITIONS IN THE THREE-DIMENSIONAL FORMULATION

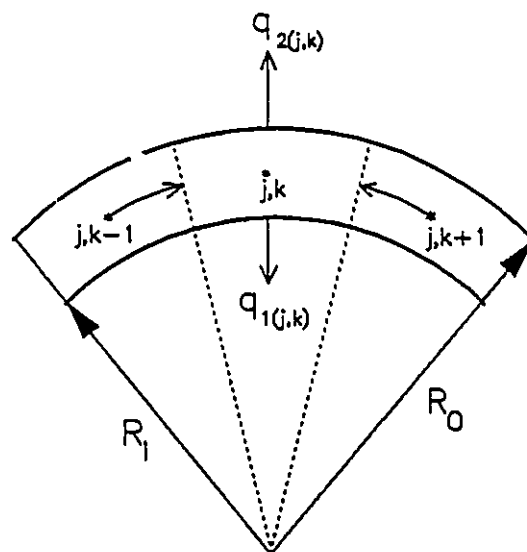


FIGURE 7-6 TWO-DIMENSIONAL FORMULATION WITH CONVECTIVE BOUNDARY CONDITIONS

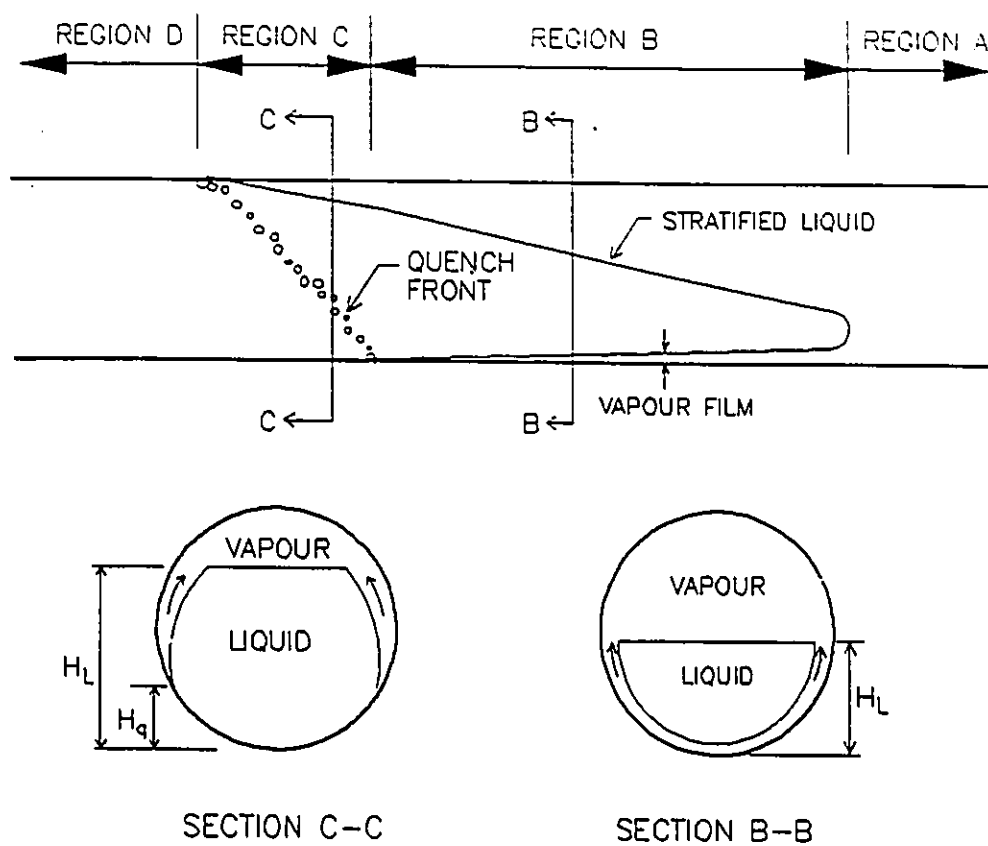


FIGURE 7-7 REGIONS OF HEAT TRANSFER FOR
MODERATE TUBE HEAT CAPACITY AND
MODERATE MASS FLUX

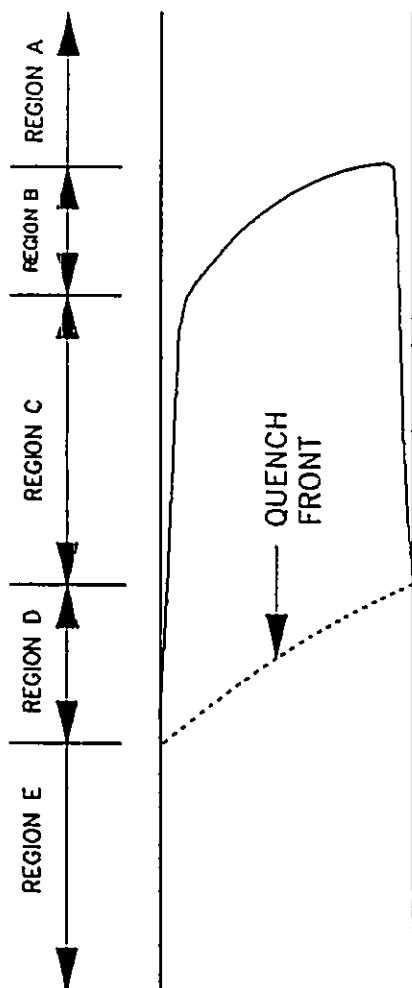


FIGURE 7-8 REGIONS OF HEAT TRANSFER FOR HIGH TUBE HEAT CAPACITY AND HIGH MASS FLUX

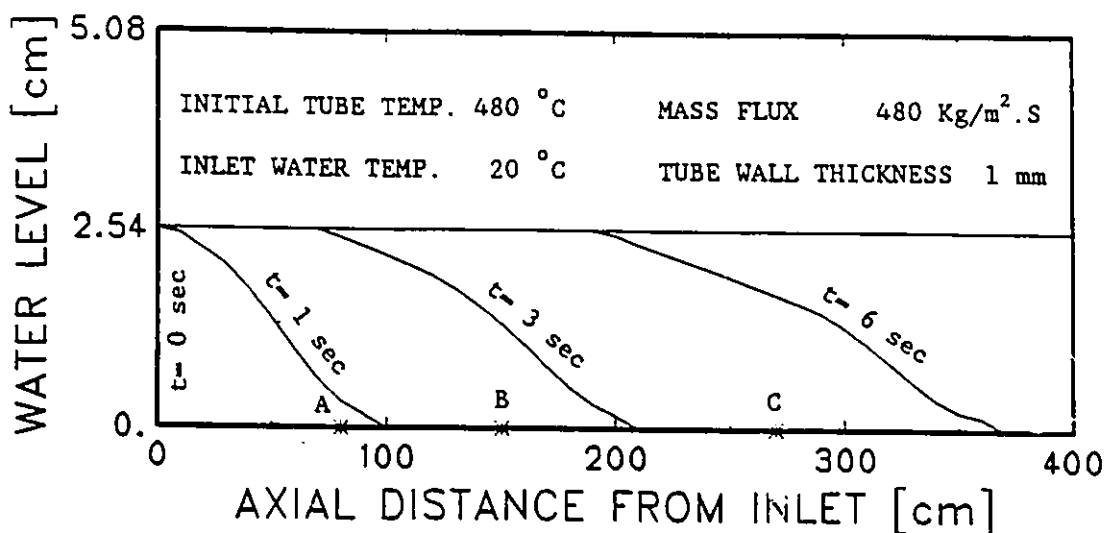


FIGURE 7-9 REFILLING AND QUENCH FRONT PROPAGATION

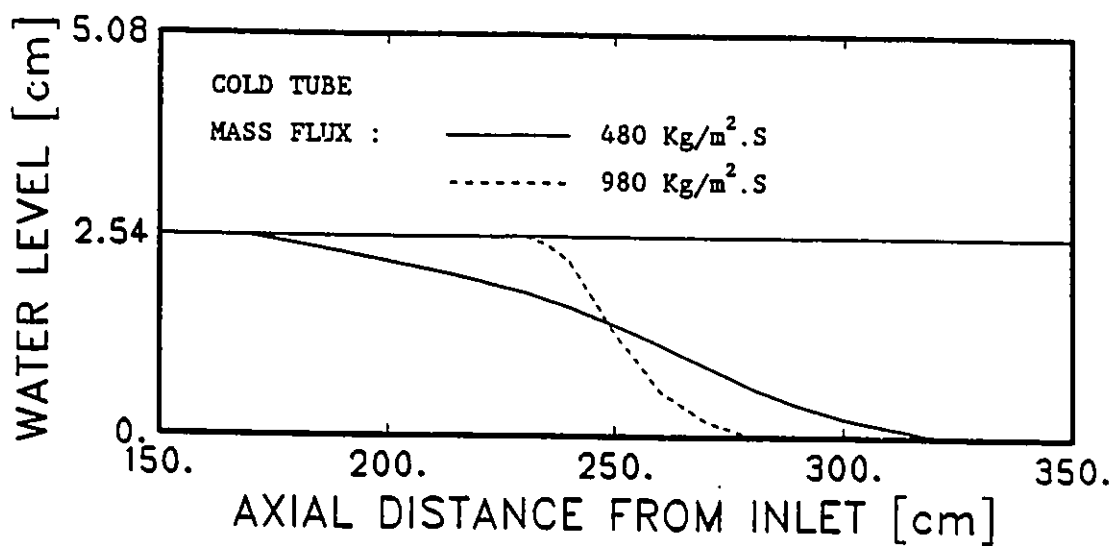


FIGURE 7-10 EFFECT OF MASS FLUX ON STRATIFICATION

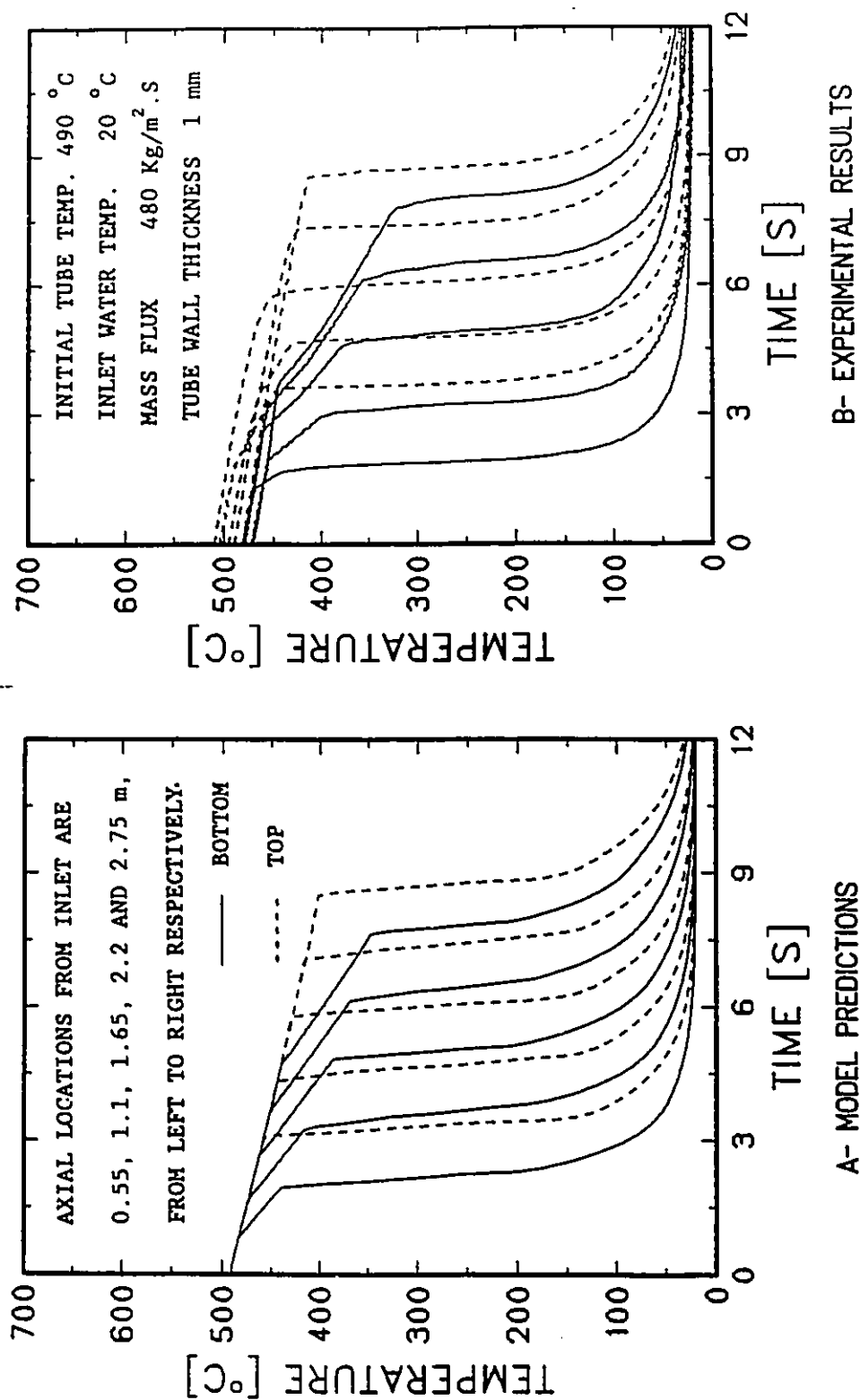


FIGURE 7-11
 TRANSIENT TEMPERATURE CURVES AT DIFFERENT
 AXIAL LOCATIONS FOR LOW MASS FLUX

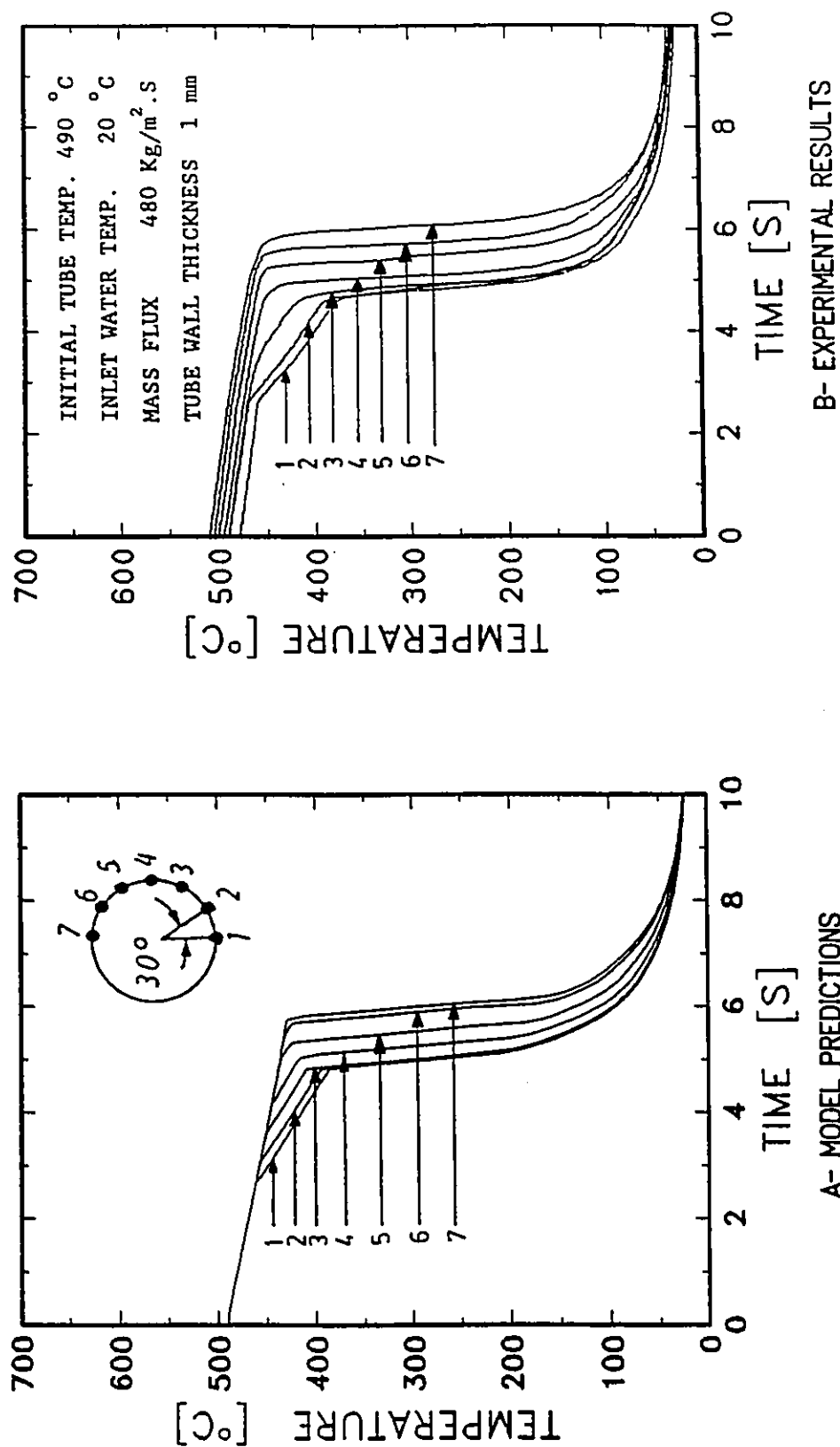


FIGURE 7-12
TRANSIENT TEMPERATURE CURVES AT DIFFERENT
CIRCUMFERENTIAL LOCATIONS FOR LOW MASS FLUX

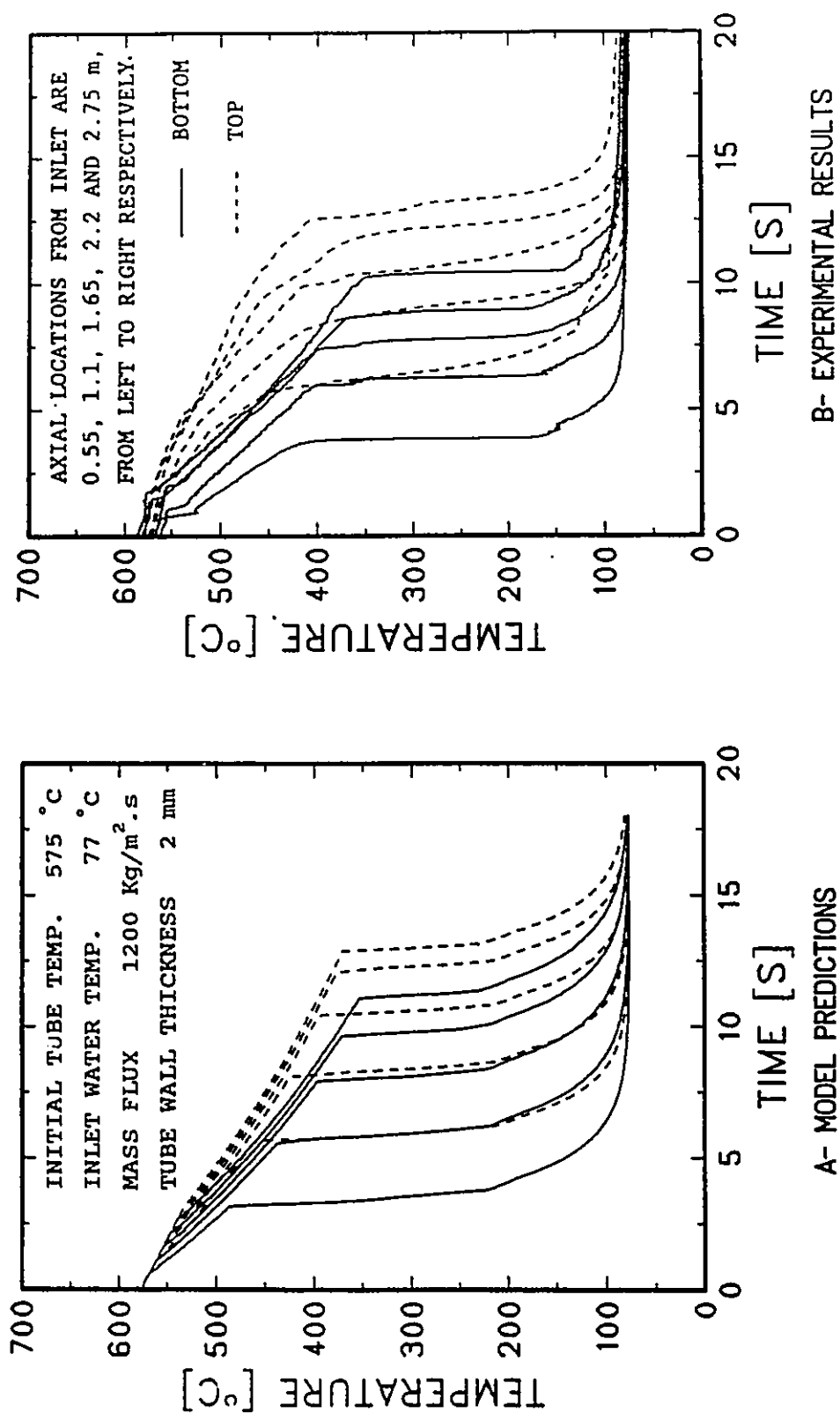


FIGURE 7-13
TRANSIENT TEMPERATURE CURVES AT DIFFERENT
AXIAL LOCATIONS FOR HIGH MASS FLUX

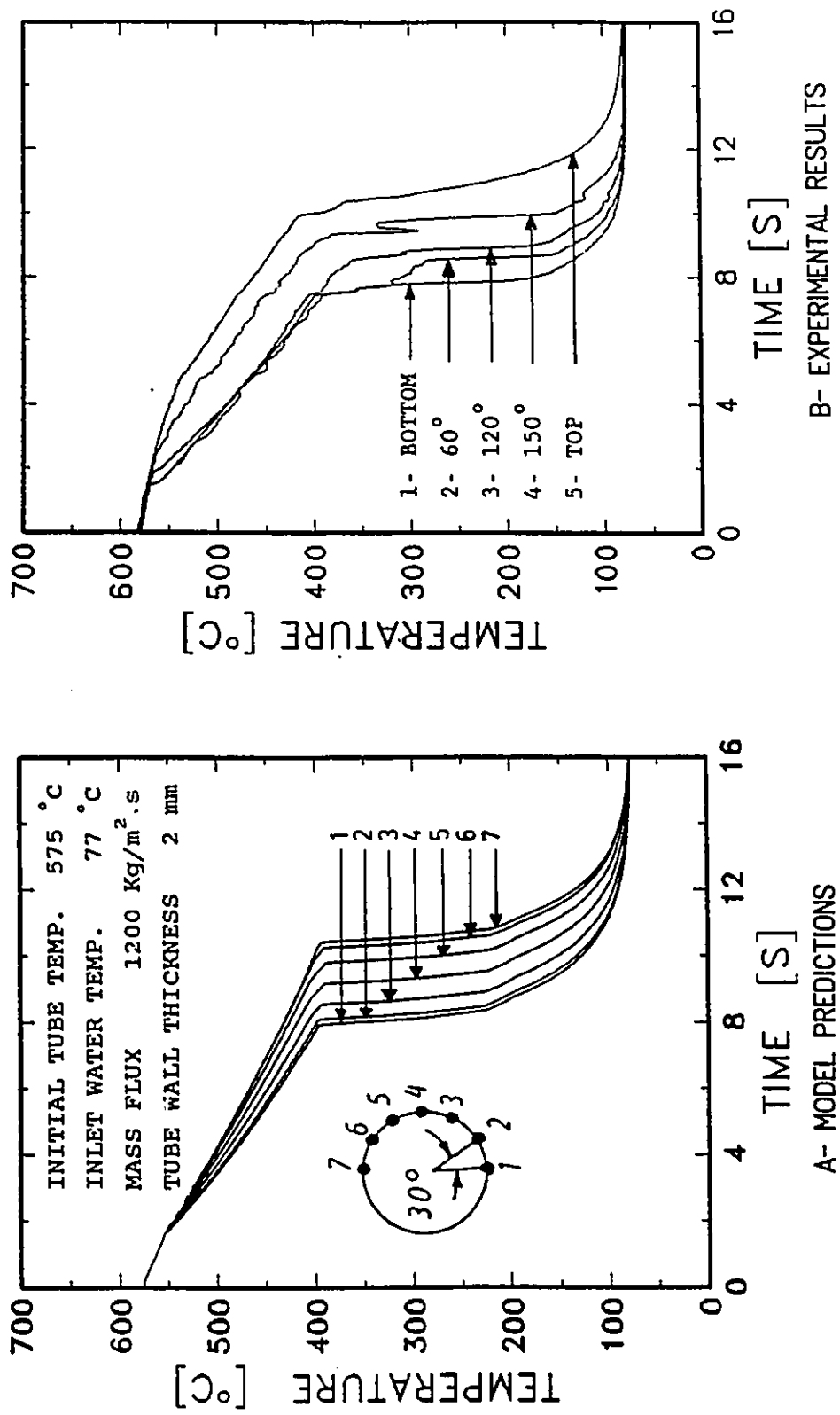


FIGURE 7-14
 TRANSIENT TEMPERATURE CURVES AT DIFFERENT
 CIRCUMFERENTIAL LOCATIONS FOR HIGH MASS FLUX

CHAPTER 8

CONCLUSIONS

An experimental and analytical study of the refilling and rewetting of hot horizontal tubes has been conducted. This chapter summarizes the major findings and contributions as follows:

1- A new set of data on refilling and rewetting of hot horizontal tubes for a wide range of initial and boundary conditions has been obtained. The data has played an important role in formulating the physical model and verifying code calculations. This data is also well suited to be used as benchmark data for future model development and code verification.

2- The effect of different parameters (mass flux, subcooling, initial tube temperature and tube wall thickness) on the rewetting velocity agreed well with those reported in previous investigations for both vertical channel reflooding and horizontal rewetting. In particular, increasing mass flux and/or coolant subcooling increases the rewetting velocity while increasing the initial tube temperature and/or tube wall thickness decreases the rewetting velocity.

3- The experiments were designed such that the simultaneous transient void fraction and the transient circumferential surface temperature distribution at a given cross section of the tube were measured. This

allowed the identification of the flow patterns associated with the quench front propagation. Although the stratified flow pattern was found to be the most dominant regime, inverted annular and skewed annular flow patterns were observed as well. The inverted annular flow pattern was obtained at relatively high mass flux and high tube heat capacity while the skewed annular flow pattern was limited to a very low tube heat capacity and very low mass flux.

4- Quench curves at different axial and circumferential locations were obtained to evaluate the various modes of heat transfer associated with the rewetting process. For the case of the thin tube (1 mm wall thickness), the temperature was assumed uniform across the tube thickness and the measured temperature transients at the outside surface was utilized in obtaining the quench curves. For the case of the thick tube (2 mm wall thickness), the same lumped parameter approach was used but the measured average transient tube wall temperature was utilized in obtaining the quench curves. The average transient tube wall temperature was calculated by integrating the transient radial temperature distribution. This analysis showed that a decrease in rewetting temperature, caused by changing any flow parameter, was always associated with longer duration of the film boiling region. Longer film boiling duration resulted not only in lower rewetting temperature but also in lower maximum heat flux and surface heat flux in the transition boiling period. Moreover, the analysis showed that the axial heat conduction represents a very small fraction of the total heat flux.

5- From the analysis of the present experimental results as well as a review of the available literature, a general rewetting criterion which marks the end of the stable film boiling due to the vapour film collapse was proposed. This criterion represents the necessary (but may not be sufficient) condition for initiating tube wall rewetting. It suggests that rewetting is initiated when the vapour film thickness reduces down to a value equal to the sum of the amplitude of the liquid-vapour interface fluctuations and the solid surface roughness.

6- A theoretical model for predicting the dynamic behaviour of the liquid-vapour interface in the film boiling region near the bottom of a horizontal tube was developed. This study showed that the hydraulic disturbances represented by the system pressure fluctuations could induce interface fluctuations capable of rewetting the surface when the equilibrium vapour film thickness was close to the experimentally estimated critical value.

7- Theoretical models for the partition factor (portion of heat used in evaporation) and the film boiling heat transfer coefficient in the film boiling region during the refilling of hot horizontal tubes were developed.

8- A two-fluid model, incorporating the proposed rewetting criterion as well as the models for the partition factor and the film boiling heat transfer coefficient, was developed to predict the transients of the refilling and rewetting of hot horizontal tubes. This showed a good

capability of predicting the thermal-hydraulic transients of the process.

REFERENCES

- Agee, L.J., Banerjee, S., Duffey, R.B., and Hughes, E.D. , "Some Aspects of Two-Fluid Models and Their Numerical Solutions", Paper Presented at Second OECD/NEA Specialists Meeting on Transient Two-Phase Flow, Paris, 1978.
- Ahluwalia, A.K., Chan, A.M.C., and Shoukri, M. , "Refilling and Rewetting of Hot Horizontal Tubes : Interim Report II" , Ontario Hydro, Canada, Report No. B85-29-K, 1985.
- Andreoni, D., and Courtant, M. , "Study of Heat Transfer During the Reflooding of a Single Rod Test Section" , Proceedings of the CREST Specialist Meeting on Emergency Core Cooling for Light Water Reactors, Garching/Munich, October 18-20, MRR 115, Volume 1, 1972.
- Andreoni, D., Courtant, M., and Deruaz, R. , "Heat Transfer During the Reflooding of a Tubular Test Section" , European Two-Phase Flow Meeting, Harwell, 3-7 June, 1974.
- Avidisian, C.T., and Koplik, J. , "Leidenfrost Boiling of Methanol Droplets on Hot Porous/Ceramic Surfaces", Int. J. Heat Mass Transfer, Vol. 30, No. 2, pp. 379-393, 1987.
- Banerjee, S., and Chan, A.M.C. , "Separated Flow Models - I: Analysis of the Averaged and Local Instantaneous Formulation" Int. J. Multi-Phase Flow, Vol. 6, pp. 1-24, 1980.
- Baumeister, K.J., Hendricks, R.C., and Hamill, T.D., "Metastable Leidenfrost States", Natl. Aeronaut. Space Admin., Tech. Note D-3226, 1966.
- Baumeister, K.J., and Simon, F.F. , "Leidenfrost Temperature - Its Correlation for Liquid Metals, Cryogenes, Hydrocarbones and Water" , J. Heat Transfer, Vol. 95, pp. 166-173, 1973.
- Bell, K.J. , "The Leidenfrost Phenomenon - a Survey", Chemical Engineering Progress Symposium Series, Vol. 6, No. 7, , 1967.
- Bennett, A.W., Hewitt, G.F., Kearsey, H.A., and Keeys, R.K.F. , "The Wetting of Hot Surfaces by Water in a Steam Environment at High Pressures" , UKAEA Report , AERE-5416 , 1966.
- Berenson, P.J., "Film Boiling Heat Transfer From a Horizontal Surface", J. Heat Transfer, Vol. 83, pp. 351-358, 1961.

Blair, J.M., "An Analytical Solution to a Two-Dimensional Model of the Rewetting of a Hot Dry Rod" , Nucl. Eng. & Design, Vol. 97, pp. 159-170, 1975.

Bonakdar, H., and Mcassey, Jr.E.V., "A Method for Determining Rewetting Velocity under Generalized Boiling Conditions" , Nucl. Eng. & Design, Vol. 66, pp. 7-12, 1981.

Bradfield, W.S., "Wave Generation at Stagnation Point in Stable Film Boiling", Proc. of the Two-Phase Flow Symposium, University of Exeter, England, 1965.

Butterworth, D., and Owen, R.G., "The Quenching of Hot Surfaces by Top and Bottom Flooding - a Review" , AERE-R7992, 1975.

Chan, A.M.C., "Transient Two Phase Flows : Refilling and Rewetting of Hot Horizontal Tube" , Ph.D Thesis, McMaster University, Hamilton, Ontario, Canada, 1980.

Chan, A.M.C., and Banerjee, S., "Refilling and Rewetting of Hot Horizontal Tube, Part I : Experiments" , J. of Heat Transfer, Vol. 103, May 1981a.

Chan, A.M.C., and Banerjee, S., "Refilling and Rewetting of Hot Horizontal Tube, Part II : Structure of a Two Fluid Model" , J. of Heat Transfer, Vol. 103, May 1981b.

Chan, A.M.C., and Banerjee, S., "Refilling and Rewetting of Hot Horizontal Tube, Part III : Application of a Two Fluid Model to Analyze Rewetting" , J. of Heat Transfer, Vol. 103, Nov. 1981c.

Chan, A.M.C., and Banerjee, S., "Design Aspects of Gamma Densitometer for Void Fraction Measurements in Small Scale Two-Phase Flows" , Nuclear Instruments and Methods, Vol. 190, pp. 135-148, 1981.

Chan, K.C., and Yadigaroglu, G., "Calculations of Film Boiling Heat Transfer Above the Quench Front During Reflooding", Proc. of National Heat Transfer Conference, Vol. 7, pp. 65-72, 1980.

Chang, Y.P., "A Theoretical Analysis of Heat Transfer in Natural Convection and in Boiling" , Tran. ASME, Vol. 79, pp. 1501-1513, 1957.

Chen, W.J., Lee, Y., and Groeneveld, D.C., "Measurement of Boiling Curves During Rewetting of a Hot Circular Duct" , J. of Heat Mass Transfer, Vol. 22, pp. 973-976, 1979.

Cheng, S.C., Lau, P.W.K., and Poon, K.T., "Measurements of True Quench Temperature of Subcooled Water under Forced Convective Conditions" , Int. J. Heat Mass Transfer, Vol. 28, No. 1, pp. 235-243, 1985.

Cheng, S., Ng, W., and Heng, K., "Measurements of Boiling Curves of Subcooled Water under Forced Convective Conditions", Int. J. Heat Mass Transfer, Vol. 21, pp. 1385-1392, 1978.

Cheng, S.C., and Poon, K.T., "Correlation of True Quench Temperature for Water", Int. Comm. Heat Mass Transfer, Vol. 12, pp. 629-633, 1985.

Chun, M.H., and Chung, B.D., "A Numerical Model for Analysis of Reflooding Phase of a LOCA", ASME Paper 82-WA/HT-32, 1982.

Coney, M.W.E., "Calculations on the Rewetting of Hot Surfaces", Nucl. Eng. and Design, Vol. 31, pp. 246-259, 1974.

Delhaye, J.M., and Achard, J.L., "On the Averaging Operators Introduced in Two-Fluid Modelling", Paper Presented at First OECD/NEA Specialists Meeting on Transient Two-Phase Flow, Toronto, August, 1976.

De Salve, M., and Panella, B., "Thermal-Hydraulics of the Bottom Reflooding in Tubes with Different Thickness and Length", NUREG/CP-0014, 2, 1196, 1980.

De Salve, M., and Panella, B., "Validation of a Bottom Flooding Model", Nucl. Eng. & Design, Vol. 99, pp. 213-222, 1987.

Duffey, R.B., and Porthouse, D.T.C., "The Physics of Rewetting in Water Reactor Emergency Core Cooling", Nucl. Eng. & Design, Vol. 25, pp. 379-394, 1973.

Elias, E., and Yadigaroglu, G., "A General One-Dimensional Model for Conduction-Controlled Rewetting of a Surface", Nucl. Eng. & Design, Vol. 42, pp. 185-194, 1976.

Elias, E., and Yadigaroglu, G., "The Reflooding Phase of the LOCA in PWRs. Part II : Rewetting and Liquid Entrainment", Nuclear Safety, Vol. 19, No. 2, March-April 1978.

Elliot, D.F., and Rose, P.W., "The Quenching of a Heated Surface by a Film of Water in a Steam Environment at Pressures up to 53 Bar", UKAEA Report, AEEW-M976, 1970.

Elliot, D.F., and Rose, P.W., "The Quenching of a Heated Zircaloy Surface by a Film of Water in a Steam Environment at Pressures up to 53 Bar", UKAEA Report, AEEW-M1027, 1971.

Elphick, I., Chan, A.M.C., Ahluwalia, A.K., and Shoukri, M., "Surface Temperature and Heat Flux Measurements Using Subminiature Thermocouples", Proc. ANS/ASME/AICHE 3rd Int. Topical Meeting on Nuclear Thermal Hydraulics, Vol. I, Paper 4A.1, Rhode Island, October 1985.

Fung, K.K. , "Subcooled and Low Quality Film Boiling of Water in Vertical Flow at Atmospheric Pressure", Ph.D. Thesis, University of Ottawa, 1981.

Ghiaasiann, S.M., Catton, I., and Duffey, R.B., "A Single Channel Reflood Model" , ASME Paper 82-WA/HT-32, 1982.

Groeneveld, D.C., and Snoek, C.W., "A Comprehensive Examination of Heat Transfer Correlations Suitable for Reactor Safety Analysis", Multiphase Science and Technology, Vol. 2, Chapter 3, 1986.

Groeneveld, D.C., and Stewart, J.C., "The Minimum Film Boiling Temperature for Water During Film Boiling Collapse" , Proc. of the 7th Int. Heat Transfer Conf., Vol. 4, pp. 393-398, Munich, Fed. Rep. of Germany, 1982.

Groeneveld, D.C., and Young, J.M., "Film Boiling and Rewetting Heat Transfer During Bottom Flooding of a Hot Tube" , 6th International Heat Transfer Conference, Vol. 5, pp. 89-94, Toronto, 1978.

Henry, R.E., "A Correlation for the Minimum Film Boiling Temperature" , AIChE Symposium Series, Vol. 70, No. 138, pp. 81-90, 1974.

Holman, J.P., "Heat Transfer " , McGraw-Hill Book Company, Fourth Edition, p. 253, 1976.

Iloeje, O.C., Plummer, D.N., Griffith, P., and Rohsenow, W.M., "An Investigation of the Collapse and Surface Rewet in Film Boiling in Forced Vertical Flow", ASME Paper, No. 73-WA/HT-20 , 1973.

Ishii, M., "Thermo-Fluid Dynamic Theory of Two-Phase Flow", Eyrolles, Paris, 1975.

Ishii, M., and Jarlais, G., "Flow Regime Transition and Interfacial Characteristics of Inverted Annular Flow " , J. of Nuclear Engineering and Design, Vol. 95, pp. 171-184, 1986.

Jens, W.H., and Lottes, P.A. , "Analysis of Heat Transfer Burnout, Pressure Drop and Density Data for High Pressure Water", ANL-4627, 1951.

Johannsen, K. , "Low Quality Transition and Inverted Annular Flow Film Boiling of Water : An Updated Review", Proc. of 1st World Conf. on Experimental Heat Transfer, Fluid Mechanics and Thermodynamics, pp. 1416-1429, Dubrovnik, Yugoslavia, 1988.

Kawaji, M., and Banerjee, S., "Application of a Multifield Model to Reflooding of A Hot Vertical Tube : Part 1 - Model Structure and Interfacial Phenomena" , J. of Heat Transfer, Vol. 109, pp. 204-211, February 1987.

Kawaji, M., and Banerjee, S., "Application of a Multifield Model to Reflooding of A Hot Vertical Tube : Part II - Analysis of Experimental Results" , J. of Heat Transfer, Vol. 110, pp. 710-720, August 1988.

Kawaji, M., Ng, Y.S., Banerjee, S., and Yadigaroglu, G., "Reflooding with Steady and Oscillatory Injection : Part I - Flow Regimes, Void Fraction, and Heat Transfer" , J. of Heat Transfer, Vol. 107, pp. 670-678, August 1985.

Kim, A.K., and Lee, Y., "A Correlation of Rewetting Temperature", Letters in Heat and Mass Transfer, Vol. 6, pp. 117-123, 1979.

Klimenko, V.V., and Snytin, S.Yu., "Film Boiling Crisis on a Submerged Heating Surface" , Proc. of the 1st World Conf. on Experimental Heat Transfer, Fluid Mechanics and Thermodynamics, pp. 551-563, Dubrovnik, Yugoslavia, 1988.

Kreyszig, E., "Advanced Engineering Mathematics", Fifth Ed., John Wiley & Sons, p. 844, 1983.

Laurinat, J., "Studies of the Effects of Pipe Size on Horizontal Annular Two-Phase Flows" , Ph.D. Thesis, University of Illinois at Urbana-Champaign, 1982.

Laurinat, J. et al, "Film Thickness Distribution Around a Horizontal Pipe for Annular Two-Phase Flow" , Proc. Int. Symposium on Two-Phase Annular and Dispersed Flows, Pisa, Italy, June 1984.

Lee, Y., Chen, W.J., and Groeneveld, D.C., "Rewetting of Very Hot Vertical and Horizontal Channels by Flooding" , 6th International Heat Transfer Conference, Toronto, Vol. 5, pp. 95-100, 1978.

Lienhard, J.N. and Wong, P.T.Y., "The Dominant Unstable Wave Length and Minimum Heat Flux During Film Boiling on a Horizontal Surface" , J. Heat Transfer, Vol. 86, pp. 220-228, 1964.

Lin, D.Y.T., and Westwater, J.W., "Effect of Metal Thermal Properties on Boiling Curves Obtained by the Quenching Method" , Proc. of the Seventh Int. Heat Transfer Conference, Fed. Rep. of Germany, 1982.

Martini, R., and Premoli, A., "Bottom Flooding Experiments with Simple Geometries under Different ECC Conditions" , Energia Nucleare, Vol. 20, p. 540, 1973.

Michiyoshi, I., Takahashi, O., and Kikuchi, Y., "Heat Transfer and Low Limit of Film Boiling" , Proc. of the 1st World Conf. on Experimental Heat Transfer, Fluid Mechanics and Thermodynamics, pp. 1404 -1415, Dubrovnik, Yugoslavia, 1988.

Naylor, P., and Patrick, M.A., "Film Boiling Destabilization", Proc. of the 8th Int. Heat Transfer Conf., Vol. 4, pp. 2037-2042, 1986.

Nishikawa, K., Fujita, Y., Uchida, S., and Ohta, H., "Effect of Surface Configuration on Nucleate Boiling Heat Transfer ", Int. J. Heat Mass Transfer, Vol. 27, No. 9, pp. 1559-1571, 1984.

Olek, S., "Solution to a Fuel-and-Cladding Rewetting Model" , Int. Comm. Heat Mass Transfer, Vol. 16, pp. 143-158, 1989.

Olek, S., Zvirin, Y., and Elias, E., "Rewetting of Hot Surfaces by Falling Liquid Films as a Conjugate Heat Transfer Problem" , Int. J. Multiphase Flow, Vol. 14, No. 1, pp. 13-33, 1988.

Orozco, J., and Stellman, R., "Oscillation of a Liquid-Vapour Interface During Flow Film Boiling" , Int. Comm. Heat Mass Transfer, Vol. 15, pp. 125-140, 1988.

Orozco, J., Stellman, R., and Poulikados, D., "Dynamic Response of a liquid-Vapour Interface During Flow Film Boiling from a Sphere" , J. Heat Transfer, Vol. 109, pp. 1051-1055, 1987.

Owens, F.L., and Florschuetz, L.W., "Transient Versus Steady-State Nucleate Boiling ", J. of Heat Transfer, Technical Briefs, pp. 331-333, August, 1972.

Peyayopanakul, W., and Westwater, J.W., "Evaluation of the Unsteady-state Quenching Method for Determining Boiling Curves ", Int. J. Heat Mass Transfer Vol. 21, pp. 1437-1445, 1978.

Piggott, B.D.G., and Duffey, R.B., "The Quenching of Irradiated Fuel Pins" , Nucl. Eng. & Design, Vol. 32, pp. 182-190, 1975.

Plummer, D.N., Iloeje, O.C., Griffith, P., and Rohsenow, W.M., "A Study of Post Critical Heat Transfer in a Forced Convection System" , MIT Report NO. 73645-80, 1973.

Raj, V.V., "Experimental and Analytical Studies on the Rewetting of Hot Surfaces" , Ph.D Thesis, Indian Institute of Technology, Bombay, India, 1984.

Salcudean, M., and Bui, T.M., "Heat Transfer during the Rewetting of Hot Horizontal Channels" , Nucl. Eng. & Design, Vol. 59, pp. 369-377, 1980.

Salcudean, M., and Rahman, M., "An Analytical Solution for the Heat Conduction during the Rewetting of Hot Horizontal Channels" , Transactions of the CSME, Vol. 6, No. 2, pp. 106-114, 1980/1981.

Sawan, M.E., and Carbon, M.W., "A Review of Spray Cooling and Bottom Flooding Work for LWR Cores" , Nucl. Eng. & Design, Vol. 32, pp. 191-207, 1975.

Sawan, M.E., and Temraz, H.M., "A Three Regions Semi-Analytical Rewetting Model" , Nucl. Eng. & Design , Vol. 64, pp. 319-327, 1981.

Semeria, R., and Martinet, B., "Calefaction Spots on a Heating Wall : Temperature Distribution and Resorption" , Proc. Inst. Mech. Eng., Vol. 180, pp. 192-205, 1965.

Sheppard, J.J., and Bradfield, W.S., "Stagnation Point Free-Convection Film Boiling on a Hemisphere" , Progress in Heat and Mass Transfer, Vol. 6, pp. 227-293, 1972.

Shires, G.L., Pickering, A.R., and Blacker, P.T., "Film Cooling of Vertical Fuel Rods" , UKAEA Report, AEEW-R343, 1964.

Sollychin, R., "The Verification and the Preliminary Development of Physical Models for Analyses of the Vertical and the Horizontal Rewetting Phenomena" , M.Sc. Thesis, University of Toronto, Ontario, Canada, 1983.

Spiegler, P., Hopenfeld, J., Silberberg, M., Bumpus Jr., C.F., and Norman, A., "Onset of Stable Film Boiling and the Foam Limit" , Int. J. Heat Mass Transfer, Vol. 6, pp. 987-994, 1963.

Stoker, J.J., "Water Waves - The Mathematical Theory and Applications", Interscience Publishers, pp. 480-481, 1957.

Sun, K.H., Dix, G.E., and Tien, C.L., "Cooling of a Very Hot Vertical Surface by a Falling Liquid Film" , J. of Heat Transfer, Vol. 22, pp. 126-132, 1974.

Sun, K.H., Dix, G.E., and Tien, C.L., "Effect of Precursory Cooling on Falling Film Rewetting" , J. of Heat Transfer, Vol. 97, pp. 360-365, 1975.

Thompson, T.S., "An Analysis of the Wet-Side Heat Transfer Coefficient during Rewetting of a Hot Dry Patch" , Nucl. Eng. & Design, Vol. 22, pp. 212-224, 1972.

Thompson, T.S. , "On the Process of Rewetting a Hot Surface by a Falling Liquid Film" , Nuclear Eng. & Design, Vol. 31, pp. 234-245, 1974.

Toda, S., and Mori, M., "Subcooled Film Boiling and the Behaviour of Vapour Film on a Horizontal Wire and a Sphere" , Proc. of the 7th Int. Heat Transfer Conf., pp. 173-178, Munchen, Fed. Rep. of Germany, 1982.

Tong, L.S., "Heat Transfer Mechanisms in Nucleate and Film Boiling", Nuclear Eng. & Design, Vol. 21, pp. 1-25, 1972 .

Ueda, T., and Inoue, M., "Rewetting of a Hot Surface by a Falling Liquid Film - Effects of Liquid Subcooling ", Int. J. Heat Mass Transfer, Vol. 27, No. 7, pp. 999-1005, 1984.

Ueda, T., Tsunenari, S., and Koyanagi, "An Investigation of Critical Heat Flux and Surface Rewet in Flow Boiling System, "Int. J. Heat Mass Transfer, Vol. 26, No. 8, pp. 1189-1198, 1983.

Ueda, T. et al, "Rewetting of a Hot Surface by a Falling Liquid Film ", Int. J. Heat Mass Transfer, Vol. 26, No. 3, March 1983.

Veres, D.R., and Florschütz, L.W., "A Comparison of Transient and Steady-state Pool-Boiling Data Obtained Using the Same Heating Surface", J. of Heat Transfer, Technical Briefs, pp. 229-232, May 1971.

Vernier, P., and Delhay, J.M., "General Two-Phase Flow Equations Applied to the Thermodynamics of Boiling Nuclear Reactors", Energie Primaire, Vol. 4, No 1, 1968.

Wallis, G.B., "One Dimensional Two-Phase Flow", McGraw Hill, Chapter 2, 1969.

Wachters, L.H.J., Bonne, H., and Van Nouhuis, H.J., "The Heat Transfer from a Hot Horizontal Plate to Sessile Water Drops in the Spheroidal State" , Chem. Eng. Sc., Vol. 21, pp. 923-936, 1966.

Werner, M.F., Dokainish, M.A. and Shoukri, M., "Finite Element Analysis of Transient Heat Conduction With Moving Convective Boundaries" , Numerical Heat Transfer, Vol. 15, 1988.

Yadigaroglu, G., Arrieta, L.A., and Greif, R., "Heat Transfer during the Reflooding Phase of the LOCA-State of the Art" , EPRI 248-1 Topical Report, September 1975.

Yamanouchi, A., "Effect of Core Spray Cooling in Transient State After Loss of Coolant Accident" , J. Nucl. Sci. Tech., Vol. 5, pp. 547-558, 1968.

Yeh, H.C., "An Analysis of Rewetting of a Nuclear Fuel Rod in Water Reactor Emergency Core Cooling" , Nucl. Eng. & Design, Vol. 34, pp. 317-322, 1975.

Yeh, H.C., "An Analytical Solution to Fuel-and-Cladding Model of the Rewetting of a Nuclear Fuel Rod" , Nucl. Eng. & Design, Vol. 61, pp. 101-112, 1980.

Yuzda, G., and Pham, C., "Gamma Attenuation Method for Measuring Void Fraction in Two-phase Flow", B. Eng. Thesis, Mech. Eng. Dept., McMaster Univ., 1986.

Zvonarev, Yu.A., Komendantov, A.S., and Kuzma-kichta, Yu.A., "An Experimental Investigation of Heat-Transfer Characteristics During Rewetting of a Heating surface", Thermal Engineering, Vol. 31, Issue 5, 1984.

Zuber, N., "On the Stability of Boiling Heat Transfer" , Trans. of ASME, Vol. 58, pp. 711-720, 1958.

APPENDIX A
MATRIX OF EXPERIMENTAL RESULTS

Table A-1

Test Matrix of the Thin Tube

First Group

A- Initial Tube Temperature 290 °C

Mass Flux (kg/m ² .s)	Inlet Water Temperature (°C)		
	20	60	80
420	T.R. 1 Feb-2-1987	T.R. 2 Feb-9-1987	T.R. 3 Feb-10-1987
480	T.R. 4 Jan-29-1987	T.R. 5 Jan-21-1987	T.R. 6 Jan-23-1987
650	T.R. 7 Feb-2-1987	T.R. 8 Feb-6-1987	T.R. 9 Feb-4-1987
720	T.R. 10 Jan-19-1987	T.R. 11 Jan-21-1987	T.R. 12 Jan-22-1987
970	T.R. 13 Jan-20-1987	T.R. 14 Jan-21-1987	T.R. 15 Jan-22-1987
1200	T.R. 16 Jan-20-1987	T.R. 17 Jan-21-1987	T.R. 18 Jan-22-1987

Table A-2
 Test Matrix of the Thin Tube
 First Group
 B- Initial Tube Temperature 390 °C

Mass Flux (kg/m ² .s)	Inlet Water Temperature (°C)		
	20	60	80
420	T.R. 19 Feb-12-1987	T.R. 20 Feb-9-1987	T.R. 21 Feb-10-1987
480	T.R. 22 Jan-26-1987	T.R. 23 Jan-27-1987	T.R. 24 Jan-26-1987
650	T.R. 25 Feb-2-1987	T.R. 26 Feb-6-1987	T.R. 27 Feb-6-1987
720	T.R. 28 Jan-26-1987	T.R. 29 Jan-27-1987	T.R. 30 Jan-27-1987
970	T.R. 31 Feb-17-1987	T.R. 32 Feb-18-1987	T.R. 33 Feb-20-1987
1200	T.R. 34 Feb-19-1987	T.R. 35 Feb-19-1987	T.R. 36 Feb-23-1987

Table A-3

Test Matrix of the Thin Tube

First Group

C- Initial Tube Temperature 490 °C

Mass Flux (kg/m ² .s)	Inlet Water Temperature (°C)		
	20	60	80
420	T.R. 37 Feb-12-1987	T.R. 38 Feb-9-1987	T.R. 39 Feb-10-1987
480	T.R. 40 Jan-29-1987	T.R. 41 Jan-28-1987	T.R. 42 Jan-29-1987
650	T.R. 43 Feb-2-1987	T.R. 44 Feb-6-1987	T.R. 45 Feb-5-1987
720	T.R. 46 Jan-29-1987	T.R. 47 Jan-28-1987	T.R. 48 Jan-29-1987
970	T.R. 49 Feb-17-1987	T.R. 50 Feb-19-1987	T.R. 51 Feb-20-1987
1200	T.R. 52 Feb-19-1987	T.R. 53 Feb-19-1987	T.R. 54 Feb-23-1987

Table A-4

Test Matrix of the Thin Tube

Second Group : Repeated Runs

Case No.	Initial Tube Temperature (°C)	Water Temperature (°C)	Mass Flux (kg/m ² .s)	Test Runs
1	390	20	480	T.R. 55 - 59
2	390	20	720	T.R. 60 - 64
3	390	80	720	T.R. 65 - 69
4	490	80	720	T.R. 70 - 74

Table A-5

Test Matrix of the Thick Tube

A- Initial Tube Temperature 390 °C

Mass Flux (kg/m ² .s)	Inlet Water Temperature (°C)		
	20	60	80
420	T.R. 75 Dec-7-1987	T.R. 76 Dec-17-1987	T.R. 77 Dec-8-1987
480	T.R. 78 Nov-27-1987	T.R. 79 Dec-16-1987	T.R. 80 Dec-5-1987
720	T.R. 81 Nov-27-1987	T.R. 82 Dec-17-1987	T.R. 83 Dec-3-1987
970	T.R. 84 Dec-1-1987	T.R. 85 Dec-16-1987	T.R. 86 Dec-10-1987
1200	T.R. 87 Dec-14-1987	T.R. 88 Jan-1-1988	T.R. 89 Dec-14-1987

Table A-6

Test Matrix of the Thick Tube

B- Initial Tube Temperature 490 °C

Mass Flux (kg/m ² .s)	Inlet Water Temperature (°C)		
	20	60	80
420	T.R. 90 Dec-7-1987	T.R. 91 Dec-17-1987	T.R. 92 Dec-8-1987
480	T.R. 93 Dec-1-1987	T.R. 94 Dec-16-1987	T.R. 95 Dec-3-1987
720	T.R. 96 Dec-7-1987	T.R. 97 Dec-17-1987	T.R. 98 Dec-8-1987
970	T.R. 99 Dec-10-1987	T.R. 100 Dec-16-1987	T.R. 101 Dec-10-1987
1200	T.R. 102 Dec-14-1987	T.R. 103 Jan-29-1988	T.R. 104 Dec-14-1987

Table A-7

Test Matrix of the Thick Tube

C- Initial Tube Temperature 590 °C

Mass Flux (kg/m ² .s)	Inlet Water Temperature (°C)		
	20	60	80
420	T.R. 105 Jan-6-1988	T.R. 106 Feb-10-1988	T.R. 107 Jan-7-1988
480	T.R. 108 Jan-6-1988	T.R. 109 Feb-10-1988	T.R. 110 Jan-7-1988
720	T.R. 111 Jan-6-1988	T.R. 112 Feb-10-1988	T.R. 113 Jan-29-1988
970	T.R. 114 Jan-22-1988	T.R. 115 Feb-10-1988	T.R. 116 Jan-29-1988
1200	T.R. 117 Jan-22-1988	T.R. 118 Feb-9-1988	T.R. 119 Jan-26-1988

APPENDIX B

TWO-DIMENSIONAL HEAT CONDUCTION MODEL

The two-dimensional heat conduction equation in cylindrical coordinates is

$$\frac{\partial^2 T}{\partial r^2} + \frac{1}{r} \frac{\partial T}{\partial r} + \frac{\partial^2 T}{\partial z^2} = \frac{1}{\alpha} \frac{\partial T}{\partial t} \quad (\text{B.1})$$

where α is the thermal diffusivity of the wall. Considering a coordinate Z which moves with the wet front at velocity U and has its origin at the wet front point

$$Z = z - Ut \quad (\text{B.2})$$

Hence, equation (B.1) could be reduced to

$$\frac{\partial^2 T}{\partial r^2} + \frac{1}{r} \frac{\partial T}{\partial r} + \frac{\partial^2 T}{\partial Z^2} = - \frac{U}{\alpha} \frac{\partial T}{\partial Z} \quad (\text{B.3})$$

The Z -coordinate ranges from $-\infty$ to $+\infty$. The origin is taken at the apparent quench temperature. For the wet side, the coordinates could be transformed from $-\infty < Z < 0$ to $0 < Z < \infty$ by substituting $\partial T / \partial Z$ by $-\partial T / \partial Z$.

Hence equation (B.3) is reduced to

$$\frac{\partial^2 T}{\partial r^2} + \frac{1}{r} \frac{\partial T}{\partial r} + \frac{\partial^2 T}{\partial Z^2} - \frac{U}{\alpha} \frac{\partial T}{\partial Z} = 0 \quad (\text{B.4})$$

Discretizing the tube wall along r -direction and Z -direction as shown

in figure B-1, each term of equation (B-4) is reduced as follows:

$$\partial T / \partial r = [T_{A(i,j)} - T_{(i-1,j)}] / 2 \Delta r_{i-1}$$

where

$$T_{A(i,j)} = [T_{(i+1,j)} \Delta r_{i-1} + T_{(i,j)} (\Delta r_i - \Delta r_{i-1})] / \Delta r_i$$

$$\begin{aligned} \partial^2 T / \partial r^2 = & [(T_{(i+1,j)} - T_{(i,j)}) / \Delta r_i] \\ & - [(T_{(i,j)} - T_{(i-1,j)}) / \Delta r_{i-1}] / \Delta r_{i-1} \end{aligned}$$

$$\partial T / \partial z = (T_{(i,j+1)} - T_{(i,j-1)}) / 2 \Delta z$$

Substituting into equation (B-4) and rearranging gives the following difference equation for the inner mesh points.

$$\begin{aligned} T_{(i,j)} = & [C_1 T_{(i+1,j)} + C_2 T_{(i,j+1)} + C_3 T_{(i,j-1)} \\ & + C_4 T_{(i-1,j)}] / C_5 \end{aligned} \quad (B-5)$$

where

$$C_1 = rr1 + rr3$$

$$C_2 = ZZ1 - ZZ2$$

$$C_3 = ZZ1 + ZZ2$$

$$C_4 = rr2 - rr4$$

and

$$C_5 = 2 ZZ1 + rr1 + rr2 + rr3 - rr4$$

where

$$ZZ1 = 1 / \Delta z^2$$

$$ZZ2 = U / (2 \alpha \Delta z)$$

$$rr1 = 1 / (\Delta r_i * \Delta r_{i-1})$$

$$rr2 = 1/(\Delta r_{i-1})^2$$

$$rr3 = 1/(2 r_i \Delta r_i)$$

and

$$rr4 = 1/(2 r_i \Delta r_{i-1})$$

The radial boundary conditions are defined by substituting the measured outside surface temperature and the extrapolated inner surface temperature. For the boundary conditions in Z-direction, zero net axial conduction is assumed as the experimental results showed clearly that axial conduction becomes less significant away from the quench front.

Equation (B-5) is solved by iteration, terminating the computation when the converged temperature distribution is obtained. The smallest radial mesh size (Δr_i) of 0.01 mm and ΔZ of 0.02 mm were used.

Once the temperature distribution in the tube wall has been solved, the surface heat flux is obtainable. From the heat balance for the hatched area in figure B-2

$$\begin{aligned} q_{(1,j)} \Delta Z = & k_{(1,j)} \Delta r_i (T_a - T_b)/(2\Delta Z) + k_{(1,j)} \Delta r_i (T_a - T_c)/(2\Delta Z) \\ & + k_{(1,j)} \Delta Z (T_{(2,j)} - T_{(1,j)})/\Delta r_i \end{aligned} \quad (B-6)$$

where

$$T_a = (3 T_{(1,j-1)} + T_{(2,j-1)}) / 4$$

$$T_b = (3 T_{(1,j+1)} + T_{(2,j+1)}) / 4$$

$$T_c = (3 T_{(1,j)} + T_{(2,j)}) / 4$$

Substituting for T_a , T_b and T_c , equation (B-6) is reduced to

$$q_{(1,j)} = C_6 T_{(1,j)} + C_7 T_{(2,j)} + C_8 [3 T_{(1,j-1)} + T_{(2,j-1)} + 3 T_{(1,j+1)} + T_{(2,j+1)}] \quad (B-7)$$

where

$$C_6 = - [k_{(1,j)} / \Delta r_1 + 3 k_{(1,j)} \Delta r_1 / (4 \Delta Z^2)]$$

$$C_7 = [k_{(1,j)} / \Delta r_1] - [k_{(1,j)} \Delta r_1 / (4 \Delta Z^2)]$$

$$C_8 = [k_{(1,j)} \Delta r_1] / \Delta Z^2$$

where $k_{(1,j)}$ is the wall thermal conductivity at $T_{(1,j)}$

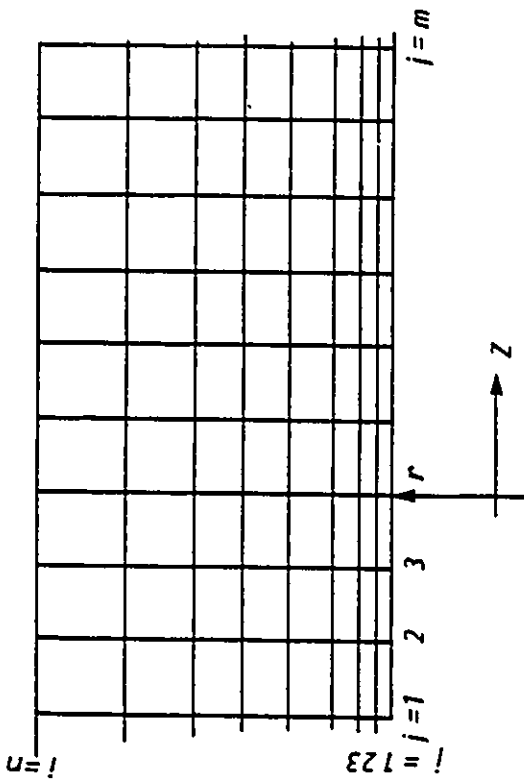


FIGURE B - 1 :

NODAL NETWORK FOR THE TWO-DIMENSIONAL
ANALYSIS.

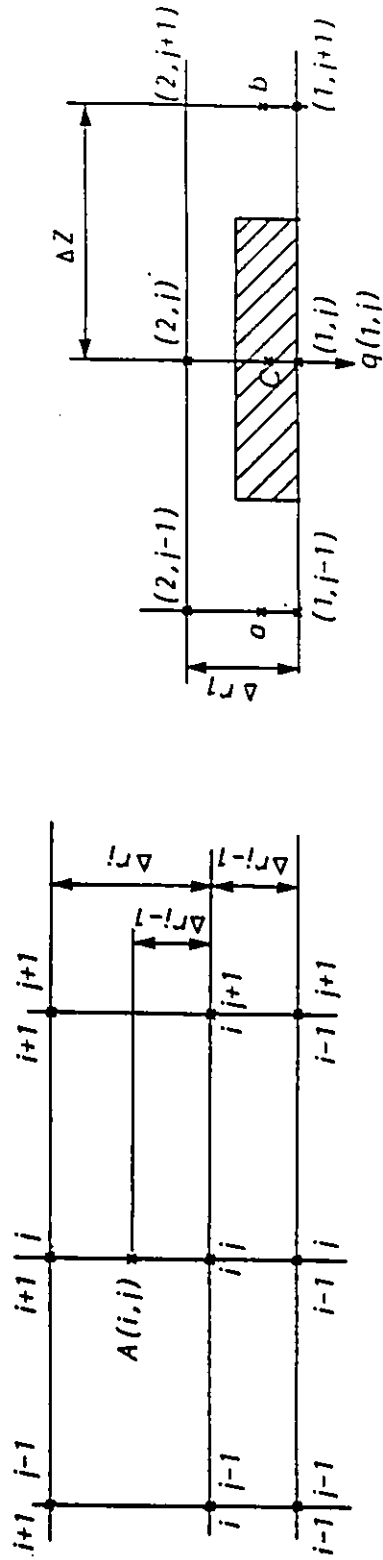


FIGURE B - 2 :

NODAL NETWORK FOR CALCULATION OF
SURFACE HEAT FLUX.